

Small changes, unexpected consequences:

Molecular insights into substrate-dependent adaptation of
KsgA/Dim1-dependent ribosomal RNA modifications in
archaea



DISSERTATION

ZUR ERLANGUNG DES
DOKTORGRADES DER NATURWISSENSCHAFTEN (DR. RER. NAT.)
DER FAKULTÄT FÜR BIOLOGIE UND VORKLINISCHE MEDIZIN
DER UNIVERSITÄT REGENSBURG

vorgelegt von

Robert Michael Knüppel

aus München

im August 2020

Das Promotionsgesuch wurde eingereicht am 7.8.2020:

Die Arbeit wurde angeleitet von:

PD Dr. Sébastien Ferreira-Cerca

Unterschrift:

Robert Knüppel

“Doing a PhD is a traumatic experience”

Dr. Brian Cusack – on the first day of the scientific writing course

INHALTSVERZEICHNIS

1	Abstract	1
2	Zusammenfassung.....	2
3	Introduction	3
3.1	A brief archaeal history	3
3.1.1	From untamed to genetically tractable	5
3.1.2	<i>Haloferax volcanii</i>	6
3.1.3	<i>Sulfolobus acidocaldarius</i>	7
3.2	The Ribosome.....	7
3.2.1	Ribosome Biogenesis.....	10
3.2.1.1	Ribosome biogenesis in <i>Escherichia coli</i>	11
3.2.1.2	Ribosome Biogenesis in <i>Saccharomyces cerevisiae</i>	13
3.2.1.3	Ribosome biogenesis in archaea.....	17
3.2.2	Conservation of ribosome biogenesis	18
3.2.3	Comparative late small subunit biogenesis, an <i>E. coli</i> perspective	19
3.2.3.1	RimM.....	20
3.2.3.2	RbfA	21
3.2.3.3	Era.....	21
3.2.3.4	Rio Proteins.....	22
3.2.3.5	KsgA/Dim1	22
3.2.3.5.1	Structure, positioning and mechanism of KsgA/Dim1.....	23
3.2.3.5.2	KsgA's role in the final biogenesis steps of <i>E. coli</i>	26
3.2.3.5.3	Dim1's role in the last steps of biogenesis in eukaryotes.....	29
3.3	Tracing of RNA metabolisms and structure	30
3.3.1	RNA Labelling.....	31
3.3.2	Chemical RNA structure probing	32
3.4	Goal of this work	34
4	Results.....	35
4.1	Establishment of RNA modifications methods	35
4.1.1	4-Thio Uracil Pulse labelling in archaea	35
4.1.2	<i>In Vivo</i> RNA chemical foot-printing in archaea.....	39
4.2	A detailed analysis of the archaeal KsgA/Dim1 methyltransferase.....	42
4.2.1	KsgA is not essential in three model archaea	42

4.2.2	The functional conservation of archaeal KsgA/Dim1	44
4.2.2.1	Abnormal methylation status in <i>Haloferax volcanii</i>	44
4.2.2.1.1	Complementation and overexpression does not resolve the abnormal methylation pattern 46	
4.2.2.1.2	Substrate dependency and structure	48
4.2.2.2	Binding and release assay of hvKsgA to the SSU	56
4.2.3	Cellular consequences of KsgA deficiency	58
4.2.3.1	KsgA deficient strains do not grow slower	58
4.2.3.2	Loss of dimethylation leads to decreased motility	59
4.2.3.3	Loss of KsgA can lead to increased biofilm formation	62
4.2.3.4	KsgA deficient cells are on average slightly longer	63
4.2.4	Translational landscape	64
5	Discussion.....	69
5.1	Pleiotropic effects from loss of KsgA in at least one Archaeal Model organism.....	69
5.2	Structural dependency for KsgA dependent methylation	73
5.3	The release mechanism of KsgA remains uncertain in archaea	79
5.4	Most RNA structure probing chemicals are suitable for model archaea	83
5.5	4-TU labelling is working in archaea.....	84
6	Conclusion.....	85
7	Material and Methods.....	87
7.1	Materials	87
7.1.1	Chemicals.....	87
7.1.2	Buffers	87
7.1.3	Media.....	90
7.1.4	Nucleic Acids.....	93
7.1.4.1	Oligonucleotides	93
7.1.4.2	Nucleotides	99
7.1.4.3	Plasmids	99
7.1.4.4	Gene synthesis.....	99
7.1.5	Kits	99
7.1.6	Enzymes.....	99
7.1.7	Strains	100
7.1.8	Consumables	100
7.1.9	Software	101

7.2	Methods.....	101
7.2.1	Microbiology.....	101
7.2.1.1	<i>Escherichia Coli</i>	101
7.2.1.1.1	Making chemically competent cells	101
7.2.1.1.2	Transformation of Plasmids via Heat-shock	102
7.2.1.1.3	P1 Transduction.....	102
7.2.1.2	<i>Haloferax volcanii</i> workflow	103
7.2.1.2.1	Transformation of Plasmids.....	103
7.2.1.2.2	Preparation of plates.....	104
7.2.1.3	Growth rate measurements	104
7.2.1.3.1	<i>H. volcanii</i> / <i>E. coli</i>	104
7.2.1.3.2	<i>S. acidocaldarius</i>	104
7.2.1.3.3	<i>P. furiosus</i>	104
7.2.1.4	Motility Assays.....	104
7.2.1.5	Microscopy.....	105
7.2.1.6	Biofilm.....	105
7.2.1.7	4TU Labelling	105
7.2.2	DNA work.....	106
7.2.2.1	Polymerase Chain Reaction	106
7.2.2.1.1	Two-step site mutation	106
7.2.2.1.2	Site Directed Mutagenesis.....	106
7.2.2.2	Restriction enzyme digest.....	106
7.2.2.3	Agarose Gel electrophoresis	107
7.2.2.4	Polyacrylamide Gel electrophoresis of DNA	107
7.2.2.4.1	Crush and Soak extraction	107
7.2.2.5	DNA Ligation	107
7.2.2.5.1	pTA_1228 Vector multiple cloning site	107
7.2.2.6	DNA Sequencing	108
7.2.2.7	DNA quantification	108
7.2.2.8	cDNA Synthesis	108
7.2.2.9	Quantitative real-time PCR	109
7.2.2.10	Dideoxy chain-termination sequencing ladder	109
7.2.2.11	Genomic Miniprep by DNA spooling.....	109
7.2.2.12	Southern blotting.....	110
7.2.2.12.1	Detection	110
7.2.3	Protein Work	110
7.2.3.1	Expression of recombinant Protein in <i>E. coli</i>	110
7.2.3.1.1	Expression.....	110
7.2.3.1.2	Extraction and purification	111

7.2.3.2	Plasmid based Protein overexpression in <i>H. volcanii</i>	112
7.2.3.2.1	Expression.....	112
7.2.3.2.2	Extraction	112
7.2.3.3	Single turnover ATPase assay	112
7.2.3.4	Adenylate cyclase reaction	112
7.2.3.5	Methanol Chloroform precipitation	112
7.2.3.6	TCA-precipitation	112
7.2.3.7	Sucrose gradient separation and fractionation	113
7.2.3.8	<i>In vitro</i> reconstitution KsgA dependent dimethylation of $\Delta ksgA$ cells.....	113
7.2.3.9	Single molecule methods.....	114
7.2.3.10	Ribosomal subunit pelleting	114
7.2.3.11	Polyacrylamide Gel Electrophoresis of Proteins	114
7.2.3.11.1	Coomassie stain.....	115
7.2.3.11.2	Silver stain	115
7.2.3.12	Western Blotting.....	115
7.2.4	Mass spectrometry	115
7.2.4.1	Protein extraction	115
7.2.5	RNA Work	116
7.2.5.1	RNA extraction	116
7.2.5.2	DNase digestion and RNA precipitation	116
7.2.5.3	RNA biotinylation.....	117
7.2.5.4	Northern blotting and Detection of RNAs	117
7.2.5.4.1	Methylen Blue	117
7.2.5.4.2	Radioactive	117
7.2.5.4.3	4TU labelled RNA.....	117
7.2.5.5	Fluorescent Primer extension	117
7.2.5.6	RNA Foot-printing	118
7.2.5.6.1	CMCT	118
7.2.5.6.2	DMS	119
7.2.5.6.3	SHAPE	119
7.2.5.7	RNA Affinity purification	119
7.2.5.7.1	MS2 Aptamer purification	119
7.2.5.7.2	Biotinylated RNA purification	120
7.2.6	Miscellaneous.....	120
7.2.6.1	TECAN-Reader.....	120
7.3	Statistics.....	120
8	List of Figures	121

9	<i>List of Tables</i>	123
10	<i>Supplements</i>	123
10.1	Identifiers for ArCOGs:	123
10.2	Supplementary Figures	125
11	<i>References</i>	137
12	<i>Publications</i>	164
13	<i>Danksagung</i>	165

1 ABSTRACT

Classically, life is divided into three phylogenetically interconnected groups of organisms, the archaea, bacteria and eukarya. However, they all share a central and universally conserved molecular component of the cell, a ribonucleoprotein complex known as the ribosome. The assembly of this molecular machine is an orchestration of RNA folding/modification events, hierarchical and cooperative incorporation of ribosomal proteins, and the association, dissociation, and interplay of various ribosomal biogenesis factors. Remarkably, this process has become increasingly complex over the course of evolution and has been studied best in bacterial and eukaryotic model organisms. In contrast, the *in vivo* archaeal ribosome biogenesis pathway(s) lack this detailed insight. Previous *in vitro* and *in silico* studies suggested bacterial as well as eukaryotic-like aspects of archaeal ribosome biogenesis. In this work, I have functionally characterized the archaeal homologue of the almost universally conserved ribosomal RNA dimethyltransferase KsgA/Dim1 *in vivo*.

We could show that this ribosome biogenesis factor is dispensable in the Euryarchaeon *Haloferox volcanii* and *Pyrococcus furiosus*, as well as in the Crenarchaeon *Sulfolobus acidocaldarius*. The loss of this ribosome biogenesis factor in *H. volcanii* is associated to a decreased cellular fitness and stress adaptation, as well as a differential translational landscape which may correlate with altered translation initiation. Moreover, in this and phylogenetically related organism we observed an unusual heterogeneous/ hypomethylated KsgA/Dim1 dependent methylation pattern. Using phylogenetic-based comparison and genetic analysis, we show that the molecular determinant of this unusual methylation status is based on a single nucleotide exchange within the KsgA/Dim1 targeted rRNA substrate. The structural consequences of this variability could be verified with chemical RNA foot-printing and support a model where KsgA/Dim1-dependent modification disrupts local intramolecular interaction and promotes inter-molecular interaction of 16S/18S rRNA helices. Based on these observations and *in vitro* reconstitution experiments, this study suggests that release competence of KsgA from the 30S subunit is not dependent on full methylation completion but rather on cooperative local and distant rRNA conformational changes controlled by methylation-induced (intra-molecular) destabilization of the KsgA/Dim1 substrate. Finally, and in addition to this functional analysis, I have implemented and applied chemical RNA foot-printing and 4TU pulse (chase) labelling protocol for *H. volcanii* and *S. acidocaldarius*.

Together, this work contributes to a better understanding of archaeal ribosome biogenesis, KsgA/Dim1 biology, and also expands the archaeal tool-box to study RNA metabolism.

2 ZUSAMMENFASSUNG

Die klassischen Lebewesen sind in drei phylogenetisch verbundene organismische Gruppen aufgeteilt, den Archaeen, Bakterien und Eukaryonten. Was alle drei miteinander verbindet ist eine Zentrale konservierte molekulare Maschine der Zelle, ein ribonuklearer Protein-Komplex, besser bekannt als das Ribosom. Die Assemblierung einer solchen molekularen Maschine ist eine Orchestrierung von RNA Faltung/Modifizierung, dem hierarchischen und kooperativen Einbau ribosomaler Proteine, sowie die Assoziierung, Dissoziierung und das Zusammenspiel vieler ribosomaler Biogenesefaktoren. Bemerkenswerterweise ist dieser Prozess im Verlauf der Evolution zunehmend komplexer geworden und am besten in Bakterien und Eukaryonten untersucht. Im Vergleich zu Bakterien und Eukaryonten, fehlen detaillierte *in vivo* Studien zur archaeellen Ribosomenbiogenese. Frühere, *in vitro* und *in silico* Untersuchungen wiesen auf sowohl bakterielle als auch eukaryontische Merkmale der archaeellen Ribosomenbiogenese hin. In dieser Arbeit präsentiere ich eine funktionelle Charakterisierung des archaeellen Homologes, der fast universell konservierten ribosomalen RNA Methyltransferase KsgA/Dim1 *in vivo*.

Wir konnten zeigen, dass dieser Biogenesefaktor in den Euryarchaeota *Haloferax volcanii* und *Pyrococcus furiosus*, sowie im Crenarchaeoten *Sulfolobus acidocaldarius* nicht essenziell sind. Der Verlust dieses Faktors führt in *H. volcanii* zu reduzierter zellulärer Fitness und Stresstoleranz sowie einer differenziellen Proteinexpression, die vermutlich mit einer veränderten Translations-Initiation assoziiert ist. Zusätzlich haben wir in diesem und anderen verwandten Organismen einen unerwarteten, heterogenen bzw. hypomethylierten, durch KsgA/Dim1 induzierten, Methylierungszustand entdeckt. Wir konnten anhand von phylogenetischen Vergleichen und genetischen Analysen den molekularen Ursprung dieses unerwarteten Methylierungszustandes, auf einen einzelnen Basenaustausch im rRNA Substrat von KsgA/Dim1 zurückführen. Die strukturellen Konsequenzen dieser Veränderung konnten wir mithilfe von „chemical RNA foot-printing“ nachweisen. Diese bestärken ein Modell, in dem die KsgA/Dim1 vermittelte RNA Modifizierung lokale intramolekulare Interaktionen destabilisiert und dadurch intermolekulare Interaktionen zwischen Helices der 16S/18S rRNA herstellt. Diese Beobachtungen, sowie *in vitro* Rekonstitutionsexperimente deuten darauf hin, dass die Dissoziationskompetenz von KsgA/Dim1 von der 30S Untereinheit nicht von der vollen Methylierung abhängig ist, sondern eher von kooperativen, lokalen und entfernten strukturellen Veränderungen, die aus der methylierungsinduzierten Destabilisierung des Substrats resultieren. Zu guter Letzt und zusätzlich zu der funktionellen Analyse, habe ich „chemical RNA foot-printing“ und „4TU-Pulse (chase) labelling“ Protokolle für *H. volcanii* und *S. acidocaldarius* etabliert.

Zusammenfassend trägt diese Arbeit zu einem besseren Verständnis der archaeellen Ribosomenbiogenese und der Beschreibung von KsgA/Dim1 bei, sowie eine Erweiterung des Werkzeugkastens zur Analyse des archaeellen RNA Metabolismus.

3 INTRODUCTION

3.1 A brief archaeal history

Given the vast diversity of organisms, discovering a new one has always been a great success for scientists. However, the classification and how a newly discovered species fits in with the already discovered organisms, has been, and still is, a challenging and highly debated endeavor (Balter, 2004; Da Cunha et al., 2018; Laurentii Salvii. and Linné, 1753; MacLeod et al., 2019). Especially proposing a new kingdom, the Archaeobacteria (now archaea) (Woese and Fox, 1977), sparked controversy back in the earlier times of modern microbiology (Pühler et al., 1989; Zillig, 1991; and reviewed in Albers et al., 2013). This spark however, led to a new age in modern microbiology and classification using the 16S/18S ribosomal RNA (rRNA) as a phylogenetic marker (Fox et al., 1977; reviewed in Olsen et al., 1994 and; Woese, 1994) and to several advances in many fields of research and industry (Breithaupt, 2001; Chien et al., 1976; Jenney Jr and Adams, 2008; Synowiecki et al., 2006). At the end of the 20th century Carl Woese proposed the three domain of life model based on sequence homology analysis of the 16S/18S rRNA (Woese et al., 1990). It established bacteria, eukaryotes and archaea as independent monophyletic groups. Novel large scale homology analysis of RNA polymerase genes have renewed support to this model (MacLeod et al., 2019) and is shown in Figure 3.1.

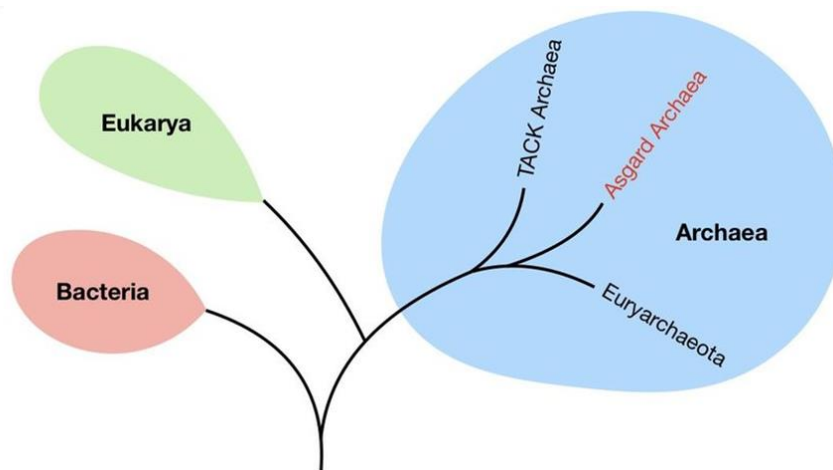


Figure 3.1 **Three Domains of life tree.**
Phylogenetic analysis of RNA Polymerase genes, reproduced from MacLeod et al., 2019.

However, this model and especially the placement of the eukaryotic origin have been a matter of debate early on. Based on structural comparison of bacterial, archaeal, and eukaryotic ribosomes, the Eocyte hypothesis proposed that eukaryotes emerged from within archaea (Lake et al., 1984). Especially, the recent renaissance of archaeal phylogeny, on the basis of sequence analysis from metagenomes, added support for the Eocyte hypothesis and further challenged the placement of eukaryotes in the tree of life (Dombrowski et al., 2019; Spang et al., 2015; Zaremba-Niedzwiedzka et al., 2017). Early metagenomic studies have placed eukaryotes next to the TACK superphylum

(Guy and Ettema, 2011), but with increasing numbers of metagenomes newer studies revealed a large, closer related group of deep sea sediment archaea, the Asgard archaea (Dombrowski et al., 2019; Zaremba-Niedzwiedzka et al., 2017). Within this group it is proposed that the eukaryotes arose as a sister group to the Asgard archaea, specifically the Heimdallarchaeota (see Figure 3.2) (Zaremba-Niedzwiedzka et al., 2017). If the two domain of life tree is correct, it puts the kingdom of eukaryotes and our own deep ancestry within archaea (Liu et al., 2018; López-García and Moreira, 2020). The additional data can be used to elucidate the origin of eukaryotes perhaps even by testing ideas about the origins of single constituents of eukaryotic cells. But in the end, additional genomic data will strengthen the correct model and it makes these somewhat overlooked organisms even more interesting to study. Independently of which tree is correct, at the base of either lies the **last universal common ancestor (LUCA)** (Theobald, 2010). The ability to discover and sequence unculturable novel organisms from remote habitats expands our knowledge of phylogeny and cellular diversity and will inevitably help to paint a clearer picture of LUCA.

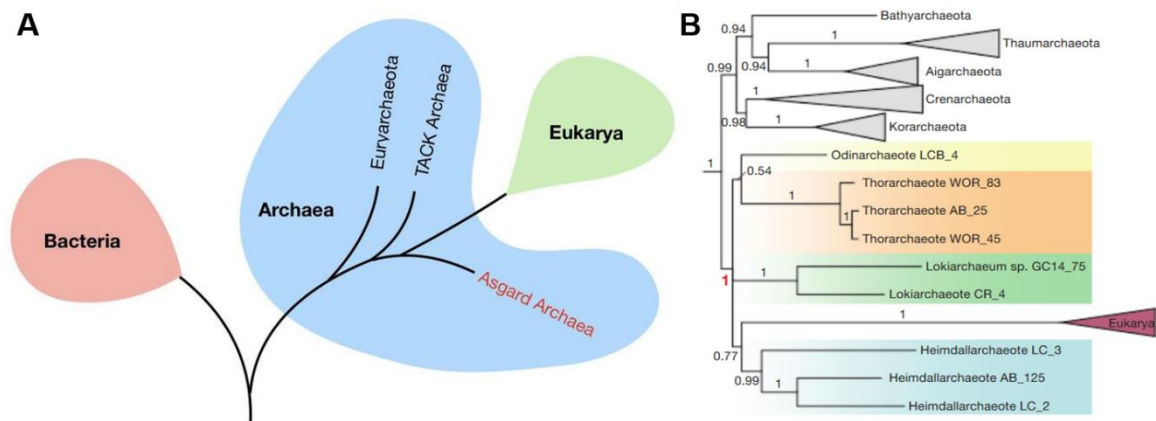


Figure 3.2 **Eukaryo-archaeal ancestry.**

[A] Phylogenetic overview based on conserved markers: rRNA and ribosomal proteins from MacLeod et al., 2019 **[B]** Detailed phylogenetic ancestry based on ribosomal proteins reveal Eukaryotes as a sister group to the Heimdallarchaeota. (Zaremba-Niedzwiedzka et al., 2017)

However, archaea are not only comprised of rare unculturable species in inaccessible habitats. It is believed that roughly 20% of the marine biomass is comprised of archaea (DeLong and Pace, 2001). Furthermore, the increasing focus on (gut-) microbiomes has revealed an omnipresence of archaea in multicellular eukaryotic hosts (Koskinen et al., 2017; Moissl-Eichinger et al., 2018). Especially, anaerobic methanogens are a crucial part of our gut microbiome (Nkamga et al., 2017). Contrary, to bacteria and eukarya, pathogenic archaea are virtually nonexistent (Gill and Brinkman, 2011) with some proposed exceptions (Vierbuchen et al., 2017). With growing relevance and popularity, archaea now have found their way into laboratories around the world and are increasingly feasible to work with.

3.1.1 From untamed to genetically tractable

The first thing that comes to mind when talking about archaea are the diverse environments they can inhabit (Merino et al., 2019). Basically, no niche no matter how extreme, is left uninhabited. Ranging from high pressure to high temperature, down to freezing temperatures (Mancinelli et al., 2004), very high and low pH and also extreme salinity (Bowers and Wiegel, 2011; Rampelotto, 2013). A closer look at the phylogeny of archaea reveals that the class and family name are generally a good indicator to the environmental conditions they thrive in (see Figure 3.3). *Pyrococcus furiosus* enjoys temperatures of 100 °C (Fiala and Stetter, 1986), *Thermococcus barophilus* lives at very high pressure (Marteinsson et al., 1999), *Sulfolobus acidocaldarius* is able to survive in acidic conditions (Brock et al., 1972), *Natronorubrum bangense* is located on the other side of the pH scale accompanied by a high salinity tolerance (Xu et al., 1999). However, not all extremophiles are reliant on extreme conditions, some also are able to grow in “normal” conditions but tolerate extreme variances in for example temperature and salt (Moissl-Eichinger et al., 2012).

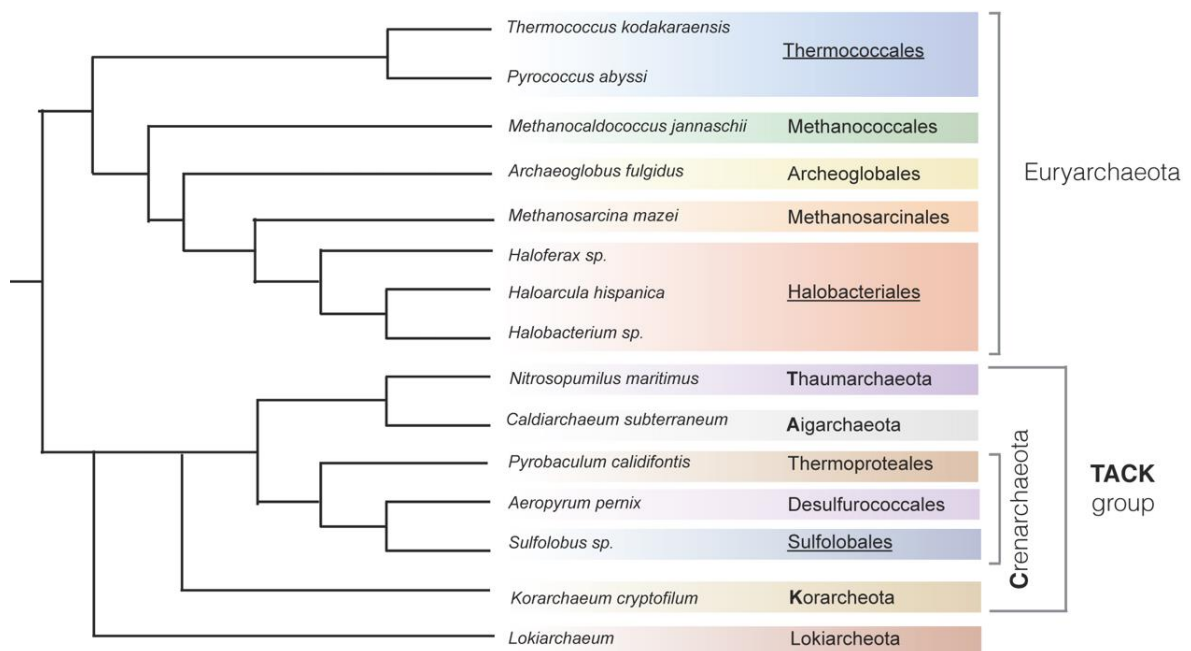


Figure 3.3 Archaeal groups with representative species. (Ausiannikava and Allers, 2017)

Implementing these organisms into laboratories means adapting culture conditions (Imachi et al., 2020; Sun et al., 2020). This can involve using pressure flasks, high temperature incubators, creating pH adjusted media or large amounts of salt. Depending on the facility, using anaerobic organisms might be impossible. Luckily, pioneers have established cultivation techniques and genetic tools for a selected range of archaea (Allers et al., 2004; Hileman and Santangelo, 2012; Huber et al., 2002; Kreuzer et al., 2013; Waegel et al., 2010; Wagner et al., 2012). Among the genetically tractable organisms, the majority is found in the phylum of Euryarchaeota while the Sulfolobales are the only genetically tractable Order of the Crenarchaeota (reviewed in Peng et al., 2017). In our lab we have

established to work with both, *Haloferax volcanii* (Euryarchaeota) and *Sulfolobus acidocaldarius* (Sulfolobales/TACK) (Figure 3.4).

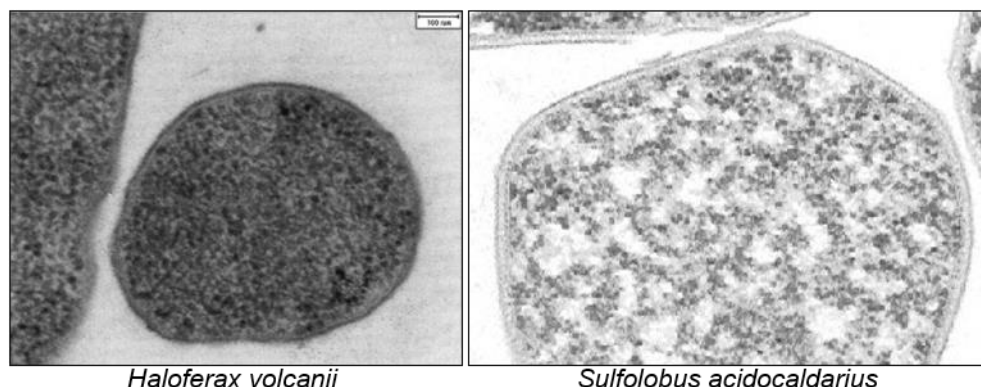


Figure 3.4 **Electron micrographs of *Haloferax volcanii* and *Sulfolobus acidocaldarius*.** (Hölzle et al., 2008) and (alchetron.com/Sulfolobus), respectively

3.1.2 *Haloferax volcanii*

The formerly called *Halobacterium volcanii* (*Hv*) was named after Benjamin Elazari Volcani who was the first to discover microorganisms in the Dead Sea (Elazari-Volcani, 1943). As a member of the Euryarchaeota phylum, it inhabits the most saline environments on earth and lives an aerobic, mesophilic and heterotrophic lifestyle. The cells display pleiomorphism depending on their growth phase (Duggin et al., 2015) and maintain an osmotic balance with the surrounding medium by accumulating salt in the cytoplasm (Gunde-Cimerman et al., 2018; Oren, 2008). They show a high tolerance for varying salt concentrations, ranging from 1.5 to ~5 M NaCl, with an optimum of 1.5 - 2.5 M NaCl and 75 mM MgCl₂ at 45 °C (Boone, 2001, pp. 1089–1105; Oren, 2008; Oren et al., 2009). Based on its high radiation and salt tolerance, this organism was curated for astrobiology as a model organism to test on Mars by researchers at University of California, Berkeley (DasSarma, 2006).

The genome of the strain type “DS2” contains a polyploid genome ranging from 15 to 30 copies which was fully sequenced in 2010 (Breuert et al., 2006; Hartman et al., 2010). The polyploidy changes with growth phase, exponential cells have a higher copy number than stationary cells (Breuert et al., 2006). The genome is composed of a circular chromosome (2.8 Mb) and four plasmids pHV1 (85kb), pHV2 (6.3 kb), pHV3 (437 kb) and pHV4 (635 kb) with a total of about 4100 predicted genes on 4 Mb with a GC content of 65 %. This high GC content is a potential mechanism to avoid UV induced thymidine dimers (Hartman et al., 2010). The overall amino acid composition is adapted to the hypersaline cytoplasm by favoring acidic amino acids (Aspartate/Glutamate) and thus lowering the isoelectric point to an average of 5.2 (Hartman et al., 2010).

Haloferax volcanii has been a model organism for roughly 30 years and the genetic toolbox has steadily expanded. The introduction of proto-/auxotrophic markers has opened the organisms to easy

shuffle plasmid transformation that enable overexpression systems as well as gene knock outs (Allers et al., 2010; Cline et al., 1989; Lam and Doolittle, 1989; Leigh et al., 2011; Sowers and Schreier, 1999). Recent advances in CRISPR technology have added the possibility to knock down (essential) genes (Stachler and Marchfelder, 2016).

3.1.3 *Sulfolobus acidocaldarius*

The second species used in this work is *Sulfolobus acidocaldarius* (*Saci*). It is part of the only genetically tractable group (Sulfolobales) in the phylum of Crenarchaeota (Peng et al., 2017). It was first isolated by Thomas Brock in 1972 in the hot springs of Yellowstone National Park (Brock et al., 1972). It is cultured aerobically at 70 – 85 °C with a pH of 2 – 3, underlining its thermo- and acidophile properties.

The strain used in this study, MW001, also has a fully sequenced genome available (Chen et al., 2005). The circular genome consists of 2.3 Mb with a low GC content of only 37 % and a predicted gene count of 2,292.

Similarly to *H. volcanii*, the introduction of proto-/auxotrophic markers enabled easy gene deletion as well as plasmid-based gene expression (Wagner et al., 2012).

3.2 The Ribosome

While ribosome research predates the discovery of archaea, the 16S/18S sequence homology analysis has created a historical link between the two fields of research (Fox et al., 1977; Palade, 1955). This history, the conserved biological relevance of the ribosome (translation) and being an archetype **ribonucleoprotein particle (RNP)** is one of the many fundamental reasons to study the biogenesis of this complex machine in detail. The assembly of such a large and essential macromolecule is subjected to heavy evolutionary pressure, where small mistakes can have grave consequences for the cell, e.g. ribosomopathies (Nakhoul et al., 2014).

The conserved function of translation is also reflected in the architecture of the ribosome. All three kingdoms of life have a large (**LSU**) and a small (**SSU**) ribosomal **subunit** that join to form the mature ribosome (see Figure 3.5) (Fox, 2010). These ribosomal subunits consist of rRNA and ribosomal proteins. The rRNA is not only the scaffold to which the ribosomal proteins bind but also serves as the catalyst for peptide bond formation (Alberts, 2002, chap. 6; Moore, 2003). The SSU is made up of 5 subs-structures (see Figure 3.6A-D): ‘head’, ‘body’, ‘platform’, ‘beak’ and ‘shoulder’ (Barandun et al., 2017). At the interface sits the decoding center, which is responsible for codon/anti-codon recognition, as well as the base of the three tRNA binding sites A, P and E (Aminoacyl, Peptidyl, and Exit) (Alberts, 2002, chap. 6). A tunnel between the head and the SSU shoulder conducts the mRNA through the translating ribosome to exit at the head and the platform (Yusupova et al., 2001).

The sub-structures of the LSU (see Figure 3.6E-H) are the ‘central protuberance’, ‘L1-stalk’ and the ‘L7/L12-stalk’ (‘P-stalk’ in eukaryotes) (Klinge et al., 2011). The complementary tRNA binding pockets are located at the interface of the LSU (opposing the SSU). Here the peptide bonds are formed in the peptidyl transferase center and nascent peptides exit the ribosome through the peptide exit tunnel (Voss et al., 2006). These sites are essential for proper translation and are found in all ribosomes.

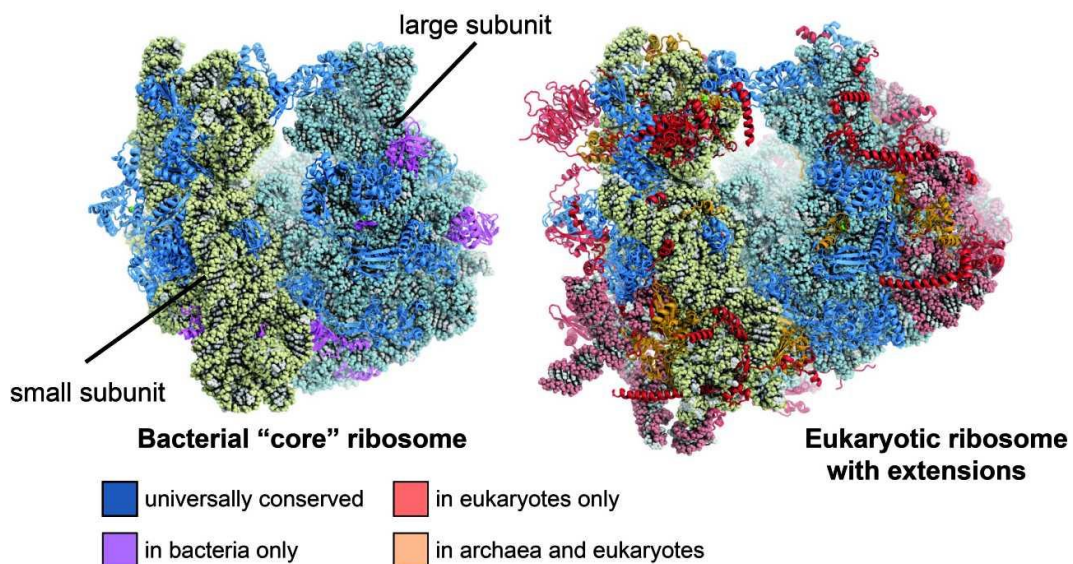


Figure 3.5 **Structural comparison of the bacterial and Eukaryotic ribosome.** (“The Ban Lab ETH Zurich,” 2020)

However, when comparing the ribosomes from all the kingdoms, the differences in size and mass were visible early on (Lake et al., 1984). Not only the nomenclature for the individual subunits (the sedimentation coefficient “Svedberg”, 30S : 50S and 40S : 60S) already indicates a different size and mass, but when isolating the individual components (RNA and protein) the differences become apparent (see Table 3.1).

In bacteria and archaea, the rRNA shows a sedimentation coefficient of 16S for the small and 23S and 5S for the large subunit. The eukaryotic ribosomes have a higher variance in size, the SSU consists of 18S rRNA, and the large subunits contains 5S, 5.8S and 25S (28S in higher eukaryotes) rRNA. In archaea and eukarya the rRNA shows varying amounts and sizes of rRNA expansion segments which are not present in bacteria (Armache et al., 2013; Fujii et al., 2018; Greber et al., 2012; Klinge et al., 2011; Penev et al., 2019; Rabl et al., 2011).

al., 2010), it is rarer in Euryarchaeota with the exception of *Haloarchaea* (Benelli et al., 2017; Kramer et al., 2014). Eukaryotic initiation, on the other hand, mostly starts by recognizing the 5'-CAP structure of the mRNA following scanning until the start codon is reached (Hinnebusch, 2014). In regard to initiation factor usage, archaeal ribosomes use a set of 5 factors (aIF1, aIF1A, aIF2, aIF6, aIF5B) of which homologues are found in eukarya (3) or bacteria (2), while the latter is universally conserved (Benelli et al., 2016). The usage of proprietary translation initiation factors is very likely a result from the evolution of ribosomal composition of each domain or organism, i.e. different ribosomal proteins provide different interaction interfaces (Melnikov et al., 2012).

Interestingly bacteria does not share any ribosomal constituents exclusively with archaea or eukarya, yet some r-proteins are exclusively shared among archaea and eukarya, emphasizing the common ancestry as discussed earlier (Liu et al., 2018; Zaremba-Niedzwiedzka et al., 2017).

With the increasing number of structural components, the assembly process becomes increasingly complex and has occupied scientists for the last 60 years.

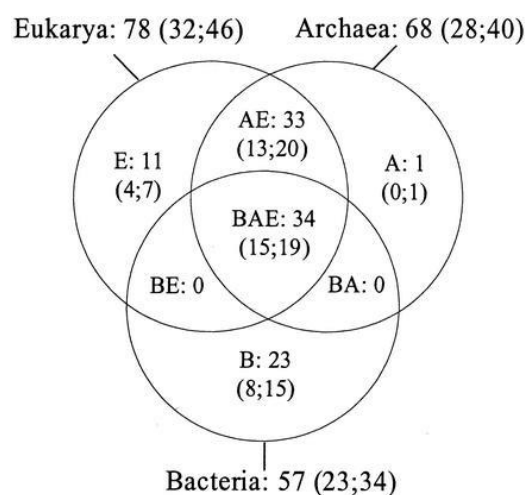


Figure 3.7 **Venn diagram of shared ribosomal proteins of all three kingdoms.** Number in brackets: SSU;LSU (Lecompte et al., 2002)

3.2.1 Ribosome Biogenesis

Ribosome biogenesis is one of the most energy demanding processes in a cell and thus must be highly efficient and optimized (Warner, 1999). The flawless orchestration of a complex event such as ribosome assembly involves numerous hierarchical steps and is aided by several additional biogenesis factors along the way. To disentangle the steps and identify the factors involved, a solid genetic system and applicable biochemistry are of great value. Both and more can be found in the two model organisms *Saccharomyces cerevisiae* and *Escherichia coli*, which helped elucidate this complex matter, that is ribosome biogenesis. From a historical standpoint, bacterial ribosome biogenesis was studied first and thus will be discussed first (Traub and Nomura, 1968).

3.2.1.1 Ribosome biogenesis in *Escherichia coli*

Back in 1968 a major milestone in the ribosome biogenesis field was set by Traub and Nomura, with the complete assembly of an active 30S subunit *in vitro* from free 16S rRNA and purified ribosomal proteins (Traub and Nomura, 1968). The complementary milestone was achieved a few years later by Nierhaus and Dohme with the *in vitro* assembly of the 50S subunit (Nierhaus and Dohme, 1974). Both painted the picture of a hierarchical assembly pathway, illustrated in the famous Nomura and Nierhaus maps (see Figure 3.8) (Held et al., 1974a; Herold and Nierhaus, 1987; Mizushima and Nomura, 1970; Röhl and Nierhaus, 1982). This hierarchy indicated that the assembly process follows an encoded blueprint in the rRNA and the r-proteins, revolving around assembly check points that facilitate progression (Nierhaus, 1991, 1980).

To produce a mature ribosome *in vivo* with correctly cleaved, folded and modified rRNA as well as the correct binding of all the ribosomal proteins, indicates that the cell has evolved a system that catalyzes this process.

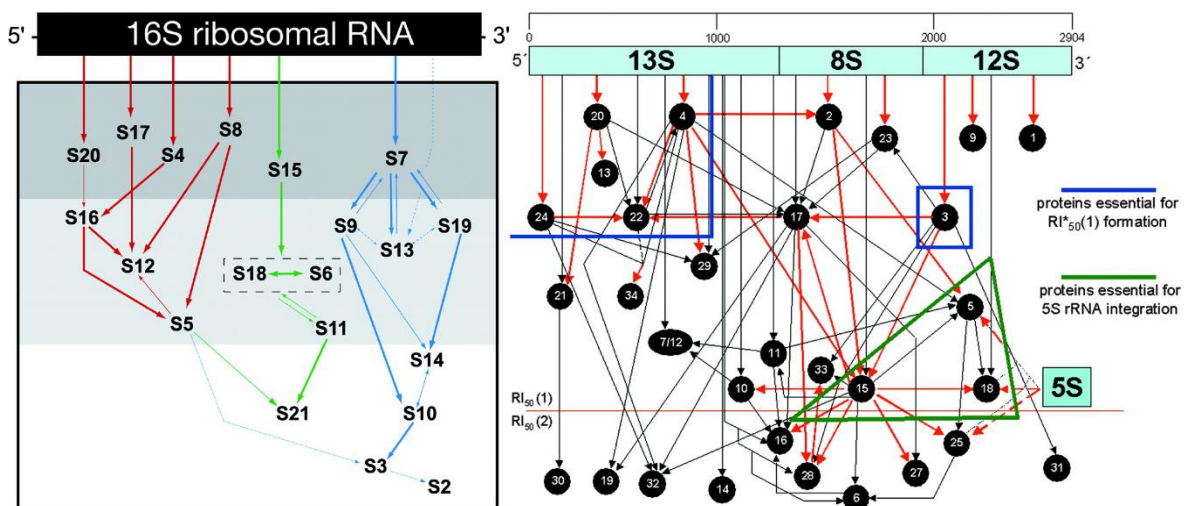


Figure 3.8 **Assembly maps of the 30S and 50S subunits, reinterpreted from Nomura and Nierhaus.**

Left panel: “Assembly map of the 30S subunit [...]. The 16S rRNA is represented by a rectangle, and the binding order of the ribosomal proteins is shown. The dark gray area indicates the primary binding proteins, the light gray area indicates the secondary binding proteins, and the white area indicates the tertiary binding proteins. The thick, thin, and dashed arrows show strong, weak, and very weak interactions between the proteins, respectively. Proteins S6 and S18 bind as a complex and are therefore enclosed in a dashed box. Red arrows indicate the assembly of the body, green arrows indicate the platform, and blue arrows indicate the head.” **Right panel:** “Assembly map of the 50S subunit. The 23S rRNA is represented by a rectangle with its main fragments and the binding order of the ribosomal proteins and 5S rRNA. The red arrows indicate strong dependence for binding, and the black arrows indicate weaker dependence. The blue line encloses proteins essential for R1*50(1) complex formation, and the green triangle encloses proteins essential for 5S rRNA integration. The horizontal orange line shows the division between the R150(1) and R150(2) proteins.” (Reproduced from Kaczanowska and Rydén-Aulin, 2007)

In *E. coli* the rRNA is transcribed as one primary transcript by the RNA polymerase and is processed by at least 9 nucleases (see Figure 3.9). The first cleavage by RNase III yields the precursor- 17S rRNA, pre-23S rRNA and 9S rRNA. The 17S rRNA is then further cleaved by RNase G, AM, E, R PH, II, PNPase and YbeY to mature 16S rRNA (Jain, 2020; Zhongwei Li et al., 1999; Sulthana and Deutscher, 2013; Vercruyssen et al., 2016; Young and Steitz, 1978). The 23S precursor is further processed by RNase III, T and AM (Jain, 2020; Z. Li et al., 1999; Song et al., 2011). The 9S particle

is cleaved by RNase E, T, III and AM (Jain, 2020; Li and Deutscher, 1995; Misra and Apirion, 1979; Roy et al., 1983).

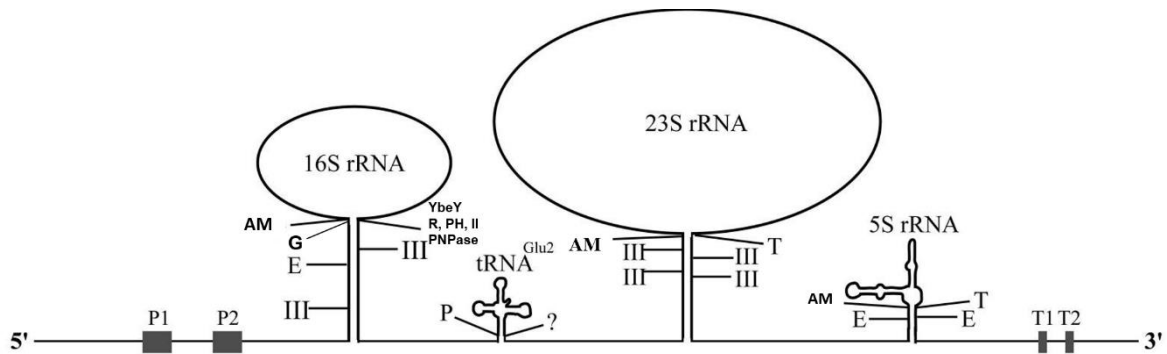


Figure 3.9 **Schematic drawing of the *rrnB* operon.**

Nucleolytic processing of the *rrnB* primary transcript. The rRNA and tRNA species, promoters P1 and P2, and terminators T1 and T2 are indicated, as well as the processing sites of RNase III (III), RNase G (G), RNase AM (AM), RNase E (E), RNase P (P), RNase T (T), RNase R (R), RNase PH (PH), RNase II (II), PNPase, YbeY. Modified from Kaczanowska and Rydén-Aulin, 2007

While the rRNA is being transcribed, cleaved, and is folding, early ribosomal proteins bind in a co-transcriptional manner and thereby chaperone the rRNA for subsequent binders (Duss et al., 2019; Rodgers and Woodson, 2019). The early *in vitro* experiments of Nomura and Nierhaus classified the ribosomal proteins based on their binding dependency (“primary, secondary and tertiary” binders) (Mizushima and Nomura, 1970; Röhl and Nierhaus, 1982; and reviewed in Nierhaus and Wilson, 2004, chap. 3). This classification was later confirmed *in vivo* (Davis et al., 2016; Mulder et al., 2010).

To avoid pitfalls, such as premature or non-native r-protein binding, RNA misfolding or other errors, assembly factors (AF) aid to prevent these. These ribosome biogenesis factors (AFs) include GTPases (Britton, 2009), ATP-dependent RNA helicases (Fuller-Pace et al., 1993), rRNA modification enzymes (Lesnyak et al., 2006) and other maturation factors (Davis and Williamson, 2017).

Most of these assembly factors are very low abundant and have a very short “intermezzo” with the maturing ribosome (Li et al., 2014; Thurlow et al., 2016). This, in combination with a very low affinity to mature ribosomes increases specificity and rapid transition from one immature ribosome to the next. Interestingly, many of these factors are not essential and their absence may only cause assembly defects under stress conditions, indicating alternative pathways (Bubunenko et al., 2006; Gupta and Culver, 2014; Talkington et al., 2005). Traceable interactions are left behind in the mature ribosome by RNA modifying enzymes. The 16S rRNA is modified 11 times (1 pseudouridylation and 10 methylations) and the 23S rRNA undergoes 25 modifications (1 unknown, 14 methylations, 9 pseudouridylation, and 1 methylated pseudouridylation) (Chow et al., 2007; Decatur and Fournier, 2002; Kaczanowska and Rydén-Aulin, 2007).

For bacteria in general it needs to be noted, that there are some processing differences between gram negative and positive species (Britton et al., 2007; O'Farrell and Rife, 2012; Uicker et al., 2006). However, these differences are marginal when comparing bacterial and eukaryotic ribosome biogenesis.

3.2.1.2 Ribosome Biogenesis in *Saccharomyces cerevisiae*

Cell compartmentalization in eukaryotes is one of the major differences to bacteria. As a consequence, eukaryotic ribosomes must travel from the nucleolus through the nucleoplasm, exit the nuclear membrane through the nucleopore to reach the cytoplasm, whilst being correctly assembled. The highly complex interplay of biogenesis factors during the assembly is reviewed and updated regularly (Henras et al., 2015; Klinge and Woolford, 2019; Konikkat and Woolford, 2017; Thomson et al., 2013; Tschochner and Hurt, 2003; Woolford and Baserga, 2013) and a less detailed summary of *S. cerevisiae* ribosome biogenesis (unless stated otherwise) will be given here.

The encoding information for the rRNA is stored in 150-200 copies on the rDNA loci on chromosome 12, which concentrate in a sub-compartment of the nucleus, the nucleolus. The RNA Polymerase I transcribes the polycistronic 35S precursor rRNA encoding for the 18S, 5.8S, 25S rRNA, while the RNA polymerase III transcribes the 5S rRNA in the opposite direction (see Figure 3.10). Each rRNA is separated by Internal and/or flanked by External transcribed spacers (ITS/ETS) which are then further processed by (in part co-transcriptional) endo- and exonucleolytic cleavages (Kos and Tollervey, 2010; Venema and Tollervey, 1995).

The processing of this large precursor (defined as the 90S pre-ribosome (Trapman et al., 1975)) is initiated by cleavage at the 3' end (Kufel et al., 1999), followed by two consecutive cleavage steps in the 5' ETS (Beltrame et al., 1994; Beltrame and Tollervey, 1992) before the particle is separated into the precursors for the small (20S) and large subunit (27SA₂) (Kos and Tollervey, 2010), the 43S- and 66S pre-ribosome respectively (see Figure 3.11 and Figure 3.12). After that, the small subunit has only one remaining processing step, while the large subunit requires 5-6 additional steps, depending on the processing pathway (see Figure 3.11 and described later).

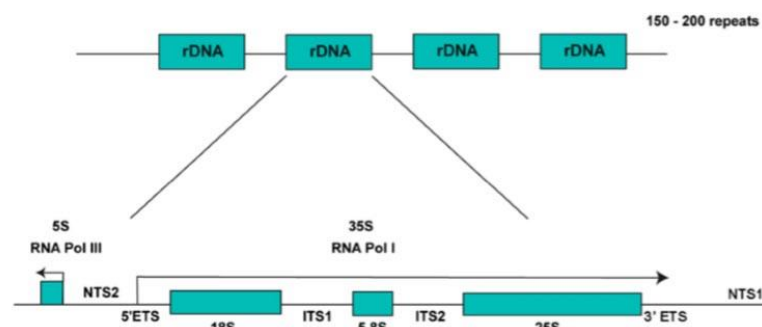


Figure 3.10 **Schematic representation of the yeast rDNA locus.**

ETS: External transcribed spacers, ITS: Internal transcribed spacers NTS: Non transcribed spacer (Woolford and Baserga, 2013)

The correct assembly, modification and folding of the rRNA in the ribosome requires at least 64 ribosomal proteins (Steffen et al., 2012) and all of them interact directly with the rRNA of the mature ribosome. The importance of these interaction surfaces is highlighted by the corresponding rRNA processing defects when certain r-proteins are absent (Ferreira-Cerca et al., 2005; Ohmayer et al., 2013; Pöll et al., 2009). In addition to the core ribosomal proteins, around 200 different assembly factors play a pivotal role in ribosome completion (Ebersberger et al., 2014; Thomson et al., 2013). Most of these proteins are usually conserved throughout eukaryotes and are commonly essential for cell viability (Woolford and Baserga, 2013, chap. 6). The broad spectrum of functional classes ranges from RNA-Helicases, ATPases, GTPases, kinases, phosphatases, diverse types of RNA-modification enzymes, snoRNPs (small nucleolar **RNPs**) and even to some homologs to r-proteins (reviewed in Woolford and Baserga, 2013 Table 3). These enzymes are in a strict interplay with each other and the maturing ribosomal subunit (Lamanna and Karbstein, 2009; Woolls et al., 2011). These assembly factors act as check points, placeholders, export factors and inhibitors of progression that tightly regulate the maturation by timely associating and dissociating from the maturing ribosome to avoid errors (e.g. Ferreira-Cerca et al., 2014; Lafontaine et al., 1995; Strunk et al., 2011; Turowski et al., 2014) (see Figure 3.12). Most assembly factors have already associated to the 90S pre-ribosome, and both the 60S and 40S precursor start out as very complex particles (Kornprobst et al., 2016). Both pathways experience extensive remodeling of rRNPs by the addition of ribosomal proteins and by the association and dissociation of assembly factors as they progress to maturity. This remodeling increases the binding strength of the r-proteins to its core (Ferreira-Cerca et al., 2007; Ohmayer et al., 2013). Additional structural rigidity is conferred by rRNA modification from RNA modifications enzymes and snoRNPs (Sloan et al., 2016). The latter produce the most prominent rRNA modifications, 2'-O-methylation (Kiss-László et al., 1996) of the ribose and pseudouridylation (Ψ) (Ni et al., 1997), ranging from 55 (yeast) – 100 (human) and 45 (y) – 100 (h) per ribosome respectively (Sloan et al., 2016).

The 43S pre-ribosome is believed to be processed in only three major steps (see Figure 3.12 lower pathway or in detail Figure S1). The first step is the binding of the tUTP/UTP-A complex to the 5'ETS of the 90S precursor particle, enabling the binding of the Mpp10 complex, UTP-B complex and U3 snoRNP (Cheng et al., 2017; Dragon et al., 2002; Gallagher et al., 2004; Pérez-Fernández et al., 2007; Sá-Moura et al., 2017). Early studies have termed the 90S, 5'ETS containing particle the SSU-processome (Grandi et al., 2002; Phipps et al., 2011), however newer studies show that the SSU processome contains only pre-18S rRNA, i.e. after A₂ cleavage (Chaker-Margot et al., 2017; Sun et al., 2017). Independent of the confusing terminology, all SSU processome particles contain the U3-snoRNP. The U3 is the major structural organizer for SSU and base pairs in both the 5' ETS and the pre-18S rRNA, conferring structural rigidity (Barandun et al., 2018; Beltrame and Tollervy, 1992; Dragon et al., 2002; Marmier-Gourrier et al., 2011). The UtpA- and UtpB-complexes act in cooperation with U3 as RNA chaperons (Hunziker et al., 2016). Aside from these three complexes,

numerous other assembly factors aid in the correct folding of all the structural subdomains (Phipps et al., 2011; Zhang et al., 2016). Once every subdomain of the SSU has been folded correctly, a large number of AFs dissociate and the pre-43S particle is ready for export through the nucleopore (Barandun et al., 2017). On the way to the nuclear pore complex the particle is further matured and additional AFs associate to the particle, facilitating export through the nuclear pore complex (Peña et al., 2017). The immature pre 40S subunit in the cytoplasm still lacks some r-proteins and translation initiation is inhibited by AFs occupying positions at the subunit interface (Strunk et al., 2011). These AFs further mature the 40S, while also being dependent on the correct maturation of the 60S subunit (García-Gómez et al., 2014; Gregory et al., 2019; Tamm et al., 2019). As a final “test-drive” before translation is initiated, the (late-AF-bound) pre-40S binds the mature 60S with the help of eIF5B forming the “80S-like” particle for functional proofreading. If everything is in order final maturation of the pre-40S takes place and the remaining AFs are released and translation can be initiated (Strunk et al., 2012a, 2012b).

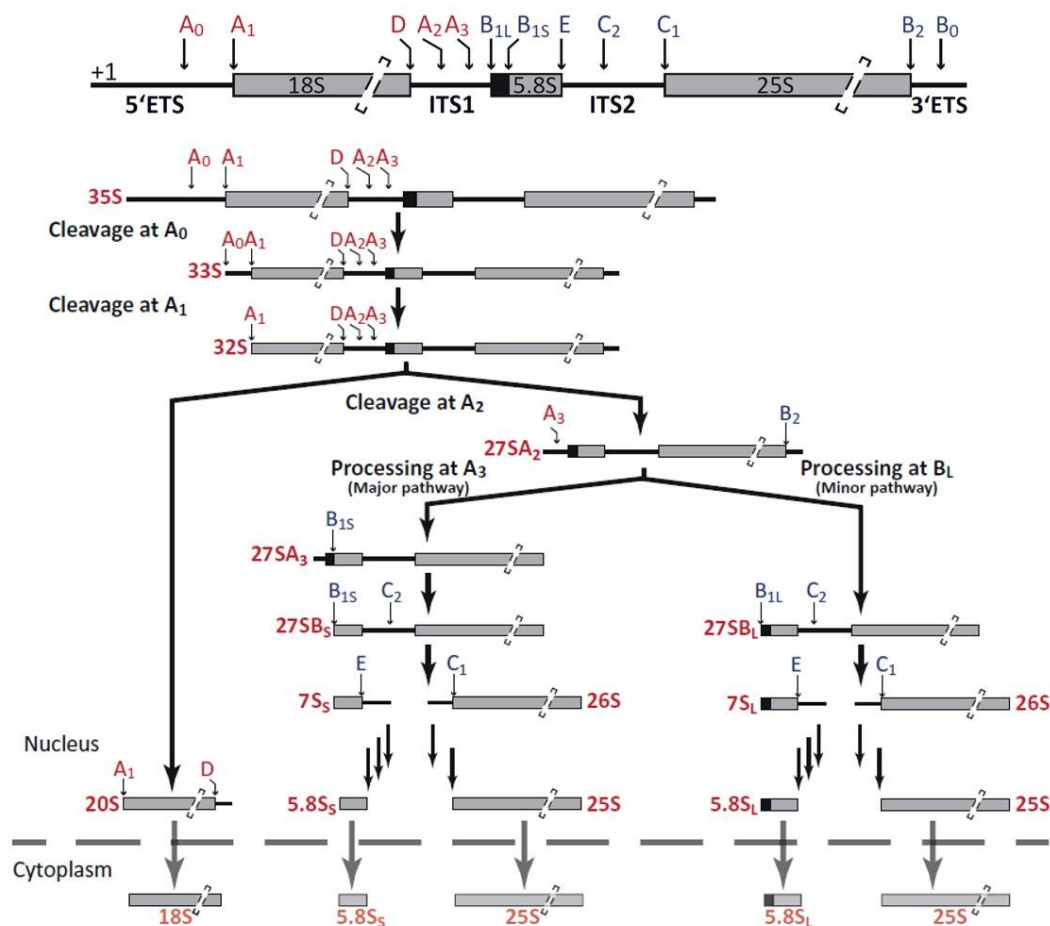


Figure 3.11 Schematic representation of the pre-rRNA processing pathways in *S. cerevisiae*.

Precursors are colored dark red, mature in light red. SSU cleavage sites are colored red, LSU cleavage sites are colored in blue. (Adapted from Braun et al., 2020)

The 66S precursor on the other hand undergoes a more gradual processing in all three compartments of the cell due to its higher complexity (see Figure 3.12 upper pathway or in detail Figure S 2)

(Harnpicharnchai et al., 2001; Milkereit et al., 2001; Nissan et al., 2002). In the beginning the nascent 35S pre-rRNA is being co-transcriptionally modified by snoRNPs while folding into a more compact structure (Kos and Tollervey, 2010; Sloan et al., 2016). Interestingly, cleavages in ITS1 and the 3' ETS are dependent on an sufficient distance or even termination of RNA Polymerase I (Allmang and Tollervey, 1998; Kos and Tollervey, 2010; Turowski and Tollervey, 2015), suggesting that most AFs and r-proteins cannot bind stably co-transcriptionally (Chaker-Margot and Klinge, 2019; Chen et al., 2017). The very early steps (before A₂ cleavage) have not been resolved as well as later steps and the very early binders (AFs and r-proteins) are thought to compact the structure and convey structural rearrangements that lead to a stable precursor RNP (de la Cruz et al., 2004; Rosado et al., 2007b, 2007a). The individual domains are then assembled, including the addition of the 5S rRNA, in a hierarchical manner with the help of several domain specific AFs (Hierlmeier et al., 2013; Kater et al., 2017; Sanghai et al., 2018; Zhang et al., 2007; Zhou et al., 2019). Before being exported to the cytoplasm, no longer required biogenesis factors are stripped from the precursor (Ho et al., 2000; Kressler et al., 2012, 2008; Stage-Zimmermann et al., 2000). The final steps are performed in the cytoplasm, including complete trimming of the 3' end of the 5.8S (Thomson and Tollervey, 2010) and removing the remaining assembly factors, that also inhibit binding to the 40S subunit (Gartmann et al., 2010; Sengupta et al., 2010). After the last r-proteins have been assembled and the catalytic centers are folded correctly, the large subunit is ready for translation and/or functional proofreading (Lebaron et al., 2012; Lo et al., 2010; Ma et al., 2017).

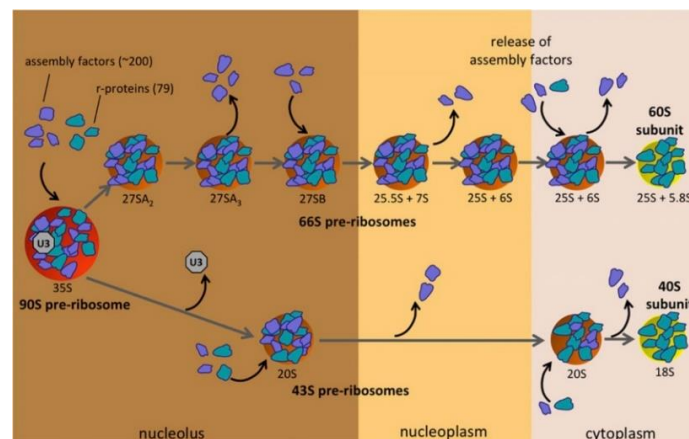


Figure 3.12 **Ribosome assembly and maturation pathway.**

Dark blue: Assembly factors, Light blue: r-proteins (Woolford and Baserga, 2013)

The “widespread” availability of Cryo-EM and the advances in electron detector quality in combination with the historically grown biochemical experience in yeast ribosome biogenesis have facilitated the visualization of precursor ribosomal particles and even intermediate processing steps of both the SSU (Heuer et al., 2017; Scaiola et al., 2018) and LSU (Kater et al., 2017; Sanghai et al., 2018; Zhou et al., 2019) as well as even earlier 90S (Cheng et al., 2017; Sun et al., 2017). With novel methods allowing for time resolved Cryo-EM (Kontziampasis et al., 2019), the temporal interplay of assembly factors can potentially be pushed even further (Kaledhonkar et al., 2019).

3.2.1.3 Ribosome biogenesis in archaea

Archaeal ribosome biogenesis is not as well documented as bacterial or eukaryotic ribosome biogenesis. Archaea, as bacteria, only have one RNA polymerase to transcribe the polycistronic rRNA precursor. The 16S and 23S pre-rRNA in Euryarchaeota are sometimes spaced by an internal tRNA^{Ala} and an external tRNA^{Cys} following the 5S rRNA at the 3' end (see Figure 3.13A). Many species from the TACK superphylum are missing these tRNAs and have externalized the 5S rRNA to another genomic region (Durovic and Dennis, 1994; Elkins et al., 2008; Hallam et al., 2006; Ikeda et al., 2017; Nunoura et al., 2011). In some rare cases each rRNA gene is transcribed individually (Ree and Zimmermann, 1990; Waters et al., 2003).

Another highly variable part of the rRNA composition is the amount and types of rRNA modifications that are present in archaea. Like eukaryotes, these modifications are mediated by sRNPs (no nucleolus in archaeal cells \neq eukaryotes: snoRNPs) and standalone RNA modification enzymes alike (Yip et al., 2013). The types of modification are similar to those found in bacteria and eukaryotes. However, the amount of modifications, ranges from very abundant in thermophilic- (*S. acidocaldarius*: >70) to very low in halophilic archaea (*H. volcanii*: ~13) (Dennis et al., 2015; Sas-Chen et al., 2020).

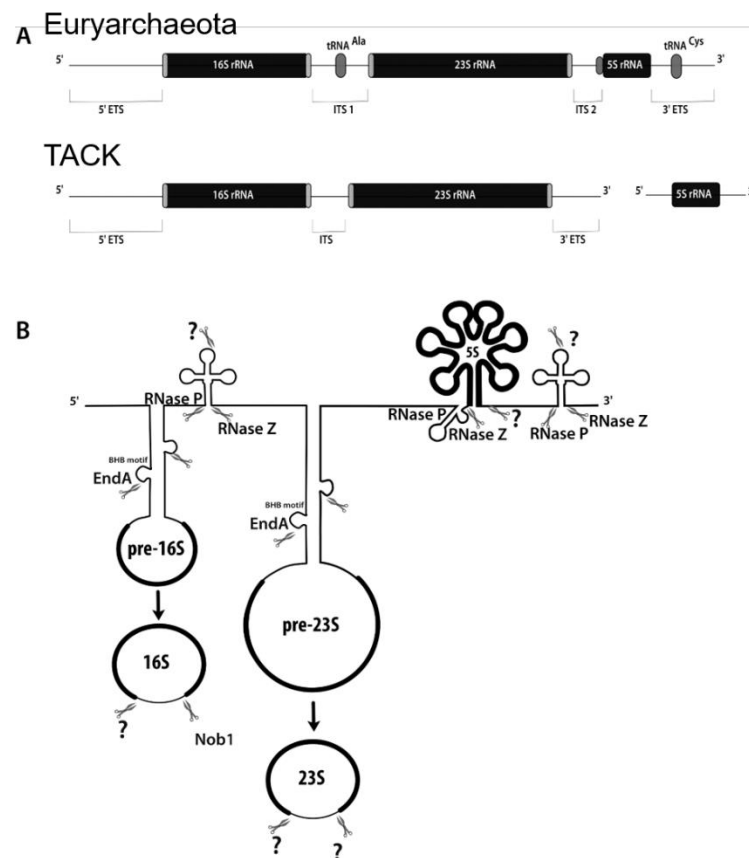


Figure 3.13 Polycistronic organization of two representative archaeal rDNA loci. [A] and processing scheme in *H. volcanii* [B]. (modified from Clouet-d'Orval et al., 2018)

The pre-rRNA is structured similarly to bacteria. Each rRNA forms a loop that is “sitting” on a dsRNA processing stem formed by flanking inverted repeat regions at the 5′-leader and 3′-trailer of the respective rRNA (see Figure 3.13B). The tRNA and 5S pre-rRNA on the polycistronic rRNA precursor are cleaved by the RNase Z and P (Frank and Pace, 1998; Vogel et al., 2005) and for the 5S pre-rRNA an additional unknown endonuclease. Contrary to bacteria there is no clear RNase III homolog present to perform the initial cuts at the two major rRNAs, this is supposedly replaced by the tRNA endonuclease *endA* that recognizes **bulge helix bulge (bhb)** structures that form in the processing stems (Clouet-d’Orval et al., 2018). The resulting nick is most likely ligated by another component of the tRNA splicing machinery, the tRNA ligase *rtcB* (Clouet-d’Orval et al., 2018; Ferreira-Cerca, 2017). This results in circular pre-rRNAs that could be detected in both Eury- and Crenarchaeota (Danan et al., 2012; Jüttner et al., 2020; Qi et al., 2020; Tang et al., 2002). The functional significance behind this circulation is unclear. It could be a strategy to prematurely bring the 3′ and 5′ ends into close proximity as observed in the mature structure, thus perhaps providing a stabilized structure that serves as a processing scaffold for (early) maturation events (Ferreira-Cerca, 2017). Moreover, it could be a method to avoid unspecific exonuclease degradation. The processing of this circular intermediate is not fully understood (see Figure 3.13B). However, gene orthology analysis (Ebersberger et al., 2014), initial *in vitro*, and some *in vivo* studies (Jia et al., 2010; Knüppel et al., 2018; Veith et al., 2012), show that the factors involved for further processing are rarely universally conserved and are either found in bacteria or eukarya.

3.2.2 Conservation of ribosome biogenesis

With the ribosome being a universal molecular machine, the similarities, and differences among the three kingdoms have evolved to essentially facilitate the production of the similar final product with varying degrees of complexity. While archaea and bacteria only possess one RNA Polymerase to transcribe all their RNA, eukaryotes have distributed their ribosomal component production to three polymerases. This is mirrored in the additional rRNA that is present in the final ribosome, as well as in the number of proteins that compose the final product (review Table 3.1 and references therein).

The production of snoRNAs (small nucleolar RNAs; hereafter sRNA/P) in eukaryotes by RNA Polymerase II and III (Darzacq et al., 2002; Ikegami and Lieb, 2013), has already been accomplished by the single RNA Polymerase in archaea (Gaspin et al., 2000; Thore et al., 2003), yet not in bacteria (Lafontaine and Tollervey, 1998). The two main classes of sRNA are C/D box and H/ACA box sRNAs, that methylate or pseudourinylate RNA respectively in a sequence specific manner (reviewed in Kiss, 2002). The base modification is conveyed by the proteins attached to the guide sRNA, i.e. the sRNP. The consequence being, that bacteria rely solely on rRNA modification by standalone enzymes while archaea and eukaryotes use both, standalone enzymes and sRNPs (Gaspin et al., 2000; Lafontaine and Tollervey, 1998). This enables these organisms to readily modify less structured rRNA at very early stages with RNA guided sRNPs and thereby aiding the structural

dynamics during assembly by chaperoning the folding rRNA (Dennis et al., 2015; Rozhdestvensky et al., 2003; Sloan et al., 2016; Yip et al., 2013). The usage of standalone modification enzymes in eukaryotes and possibly archaea mostly occur at the late stage of the assembly (Sloan et al., 2016). In bacteria this is also true for the small subunit, where the majority of modifications take place at the late stages of assembly (Siibak and Remme, 2010) in a 5' to 3' sequential order (Popova and Williamson, 2014). The large subunit, however is modified at early stages due to the majority of modifications being deeply buried in the active centers of the ribosome and thus inaccessible to bulky modifying enzymes once folding has progressed (Siibak and Remme, 2010).

The pre-rRNA is organized in a pseudo-circular manner before the initial cleavage in both, bacteria and archaea (compare Figure 3.9 and Figure 3.13). A related pseudo-circularization step is also suggested in eukaryotes by either self-base-pairing of the pre-18S rRNA with the spacers (Ferreira-Cerca, 2017; Veldman et al., 1981) and also mediated by the U3 snoRNP that base-pairs with the 5' leader sequence of the pre 18S-rRNA (Dutca et al., 2011; Henras et al., 2015). A similar system has also been proposed in bacteria, where the transcription elongation factors NusA and NusB hold the 5' end of the nascent transcript in place to facilitate the hairpin base-pairing required for RNase III cleavage (Bubunencko et al., 2013). Homologs of this factor are also found in archaea indicating a similar mechanism (Ferreira-Cerca, 2017). However, the enzymes that perform the initial cuts and many other ribosome biogenesis factors are not conserved across the three kingdoms.

This is especially true for the biogenesis of the large subunit. The additional solitary 5.8S rRNA strand that needs to be “captured” and incorporated into the folding LSU while using two alternative processing pathways (see above and Figure 3.11) and a comparably large number of assembly factors has made the biogenesis of this subunit in eukaryotes a lot more complex. While *E. coli* only requires the help of 4 Helicases, 2 GTPases, and ~4 protein/RNA chaperones to assemble the LSU, *S. cerevisiae*, requires the help of at least twice as many respective assembly factors (Hage and Tollervey, 2004). In archaea, little is known about how the circular pre-23S rRNA is processed, and from homology analysis very few putative LSU biogenesis factors could be identified (Ebersberger et al., 2014).

The similarities in the processing of the small subunit, especially in the late steps, appears to follow a more conserved functional pattern among the three kingdoms and will be discussed in more detail due to the focus of this work.

3.2.3 Comparative late small subunit biogenesis, an *E. coli* perspective

In *E. coli* the SSU pre-rRNA is relieved from the primary pre-rRNA transcript by the cleavage of RNase III, similar to the endA cleavage of the bhb motif in archaea (Xue, 2006). Whereas, in eukaryotes the cleavages at A₀, A₁ and A₂ by an unknown endonuclease and Utp24 are required to liberate the SSU precursor from the nascent transcript (Tomecki et al., 2015; Wells et al., 2016).

Unlike eukaryotes, *E. coli* is still in need for further 5' trimming by RNase G, E and AM resembling the A₁ and A₂ cleavage sites in Yeast. In archaea the further processing of the 5' end is still unknown, yet a Utp24-like (HVO_1900) putative RNA-binding protein has been found in *H. volcanii* and appears to be essential for cell viability (own observations). The 3' end cleavage in *E. coli* is orchestrated by four 3'-to-5' exoribonucleases, RNase II, RNase PH, RNase R, and polynucleotide phosphorylase (PNPase) with help of the multifunctional endonuclease YbeY (Jacob et al., 2013; Sulthana and Deutscher, 2013; Vercruyse et al., 2016), which is also involved in the mitochondrial ribosome biogenesis in eukaryotes (Summer et al., 2020). The idea being that the RNases degrade the 3' end until they reach the YbeY protected 3' end, which will receive final cleavage once the time is right and accessible (Ghosal et al., 2018; Vercruyse et al., 2016). The yeast ribosome, however has its remaining 3' ends of the 20S rRNA cleaved by the PIN domain containing endonuclease Nob1 (Fatica et al., 2003). Interestingly, Nob1 is also found in archaea and is likely involved in a similar process (Qi et al., 2020; Veith et al., 2012).

Apart from nucleases many other assembly factors are involved in ribosomal maturation. Here I will focus on the late steps of the SSU maturation, in *E. coli* after the primary and secondary ribosomal proteins have already bound (compare Figure 3.8 left, white area) and in yeast once the pre 40S particle has left the nucleolus and is ready to be transported through the nuclear pore complex (see Figure 3.12 and Figure S1). The focus will be on the *E. coli* side and will be compared to what is going on in yeast and potentially in archaea. For ease of understanding the r-proteins will be labelled according to (Ban et al., 2014) as oSX (o being the u=universally conserved, b=bacteria-only, a=archaea-only, e=eukarya-only, y or h for yeast or human if necessary, S= small ribosomal protein, X being the numeral for the protein)

3.2.3.1 RimM

In *E. coli* the ribosome maturation factor M (RimM) is one the first binders at the late stage of SSU assembly as it binds with increasing affinity once uS19 and uS13 (both secondary binders) have assembled to the SSU (Lövgren et al., 2004; Wilson and Nierhaus, 2007). The binding of RimM facilitates the assembly of S3 by controlling the folding of the pre-16S rRNA (Clatterbuck Soper et al., 2013). A similar mechanism is observed in yeast, where the release of the non-essential assembly factor Ltv1 from the SSU processome enables binding of the ribosomal proteins uS10 and uS3 (Johnson et al., 2017; Mitterer et al., 2019; Strunk et al., 2011). Ltv1-less cells show mispositioning of uS3 resulting in a misfolded head structure, resembling that of RimM-less cells (Collins et al., 2018). The absence of RimM is additionally associated with reduced amounts of ribosomal proteins uS3, uS10, uS13, uS14, and uS19 suggesting an overall increase in assembly stability with RimM present (Guo et al., 2013; Thurlow et al., 2016). So far, no homologues have been found in archaea, none for Ltv1 and none for RimM. While the RimM typical PRC barrel is present in archaea but only in a stand-alone version (Anantharaman and Aravind, 2002). BLAST results show some RimM

candidates in archaeal organisms but none for curated single cultured genomes (Cobalt RID DS7J90G1212). When considering gene neighborhoods, one PRC barrel containing protein HVO_1964 is located upstream of the predicted Nob1 homologue (HVO_1965) in *H. volcanii*, but is missing the N-Terminal RimM-specific domain (PF05239). The effect of Δ RimM (17S pre-rRNA accumulation and slow growth) can be suppressed by the overexpression of the next assembly factor, **Ribosomal binding factor A (RbfA)** (Bylund et al., 2001, 1998).

3.2.3.2 RbfA

RbfA (Inoue et al., 2006), binds to the immature SSU at the 5' end at helix 1 (Dammel and Noller, 1995), which is in close proximity of helix 44 (shown later in Figure 3.17A). Binding of RbfA stabilizes a conformational change in the helix 44 that is unsuitable for translation, preventing the subunit from entering the translational pool (Datta et al., 2007). Moreover, recent studies have suggested that RbfA is a “gate keeper”, that remains bound until the SSU is fully matured (Sharma and Woodson, 2020). Once this mature state is reached the GTPase RsgA (or YjeQ) is able to bind to the SSU and releases RbfA via GTP hydrolysis (Goto et al., 2011; Jeganathan et al., 2015; Razi et al., 2017). A second release mechanism for RbfA, utilizes IF3, which in turn remains bound after RbfA release to initiate translation (Sharma and Woodson, 2020). Clear homologues to RbfA or RsgA in yeast or archaea are not known, and their respective function may have been replaced by other biogenesis factors. Plants show a homologue (RBF1) participating in Chloroplast 16S processing (Fristedt et al., 2014). Here, again, the effect of Δ RbfA can be complemented by overexpression of the next AF, Era (Inoue et al., 2003).

3.2.3.3 Era

The GTPase Era (Chen et al., 1999) can only bind in the GTP bound state between the head and platform of the SSU in a cavity formed by the r-proteins uS2, uS7, uS11, and bS18 (Sharma et al., 2005; Vercruyse et al., 2016). Upon GTP hydrolysis a significant structural change in Era is induced, that triggers its release from the maturing SSU, thereby facilitating access of the 3' end of the 17S rRNA precursor for cleavage (Razi et al., 2019) while also enabling the binding of bS1 and thereby permitting mRNA recruitment (Sharma et al., 2005). Rendering an Era bound SSU non-functional while retaining it from final processing. The binding of S1 and the interaction of Era with YbeY (Vercruyse et al., 2016), the proposed functional homologue of the endonuclease Nob1, also underlines this very late participation. Most importantly, the 3' cleavage is the last processing step, as Nob1 is one of the last assembly factors to leave the maturing 40S subunit in yeast (Lamanna and Karbstein, 2011, 2009). In several archaeal genomes there are annotations for Era-like GTPase, however, from sequence comparison the KH domain appears to be missing and the function remains unclear (Ferreira-Cerca, 2017). This KH-Domain of Era binds a specific sequence motif downstream of the helix 45 at the 3' end in *E. coli* (Tu et al., 2011), which was also shown to be bound by a proposed KH-Domain containing archaeal Dim2 (or Pno1) homologue (Jia et al., 2010). Indicating

a possible outsourcing of the Era KH domain. In addition, Dim2 interacts with Nob1 in yeast (Strunk et al., 2011; Woolls et al., 2011), underlining the functional conservation of assembly factors interactions.

Another interactor and also a suppressor of a catalytic Era mutant (Inoue et al., 2007; Lu and Inouye, 1998), is the universally conserved methyltransferase KsgA/Dim1, which will be discussed in detail later.

3.2.3.4 Rio Proteins

In eukaryotes along with KsgA/Dim1 and others, the essential Kinase/ATPase Rio2 associates to the maturing pre 40S in the nucleus before being exported to the cytoplasm (Ferreira-Cerca et al., 2012; Peña et al., 2017; Schäfer et al., 2003; Vanrobays et al., 2003). Once exported via the nuclear pore complex, Rio2 is released from the SSU, and the other essential Kinase/ATPase Rio1 associates to the pre 40S complex before joining with the LSU to initiate functional proofreading (Ferreira-Cerca et al., 2014; Lebaron et al., 2012; Strunk et al., 2012b; Widmann et al., 2012). Interestingly both Rio proteins are also present in many archaea (Esser and Siebers, 2013; LaRonde, 2014; LaRonde-LeBlanc and Wlodawer, 2005) and share the common ATPase function (Knüppel et al., 2018). Some archaea lack Rio1 and instead contain RioB homologue, a poorly characterized RIO domain containing protein with unknown function in ribosome assembly, also present in bacteria (Esser and Siebers, 2013). Moreover, multicellular eukaryotes contain an additional Rio protein, Rio3 (Baumas et al., 2012).

3.2.3.5 KsgA/Dim1

The almost universally conserved S-adenosylmethionine (SAM or AdoMet) dependent methyltransferase KsgA(B/A)/Dim1(E) is found in all three kingdoms of life (see sequence alignment Figure 3.15) (Ebersberger et al., 2014; Seistrup et al., 2016). Its main function as a ribosome biogenesis factor is to dimethylate two adjacent adenosines (A1518, A1519 in *E. coli* and A1779, A1780 in *S. cerevisiae*) in the GGAA tetraloop of helix 45 at the 3' end of the 16S/18S rRNA (see Figure 3.14) (Connolly et al., 2008; Helser et al., 1972; Lafontaine et al., 1994). Like most bacterial ribosome biogenesis factors, KsgA is not essential and its loss leads to Kasugamycin resistance (van Buul et al., 1984). Also when confronted with cold stress the *ΔksgA* cells accumulate 17S precursor rRNA (i.e. RNase III cleavage only, review Figure 3.9) (Connolly et al., 2008). Eukaryotic Dim1 on the other hand is essential for cell viability, most likely due to its proposed earlier participation in the 90S processome prior to the methylation reaction (Lafontaine et al., 1995). Eukaryotes have some additional orthologs in their organelles. *Arabidopsis thaliana*, for example uses the ortholog Pfc1 to methylate its small subunit rRNA of the chloroplast to circumvent negative temperature effects (Tokuhisa et al., 1998). Another orthologue mtTFB, is transported into the mitochondria of eukaryotes. In yeast, and fungi in general, one copy mtTFB serves as a mitochondrial transcription factor at the expense of methylation capabilities (Klootwijk et al., 1975; O'Farrell et

al., 2008), whereas most metazoans have two copies, mtTFB1 and mtTFB2, with mtTFB1 excelling at methylation while mtTFB2 is the better transcription factor, though both can complement for each other to a lesser extent (Bonawitz et al., 2006; Cotney et al., 2009, 2007). The function in archaea is supposedly similar to bacterial and eukaryotic KsgA/Dim1 and experiments with *Methanocaldococcus jannaschii* KsgA have shown that it can complement the function in *E. coli* but not in Yeast (Pulicherla et al., 2009).

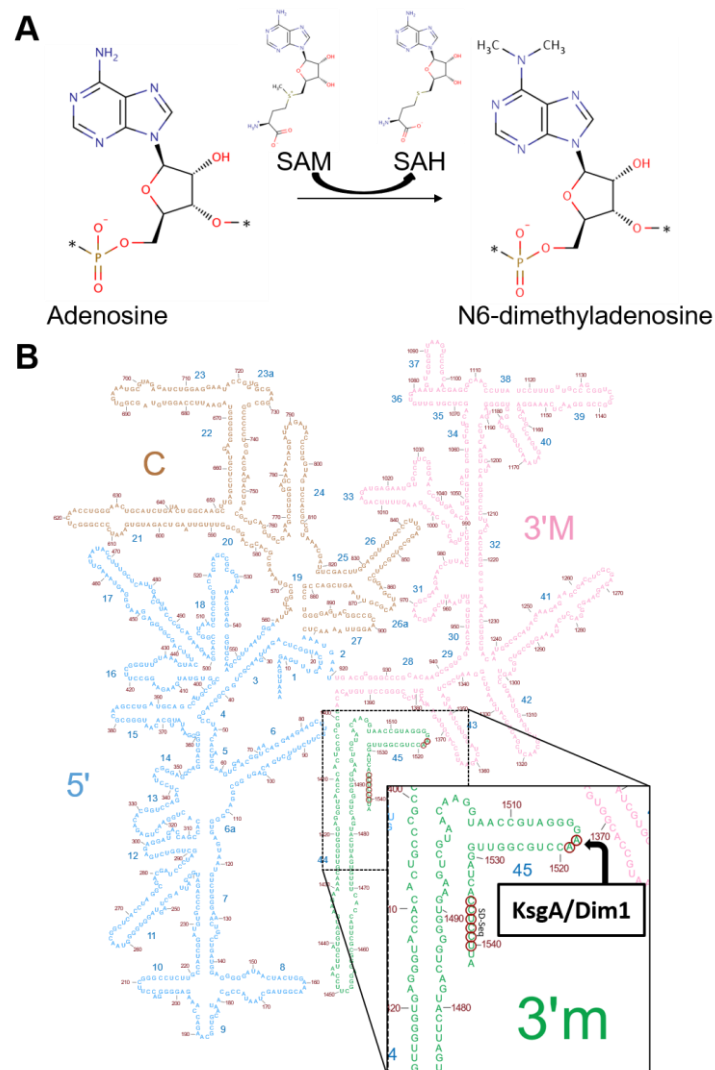


Figure 3.14 **Methylation reaction and 2D-Structure of 16S rRNA in *E. coli*.**

[A] Chemical reaction catalyzed by KsgA/Dim1. It transfers a total of four methyl groups, two to each of the two adjacent adenosines. SAM is the methyl donor, while SAH (S-adenosylhomocysteine) is the product. [B] Helix 45 with the two adjacent adenosines A1518, A1519 and anti-Shine-Dalgarno sequence are circled in red. Helices are annotated in blue. Nucleotides matching blue, pink, green and brown represent the 5'-, 3' major-, 3' minor- and the central domain respectively (created with Ribovision (Bernier et al., 2014)).

3.2.3.5.1 Structure, positioning and mechanism of KsgA/Dim1

The protein consists of two major structural domains and the structure is overall very well conserved among the three kingdoms of life (see Figure 3.16C), the N-Terminal part comprises the methyltransferase/catalytic domain and a C-Terminal domain that is highly unstructured and most likely involved in stabilizing its binding to the 30S (see Figure 3.15 and Figure 3.16D) (Boehringer

et al., 2012). The methyltransferase center shows the well conserved β -sheets (Figure 3.16D) shared among SAM dependent DNA-, RNA-, and small-molecule methyltransferases (Boehringer et al., 2012; Cheng, 1995; Schluckebier et al., 1999).

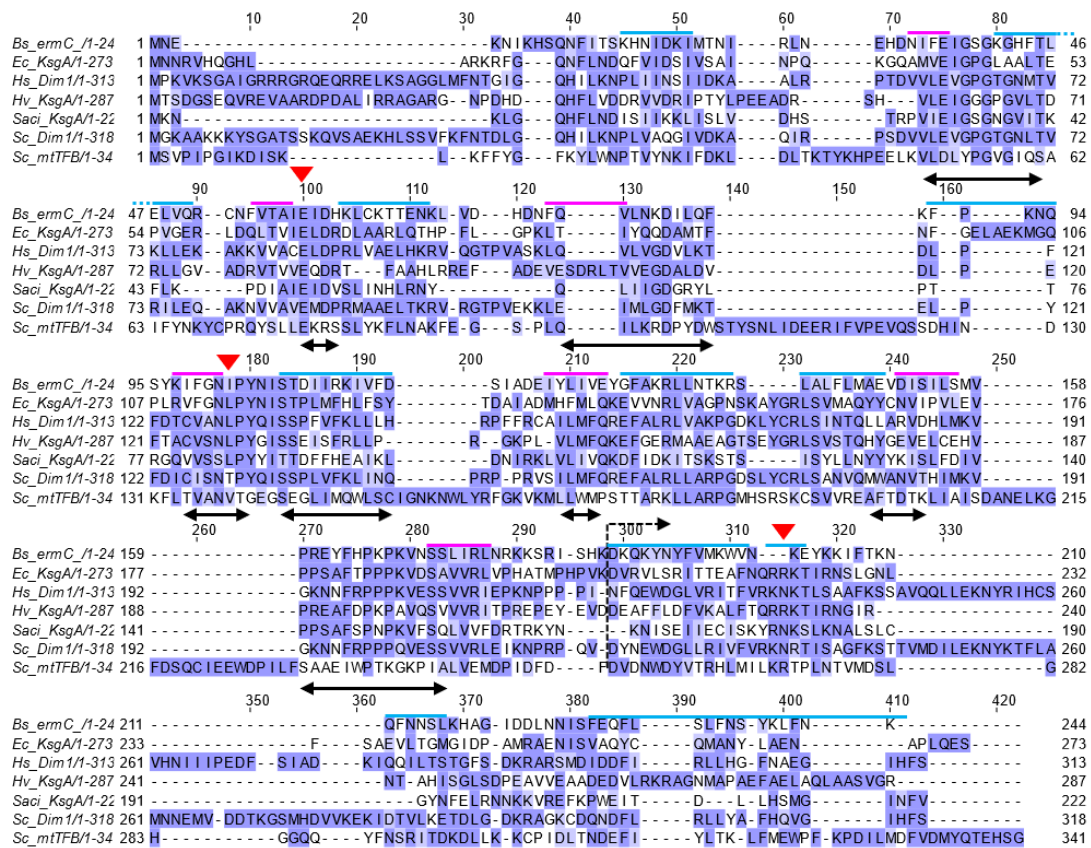


Figure 3.15 T-Coffee multiple sequence alignment of KsgA from four representative organisms and two other methyltransferases.

BLOSUM62 Score is depicted in a shade of blue. Double-headed arrows indicate motifs common to S-adenosylmethionine-dependent methyltransferases (O'Farrell et al., 2004). Magenta Bars are β -sheets, light blue bars are α -helical, Red triangles indicate introduced mutations in this work. Dashed black arrow indicates the start of the C-Terminal Domain. Uniprot Identifiers: *B. subtilis* ermC (P13956), *E. coli* KsgA (P06992), *H. sapiens* Dim1 (Q9UNQ2), *H. volcanii* KsgA (D4GWA1), *S. acidocaldarius* KsgA (M1ITD0), *S. cerevisiae* Dim1 (P41819), *S. cerevisiae* mtTFB (P14908). Generated with Jalview 2.11.1.0

Complementation experiments with varied N- and C-Terminal domains from either eukaryotic, bacterial or archaeal KsgA/Dim1, suggest that the eukaryote specific domain resides in the N-Terminal region (Pulicherla et al., 2009). The protein binds in between the body and the platform of the SSU (see Figure 3.16A, B). Yet there is no clear Cryo-EM data with natively bound KsgA to a SSU in bacteria, basing most interactions on *in vitro* reconstitutions and hydroxyl radical footprints (Boehringer et al., 2012; Xu et al., 2008). The C-Terminal part of EcKsgA is in contact with helix 24 and 27 (Boehringer et al., 2012) while ScDim1's C-Terminal region contacts helix 11 and 28 (Granneman et al., 2010). The N-Terminal part of KsgA/Dim1 is in contact with the immature helix 44 and in close proximity to helix 45 (see Figure 3.16A, B), thereby preventing premature folding of the decoding center of the SSU and preventing entry into the translational pool (Xu et al., 2008). This idea is supported by the fact that KsgA/Dim1 resides in the same spot as the C-Terminal domain of

the initiation factor IF3 in bacteria (Xu et al., 2008), and eIF1, and eIF1A in eukaryotes (Strunk et al., 2011). Moreover, the presence of S21, a late platform ribosomal protein involved in translation initiation (see Figure 3.8 left) (Held et al., 1974b), is inhibitory of KsgA activity *in vitro* (Poldermans et al., 1979; Thammana and Held, 1974). The eukaryotic functional homologue of bS21, eS26, however binds to the binding site of Dim2/Pno1, the interactor of Nob1 (Strunk et al., 2011).

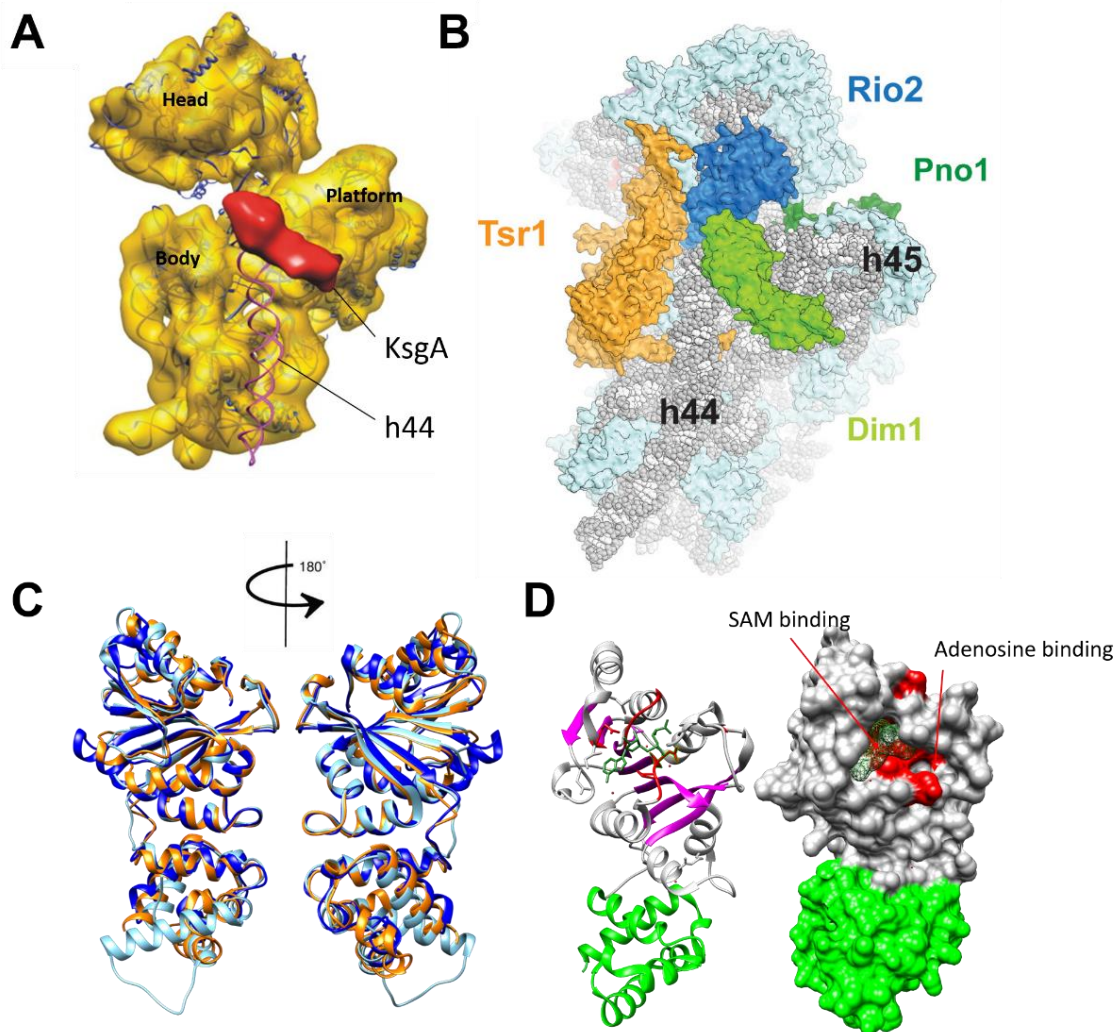


Figure 3.16 Binding Sites and Structure of KsgA/Dim1. Binding of KsgA/Dim1 to the SSU in *E. coli* [A] and *S. cerevisiae* [B]. [C] Overlay of MjDim1 (Orange, PDB 3GRV), HsDim1 (light blue, PDB: 1ZQ9) and EcKsgA (Dark blue, PDB: 1QYR). Created in Chimera [D] Crystal structure of MjKsgA with bound SAM (PDB: 3GRY), Dark grey N-terminal, Green C-Terminal part. Dark green Residue/Mesh: SAM. Catalytic centers are highlighted in red, characteristic mTase β -sheets are highlighted in magenta, SAM and Adenosine binding pockets are marked. Images taken and modified from [(Boehringer et al., 2012) A] and [(Scaiola et al., 2018) B]

The structure and catalytic domains of this highly conserved methyltransferase have been studied best in *E. coli*. The catalytic center is clearly visible at the surface of the crystal structure and it shows two distinct binding pockets (see Figure 3.16D), one for SAM, one for the respective adenosine (only fits one at a time). This structure has a strong resemblance to the ermC SAM dependent adenosine methyltransferases involved in 23S rRNA (A2058) dimethylation in *Bacillus subtilis* and

Staphylococcus aureus, (view structure comparison in Figure S 3). Interestingly, absence of ermC induced dimethylation leads to sensitivity to various antibiotics (Champney et al., 2003; Weisblum, 1995), whereas absence of KsgA leading to antibiotic resistance. Both show a very high specificity towards their targets and do not methylate if the structural context is incorrect or missing. Yet the major difference is that ermC is able to mono- and dimethylate the naked 23S RNA *in vitro* (Denoya and Dubnau, 1989; Schluckebier et al., 1999; Zhong et al., 1995), indicative of early LSU biogenesis participation, whereas KsgA requires a minimal RNP context in order to methylate its substrate. KsgA can bind naked 16S rRNA but requires a core set of body and platform r-proteins (uS4, bS6, uS8, uS11, uS15, bS16, uS17 and bS18) attached to the RNA in order to methylate the substrate *in vitro* (Desai and Rife, 2006). In order to methylate *ΔksgA* 30S subunits *in vitro*, the SSU needs to be “reprogrammed” into an inactive state by lowering magnesium concentrations (Poldermans et al., 1979; Thammana and Held, 1974). The reaction has no clear obligate order of which adenosine is methylated first (Cunningham et al., 1990). However, when lowering the temperature and SAM concentrations only A1519, i.e. the most 3' Adenosine, is methylated, indicating a preferred order of methylation (Van Buul et al., 1984). Whether the enzyme dimethylates in one go or must undergo dissociation/reassociation after every methylation, i.e. four times, is not completely clear, but unlikely (O'Farrell et al., 2006). Once helix 45 has reached its mature status (complete methylation) the binding affinity of KsgA to the SSU is decreased and it dissociates (Poldermans et al., 1979).

3.2.3.5.2 KsgA's role in the final biogenesis steps of *E. coli*

The exact order of the final steps in *E. coli* has been rescheduled over the years. On the one hand the suppression of a catalytic (E200K) Era mutant by overexpression of KsgA and the accumulation of 17S rRNA from a catalytically inactive KsgA and under low temperatures in *ΔksgA* (Connolly et al., 2008; Inoue et al., 2007; Lu and Inouye, 1998) suggests that after RbfA dissociation, KsgA is able to bind and further stabilizes the translationally inactive helix 44 conformation (Boehringer et al., 2012; Clatterbuck Soper et al., 2013; Xu et al., 2008). However, newer studies give strong evidence for KsgA acting and dissociating prior to the postulated “gate keeper” RbfA (Connolly and Culver, 2013; Sharma and Woodson, 2020). In this case how and when exactly KsgA binds is a bit unclear and will possibly be revealed in future studies. In any case, once KsgA has bound to the appropriate maturation state (likely after RimM has completed its task), further maturation of the SSU (RNA-folding, addition of r-proteins) possibly increases the proximity of the two Adenosines to the binding pockets of KsgA (Boehringer et al., 2012; Tu et al., 2011). This is supposedly a passive detector of maturation and the methylations can be considered as a “timestamp”. These methylations are vital to relax the “tense” GGAA tetraloop of helix 45 to a more “flexible” GGm₂⁶Am₂⁶A conformation that is capable to turn outward and form hydrogen bonds to helix 44 and thereby stabilizing the A and P sites of the ribosome (Demirci et al., 2010; Rife and Moore, 1998). After the dimethylation reaction is completed *in vitro*, the binding affinity to the SSU decreases and KsgA dissociates (Poldermans et al., 1979). The *in vivo* scenario very likely involves RbfA competing with KsgA for SSU binding,

since both occlude the same binding site (Figure 3.17A & C and Figure S 4). Coupled to the decreased binding affinity to, and structural rearrangements of the SSU after methylation could shift affinity towards RbfA. RbfA then further stabilizes the KsgA induced rearrangement of helix 44 and 45 towards the mature state (Demirci et al., 2010; López-Alonso et al., 2017) while still retaining it from the translational pool. Either the binding of RbfA or the structural rearrangements by KsgA are then most likely detected by the Era/YbeY complex. Era is bound across from KsgA or RbfA (see Figure 3.17) and is in contact to the anti-Shine-Dalgarno sequence of the 3' end of h45 (Tu et al., 2011). Activation of the Era/YbeY complex then leads to final cleavage of the 3' end of the 16S rRNA (Ghosal et al., 2018; Vercruyssen et al., 2016). If this happens before or after RbfA dissociation is not completely clear. However, two recent studies favor cleavage before RbfA dissociation. First, having the translation initiation factor IF3 involved in the release of RbfA, with the subsequent entry in the translational pool (Sharma and Woodson, 2020) and second, the fact that Era bound 30S subunits prevent binding of RsgA, the release factor of RbfA (Razi et al., 2019).

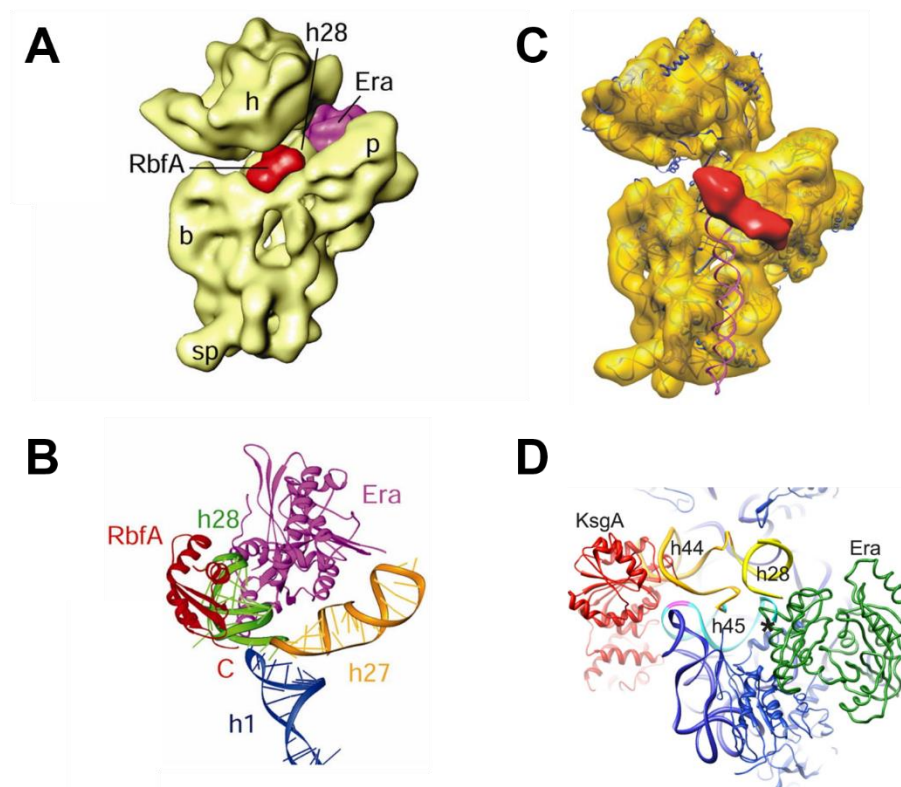


Figure 3.17 **Proximity of Era to RbfA and KsgA on the SSU.**

[A] Binding position of RbfA (red) and Era on the 30S subunit. **[B]** RbfA (red) and Era (magenta) interact with a common structural element, h28, of the 16S rRNA (cyan). The thumbnail to the left depicts the orientation of the 30S subunit. **[C]** Binding position of KsgA (red) on the 30S subunit. **[D]** KsgA (red) binds at helix 45 (cyan, A1518 and 1519 magenta) of the 30S subunit (blue). Era is bound between the platform and the head contacting helix 28 (yellow). Helix 44 is shown in orange. (The 3' end of the 16S rRNA is labeled with an asterisk.) (modified from Boehringer et al., 2012[A,B]; Datta et al., 2007[C,D])

Era has been shown to interact with the endonuclease YbeY (Ghosal et al., 2018), yet no direct interaction could be determined between YbeY and KsgA or RsgA in a Yeast two hybrid screening (Vercruyssen et al., 2016). Furthermore, recent studies suggest that YbeY is in a complex with GTP-

bound Era and uS11 at the 3' end of the 16S rRNA precursor and thereby prevents pre-mature cleavage and/or guides accurate RNase cleavage (Ghosal et al., 2018; Razi et al., 2019) and might not be involved in the actual cleavage (Smith et al., 2018). Nevertheless, correct 3' cleavage permits Era and YbeY to dissociate from the now mature SSU via GTP hydrolysis (Ghosal et al., 2018; Sharma et al., 2005). This enables for bS1 to bind near the platform (Byrgazov et al., 2015; Vercruyse et al., 2016), and perhaps mitigates a conformational change that is detected by, or directly contacts RfbA which can now be released by RsgA, due to the dissociation of Era (Razi et al., 2019), resulting in a translational competent mature 30S subunit. A schematic summary interpretation of the late events is shown in Figure 3.18.

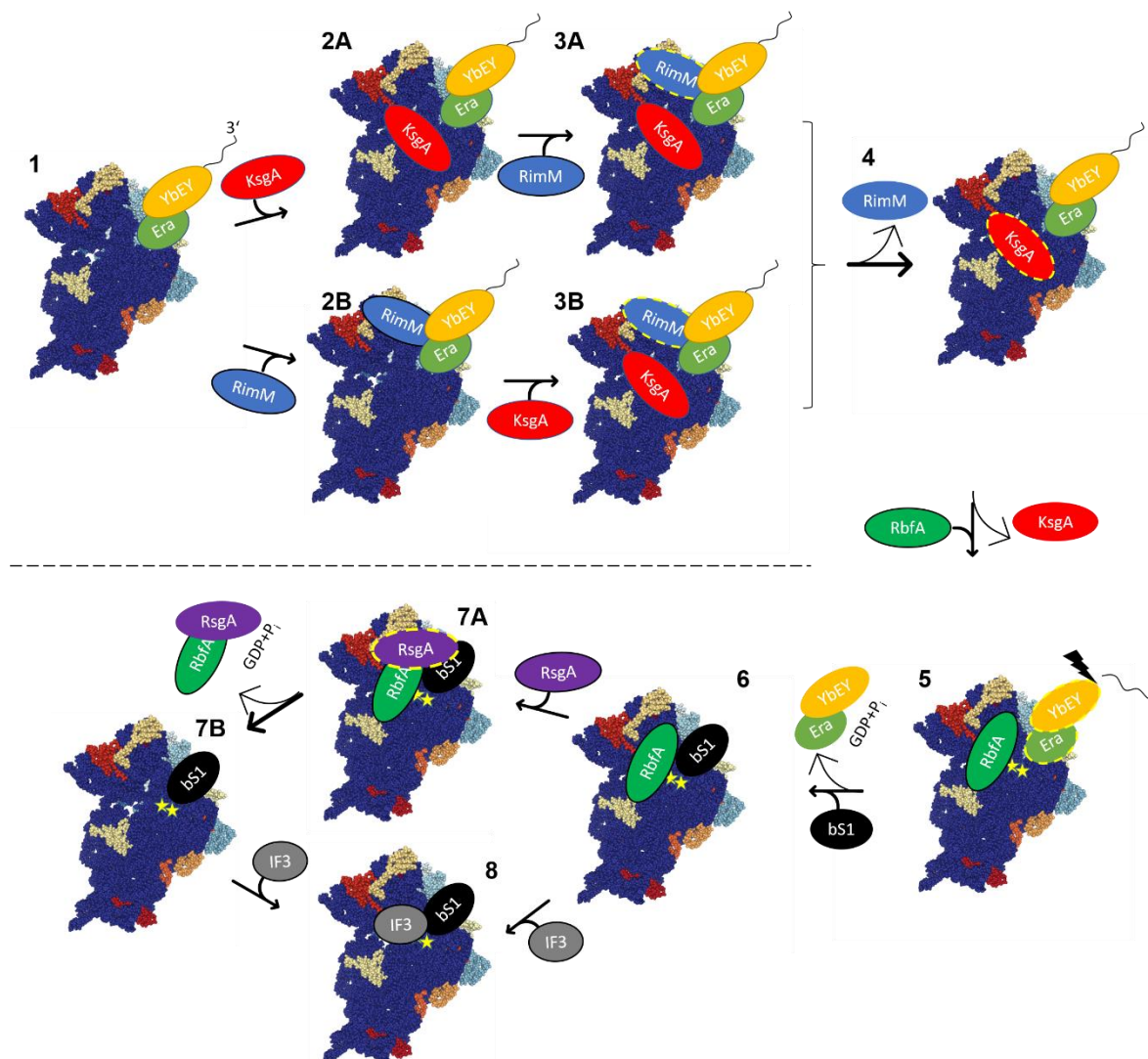


Figure 3.18 **Schematic interpretation of the late biogenesis events in *E. coli* based on my interpretation of the presented literature.**

The depicted 30S structure serves as a background placeholder and is not the actual intermediate (PDB: 1I94). Activity of an AF is indicated by the Yellow dashed border. [1] At a certain point of maturation, the Era/YbeY complex acts as a constant protector for premature cleavage of the 3' ETS [2A] KsgA binds between the platform [2B] RimM binds to the head domain. [3A] RimM joins the complex and fulfils its action by acting as a chaperone for head formation (uS3 binding, not indicated). [3B] KsgA joins the complex and RimM fulfils its action by acting as a chaperone for head formation (uS3 binding, not indicated). If pathway A or B is correct is unclear, i.e. from a KsgA perspective; if a immature head structure is required for KsgA to bind. The *in vitro* Data from Boehringer et al., (2012) and Desai and Rife (2006) suggest that, for KsgA binding necessary lowered Magnesia concentration, destabilizes the head domain, resembling a similar state to

the pre RimM status, indicates that path A could be correct. [4] RimM leaves the complex and this and other structural rearrangements in the maturing 40S particle trigger KsgA dependent methylation. [5] Either KsgA dissociates passively or is removed in competition with RbfA. The two transferred methylations are indicated by yellow stars at the previous location of KsgA. Binding of RbfA activates the Era-YbeY complex and final 3' cleavage is performed and GTP hydrolysis by Era releases the complex. [6] This enables binding of bS1, possibly contacting RbfA and indicating maturation is near completion. Depending of the growth phase and possibly availability of RsgA and IF3 (exponential growth might require both pathways), RbfA is released via the two steps [7A,7B] involving RsgA or direct exchange via competition of IF3 [8] with RsgA.

3.2.3.5.3 Dim1's role in the last steps of biogenesis in eukaryotes

As aforementioned, yeast Dim1 supposedly binds to the 90S precursor particle in the nucleolus (Lafontaine et al., 1995, 1998) and/or to a nucleoplasmic pre-40S particle (Moriggi et al., 2014; Schäfer et al., 2003). The depletion leads to the accumulation of dead end 22S rRNA resulting from the premature processing at A1 and A2 (see Figure 3.11) (Lafontaine et al., 1995) possibly due to Dim1 interactions with the 90S unfolded central pseudoknot (Granneman et al., 2010). If Dim1 truly binds to the 90S particle is debated due to the absence in both 90S Cryo-EM structures (Cheng et al., 2017; Sun et al., 2017) and in purified 90S particles (Schäfer et al., 2003). Nevertheless, the long association of Dim1 with the nascent SSU makes it difficult to determine how methylation is triggered or withheld for so long. In yeast the depletion of Pno1 (Partner of Nob1, final step in maturation), leads to an unmethylated precursor particle (Vanrobays, 2004). However, Pno1 binds shortly after Dim1, which make the downstream effects of Pno1 depletion very far-reaching (Vanrobays, 2004). The rough estimate is that methylation can occur, once the 43S particle has been exported into the cytoplasm (Brand et al., 1977). To make things even more complicated, human Dim1 is thought to methylate its substrate in the nucleolus and/or nucleoplasm (Sloan et al., 2019; Zorbas et al., 2015) and is not present in the cytoplasmic complex (Ameismeier et al., 2018). Suggesting a possible flexibility in methylation timing and underlining the possibility of KsgA/Dim1 being a passive sensor and it's activity depends strongly on the substrate competence, e.g. quality control (Karbstein, 2013). The close proximity of Rio2 (see Figure 3.16B) would suggest it being a possible activator of Dim1, but an interaction via phosphorylation has only been shown *in vitro* in the human system indicating a perhaps human specific mechanism (Sloan et al., 2019). If Rio2 is already present in the nucleus to activate Dim1 methylation via phosphorylation is unclear, since Rio2 has been proposed to join the maturing ribosome after or immediately before nuclear export (Zemp et al., 2009), also arguing against a conserved activation mechanism by Rio2. Pno1 however would be present in the nucleus in both yeast and human, with a similar proximity to Dim1 as, Era to KsgA (Vanrobays, 2004; Zhou et al., 2004). Both, human and yeast Pno1, are retained on the maturing particle and required for the final 3' cleavage by Nob1 (Ameismeier et al., 2018; Woolls et al., 2011) in analogy to the Era and YbeY (Ghosal et al., 2018; Vercruyse et al., 2016). If the trigger for methylation is mediated by an assembly factor and/or just by a conformational change that delivers the (to be methylated) adenosines of helix45 to the binding pocket, remains unclear. But, considering Dim1 as a passive sensor of conformational changes (RNA folding, r-protein assembly) and imprinting this detection onto the RNA via the methylation would make sense in *E. coli*, yeast

and human. The release of Dim1, in comparison to the postulated passive or competitive dissociation in *E. coli*, appears to utilize the activity of an ATPase/adenylate kinase, namely Fap7 or CINAP in human (Juhnke et al., 2000; Santama et al., 2005). It is proposed that Fap7 induces a rotated state in the functional proofreading 80S-like subunit (joined SSU and LSU precursor that still have AFs bound and cannot participate in translation (Lebaron et al., 2012; Strunk et al., 2012a)) via ATP hydrolysis and thereby releases Dim1 from the 80S precursor (Ghalei et al., 2017). If a similar mechanism is used in humans is unclear, as there is no evidence for 80S-like particle in the nucleus. Nevertheless, hCINAP is present in the nucleus and is, like Fap7, involved in pre-18S processing by Nob1 in an ATP dependent manner (Loc'h et al., 2014; Santama et al., 2005). In any case, in eukaryotes, the Nob1 cleavage is mediated by Pno1 and does take place after Dim1 release (Ameismeier et al., 2018; Heuer et al., 2017; Johnson et al., 2017), very similar to the respective YbeY, Era, RbfA mechanisms in *E. coli*. Where, when and by which factor exactly remains to be elucidated in detail for all organisms.

The presence of KsgA/Dim1 in all three domains of life and thus the evolutionary stability of this biogenesis factor highlights its vast importance. While being dispensable under laboratory conditions in many bacteria the real-world effect is probably more severe and impossible to sustain under competitive conditions. Otherwise nature would not have retained it over the countless years of evolution. The only known loss of KsgA has occurred in the symbiotic hyperthermophilic archaeon *Nanoarchaeum equitans* (and perhaps other nanoarchaea) and methylation activity has not been substituted by the symbionts KsgA or another endogenous methyltransferase, but rather by a mechanisms involving sRNP modification (Seistrup et al., 2016). A drastic effect of KsgA loss is very well illustrated in *Yersinia pseudotuberculosis*, where virulence to mice is lost (Mecscas et al., 2001). This along with impeded growth and accumulation of immature SSUs at cold temperatures would be major disadvantages in the wild (Connolly et al., 2008). This accumulated evidence makes it very likely that a KsgA/Dim1-Like factor was present in LUCA (Harris et al., 2003).

In conclusion, the general pattern of late SSU biogenesis in bacteria and in eukaryotes appears to be a tightly regulated interdependency of these late biogenesis factors, that enable a stepwise hierarchical progression through maturation. If a factor is missing, acquires a point mutation or is depleted, the effects are mostly associated with reduced translational fidelity, impaired initiation, rRNA processing defects or even impaired subunit joining (Bylund et al., 1998; Connolly et al., 2008; Dammel and Noller, 1995; Datta et al., 2007; Ferreira-Cerca et al., 2014, 2012; Inoue et al., 2006; Roy-Chaudhuri et al., 2010). If this holds true for the kingdom of archaea remains to be answered.

3.3 Tracing of RNA metabolisms and structure

RNA has always been an endearing molecule, its ability to form secondary structures and even catalyze reaction has not only led to the RNA-World Hypothesis (Gilbert, 1986) but to a high demand of methods that enable the study of their dynamics, metabolism and structure (Ganser et al., 2019).

Some of these methods have been established using the highly abundant ribosomal RNA as a model system and have enabled detection of percentile precursor particles (Trapman et al., 1975; Trapman and Planta, 1975) as well as resolving secondary structures of these complex RNAs (Moazed et al., 1986; Noller and Chaires, 1972; Qu et al., 1983).

3.3.1 RNA Labelling

Before the advent of genetic depletion there was no possibility to accumulate certain precursor rRNAs. Thus incorporation of traceable nucleotides was used to track short lived RNA species such as pre-rRNAs (Rovera et al., 1970; Scherrer and Darnell, 1962), mRNA (Jacob and Monod, 1961) and pre-tRNAs (Rake and Graham, 1964). Most of these early studies used the radioactively labelled nucleotide Uridine- C^{14} and/or H^3 -Uridine, as they were easy to use and did not have grave effects on transcription. Pulsing the exponentially growing cells with these traceable nucleotides revealed so far unknown precursor populations of RNAs, while chasing can reveal degradation and decay pathways (Herman and Penman, 1977). A detailed pulse analysis of yeast ribosomal rRNA postulated precursor rRNAs to the individual subunits as well as the earliest 35S pre-rRNA (Trapman and Planta, 1975). With sampling speed improving, the timescale can be pushed further and additional even shorter lived RNAs can be resolved (Kos and Tollervey, 2010).

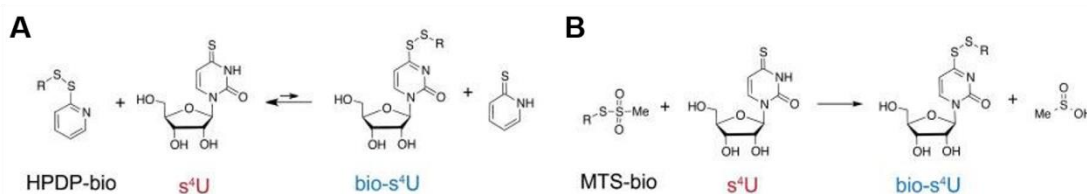


Figure 3.19 **Biotinylation of 4SU** [A] “old” reagent [B] New and improved reagent (modified from (Duffy et al., 2015))

Non-radioactive nucleotides such as 4-thiouracil- (4TU) or 4-thiouridine- (4SU), have been established in major model organisms and have provided a more accessible method for RNA labelling (Favre et al., 1986; Kenzelmann et al., 2007; Melvin et al., 1978; Miller et al., 2009). The major advantage of these analogues is that they offer thiol specific biotinylation (Dolken et al., 2008) (Figure 3.19A). This opens a door to streptavidin-based downstream applications such as antibody detection, affinity purification with subsequent high/low throughput analysis, and many more. The advances in RNA tagging chemistry have pushed the depth of analysis even further (Duffy et al., 2019, 2015) (Figure 3.19B) and transcriptome wide studies on the stability of mRNAs are now possible (Lugowski et al., 2018). Together these methods can and have provided essential insights into RNA metabolism and dynamics. Furthermore, they enable the analysis of RNA binding proteins by photo-crosslinking approaches (PAR-CLIP) (Hafner et al., 2010a, 2010b). Expanding this temporal method with the next method, RNA structure probing, has achieved great spatiotemporal results in rRNA analysis (Hulscher et al., 2016; Swiatkowska et al., 2012).

3.3.2 Chemical RNA structure probing

While RNA dynamics are not only based on synthesis and decay, its structure is also highly dynamic and can fold into a variety of structures based on inter-/intramolecular base-pairings, temperature, pH, osmolarity and chemical modifications. The formation of correct structural motifs, such as hairpins, mismatches, bulges, internal loops or pseudoknots are the epitome of enzymatic activity in ribozymes, e.g. the ribosome (Cruz and Westhof, 2009). While we now know how the complete ribosome is structured on an atomic resolution by the power of X-Ray Crystallography (Ben-Shem et al., 2011) and Cryo-EM (Greber et al., 2012), its earlier structural discoveries were made step by step, nucleotide by nucleotide (Noller and Chaires, 1972; Qu et al., 1983).

While the basics on RNA folding were clear in theory and can be calculated by computers nowadays (with its limited validity), experimental evidence is generated by using sequence specific enzymes or chemicals that target specific RNA motifs (Ziehler and Engelke, 2000). Based on their properties they can target either specific bases or the sugar backbone (see Figure 3.20). If the RNA is in a conformation that is accessible, i.e. single stranded and/or highly flexible, it can be modified (Weeks, 2010). Depending on the chemical, the transferred group can range from a small CH₃ from DMS to bulky molecules as Kethoxal or CMCT at the Watson-Crick interface, as well as large molecules from Selective 2'-hydroxyl acylation (SHA[PE]) reagents in the sugar backbone of the RNA. The readout for all of these chemicals, however, follows a similar procedure, a stop or stalling of the reverse transcriptase at the modified nucleotide, which can then be mapped to the known nucleotide sequence. Delightfully, this has remained the basis for readouts since the first Kethoxal modifications of 16S rRNA on sequencing gels (Noller and Chaires, 1972) to the modern age of next generation sequencing readouts of transcriptome wide structure probing (Rouskin et al., 2014; Talkish et al., 2014). In the 40 years in-between a lot of development has occurred. In 1986 the combined data of DMS, CMCT and Kethoxal modified 16S rRNA, verified the 2D predictions derived from comparative sequence analysis (Moazed et al., 1986). Only two years later the first *in vivo* DMS modifications were accomplished and could elucidate interaction interfaces of elongation factors with ribosomes (Moazed et al., 1988). A year later first hydroxy radical foot-printings were performed on mRNA and tRNA (Latham and Cech, 1989; Wang and Padgett, 1989) followed by the breakthrough development of SHAPE chemicals that elevated RNA structure analysis to quantitative levels (Merino et al., 2005). This was shortly before the arrival of capillary electrophoresis which allowed for a certain level of automation (Mitra et al., 2008; Wilkinson et al., 2008) and concluded in real high throughput analysis by next generation sequencing, SHAPE-seq/SHAPE-Map (Lucks et al., 2011).

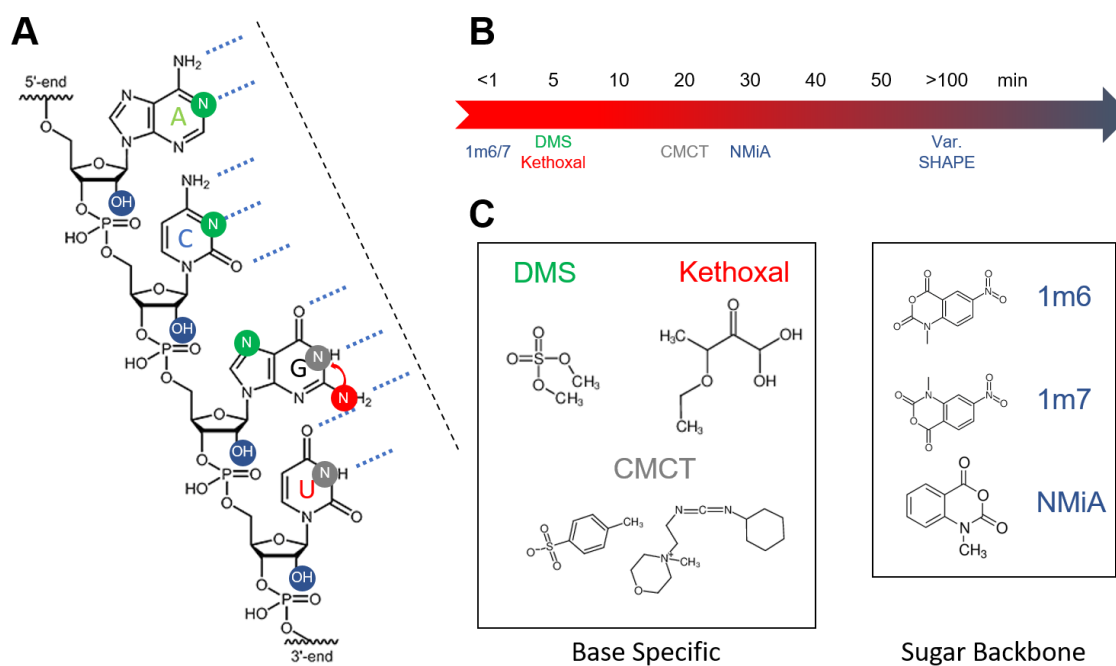


Figure 3.20 **Selection of RNA probing chemicals.**

[A] sRNA with indicated hydrogen bonds in blue dashed lines (A=Adenosine, C=Cytosine, G= Guanine, U= Uracil). Targets are colored respective to the chemical agent indicated in B and C. [B] Estimated reaction time of the respective chemicals. Actual times may vary depending on concentration, temperature and medium. SHAPE reagents are approx. 5 half-lives. [C] Chemical structures of the respective modifiers. RNA strand from biomers.net.

Even with all the advancements in the field of RNA labelling and RNA structure probing, implementing these techniques still requires a lot of testing for the system it is applied to. Differences in pH, Salinity, temperature, solubility can affect reactivity and some cell membranes are unable to take up the chemicals and only *ex vivo* or *in vitro* work is possible (reviewed in Mailler et al., 2019).

The heritage of both, RNA labelling and RNA structure probing, in the field of ribosome research are a key motivation to implement these techniques in our archaeal organisms. Especially the combination of both methods have been used for kinetic structural analysis of pre ribosomes *in vivo* (Hulscher et al., 2016; Swiatkowska et al., 2012). This could prove useful to analyze structural dynamics of short lived RNA precursors such as the (circular) pre-rRNA structures in archaea, as well as potentially mapping RNA-Protein interaction (Smola and Weeks, 2018).

3.4 Goal of this work

As mentioned earlier, ribosome biogenesis is a highly complex endeavor an organism must undertake. The assembly pathway, however, differs profoundly between the well-studied kingdoms of bacteria and eukarya, suggesting that perhaps the kingdom of archaea shows an intermediate pathway that connects the two. Yet, the overall lack of experimental data surrounding archaeal ribosome biogenesis is largely due to the for long genetic inaccessibility of these in part extreme organisms. After our previous study analyzing the conservation of the biogenesis factors Rio1 and 2 in two model archaea (Knüppel et al., 2018) we wanted to further characterize other late small subunit assembly factors. In this thesis I provide a detailed analysis of the archaeal KsgA/Dim1 dimethyltransferase, an almost universally conserved late SSU biogenesis factor. To do so we attempted to answer the following questions:

- Is KsgA/Dim1 dispensable in model archaea?
- What are the contributions of KsgA/Dim1 to archaeal physiology and translational landscape?
- What are the implications of KsgA/Dim1 dependent methylation for ribosome structure and are there any archaea specific differences?
- Is the binding and release during ribosome assembly more characteristic of yeast or *E. coli*?

To answer these questions, we used a multidisciplinary approach utilizing the genetic tools available for *H. volcanii*, *S. acidocaldarius*, *P. furiosus* and *E. coli*, a vast array of microbiological assays, biochemistry, shotgun proteomics and established chemical RNA foot-printing methods as well as 4TU pulse (chase) labelling. First, we aimed to establish knock outs in archaeal model organisms to lay the basis for further studies. Second, we investigated the effects of KsgA deficiency on cellular fitness and translational activity in *H. volcanii*. The third question was tackled by comparing the substrate structure and its implications for KsgA dependent methylation across a broad range of archaea and the tree of life. To verify these structural predictions, we also implemented chemical RNA structure probing in two archaeal organisms. To answer the fourth and final question we aimed to reconstitute a full archaeal dimethylation cycle (binding, modification, and release).

Complementary to these goals and to facilitate the study of RNA dynamics *in vivo*, we aimed to implement 4TU Pulse (Chase) labelling and chemical RNA foot-printing in both *H. volcanii* and *S. acidocaldarius*.

4 RESULTS

4.1 Establishment of RNA modifications methods

The term RNA modification can be interpreted in two ways. For one, it can mean the modification of an RNA by the addition of a group or altering the base via an enzyme or a chemical. But also, introducing modified non-canonical nucleotides that modify the composition of RNA molecules. In both cases the RNA has been replaced or modified to an extent that is distinguishable to the native form.

Here we applied two methods that make use of these two types of modification to study RNA structure and metabolism

4.1.1 4-Thio Uracil Pulse labelling in archaea

The following part is a summary of the results from, „**Toward Time-Resolved Analysis of RNA Metabolism in archaea Using 4-Thiouracil**“. *Frontiers in Microbiology* 8 (2017). **Knüppel Robert**, Corinna Kutenberger, und Sébastien Ferreira-Cerca.

Introducing traceable nucleotides into an organism enables the study of RNA metabolism and its dynamics. In the context of ribosome biogenesis this has proven to be a fruitful technique (e.g. Favre et al., 1986; Swiatkowska et al., 2012). Thus, we sought out to implement this method in our two model organisms *Haloferax volcanii* and *Sulfolobus acidocaldarius*.

The key questions that needed to be answered first was if the archaeal cells can import and process the 4TU nucleobase. Also, for an ideal testing environment, defined media with exogenously added uracil was chosen (Hv-Ca⁺, Brock Media for *H. volcanii* / *S. acidocaldarius* respectively see 7.1.3). Luckily both organisms have strains that are mutated in their respective *pyrE* genes (orotate phosphoribosyltransferase) and thus are dependent on external sources of uracil (Allers et al., 2004; Wagner et al., 2012). Based on the KEGG database (Kanehisa et al., 2016) and the presence of enzymatic homologues involved in uracil metabolism, the cells should be able to synthesize (4T)UTP from 4TU (Figure 4.1A,B). The workflow is shown in Figure 4.1C and described in detail in Chapters 7.2.1.7, 7.2.5.3 and 7.2.5.4.3. In short, cells were grown in the presence of a certain 4TU/Uracil concentration, harvested and the RNA was extracted. The 4TU containing RNA was then biotinylated using either MTSEA biotin-XX or HPDP-biotin. The biotinylated RNA was then separated on either a denaturing TBE agarose gel and following northern blotting or using affinity purification (7.2.5.7.2). The blotted RNA could then be detected via IR-Dye coupled streptavidin. Successful labelling of total RNA is shown in Figure 4.1D. The detection efficiency could be greatly improved by using the MTSEA-biotin-XX (Duffy et al., 2015) compared to HPDP-biotin (Figure 4.1E).

In the initial experiments a molar ratio of 3:1 (4TU : U) was used, however a range of 4TU/U ratios were tested for toxicity and labelling efficiency. High relative concentrations >80 % 4TU as uracil source (4:1) lead to growth defects in both archaea (see Paper), while relative concentrations below 75 % 4TU lead to decreased labelling efficiency (see Figure 4.2A). Consequently, the initial 3:1 ratio was the best choice regarding toxicity and labelling efficiency. Steady state labelling revealed that, *S. acidocaldarius* shows very strong signals in the 5S rRNA/tRNA range even in the Uracil only background (Figure 4.2B,C), indicating some unspecific biotinylation of thio-modified nucleotides (discussed in (Knüppel et al., 2017) and 5.5).

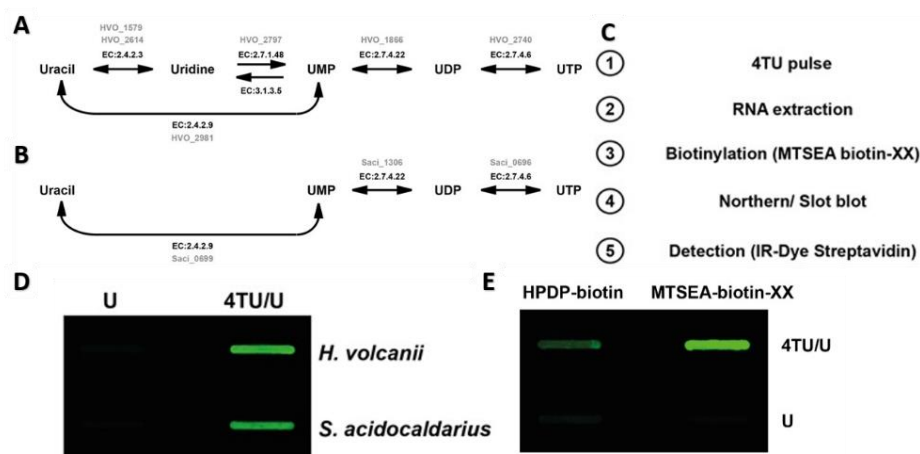


Figure 4.1 **In vivo incorporation of 4TU in model archaea.**

[A] Synthesis pathway of UTP from uracil in *Haloferax volcanii* is depicted according to KEGG pyrimidine synthesis pathway (KEGG entry: hvo00240) (Kanehisa et al., 2016). Enzyme classification number (E.C) and their corresponding open reading frame in *H. volcanii* (in gray) encoding the enzyme activity are indicated. [B] Synthesis pathway of UTP from uracil in *Sulfolobus acidocaldarius* is depicted according to KEGG pyrimidine synthesis pathway (KEGG entry: sai00240) (Kanehisa et al., 2016). Enzyme classification number (E.C) and their corresponding open reading frame in *S. acidocaldarius* (in gray) encoding the enzyme activity are indicated. [C] 4-thiouracil (4TU) labeling and detection work flow. [D] Analysis of 4TU incorporation in *H. volcanii* and *S. acidocaldarius*. *H. volcanii* (h26) and *S. acidocaldarius* (MW001) cells were grown for several generations either in medium containing a mixture of 4-thiouracil and uracil (4TU/U - 3:1) or in medium solely containing uracil (U). E Detection of 4TU with HPDP-biotin and MTSEA-biotin-XX. Biotinylated uracil was detected by infra-red fluorescence.

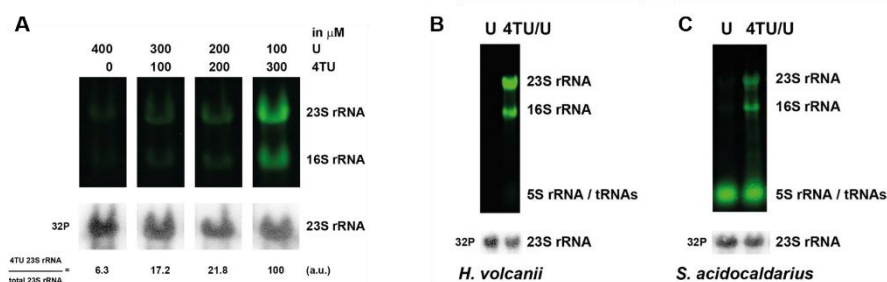


Figure 4.2 **Steady state and concentration dependent labelling of 4TU in model archaea.**

[A] Different ratios of 4TU/U tested over 2h of exponential growth in *H. volcanii*. [B] and [C] Steady state incorporation of 4TU over 20h of growth.

Compared to *H. volcanii*, the overall pulse and chase labelling experiments in *S. acidocaldarius* were difficult to handle and also the incorporation was comparably worse (Figure 4.3A). This is very likely due to the comparably long doubling times (8 - 10h) at sub optimal growth conditions (65 °C vs 75

°C) in *S. acidocaldarius*. Within the first doubling *H. volcanii* incorporated ~ 50-fold more 4TU than *S. acidocaldarius* (see Figure 4.3A). The pulse and chase labelling did work in *S. acidocaldarius* and incorporation and loss of 4TU can be seen (Figure 4.3B) but only over a very long time-span. In *H. volcanii* it was possible to detect pulse labelled RNA at very short timepoints (10-15% of a doubling) when increasing detector sensitivity (Figure 4.3C).

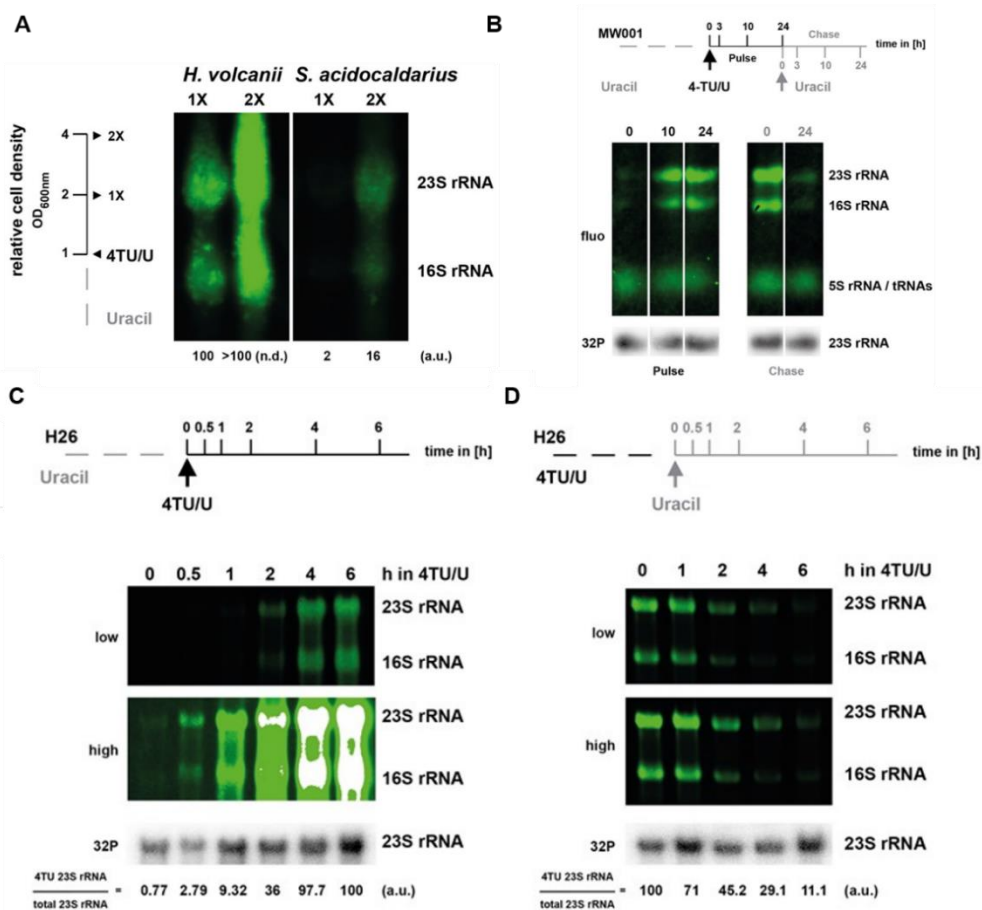


Figure 4.3 **Pulse chase comparison between two model archaea.**

The workflow overview for the respective experiments are shown above the readouts in **B**, **C** and **D**. Cell Aliquots were taken at the indicated timepoints. **[A]** exponentially grown cells were shifted into 4TU containing medium and incubated for another two doublings, Hv (4, 8 h), Saci (9, 18 h). **[B]** Pulse and chase experiment in *S. acidocaldarius*. **[C]** Pulse incorporation of 4TU in *H. volcanii*, at low and high sensitivity. **[D]** Chase of overnight 4TU pulsed *H. volcanii* cells.

The Chase experiments in *H. volcanii* show, that after roughly one doubling the majority of the labelled RNA is lost (Figure 4.3D). Overall, this demonstrates the feasibility of 4TU pulse labelling in two model archaeal organisms, with room for optimization in *S. acidocaldarius*.

However, not all organisms are genetically tractable, so having cells dependent on extracellular Uracil is not the norm. Consequently, we tested if an intact uracil metabolism (*pyrE*⁺) does affect the incorporation of 4TU in *H. volcanii*. In order to do so, we used Pop-In candidates that have genomically integrated *pyrE2::HVO_0569* from the pTA131 plasmid (analogous to Figure 4.8). These cells were then grown in the same Ca⁺ Media lacking Uracil but with added 4TU/U (3:1) for 8h. Steady state labelling worked equally well (Figure 4.4A) and time kinetic pulse labelling is just

as efficient as in *PyrE* deleted cells (Figure 4.4B, C). Overall, it can be said that for *H. volcanii* there is no difference in 4TU incorporation with Uracil auxo- or prototrophy.

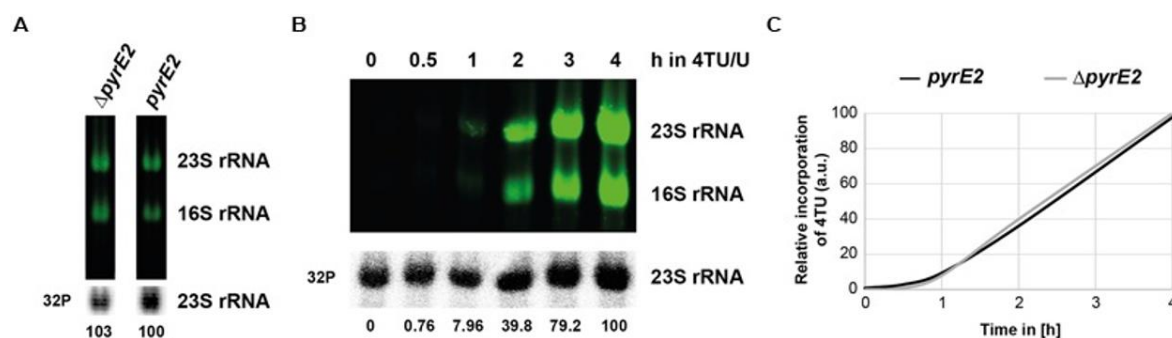


Figure 4.4 **Influence of pyrimidine *de novo* synthesis on overall 4TU incorporation.**

[A] 4TU incorporation in uracil auxotroph and prototroph strains (*pyrE2::HVO_0569*) over 8 h of exponential growth. [B] Time-dependent incorporation of 4TU in 16S and 23S rRNA in uracil prototroph strain. [C] Relative 4TU incorporation efficiency in auxotroph and prototroph cells. Results of relative quantification of 4TU incorporation in 23S rRNA from uracil auxotroph ($\Delta pyrE2$) (taken from Figure 4.3C) and from uracil prototroph (*pyrE2::HVO_0569*) B data are depicted.

The power of RNA labelling is to visualize RNA dynamics in response to genetic depletion/overexpression, compound addition, media change and more (Braun et al., 2020; Herzog et al., 2017). Regarding ribosome biogenesis, depletion of a biogenesis factor could show accumulation on rRNA precursors, however *H. volcanii* and *S. acidocaldarius* lack genetic tools such as the yeast Glucose/Galactose depletion system (Carlson, 1987). Thus a described change, the change of tryptophanase gene transcription after addition of L-tryptophan (Large et al., 2007) was tested in combination with 4TU pulse labelling. As a reaction to the addition of tryptophan, the cells elevate the expression of tryptophanase mRNA, which incorporates 4TU and can then be affinity purified as described in 7.2.5.7.2. The overall efficiency of purification and the enrichment of tryptophanase mRNA were tested in three setups described in Figure 4.5A. The biotinylated RNA was subjected to affinity purification and was then quantified via RT-qPCR. The addition of tryptophan leads to a 8-10 fold increase of tryptophanase mRNA in the input (Figure 4.5A) which is reflected in the Elution fraction in the right panel of Figure 4.5C. The overall enrichment of *de novo* synthesized RNAs is roughly 200-250 fold, here shown for highly expressed mRNAs such as the ribosomal protein L10 (left panel, Figure 4.5C).

Overall, the feasibility of affinity purifying bio labelled RNA provides a good toolset for the archaeal field and can be used for further investigations.

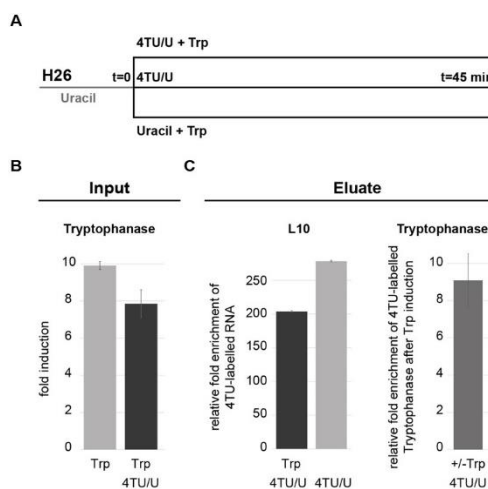


Figure 4.5 **Analysis of the transcriptionally regulated tryptophanase mRNA with 4TU.**

[A] Experimental work flow. Cells were grown in Hv-Ca⁺ medium containing uracil and lacking l-tryptophan. At the indicated time point ($t = 0$) cells were split and incubated for 45 min in presence of 4TU with or without 1 mM l-tryptophan (Trp) or Hv-Ca⁺ medium containing uracil and l-tryptophan. Bio-tagged RNA were purified by affinity purification and analyzed by RT-qPCR (see 7.2.2.8, 7.2.2.9 and 7.2.5.7.2 with primers oHv 402/403 (Trp), 404/405 (L10)). [B] Induction of tryptophanase transcription by l-tryptophan. Fold induction of tryptophanase in cells grown with Trp and with or without 4TU is depicted. Expression levels were normalized to the expression level obtained from cells grown without Trp. [C] Analysis of affinity purified 4TU-labeled mRNA. Left-panel: relative purification efficiency was obtained by comparing the enrichment of the housekeeping ribosomal protein L10 mRNA from cells labeled with 4TU with or without Trp and normalized to L10 mRNA from cells grown in absence of 4TU (background control). Right-panel: relative fold enrichment of 4TU-labeled tryptophanase after Trp induction were obtained by comparing the relative amount of purified 4TU-labeled tryptophanase after Trp induction and the relative amount of purified 4TU-labeled without Trp. Values were normalized to the amount of purified 4TU-labeled L10 mRNA obtained with and without Trp.

4.1.2 *In Vivo* RNA chemical foot-printing in archaea.

RNA is not only dynamically synthesized and degraded, but is always found bound to either Proteins, itself or both (Alberts, 2002, chap. 6). This leads to secondary, tertiary and quaternary structures that are especially important for functionality, e.g. in the ribosome. These structures can be resolved by methods such as crystallography, cryo-electron microscopy or NMR (Ameismeier et al., 2018; Ben-Shem et al., 2011; Waudby et al., 2013), but also by using RNA modifying chemicals such as CMCT, DMS, Kethoxal or Selective 2'-hydroxyl acylation (SHA[PE]) (reviewed in Weeks, 2010). These chemicals are able to modify RNA based on their nucleotide accessibility and/or flexibility, thus leaving a footprint of how the RNA is structured. An accessible non-base paired RNA nucleotide will be modified by the targeting chemical and can then be visualized by means of primer extension analysis or high throughput sequencing. This is mostly due to the addition of a bulky group at either the Watson-Crick interface of the base or at the backbone of the RNA. This bulky group then induces a primer extension stop (Youvan and Hearst, 1979).

I tried to adapt structural probing, using CMCT, DMS and Selective 2'-hydroxyl acylation for *H. volcanii* and, when mentioned, for *S. acidocaldarius*.

CMCT (1-Cyclohexyl-(2-Morpholinoethyl)Carbodiimide metho-p-Toluene sulfonate), relies almost exclusively on having Sodium Borate (Borax) in the Buffer when targeting naked RNA (Hartmann et al., 2014, chap. 10). *In vivo*, CMCT modification was not feasible for both archaea and previous

studies have shown that most cells are unable to take up the chemical and thus make it unsuitable for *in vivo* work (Harris et al., 1995; Mitchell et al., 2019). Damaged or lysed cells however can be modified by CMCT (Antal et al., 2002; Harris et al., 1995) and thus was adapted for our two archaeal model organisms. For *H. volcanii*, adding Borax to lysed cells in high Salt buffer (K1800) enabled CMCT modification *ex vivo* (method described in 7.2.5.6.1 and exemplary results are shown later in Chapter 2.3.1 in Figure 4.14). Yet, this did not work in *S. acidocaldarius*. A downside of CMCT is that it only modifies Uracil and Guanosine.

DMS can complement this gap (it modifies A and C) and works *in vivo* (Hulscher et al., 2016). However, *in vivo* modification was unsuccessful for *H. volcanii* (procedure described in 7.2.5.6.2) and *S. acidocaldarius* was not tested. The very harsh quenching conditions for DMS (high β -Mercaptoethanol and Isoamyl alcohol) led to the immediate disruption of the cells. Saturating the Isoamyl alcohol with salt water to avoid the osmotic imbalance did not amend this problem. This made pelleting or collecting of the cells impossible. *Ex vivo* whole cell extract DMS modification caused issues in the phenol extraction and most of the RNA was lost, most likely again due to the high Isoamyl/Saltwater concentrations. *In vitro* DMS probing was not used as it did not provide any additional benefits and the focus on base independent RNA foot-printing methods was prioritized.

Table 4.1 SHAPE reagent solubility in different cultivation medium.

Media	NMIA	1m6	1m7
Hv-casamino acids	Precipitate >6.5 mM	Soluble: max concentration tested ~13 mM	Soluble: max concentration tested ~6.5 mM
Hv-YPC	Soluble: max concentration tested ~6.5 mM	Soluble: max concentration tested ~13 mM	Soluble: max concentration tested ~6.5 mM
Saci-Brock	Soluble max concentration tested ~13 mM	Precipitate >6.5 mM	Not determined

The wide range of **SHAPE** (Selective 2'-hydroxyl acylation analyzed by primer extension) chemicals provided a versatile approach for our two archaeal model organisms. We decided on testing NMIA, 1m6 and 1m7 in both our model organisms. All three have been tested to work to some extent *in vivo* in *E. coli*, *S. cerevisiae* and Human cells (Spitale et al., 2013; Watters et al., 2016; Weeks and Mauger, 2011). They all target the RNA at the sugar backbone (see Figure 3.20), however compared to 1m6/1m7 the relative kinetic of NMIA is comparably low (30 min vs 5 min). Also, 1m7 is about ten times more expensive than 1m6. Since we wanted to use SHAPE chemicals *in vivo* it was crucial to test if the chemicals are soluble in the respective growth media used for *H. volcanii* and *S. acidocaldarius* (details shown in Table 4.1). The protocols for both organisms have been published (Knüppel et al., 2020). The high salt media was compatible with SHAPE chemicals, all three were soluble up to at least 6.5 mM. The low pH media was also compatible with the SHAPE chemicals but was not tested with 1m7. The overall better RNA quality and yield from *H. volcanii*

compared to *S. acidocaldarius* is also mirrored in the SHAPE results (Figure 4.6 and Figure 4.7 respectively).

Having established the SHAPE protocol in *H. volcanii*, we used it to answer further questions that arose in later experiments (see Chapter 4.2.4) and as a comparison to CMCT foot-printing (see Chapter 4.2.2.1.2). Concluding it can be said that SHAPE chemicals are very applicable for *in vivo* modification in both our archaea, especially in *H. volcanii*.

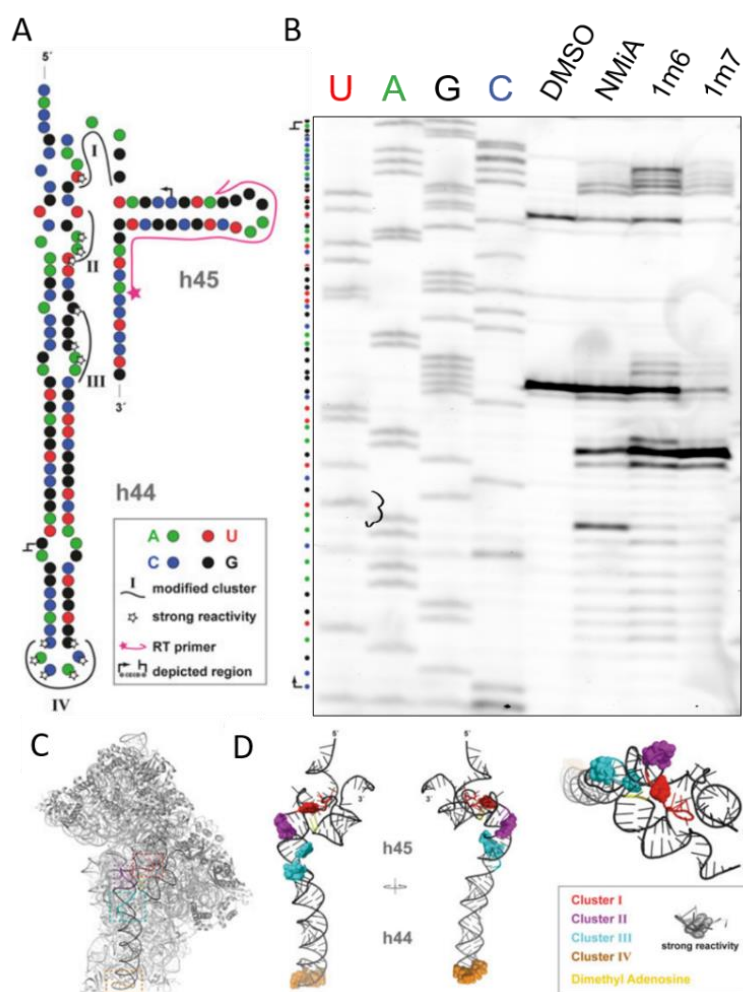


Figure 4.6 Exemplary *in vivo* SHAPE analysis of *H. volcanii* RNA using three different SHAPE reagents.

In vivo SHAPE analysis was performed with 6.5 mM (end concentration) of the indicated SHAPE reagent and analyzed by primer extension with an IR-Dye labeled primer complementary to the 3' end region of *H. volcanii* small ribosomal subunit 16S rRNA. **[A]** *H. volcanii* secondary structure model of the two most 3' end helices of the 16S rRNA, helix 44 and helix 45, is depicted. Nucleotides are color-coded as indicated in the figure panel. The depicted 2D RNA structure is adapted from the 16S rRNA 2D map from *H. volcanii* obtained at the Comparative RNA website (<http://www.rna.icmb.utexas.edu/>) (Cannone et al., 2002). Cluster and strong SHAPE-reactive residues are depicted as indicated in the figure panel. **[B]** Exemplary sequencing gel-based analysis of SHAPE reactivity. Dideoxy chain-termination reactions are shown on the left side. **[C]** Positioning SHAPE reactivity on the structure of the small ribosomal subunit from the archaeon *Pyrococcus furiosus* (PDB: 3J20) (Armache et al., 2013). Helix 44 and 45 are depicted in black. The corresponding SHAPE-modified clusters I–IV (color-coded) are depicted as indicated in the figure panel. **[D]** Close-up structure of *P. furiosus* h44 and h45 shown in different orientations. The corresponding *H. volcanii* *in vivo* SHAPE-reactive clusters I–IV (color-coded) and strong reactive nucleotides (sphere) and the dimethylated adenosines present in h45 were positioned in the structure of *P. furiosus* h44 and h45 (PDB: 3J20). Structural views were generated using Pymol. (reproduced from Knüppel et al., 2020)

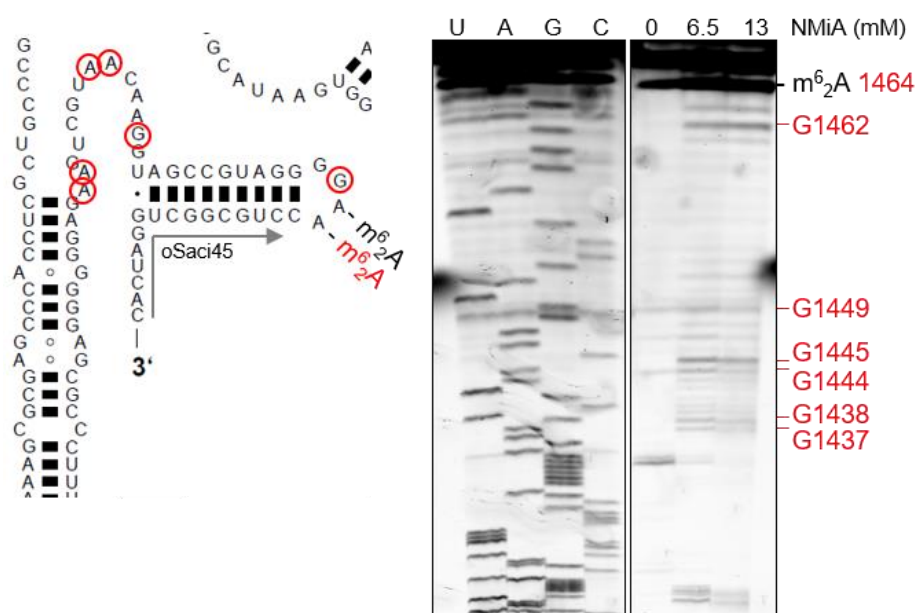


Figure 4.7 Exemplary *in vivo* SHAPE modification of WT *S. acidocaldarius* cells.

Primer extension region depicted covers the far 3' End of the 16S rRNA (helix 45) (Primer oSaci45 in grey). Decreased readthrough due to the dimethylations at 1464 and 1465. The SHAPE patterns are very likely from unmethylated precursor rRNAs that do not contain the methylation. 16S 2D structure modified from *S. solfataricus*, obtained at the Comparative RNA website (<http://www.rna.icmb.utexas.edu/>), accessible/modified nucleotides are marked in red.

4.2 A detailed analysis of the archaeal KsgA/Dim1 methyltransferase

In the following we investigated the small subunit biogenesis factor KsgA/Dim1 in our model archaea.

4.2.1 KsgA is not essential in three model archaea

As mentioned earlier the ribosome biogenesis factor KsgA, or Dim1 in eukaryotes, is present in all three Kingdoms of life. The structural conservation links the archaeal and the bacterial KsgA closer together, the eukaryotic is an overall larger protein with proposed additional functions during SSU biogenesis (Lafontaine et al., 1995; O'Farrell et al., 2008). The key structural domains that are typical for methyltransferases are present in all exemplary organisms (see alignment in introduction Figure 3.15).

This structural homology, the non-lethal deletion in *E. coli* and other bacteria, and the previously reported cross organism (B/A/E) and hybrid complementation analysis (Pulicherla et al., 2009) increased the hopes for a successful knock out in our two archaeal systems. For *H. volcanii*, the pop-in pop-out method (Allers et al., 2004) was used to generate a marker-less knock out. In Short, an upstream and a downstream region of the ORF of interest were amplified via PCR with the primers oHv091/92 and oHv93/94 respectively (see Figure 4.8). These two fragments were then assembled via PCR with the primers oHv091 and oHv094, resulting in a product that flanks the *ksgA* ORF but lacks the ORF in-between. This was then cloned into the pTA131 vector with KpnI and XbaI.

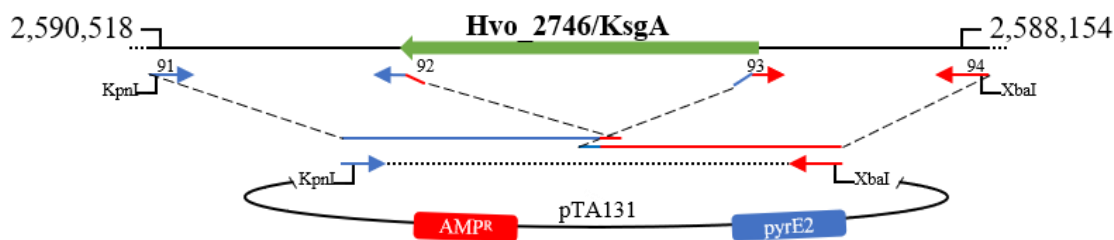


Figure 4.8 **Scheme for *ksgA* knock out cassette.**

Genomic region indicated; inner primers have 50 % overlapping region to each other. Outside primers contain matching cleavage sites to the pTA131 Vector. Linearized vector is depicted with shuffle selection markers.

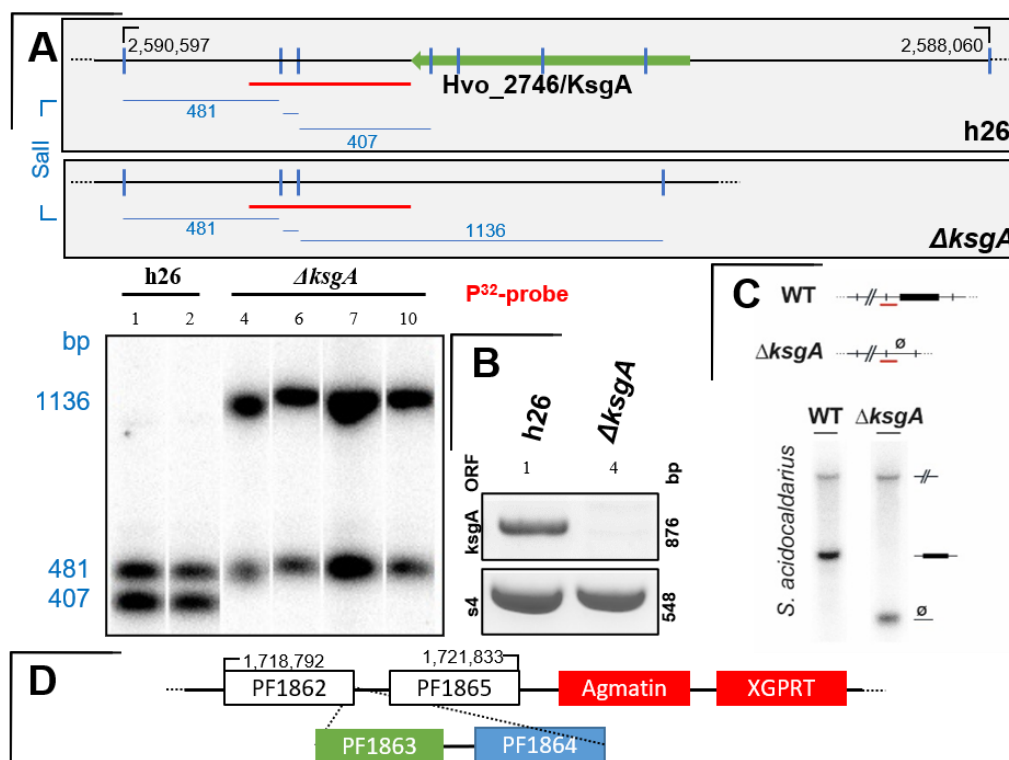


Figure 4.9 **Southern Blot and PCR Verification of Knockouts in *Haloferax volcanii* and *Sulfolobus acidocaldarius*.**

[A] The scheme shows the experimental setup in detail for *Haloferax volcanii* and is scaled to genomic distances. The genomic region is indicated by black lines, the crossing small blue bars indicate the Cut-Site of SalI and the blue lanes show the resulting fragment. The upstream PCR fragment (oHv091/092) was used as a probe (red). The ORF is depicted as a green arrow. The results from the P^{32} -probed membrane shows the differences between wild type and knock out. [B] shows an exemplary PCR verification of clone number 4. The *ksgA* ORF was amplified with oHv095/096, s4 with oHv126/127. [C] Southern blot for *Sulfolobus acidocaldarius* knock out, with less detailed scheme but similar procedure. [D] Construct for *Pyrococcus furiosus* knock out of *ksgA* (PF1863). The first construct included PF1864 which turned out to be a transposase that is present multiple times on the genome and made recombination impossible. Thus, the construct had to be modified and left out PF1864. The Construct was amplified in three PCR steps (using primers oHv512-517 and 528 and 529) and then assembled in two consecutive steps and then cloned into a TOPO blunt vector. Functional verification was done by PCR (data not shown) and screening for the loss of methylation, shown in Figure 4.10B.

After transformation, clones were given the chance to lose the integrated plasmid in uracil containing media over several re-dilution steps and by chance “popping out” the gene. These pop-out events were then selected on 5-FOA plates to ensure plasmid loss. To verify the knock out, each clone was subjected to southern blotting (Figure 4.9A) and PCR (Figure 4.9B). The gene deletion for *Sulfolobus acidocaldarius* was done in the Albers Lab in Freiburg, followed a similar method described in

(Wagner et al., 2012), and its verification is briefly shown in Figure 4.9C. Additionally, a KO in *Pyrococcus furiosus* was created in cooperation with Dr. Winfried Hausner of the Microbiology department and is essentially described in (Kreuzer et al., 2013; Waege et al., 2010). The plasmid design is shown in Figure 4.9D. Fortunately, the gene encoding for the KsgA homologue is not essential in all three archaeal model organisms. Providing a great opportunity to investigate the functional conservation of this methyltransferase in more detail.

4.2.2 The functional conservation of archaeal KsgA/Dim1

4.2.2.1 Abnormal methylation status in *Haloferax volcanii*

Having created and verified the knock out on a genomic level, the expected functional effect should be visible by analyzing the absence of the dimethylation of the two adenosines (Hv: A1451, A1452, Ec: A1518, A1519) in the helix 45 of the 16S rRNA. The method of choice is to transcribe cDNA with a labelled primer off the extracted RNA and separate it on a denaturing Acrylamide gel. The two bulky methylations prevent the reverse transcriptase (**RT**) from transcribing the RNA further and results in a distinctive primer extension stop in front of the first encountered dimethylated Adenosines, illustrated in Figure 4.10A.

Thus, the confirmation of the KO of *ksgA* would be the absence of the Methylation on the adenosines and thus read through of the reverse transcriptase. The RNA was extracted from exponentially growing cells as described in 7.2.5.1 and primer extension was performed as described in 7.2.5.5 and run on a small Novex Gel. When comparing the wild type to the KO lanes in Figure 4.10B all three archaea: *Hv*, *Saci* and *Pfu* cells show no primer extension stop at the Adenosines, similar to the KO control in *E. Coli* (Baba et al., 2006). The striking difference however is the methylation pattern we see in the h26 WT cells of *H. volcanii*. There are two primer extension stops, one for each dimethylated adenosines. This unexpected banding pattern has been reproduced many times on different gel systems, temperature stress (Figure 4.10D), as well as with different reverse transcriptases (Figure 4.10C), to exclude any artifacts. However, at lower extension temperature the reverse transcriptase (e.g. Invitrogen M-MLV-RT) struggles to read through the highly structured rRNA and thus the second extension stop is less visible. In order to verify the correct position of the stop, it was run next to a sequencing reaction (Figure 4.10E). Consider that the methylation induces a primer extension stop in “-1” to the actual methylated nucleotide, while the sequencing ladder shows the incorporated ddNTP, i.e. the actual nucleotide.

The readout by primer extension however cannot resolve the exact methylation status of the individual adenosines and only shows an overall population. So, it most likely shows a heterogeneous population of **methylated** Adenosines, i.e. a mixture of **AA**, **AA**, and/or **AA**. A major population with non-methylated Adenosines can be excluded because: 1) they are only present in very low abundance, i.e. earlier precursor particles that have not undergone KsgA-dependent methylation yet and 2) this would be visible in an ddCTP stop in the wild type run, which it is not (Figure 4.10B). As

indicated in Figure 4.10A there is no G in between the primer and two adenoses, resulting in a RT stop after the Adenosine when using ddCTP, i.e. readthrough of unmethylated populations (precursors). Additionally, direct RNA sequencing on an Oxford Nanopore platform in wild type cells showed that only precursors are unmethylated in the wild type (Grünberger et al., 2020).

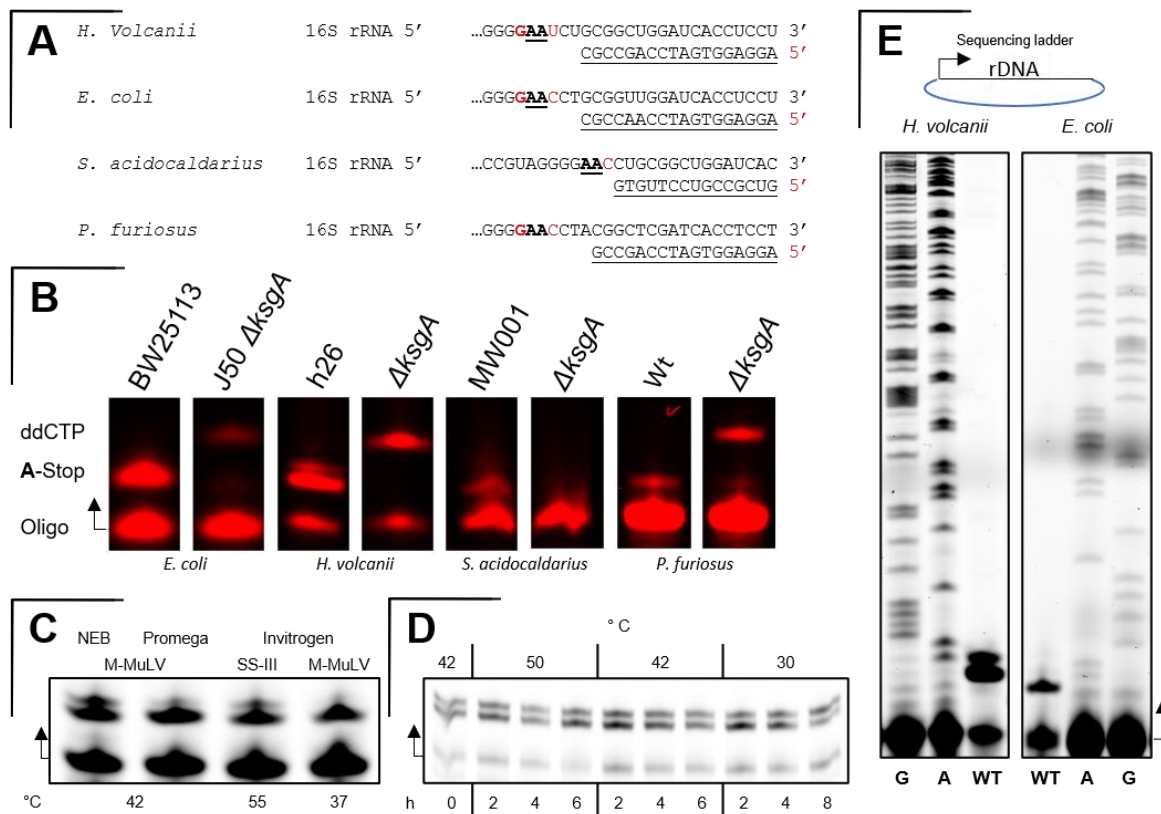


Figure 4.10 **Primer extension analysis of Knock out and Wild type constructs in four Organisms.**

[A] Illustration of Primer extension reaction in *Haloflex volcanii* (oHv356), *E. coli* (oHv357) and *S. acidocaldarius* (oSaci045) and *P. Furiosus* (oHv518). All primers are labelled at the 5' end with a UV Dye, DY682. Dimethylated adenoses are bold underlined, proposed Primer extension stop and ddCTP stop are marked red. Unless stated otherwise, every primer extension was done with Superscript III from Invitrogen at 55 °C extension temperature. (method described in 7.2.5.5)[B] Primer extension (NTP mixture (1 mM each), dA-,T-,GTP and ddCTP) readout from different organisms, directionality is indicated by an arrow, primer extension stop in front of the first A and the incorporated ddCTP stop is also indicated, i.e. visible ddCTP stop = unmethylated adenoses. Roughly 80 ng of cDNA was loaded onto each lane. In *S. acidocaldarius*, the reaction with ddCTP did not work, thus was run without ddCTP and all dNTPs (1 mM each). [C] Test of various reverse transcription kits, extension temperature and manufacturer are indicated. RNA input was the same (~1 μ g) for each (load ~80 ng per lane). [D] Temperature dependent test of methylation pattern under high and low temperatures over one and two doubling times. Cells were not diluted before temperature shift, but distributed to pre-warmed flasks. [E] Sequencing reaction to map the predicted primer extension (Hv: oHv324, Ec: oHv325) stops. Keep in mind Sanger sequencing reactions tend to stutter the first few nucleotides. Top shows sketch of plasmid containing the rDNA of the respective organism, arrow indicates the respective primer (Hv: rDNA reporter plasmid from (Jüttner et al., 2020) and Ec: pHK-rrnC⁺ from (Asai et al., 1999b).

In conclusion these results suggest, that in the case of *Haloflex volcanii*, the 16S rRNA does not show the genuine/classical dimethylation status. Leading to the question, if on the one hand the enzyme itself might be not be suited to completely methylate its target or is available in insufficient amounts or on the other hand the substrate in the highly conserved 3' minor domain of 16S rRNA is somehow different and thus leads to this specific pattern.

4.2.2.1.1 Complementation and overexpression does not resolve the abnormal methylation pattern

To distinguish the two possibilities of this abnormal methylation pattern, I first used the pTA1228 vector with a tryptophan inducible promoter to complement the *ksgA* knock out and/or overexpress the gene in Wild type cells. As a control, a point mutation was introduced (with oHv239/240) that leads to a change from Glutamate to Alanine at position 84 in the catalytic center of the enzyme and thus is expected to inhibit the methylation reaction (see Figure 3.15). These N-Terminal His₍₆₎ tagged constructs under control of a tryptophan inducible promoter (**pTna**) were then transformed as described in 7.2.1.2.1 into either the $\Delta ksgA$ cells or hv1424 Wildtype cells and grown in Hv Ca⁺ Media. Induction intensity can be varied by the addition of tryptophan (Trp). The comparable concentration of Trp in Hv-YPC, i.e. “baseline”, concentration of Trp is at around 0.25 mM, however, most likely higher than the endogenous levels of KsgA in the cells. The effect of concentrations from 0.25, 1, 2 and 4 mM Trp were tested for growth and western blot detectability. We noticed toxic effects from concentrations of ≥ 2 mM leading to growth effects in any construct (data not shown), thus 1mM was chosen as a good compromise between detectability and toxicity (data not shown).

In order to be independent of effects that may arise from tryptophan induction we also used different strong promoters, the rDNA Promotor **P2** from *H. cutirubrum* (Jolley et al., 1996), as well as the ferredoxin promoter **Pfdx** from *H. salinarum* (Gregor and Pfeifer, 2005), that were then used with differently tagged KsgA: N-His₍₆₎-ProteinA. As seen in Figure 4.11, the methylation pattern stays the same in the presence of overexpression of KsgA, the wild type complementation leads to similar results as in the Wildtype (h26) strain. P2 and Pfdx induction of His₍₆₎ tagged constructs and pTna with N-His₍₆₎-ProteinA lead to the same results (Data not shown).

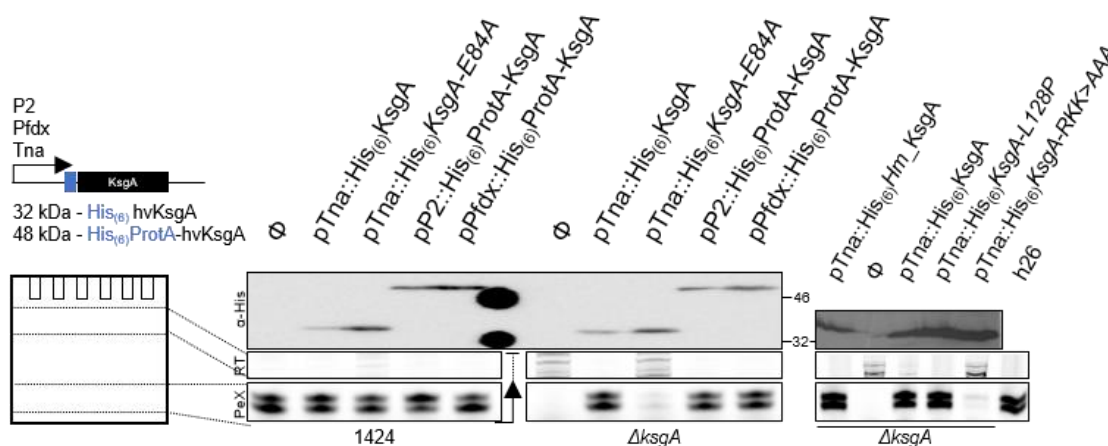


Figure 4.11 **Overexpression and complementation lead to similar results as the wild type.**

For each lane 2 OD of exponentially growing cells were used for either Protein- or RNA extraction. For good western detectability 10 % of the extract were used (as described in 7.2.3.5, 7.2.3.11 and 7.2.3.12). 1 μ g of RNA was used for Primer extension, ~ 80ng was then loaded onto each lane. Primers have been cropped off. The readthrough (RT) indicated on the upper level of the gel has an increased gain compared to the PeX, to increase visibility. Big black blobs on the western blot indicate the location of the 32 and 46 kDa band of the ladder.

The catalytic mutant shows little to no methylation in the KO and a slight dominant negative effect (reduction of methylation) on the wild type, by competing with the endogenous KsgA for the same substrate. Additionally, mutations that decrease binding affinity to the 30S Subunit in *E. coli* (231-RRK to AAA, oHv346/347) (Boehringer et al., 2012) and a mutation of a Lysine at position 128 (oHv344/345) to a Proline that leads to a monomethylation instead of dimethylation in *E. coli* (O'Farrell et al., 2012) were introduced (see red arrows in alignment Figure 3.15). KsgA from *Haloarcula marismortui* (*Hm*) was also cloned into our expression system (oHv369/370), to test cross-halophile archaeal complementation. As shown in the lower right of Figure 4.11, the L128P mutation as well as the *Hm* complementation show almost wild type results. The results for the L128P mutation, are unclear as a change from m₂⁶A to m⁶A would not display RT primer extension stops since single m⁶A requires very specific reverse transcriptases (Harcourt et al., 2013; Wang et al., 2016) or antibodies (Weichmann et al., 2020). Indicating that L128 in *H. volcanii* might not have the same function as in *E. coli* regarding the discrimination between mono- and dimethyltransferase activity. In contrast, the RRK>AAA mutation, which presumably impairs the binding affinity to the SSU, shows a massive reduction in methylation, almost comparable to the E84A catalytic dead mutant, but still two faint bands are visible.

Together these results suggest that, *in vivo*, the addition of excess amounts of biogenesis factor does not lead to a complete methylation of the two hypomethylated adenosines.

To further test, if the ratio between substrate and KsgA has an effect on the methylation pattern, I next tried to reconstitute the dimethylation reaction *in vitro* by using crude whole cell extract/lysate (WCE) and purified 30S subunits as a template for recombinant HvKsgA. Perhaps, having a defined, finite pool of substrate enables complete dimethylation. The idea being that the recombinant protein can re-associate to an already heterogeneously dimethylated 30S subunit and perhaps, given enough time, homogeneously dimethylate both Adenosines.

Interestingly, the halophile protein could be purified with higher yields in a low salt buffer compared to a high salt buffer (see Figure 4.12A). However, this was discovered later and all of the following experiments, if not noted otherwise, were done with high salt purified HvKsgA.

The *in vitro* reconstitution was performed as described in 7.2.3.8. In short: cleared cell lysates and separated 30S subunits were subjected to excess recombinant HvKsgA-His₍₆₎ or HvKsgA-E84A-His₍₆₎ (Figure 4.12A) in the presence or absence of SAM for 60 minutes at 42 °C. The extracted RNA was then used for primer extension analysis and the extracted protein was loaded onto a SDS-PAGE (Figure 4.12B). The lower gel picture in Figure 4.12A shows the impurities that come along in the high salt purification, since this does not influence the overall reaction and especially them being *E. coli* proteins they should not function/denature in the high salt environment. The *in vitro* reconstitution worked well on the WCE and the 30S subunit (Figure 4.12B, lane 3 and 5), yet did not result in full homogeneous dimethylation but rather the previously observed methylation pattern

surrounding stem, some differences become notable (Figure 4.13A) and previous work has suggested the structural importance of h45 for methylation (Formenoy et al., 1994; Van Buul et al., 1984; Vila-Sanjurjo et al., 1999). The nucleotide adjacent to the 3' methylated adenosine is changed from a C to a U in *H. volcanii*. But is one nucleotide enough to induce such a drastic difference in the substrate? Ribosomal RNA is notorious for its complex secondary structure, could this point mutation influence the structure of the helix? When running a secondary structure prediction, *E. coli*, *S. acidocaldarius* and *P. furiosus* show a Watson-Crick G-C base-pair at closing of the stem. In *H. volcanii*, however, this consists of a non-Watson-Crick G-U-wobble (Figure 4.13B). According to the prediction modelling, this single base mutation supposedly leads to a loose/flexible or open conformation of the h45. This structural prediction however does not take the RNP context into account.

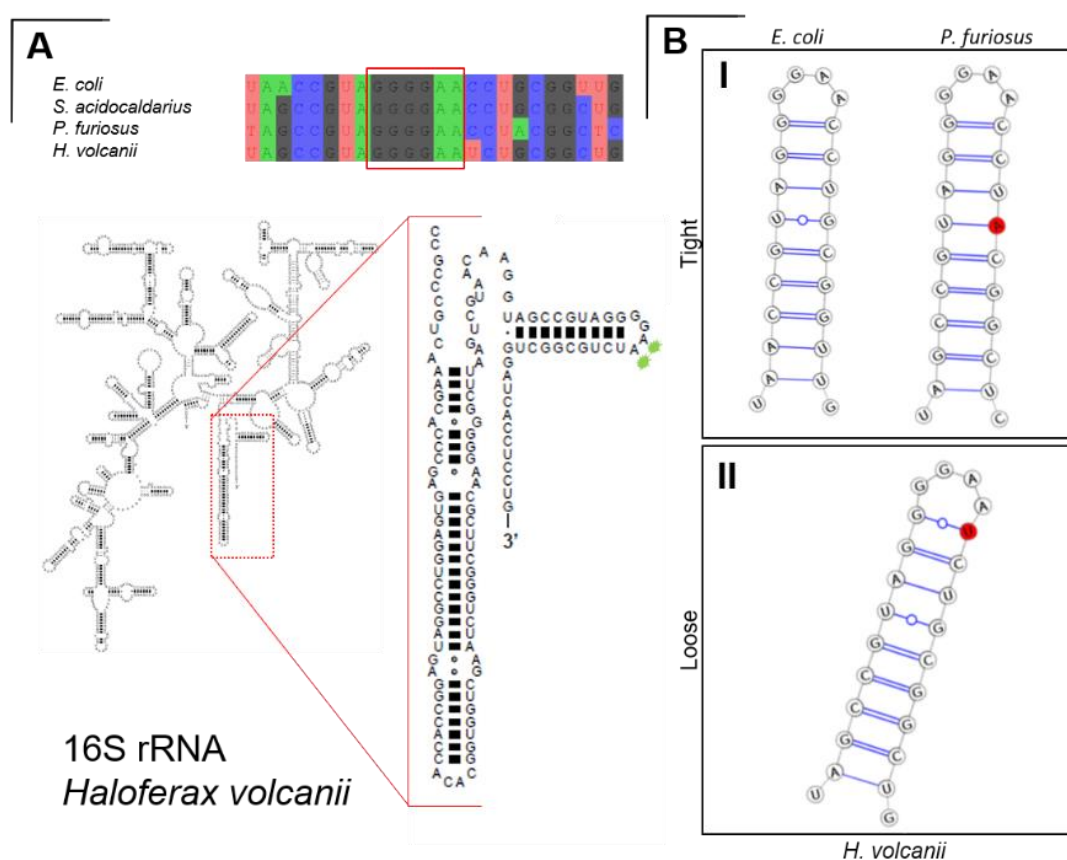


Figure 4.13 **Alignment and RNA fold prediction of helix45 of the 16S rRNA.**

[A] Shows a sequence alignment of the h45 including the stem, differences are marked with different colors. GGGAA loop is marked in red. Closeup of the 16S rRNA, h44 and h45 in view, dimethylated adenosines indicated in green. [B] RNA fold predictions from IPKnot (Sato et al., 2011). Type I: the tight loop in *E. coli* and *P. furiosus* and Type II the loose/flexible loop found in *H. volcanii*.

With help of the established RNA chemical foot-printing methods (see 4.1.2) we could verify these prediction using CMCT and SHAPE reagents (1m6, NMIA). The opening of the helix, at U1453 (Hv numbering) shows good modification in all cases, however the corresponding G1448 is only clearly visible in the 1m6 modifications (see Figure 4.14). Indicating a more flexible nucleotide 3' of the GGAA tetraloop compared to the adjacent one (G1448). Interestingly the U1445 modification is lost in the RNP context in all modification reactions, the corresponding wobble pair G1456 sits

immediately after the primer and is overlapping in signal but does show signals in both CMCT, 1m6 and NMIA particle modifications. The high reactivity of the SHAPE chemicals leads to unspecific modification in the naked RNA and never modified U1445 and U1439 in the RNP context.

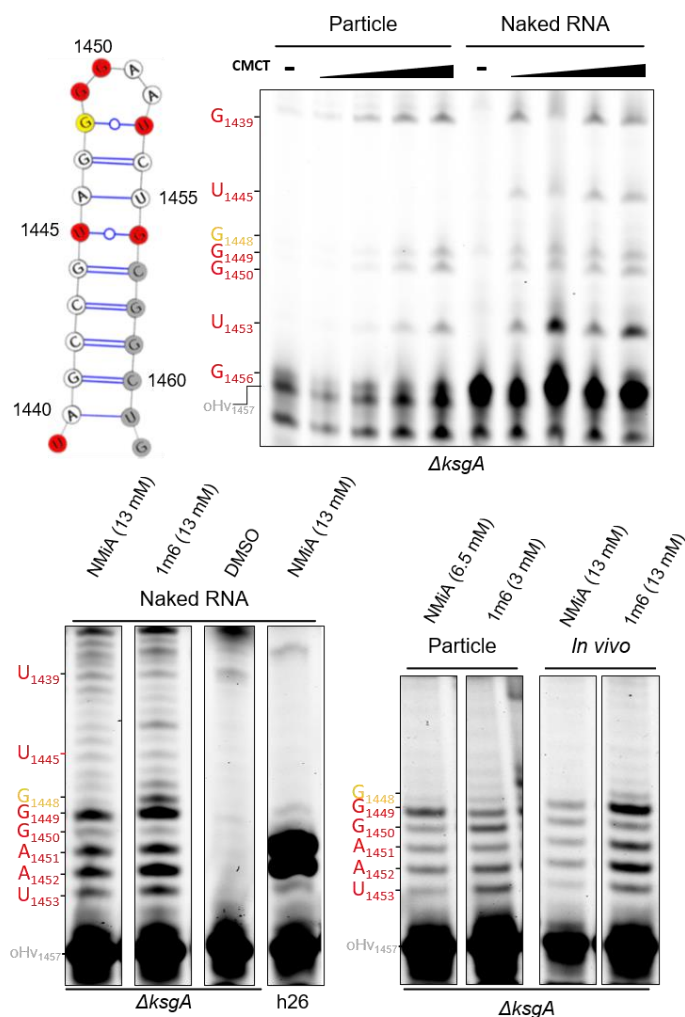


Figure 4.14 RNA foot-printing and mapping to 2D structure prediction.

All primer extension reactions were amplified with primer oHv324. Each nucleotide was mapped to a sequencing ladder with the equivalent primer but were excluded from the image. CMCT modification (as described in 7.2.5.6.1, ~500 ng per lane), SHAPE reactions (5 μ g of modified RNA was used as input and ~1 μ g of cDNA was loaded onto the gel). SHAPE foot-printing was initially performed by Martin Fenk and reproduced by me.

Overall, the 2D structure prediction could be experimentally verified. To find out if this structural change truly is the culprit to the methylation pattern in *Hv* we set out to look for other organisms that have a similar h45 conformation.

4.2.2.1.2.1 Comparison of methylation status in other archaea

The highly diverse archaeal kingdom provided many options to choose representative organisms from. To check the predicted structures, we included organisms that were available at the “Archaea Center Regensburg”, the remaining were chosen randomly as representative organisms for certain Orders. The trees were built on the inner sequence of the helix 45, e.g. *E. coli*: CCGUAGGGGAACCGCGG. This resulted in best grouping compared to using the whole helix45

sequence (+3nt on each end), as here the nucleotide variance is higher, but this did not affect the predicted structure (base/wobble pairing). Structure prediction however worked best when using the whole helix45 sequence. Among the 37 sequences 28 grouped very well together, the remaining 9 were highly variable and were put into a separate tree (see Figure 4.15). The largest group, even including two Asgard archaea, could be mapped to the genuine/classical helix45 structure, of which 3 archaeal primer extensions confirm the structure dependent single primer extension stop (see Figure 4.15 upper right in shades of cyan). The second group is inhabited solely by the Thermococcales (Figure 4.15 in red) and is missing the wobble at position 7 (respective to the depicted stem). Here I could verify the methylation status in *P. furiosus*. For the non-genuine/classical heterogeneous stop we could group three orders together and could verify two with primer extensions (see Figure 4.15 lower right in shades of green). The outlier tree consisted of 7 archaeal organisms and 1 bacteria (*B. subtilis*) (plus *E. coli* as root). Interestingly, *Haloarcula marismortui* needed to be split into two separate sequences as there is a mutation one of the three rDNA operons (A, B and C), which includes a second Wobble at position 6 (rRNA-A). The primer extension reactions were excluded due to concerns that the cultures were contaminated with *H. volcanii* as the results were not reproducible and many in the lab reported contaminations. *B. subtilis* also shows an additional wobble at position 9, yet this appears not to affect the primer extension profile. In *Methanocaldococcus jannaschii*, there is no visible difference in structure but there is a high rate of base exchanges, that apparently does not affect the primer extension profile. The remaining two organisms show an unusual variability in structure: *Nitrososphaera viennensis* has an additional wobble at position 4 and *Candidatus nanosalinarum* even shows an open confirmation at position 7. Yet, for both no biomass or RNA was available at the time.

When reviewing the phylogenetic classification of helix45, it can be said that there is a very high sequence and structural variance in this otherwise highly conserved structure of the helix. Yet, only the structural change in *H. volcanii* and other Halophiles/methanogens Class II show a difference in the methylation pattern. In other words, it appears that the mutation and structural changes in other organisms do not affect the methylation or the cells have adapted to the different substrate. For example the loss of W7 shows a great reduction of methylation *in vitro* in *E. coli* (Formenoy et al., 1994), but when looking at *P. furiosus* where this is the native structure it seems to have no negative effect on methylation (Figure 4.10B). Thus, I was interested to test if changing a single base-pair is sufficient to alter the methylation pattern *in vivo*.

4.2.2.1.2.2 *H. volcanii* and *P. furiosus* H45 mimicry using an *E. coli* rDNA shuffle strain

An ideal system to test our substrate induced methylation pattern, is the genomic rDNA knock out strain in *E. coli* (Asai et al., 1999b, 1999a), which can be shuffled with a second rDNA plasmid that contains the desired mutations. We received the strains AVS69009 and shuffle plasmid from the Vila-Sanjurjo lab in Spain (Schuwirth et al., 2006). Interestingly they have already created a mutation that fits the open loop confirmation C1520U (*E. coli* numbering), but did not comment on it (Schuwirth et al., 2006). Additionally, a mutation G1523A (no-W7) that omits the wobble at position 7 and reduces the methylation *in vitro* (Formenoy et al., 1994) was created. The “wild type” strain carried a plasmid (pHK-rrnC⁺) containing the rDNA operon (rrnC) and a KAN^R selection marker (Figure 4.16A). The shuffle plasmids (pHK-rrnC) is a modified version of the pHK-rrnC⁺ plasmid that contains a mutation at C1192U, that induces a spectinomycin (Spc) resistance (Makosky and Dahlberg, 1987) as well as KAN^R is replaced by AMP^R. The vector shuffling procedure is described in Figure 4.16D and the description therein. As shown in Figure 4.16B we can see that by introducing G1520U we could recapitulate the double banding pattern we have observed in *H. volcanii*. The loss of the wobble at 1523A retained the single primer extension stop as seen in *P. furiosus*, but in some cases showed more readthrough and weaker methylation signals, i.e. higher population of unmethylated 16S rRNA, when using ddCTP readthrough controls (Figure S 5).

An interesting side note is that the introduction of the G1520U leads to a migration shift over the first ~10 nt, in the both small and large gel system and thus leads to the primer extension stop running higher/slower, although the number of nucleotides stay the same. This is also visible on a DNA level by looking at the sequencing ladder in Figure 4.16C of the two rDNA variants G1520U and G1520, where the two Adenosines and the four Guanines run differently, thereafter running behavior is normal and all stops run at equal height. This is especially visible when co-expressing the rDNA rrnC and pHK-G1520U with both plasmids present and having both stop patterns in one lane (Figure 4.16B, lane 4).

To reproduce the observed reduction of methylation (*in vitro*) from loss of the wobble at position 7 by Formenoy et al., 1994, I wanted to introduce a *ksgA* knock out in the initial AVS69009 strain. This would enable to shuffle in various rDNA mutations while retaining the helix from methylation for downstream reconstitutions via plasmid complementation *in vivo* or *in vitro* reconstitution. In both cases it would enable to compare the appropriate enzyme to the target substrate, e.g. PfuKsgA on pHK-rrnC-1192U-G1523A vs PfuKsgA on pHK-rrnC⁺ and compare it to EcKsgA. Two methods were tried, P1 transduction and kasugamycin (ksg, 250 µg/ml) induced resistance by either rDNA mutation or mutation of the KsgA gene (Helser et al., 1972; Vila-Sanjurjo et al., 1999). The latter provided several dimethylation deficient cells but only one showed a mutation in the ORF of the gene resulting in a longer PCR product, the rest were most likely rDNA mutations (as described in Vila-Sanjurjo et al., 1999), and thus unsuitable for the experiment (Figure 4.17).

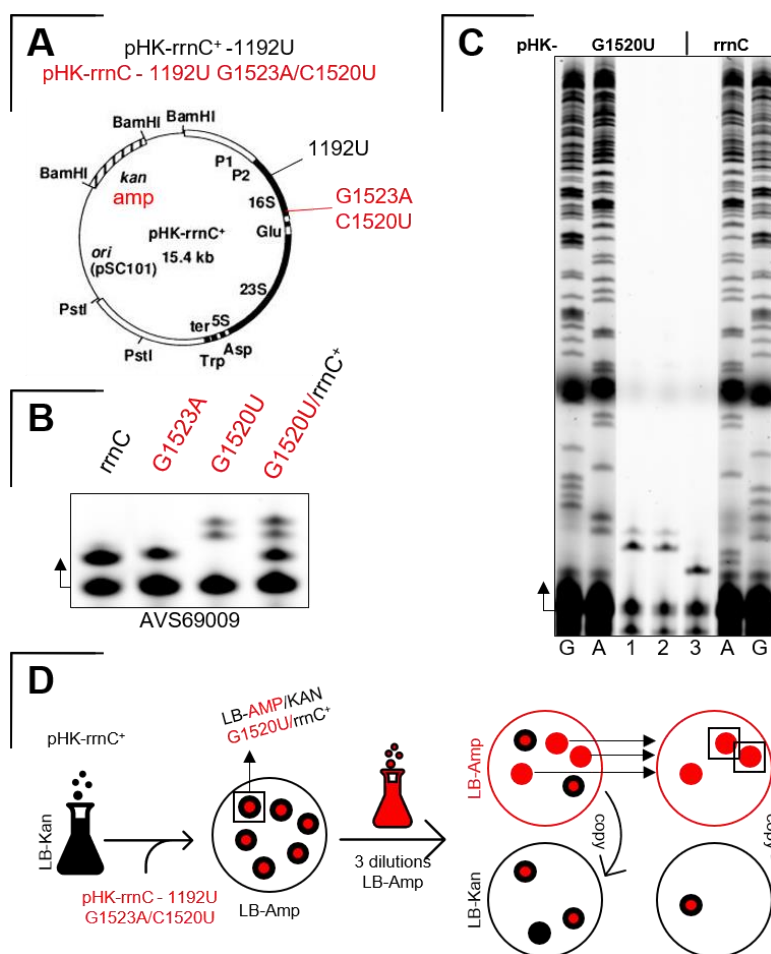


Figure 4.16 *E. coli* rDNA mutants produce predicted methylation pattern.

[A] Plasmid map of pHK-rrnC⁺, modified from (Asai et al., 1999b). Shuffle plasmid differences marked in red. [B] Primer extension readout of the various rDNA mutants from exponentially growing cells. G1520U/rrnC were co-expressed (AMP/KAN) from both plasmids. [C] Sequencing ladder on the plasmids that were transformed into AVS69009 cells. The signal of the Sequencing ladder lanes was increased. [D] rDNA-Vector shuffling schematic in AVS69009 cells. AVS69009::pHK-rrnC⁺ (Black, KAN^R) were grown in LB-KAN and made competent (as described in 7.2.1.1.1), either pHK-rrnC - 1192U G1523A or pHK-rrnC - 1192U C1520U (Both red AMP^R) were then transformed onto the cells and selected on LB-AMP plates. Both point mutations to the plasmid were introduced with the respective primer pairs oHv382/383 and oHv384/385. Transformants were picked and either inoculated in LB-KAN+AMP for co-expression of both plasmids (G1520U/rrnC⁺ in (B)) or inoculated in LB-AMP for 3 sequential over night dilutions and then spotted onto another LB-AMP plate. This plate was then copied to an LB-KAN plate. KAN^S-transformants were then spotted onto a LB-AMP+Spec plate. For final verification, this plate was once more cloned to a LB-KAN plate. The KAN^S-AMP^R-Spec^R clones (squared) were then used for the experiments in (B).

This methylation deficient strain could now be further used for *in vitro* or *in vivo* complementation experiments in a varying context helix 45 compositions using the rDNA shuffling system. Unfortunately, after transforming the appropriate plasmids carrying the desired rDNA mutations, the AVS69009^{ksg250} cells became very unstable and could not be transformed with an expression plasmid carrying the Pfu- or ECKsgA gene on an pBAD33-GM (arabinose inducible, gentamycin resistance) plasmid. Interestingly the transformation efficiency of the rDNA plasmid containing 1523A was noticeably lower compared to 1192U and 1520U (data not shown).

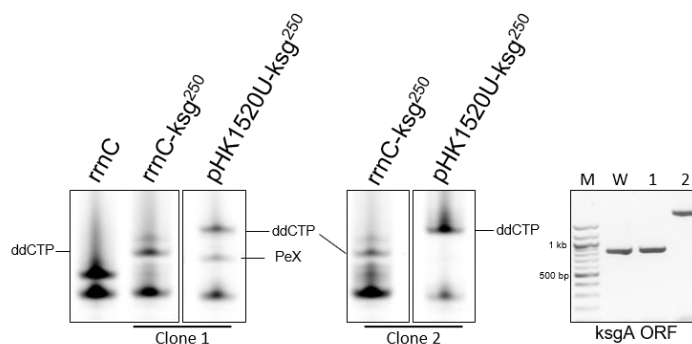


Figure 4.17 **Kasugamycin induced KsgA deficiency.**

AVS69009 cells with pHK-rrnC were subjugated to 250 μ g/ml kasugamycin. To test for rDNA mutations pHK-1520U was transformed to knock out candidate. Clone 1 shows light primer extension stop with transformed new rDNA, indicating rDNA mutation. Clone 2 shows no primer extension stop, thus endogenous ksgA should be deficient or mutated and can be seen in the PCR on the right. KsgA ORF was amplified using oHv596/597. **M** 100 bp ladder, **W** AVS69009 pHK-rrnC, **1** Clone 1, **2** Clone 2.

While we were no experts in *E. coli* gene deletion, we chose P1 transduction (see 7.2.1.1.3) as a suitable method due to the availability of the KEIO knock out strain. The J50 Δ ksgA strain from the KEIO collection was chosen as donor strain for P1 transduction. P1 transduction relies on the availability of RecA in the cells, unfortunately RecA is deleted in the AVS69009 cells to avoid genomic reintegration of the plasmid rDNA. Thus, recA was cloned into the pBAD33-GM vector to provide RecA during the transduction to enable recombination. This also failed, probably due to the AVS69009 cells being ara⁺ and prefer arabinose carbon source over promotor binding and thus no production of RecA is possible (or detectable via western blot, data not shown).

In the end both methods failed, and we were unable to test the dependency of the corresponding helix to the organisms specific KsgA.

4.2.2.1.2.3 H45 mimicry with the rDNA-reporter assay in *H. volcanii*

After having introduced the Hv-Type h45 into *E. coli*, I wanted to see if *Haloferax volcanii* would be able to accept the Ec-Type h45 and others as a substrate for methylation. Here I made use of our *cis*-acting rDNA reporter system (Jüttner et al., 2020), that enables the introduction and quantification of plasmid borne rRNA. The rt-PCR readout is briefly described in Figure 4.18B and in detail in (Jüttner et al., 2020). We introduced two tight loop mutations U1453C (*Ec*-like) and G1448A (*N. viennensis* opening A-U) and one “very open” loop with two mutations G1448C, U1453C (see Figure 4.18A). The U1453C mutations leads to the additional band visible that is corresponding to the *E. coli* results (compare Figure 4.18C with Figure 4.16B). The G1448A mutation shows no difference, but whether there is an overlapping signal, or the substrate is not suitable cannot be said. The large opening double mutation (G1448C, U1453C) leads to decreased levels of plasmid encoded rRNA, but there is also no change visible in the primer extension pattern as in the G1448A mutation.

Overall, we can summarize that the rRNA sequence/structure has an impact on the methylation pattern introduced by KsgA. This highly conserved 3' end of the 16S rRNA shows a vast structural diversity in many organisms, yet its modifying enzyme is highly conserved in its essential domains.

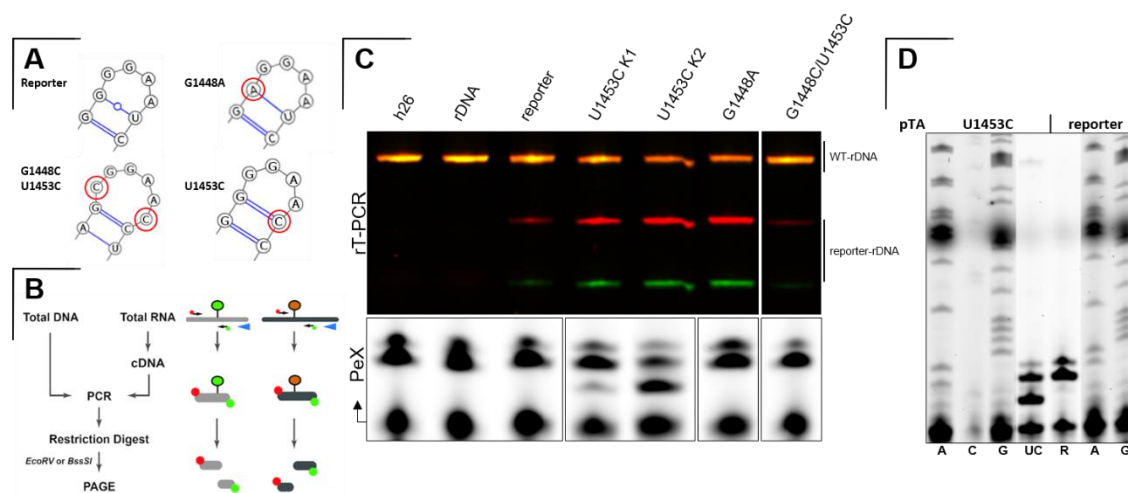


Figure 4.18 **Reporter rDNA can be methylated *in vivo*.**

[A] Shows the variants that were introduced. Point mutations were introduced by PCR via the primers (*f/r*): G1448 (oHv361/362), G1448C U1453C (oHv363/364), U1453C (oHv359/360) and amplified with the flanking primers oHv255/236. Amplicons were subcloned into a TOPO-Blunt Vector for verification and exchanged in the reporter vector via *PciI/BspHI* [B] Provides the schematics for the readout procedure of the reporter assay. [C] Shows the readout of the reporter assay with cDNA RT primer oHv040 and following PCR (24 cycles: oHv305/306) after *EcoRV* digestion. H26 and the rDNA plasmid do not carry this *EcoRV* cleavage site. The reporter and its modification carry the *EcoRV* mutation and result in the red and green band, indicating expression of the plasmid rDNA. The lower panel shows the primer extension readout, with the additional bands for the U1453C mutations. [D] Shows the primer extension alongside a sequencing reaction for the according plasmids. The signal of the Sequencing ladder lanes has been increased. UC: U1453C R: wt-rDNA-Reporter.

4.2.2.2 Binding and release assay of hvKsgA to the SSU

In yeast and perhaps human the release of Dim1 from the 40S subunit has been proposed to require assistance from other factors such as Fap7/hCINAP (Ghalei et al., 2017; Loc'h et al., 2014). In *E. coli* however, full methylation of both adenosines has been proposed as a passive dissociation requirement for KsgA from the maturing 30S subunit (Boehringer et al., 2012; Connolly et al., 2008; O'Farrell et al., 2012). Additionally, *E. coli* is devoid of any functional/sequence homologues factors to Fap7. With *H. volcanii* having this heterogeneous state of methylation it was interesting if/how the dissociation occurs and if a Fap7 homologue might be involved.

Fortunately, our previous experiments have already shown that *in vitro* reconstitution of methylation on whole cell lysate and 30S particles works (see Figure 4.12). Thus, we used a setup similar to the *in vitro* reconstitution assay (7.2.3.8, as lane 2 Figure 4.12), with a restricted reaction time of 30 minutes to avoid residual intracellular SAM to release KsgA (similar to Connolly et al., 2008). Consequently, after methylation, HvKsgA should not be detectable on the 30S subunit anymore. The reaction was then loaded onto a 5-30 % Sucrose gradient as described in 7.2.3.7. To increase confidence of association to the 30S particle, we used cells expressing a His tagged ribosomal protein (*ΔksgA::pTna::His₍₆₎-S7*) (see Figure 4.19A).

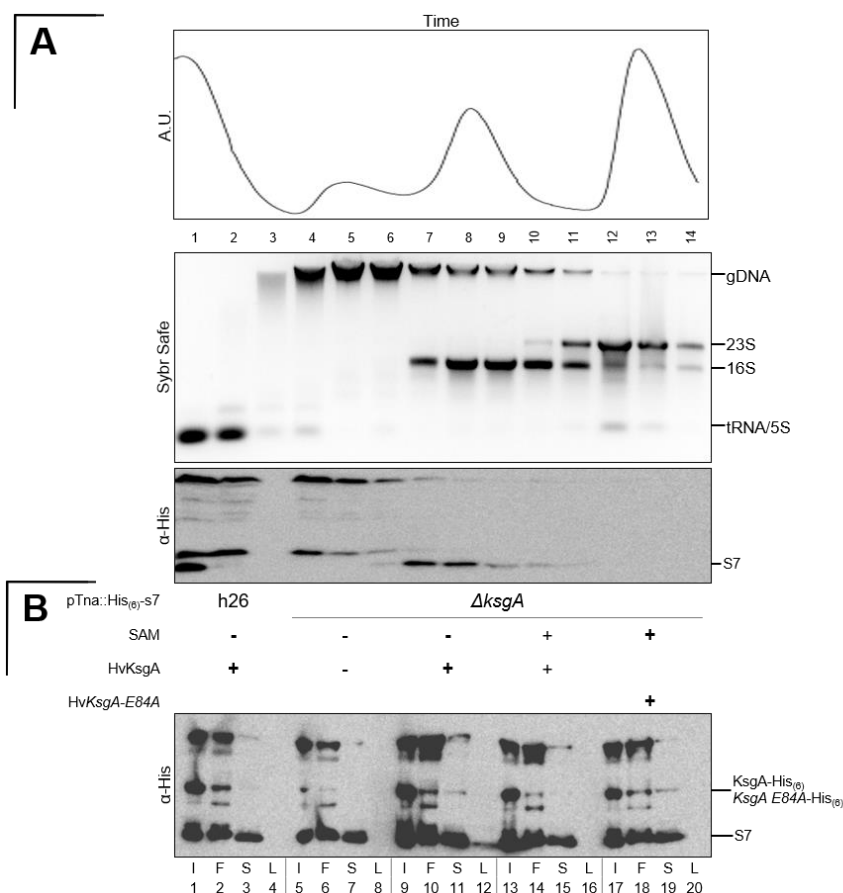


Figure 4.19 **KsgA is not detectable on the 30S fraction after adding SAM to a whole cell reconstitution.**

[A] Shows the ribosomal profile of the $\Delta ksgA::pTna::His_{(6)}-S7$ cells (Trp induction 0.25 mM), notice the peak at fractions 4-6 that result of the large amounts of gDNA in the cell lysate. Flowrate 1 ml/min, 500 μ l per fraction. The nucleic acids that are present in the fractions are shown below. The corresponding western blot shows the migration signal of S7 associated to the 30S/16S rRNA. Unfortunately, the His antibody is very unspecific on *H. volcanii* cell lysates, resulting in the many additional random background bands. [B] Shows the pooled fractions of each reaction. Lanes 3,7,11,15 and 19 show the binding status of KsgA to the 30S fractions. I: Input, F: Free pool, S: 30S, L: 50S. His₍₆₎-S7: 22 kDa, KsgA(-E84A)-His₍₆₎ 32 kDa. Experiment was repeated 3 times. Initial blot and repetition are shown in Figure S 6 and Figure S 7 respectively.

As a control h26 wild type cells were used with the same plasmid. The fractions co-sedimenting (SSU) and not showing (LSU) the S7 signal on a western blot were pooled together and then loaded onto a western blot (Figure 4.19B). Lanes 9-12 show that KsgA binds to the 30S subunit and sticks to it when there is no excess SAM available, the same binding is seen in lanes 17-20 with the catalytic mutant (E84A) that cannot methylate and is known to stay attached to the 30S subunit (Connolly et al., 2008). When having excess SAM present, KsgA is not visible in the 30S fraction, and thus has finished the methylation and has dissociated from the particle (lane 16). This is similar to the wild type context where there is no methylation needed and thus KsgA does not bind at all (lanes 1-4). Unfortunately, there is a slight background signal on the same height as KsgA (lane 5,6) but not visible in lane 7, and overall, comparably weak. The issue with this experiment was that the signal in the free pool is already very strong (large amounts of unbound, excess or unfolded/inactive recombinant KsgA) and thus there is no transition of the signal from the 30S to the free pool visible, only the loss of signal in the 30S fraction.

In order to improve this, we turned to using pre-bound 30S/KsgA (no SAM, e.g. lane 11 in Figure 4.19) and then trigger release by SAM addition. This should enable to visualize the transition from fraction to fraction and would also allow to selectively add additional biogenesis factors and will be discussed later.

In summary, we could show that KsgA can be released from the 30S subunit in a crude cell lysate by the addition of SAM (i.e. after methylation), with the limitation of not knowing if other factors contribute to this release or not.

4.2.3 Cellular consequences of KsgA deficiency

After having handled the biochemical aspects of the methylation reaction we were interested in how the loss of KsgA influences cellular fitness in various ways.

4.2.3.1 KsgA deficient strains do not grow slower

Being deficient of a ribosome biogenesis factor can have impeding effects on growth. In *E. coli* the loss of KsgA has almost no impact on growth at 37 °C but severe at 25 °C (Connolly et al., 2008). In *H. volcanii*, *S. acidocaldarius* and *P. furiosus* there is also no effect on growth at 42 °C, 65 °C and 85 °C respectively (see Figure 4.20A,B and Figure S 8). However, 65 °C (temperature limit of the incubator) is in the lower temperature range of *S. acidocaldarius* and thus could be considered a “cold treatment” with a 4-fold lower doubling time compared to the optimum of 78 °C (Grogan, 1989). Similar decreased temperatures were chosen for *P. furiosus* 85 °C vs 95 °C optimum (Fiala and Stetter, 1986). For *H. volcanii* we could not observe a decrease of doubling times at lowered temperature (Figure S 9).

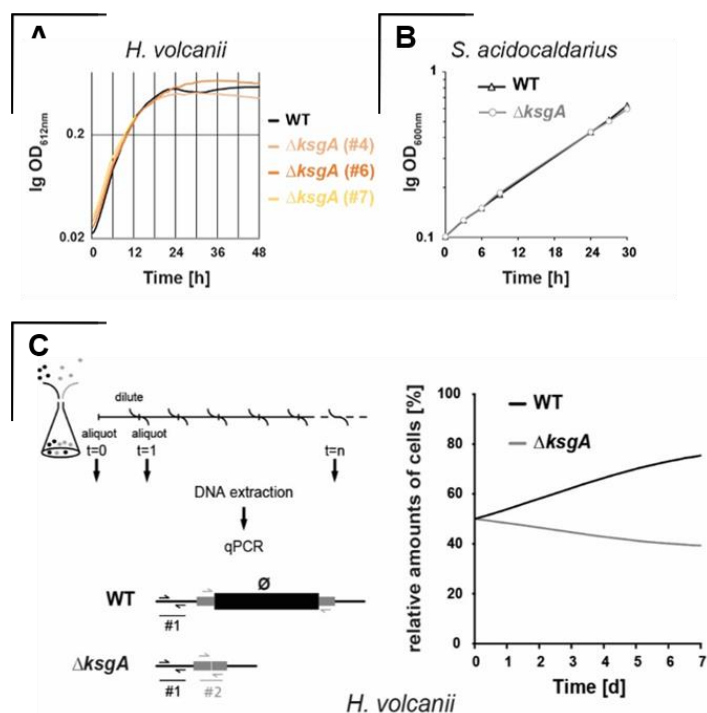


Figure 4.20 No negative growth effect of $\Delta ksgA$ but fitness advantage in competition.

[A] TECAN readout at 42 °C of wild type vs 3 knock outs of KsgA in *H. volcanii* on the left, on the right manual readout of *S. acidocaldarius* strains at 65 °C. [B] Manual readout of *S. acidocaldarius* strains at 65 °C. [C] Experimental setup for competition experiment and the qPCR results plotted over indicated amount of days. Primers used: oHv228,229;226,227. Experiments were done by Sébastien Ferreira-Cerca.

However, when pooling equal amounts of both cell types into one flask and letting them grow over several dilutions, the wild type *H. volcanii* cells outcompete the knock out (seen in Figure 4.20C).

So, when considering doubling time as growth, there is no measurable difference between the wild type and the knock out in the conditions tested. However, the competition assays indicate that the cells are sensitive to stress.

4.2.3.2 Loss of dimethylation leads to decreased motility

Growth in form of cell motility is a classic measure for adaptation of cells to environmental stress (Adler and Templeton, 1967; Amsler et al., 1993; Maurer et al., 2005). Spotted onto a semi solid agar plate, cells need to swarm away from their starting point to find new nutrients, due to increased competition with the ever-growing colony size. They do this in a circular manner, and cells that cannot adapt to the changing environment (stress) are less motile, i.e. cannot swarm as far/ react as quickly. In archaea the propelling apparatus is termed “archaellum” (see Figure 4.21A) and is similar to the type IV pilus of bacteria (Albers and Jarrell, 2015). Filament growth is associated to incorporation of large amounts of flagellin at the base of the archaellum (see Figure 4.21A).

To determine if the $\Delta ksgA$ strains in *H. volcanii* exhibit any deficiency regarding this swarming behavior I spotted equal cell densities onto semi solid agar plates and let them incubate for 3 days (described in 7.2.1.3). This was mostly done on plates containing only Casamino acid and no carbon source as this forced the cells to swarm away quickly due to more restricted nutrients conditions. For h26 and $\Delta ksgA$, Hv-YPC plates were also tested but this was done over 5-7 days as ring formation is slower due to excess nutrients. Measurements were taken as shown in Figure 4.21B.

To test if plasmid based complementation can rescue the knock out phenotype and if the catalytic mutant leads to dominant negative effects on swarming, I tested most of the His-tagged complementation and overexpression cells from Figure 4.11. To be independent of plasmid-based expression I also reintegrated the wild type and the catalytic E84A mutant genomically into $\Delta ksgA$. This was done by cloning the US/DS region including the KsgA ORF into the pTA131 Vector using oHv91/94 or PCR assembly of the two fragments amplified with oHv91/240 and oHv239/94 for the E84A mutation, and transforming them into $\Delta ksgA$ K4. The cells were screened for the KsgA ORF and methylation activity (see Figure 4.21C).

The wild type and knock out show a significant difference in swarming both on Hv-Ca media as well as on Hv-YPC plates (Figure 4.22A). The reintegration (see Figure 4.21C) of wild type KsgA into the knock out results in near wild type growth (when comparing Figure 4.22A and B, keep in mind that they were not grown on the same plates). The average swarming diameter of the catalytic mutant

lies somewhere in between the knock out and the wild type but shows a significant difference to the wild type reintegration. When overexpressing over a wild type background there is only a significant difference between the wild type *KsgA* and the E84A mutation at low tryptophan concentrations (see Figure 4.22C). The overexpression of the catalytic mutant however generates a slight dominant negative effect in mean swarming capabilities at low tryptophan concentration. When complementing the knock out with their respective plasmid constructs seen in Figure 4.22D, there is a significant negative impact of expressing the E84A mutant as well as when comparing this mutant to the wild type complementation at low tryptophan concentrations. At higher tryptophan concentrations there is an overall decrease in swarming but only a significant difference between the wild type and E84A complementation. Again, a slight dominant negative effect can be observed when comparing the mean of the empty plasmid and the catalytic mutant. Indicating, an overall dominant negative effect when expressing the catalytic mutant from a plasmid.

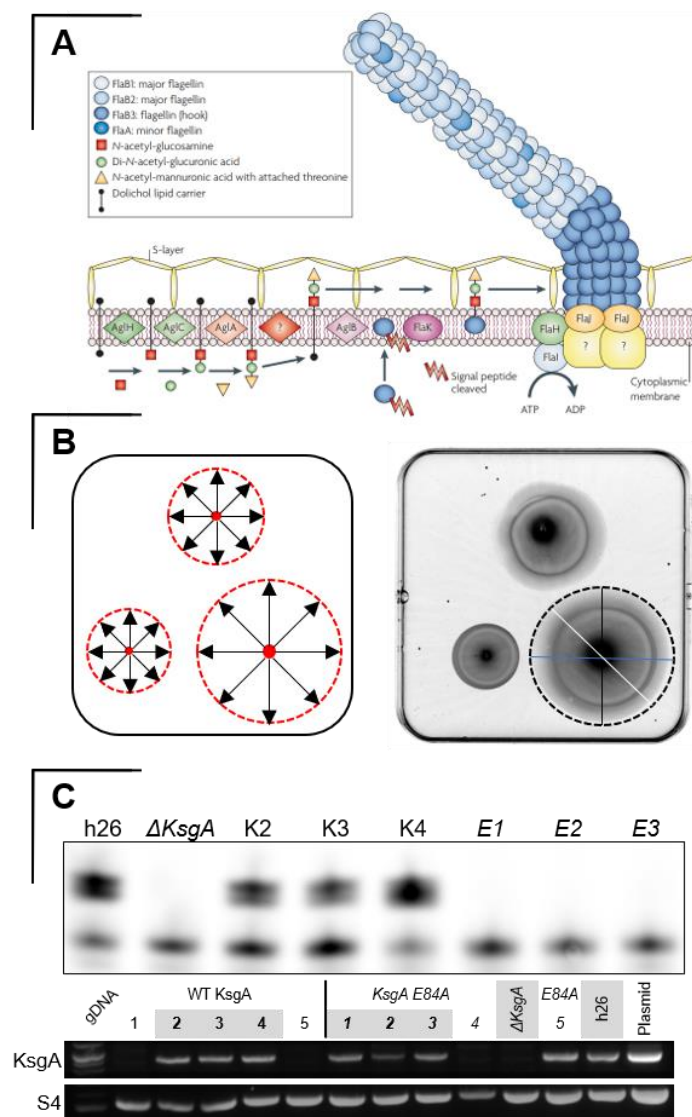


Figure 4.21 *Archaeum* structure and exemplary Motility assays.

[A] Archaeum structure from Jarrell and McBride, 2008. Nomenclature for *Methanococcus maripaludis*, Mmar FlaB1;2 = hvFlgA1;2 [B] Schematic of motility plate, small red dot is where cells are spotted and how they spread. On the right a plate scan is depicted with the measuring points for quantification (in this case $\Delta ksgA::pTna - \Phi$, - His₍₆₎KsgA and His₍₆₎KsgA E84A, clockwise orientation starting in the upper middle) [C] Reintegration of wild type and catalytic mutant into $\Delta ksgA$ K4. Primer extension readout along with PCR verification of successful reintegrations (greyed out)

To test if the loss of other late SSU biogenesis factor impair motility, I tested the strains ($\Delta rio1$, $\Delta rio2$ and $\Delta rio1\Delta rio2$) obtained from (Knüppel et al., 2018) in the same assay and compared them to their respective wild type cells (h99). Analogously to $\Delta ksgA$, swarming was impaired in all deletion constructs (see Figure S 11).

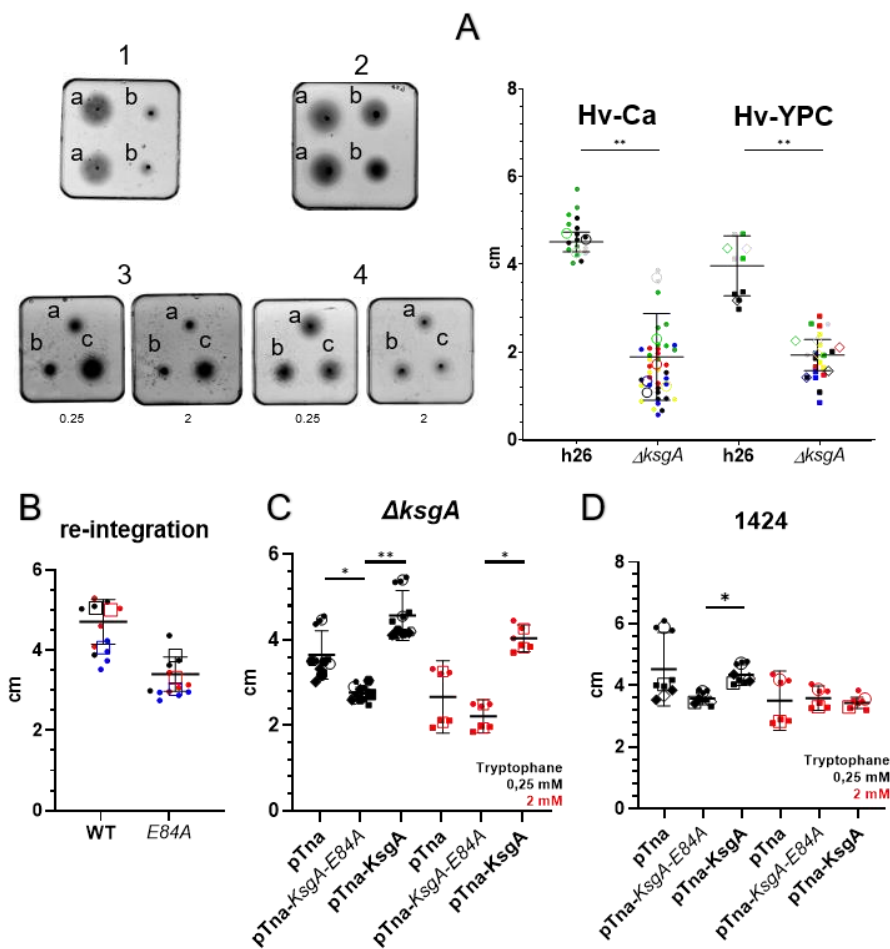


Figure 4.22 **Absence of KsgA significantly decreases motility.**

All plots were created as a “Superplot” (Fowlie and Bardsley, 2016) to improve confidence in significance. In short the technical replicates of each biological replicate were averaged (large hollow) and plotted onto a scatterplot of all individual data points (small points). The mean and SD of the averaged values are depicted as bars. These averages were then tested on their significance (unpaired T-Test). Upper left shows exemplary Hv-Ca Motility plates of the indicated graphs. Tryptophan concentration is given below the plates, e.g. 1-A, 2-B, 3-C and 4-D. Strains as follow: 1a h26, 1b $\Delta ksgA$, 2a reintegration of wildtype, 2b reintegration of catalytic mutant. 3 $\Delta ksgA$ – a pTna, b pTna-KsgA-E84A, c pTna-KsgA, 4 1424 – a pTna, b pTna-KsgA-E84A, c pTna-KsgA [A] Comparison of wild type h26 strain vs various individual knock outs of ksgA. Each color represents one biological replicate. Round shapes were done on Casamino acid plates (+uracil) (left) and rectangle shapes were done on Hv-YPC plates (right). P-Value: Ca (0.0032), YPC (0.0005). [B] Shows the swarming differences between the genomic reintegration (P= 0.0327). Each color represents one individually sourced transformant (those screened in Figure 4.21C). [C] Shows the effect overexpression on a wild type has on motility (P= 0.0264). Each shape represents one biological replicate. [D] Shows the effect on swarming by complementing the knock out with the indicated plasmids, P values from left to right: 0.0232, 0.0009, 0.0356. Doubling times for C and D shown in Figure S 10.

While swarming measures a coordinated cellular reaction resulting in a collective movement on semisolid surfaces (low percentage agar), swimming considers individual cell movement in liquid medium (Kearns, 2010). For *H. volcanii* slower swimming of $\Delta ksgA$ in liquid media could not be observed (personal communication Tessa Quaxx, Uni Freiburg).

In conclusion it can be said that the loss of KsgA and additional late SSU biogenesis factors can severely impact the swarming abilities in *Haloferax volcanii*.

4.2.3.3 Loss of KsgA can lead to increased biofilm formation

We have now learned that KsgA deficient cells cannot swarm well in semi solid agar plates, but what about the opposite action, adhesion? Many bacteria and archaea form biofilms to stick to surfaces that prevent them from being washed away, exchange genetic material and increase resilience towards antibiotics (Donlan, 2002, 2001). In *H. volcanii* the cells form a dense network that enables cell differentiation and horizontal gene transfer (Chimileski et al., 2014). If the loss of a biogenesis factor changes swarming abilities, will it also impact biofilm formation?

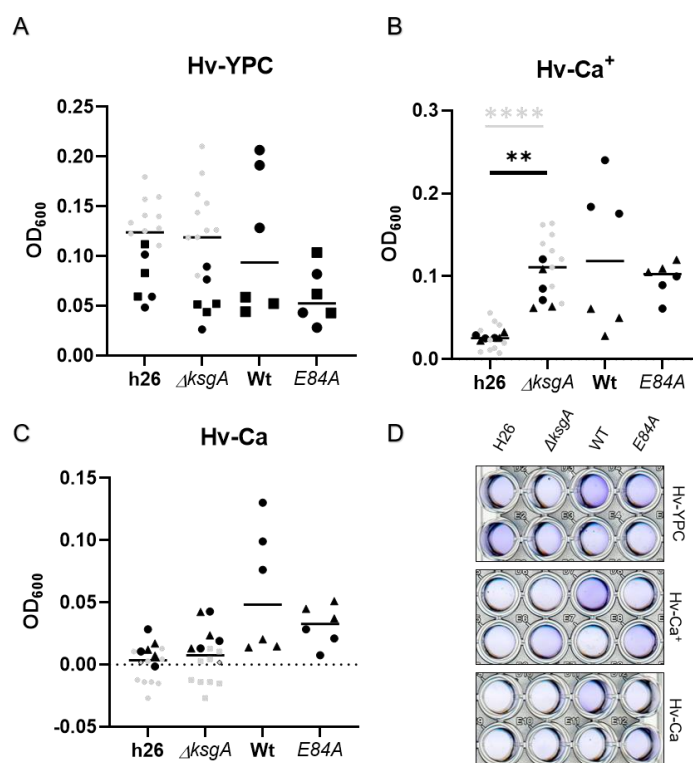


Figure 4.23 $\Delta ksgA$ cells adhere significantly better in Hv-Ca⁺ Media.

Optical densities plotted for Hv-YPC- [A] Hv-Ca⁺- [B] and Hv-Ca- [C] media. WT/E84A are the genetic reintegrations (from Figure 4.21C). The two shapes resemble two biological replicates. The grey dots (biologicals) were from another Experimental run. Here the overall staining worked poorer and the confidence of the OD measurement is not that high (near the lower detection limit of the TECAN reader). For these “grey” results the data points are equally adjusted to fit the OD range of the other two biological replicates (black). Due to additional Data points it increases the significance in B from p=0.0002(black) to <0.0001 (black + grey)). **D** Cutouts of 96-Well plate with dissolved crystal violet stained cells, each lane corresponds to one technical of a biological replicate.

To test this, I performed adhesion assays. To do this quantitatively, I stained adhering cells in a 96-Well microtiter plate and compared the amount of stained cells through optical density (shown in Figure 4.23D and described in 7.2.1.6). Cells typically form biofilms at the air-liquid interface of still media. Thus, fixing and staining them and then dissolving them enables a comparative analysis (O'Toole, 2011).

The wild type and knock out cells adhered equally well (see Figure 4.23) in Hv-YPC (A) and Hv-Ca (C) media, but the knockout adhered significantly better in Hv-Ca⁺ (B) Media. The genomic reintegrations behaved very randomly among the biological replicates and could not be compared. The dissolved crystal violet stained cells are shown in Figure 4.23D.

Concluding it can be said that opposite to being an inferior swarmer *ΔksgA* cells are able to adhere better in a certain media.

Considering *H. volcaniis* pleiomorphism, quantifying cell shapes of both wild type and knock out might reveal differences in the overall distribution of either cell shape.

4.2.3.4 KsgA deficient cells are on average slightly longer

Haloferax volcanii cells do not only differentiate in biofilms, but also show pleiomorphism during different stages of growth. During exponential and stationary growth phases, the majority of *H. volcanii* cells are round. They usually cluster together and are not very motile. A very small population shows rod shapes that are highly motile (Chimileski et al., 2014; Li et al., 2019). This pleiomorphic ratio can be shifted towards the rod shape by cultivating the cells over several days at very low densities ($OD < 0.04$) in Casamino acid only media (Figure 4.24A) (Li et al., 2019). With the results from the two previous experiments we sought out to compare the cells shapes at high and low densities in wild type and *ΔksgA*. There are slight differences visible between the two: the knock out cells show an increase in median length [low OD_{600} 2.89 μm (h26) vs. 3.18 μm (*ΔksgA*) and high OD_{600} 2.33 μm (h26) vs 2.70 μm (*ΔksgA*) μm , and Figure 4.24B] and the median rod shape increases [0.46 (h26) vs. 0.42 (*ΔksgA*) at low OD_{600} , 0.62 (h26) vs. 0.56 (*ΔksgA*) at high OD_{600} see Figure 4.24C, while 1 would be a perfect circle]. This trend strengthens when looking at the relative frequency at certain length and roundness intervals (Figure S 12). A more severe effect on roundness could be observed in the double deletion of *rio1* and *rio2* (Figure 4.24D, Figure S 12).

In conclusion, it appears the loss of KsgA results in a populational shift towards a longer rod cell morphology.

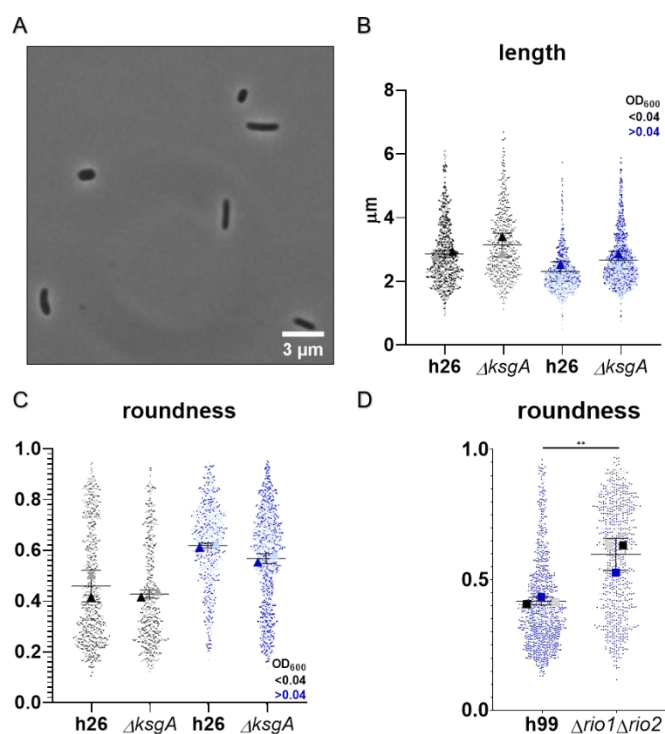


Figure 4.24 Loss of KsgA does not lead to a significant change in cell morphology.

[A] Still of h26 cells at low densities. Both shapes are present. Plotting was done as in Figure 4.22. Data acquisition is described in 7.2.1.5. Every detectable cell is characterized for length and roundness by the algorithm. Results were manually curated for dirt/artefacts. [B] Length comparison of h26 and $\Delta ksgA$ at high and low densities. No significant difference when comparing the two averages of the biological replicates. A third biological replicate was unclear in its cell state and was omitted. But when comparing the mean of both populations the knock out cells are slightly longer at low and high densities. [C] Shows the roundness, 1 being a perfect circle. The mean and overall population shows slightly less roundness in the knock out at both stages of growth. [D] Roundness of the $\Delta rio1\Delta rio2$ Knock out at OD₆₀₀ < 0.04 as comparison (low density).

4.2.4 Translational landscape

Loss of KsgA dependent modification alters the helix 45 structure and reduces the interaction with the helix 44 (Demirci et al., 2010). This change influences the accuracy (van Buul et al., 1984) and codon recognition (O'Connor et al., 1997) in the A- and P-site of the ribosome. So, linking the effects on biofilm, motility and morphology to translational levels would be interesting. Luckily, we were able to do two runs of label free whole proteome mass spectrometry. This was done for one by the company PolyQuant and by the Öffinger Lab in Montreal, CA. The amount of total proteins detected varied between the two experiments, but common major hits could be found in both analyses. PolyQuant detected 1456, the Öffinger Lab 2311 proteins. Two biological replicates were compared in each analysis with two technical replicates. The protein extraction was performed as described in 7.2.4.1 and the mass spectrometry procedure is described in . Both quantifications were done with MaxQuant, but PolyQuant used LFQ output and the Öffinger Lab iBAQ. Both are similar, but iBAQ uses global intensities that are divided by the identified peptides for the target protein (Schwanhäusser et al., 2011), while LFQ excludes some statistical outliers during the quantification but also creates the score in the same manner as iBAQ (Cox et al., 2014). Using the ArCOG database (Makarova et al., 2015), a GO term analysis could map several up/down regulated genes to their

respective organizer Figure 4.27A. The mapping proved difficult due to incompatibility of our Identifiers to those in the ArCOG database. The ArCOGs provide a good overview of the datasets but in some cases, for example motility, does include very different/opposing group of genes (biofilm vs. motility). This does not paint a very clear picture to what specifically is up- or down regulated and at which certainty.

When going into detail, a volcano plot, plots the iBAQ differences over the log P value and gives statistical power to the results (Figure 4.27B). These reveal some strongly down regulated proteins with high confidence and an overall larger population of down- regulated proteins. The dataset for the genetic reintegrations (Knock-In), showed a higher variance between the biological samples and thus show an overall decrease in its statistical significance. The identifiers for FlgA1 and prepilin are highlighted because of the relevance in our previous motility and biofilm assays. In the case of FlgA1 the downregulation supports our results from the motility assays quite well (Figure 4.25A). FlgA2 and prepilin is only detectable in the Öffinger Dataset. FlgA2 shows slight upregulation while prepilin shows a stronger upregulation. For the motility genes, the mRNA levels were compared via qPCR and showed no large differences ($<1 C_T$) and are shown in Figure 4.25B. The genetic reintegrations show similar results; down regulation of FlgA1 (Figure 4.27B) in the catalytic mutant and similar levels for the wild type reintegration (data not shown). However, due to the high variance in the samples (biofilm experiments and motility assays) coupled with the decreased statistical robustness, these results need to be interpreted carefully.

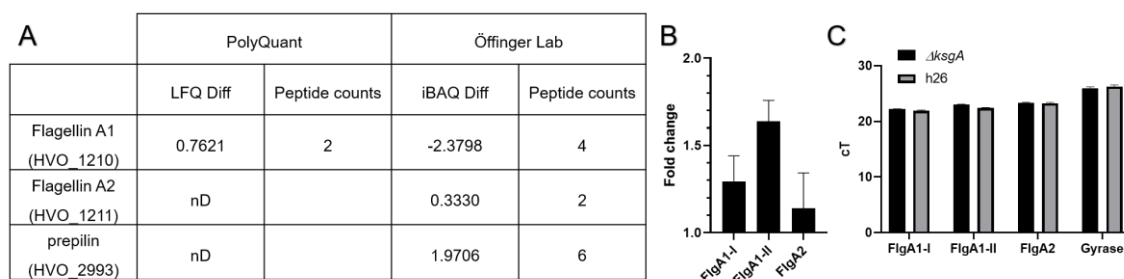


Figure 4.25 **Flagellin A1 is less abundant in KsgA Knock out cells.**

[A] Differences (WT – KO) of LFQ/iBAQ score on selected proteins. LFQ (1=equal), iBAQ (0=equal) [B] qPCR results, Expression levels of h26 over $\Delta ksgA$, normalized to Gyrase expression levels. Two primer pairs (I + II) were used for the flagellin A1 gene. Procedure described in 7.2.2.9 [C] Raw c_T values.

When filtering the datasets for AUG and non-AUG translation initiation we discovered that non-AUG usage is associated with upregulation in $\Delta ksgA$ strains in both datasets (see Figure 4.26A, B and D). In addition, the Öffinger Data revealed that a large population of down regulated genes contain an additional non-AUG codon with in the first 10 in-frame codons (see Figure 4.26C). Yet we could not associate a length bias to up or down regulated proteins (Figure S 13).

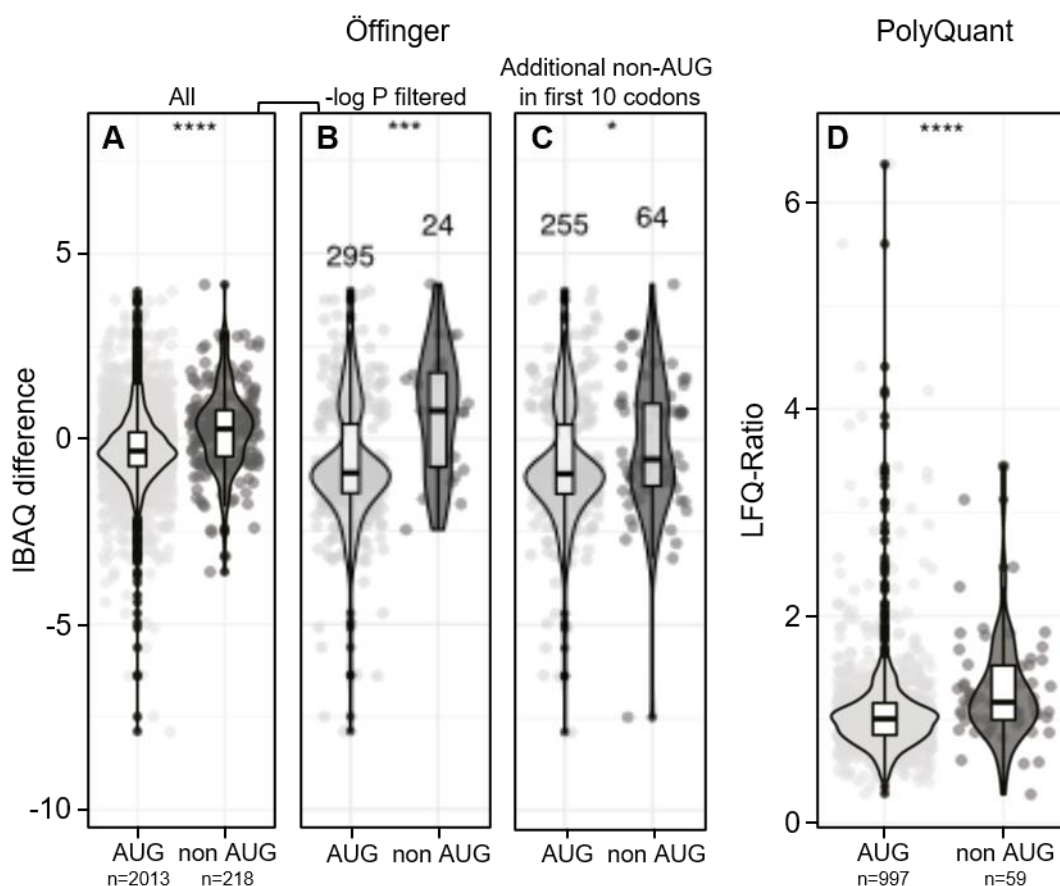


Figure 4.26 **Violin Plots of AUG vs non-AUG initiation codons usage indicate increased upregulated non-AUG initiation in *ΔksgA* in *H. volcanii*.**

[A] and [D] show the complete proteome data from both indicated data-sets sorted for AUG/non-AUG initiation and plotted for their respective IBAQ-Differences/LFQ-Ratio. [B] Shows the same as A, but filtered for $-\log P < 0.05$ (depicted in Figure 4.27B). [C] Shows the Data from A filtered for an additional non-AUG in the first 10 in-frame codons. Unpaired t-Test p-Values: A ($p=6.8^{-15}$), B ($p=0.00029$), C (0.015), D ($p=1.7^{-5}$). Data processing done with and by Felix Grünberger.

It appears as if the ribosomes lacking methylation are “struggling” to translate certain sets of mRNAs. The SHAPE experiments revealed an additional accessible nucleotide A1426 (*E. coli* numbering A1493) in the *ΔksgA* strain compared to the wild type and as well to other SSU knock outs (here Rio1 and Rio2) (shown in lane 10 in Figure 4.28A). This observation is in agreement with the data from Demirci et al., 2010 which proposed that the absence of dimethylated adenosines in the helix45 leads to a loss of hydrogen bonding between it and helix 44. This might increase flexibility of both helices and thus the accessibility for SHAPE reagents in the proximity. How this could affect the translational capability for certain mRNAs is unclear.

The conclusion from these results is that a whole proteome analysis provides a vast amount of data that can be scavenged and filtered for a myriad of settings and can be viewed under various aspects and referenced to experimental observations. Yet the statistical power of such a “shotgun” approach is comparably low if the effects are small, thus when going into detail, targeted mass spectrometry might be necessary. Yet experimental validation (motility, biofilm formation) of the observed change

in protein levels increases the confidence in the data. Finding similar results for FlgA1 in two different datasets also adds confidence to the data.

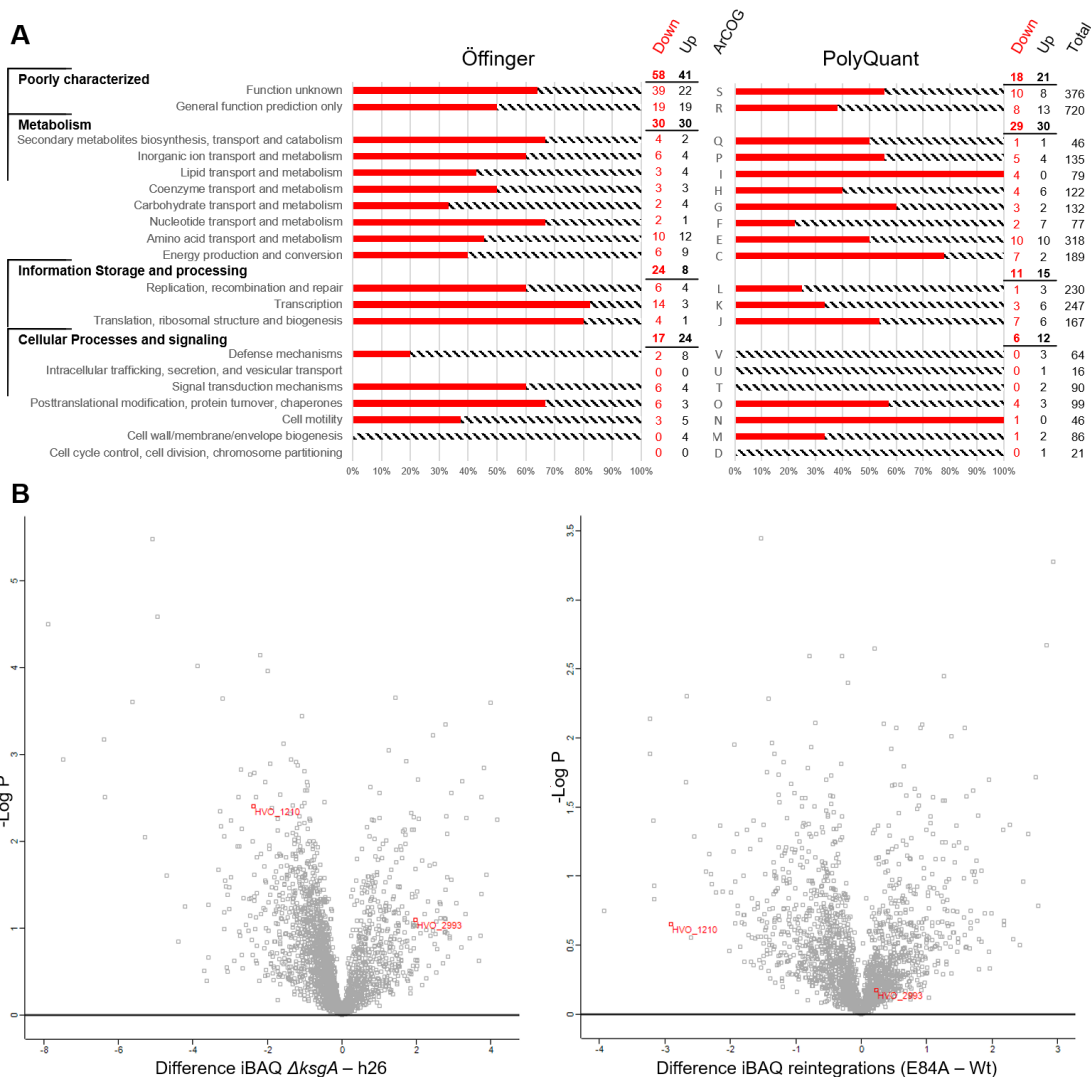


Figure 4.27 **ArCOG (GO-Term) Analysis of two Proteome Data sets and distribution effect of KsgA deficiency.** [A] ArCOG terms grouped into 4 large groups with the sum changes shown above each group. Input cutoff was >1.5 fold change in the PolyQuant data and 1.5 iBAQ difference for the Öffinger data, Wild type vs $\Delta ksgA$, identifiers listed in 10.1. [B] Volcano Plot of the Öffinger Dataset, for the Knock out vs Wild Type (left) as well as the genetic KsgA-E84A reintegration vs the KsgA Wt reintegration (right). The higher the data point the higher the confidence. HVO_1210 (FlgA1), HVO_2993 (prepilin). ArCOG analysis by Felix Grünberger, Volcano Plots by Christian Trahan (Öffinger Lab)

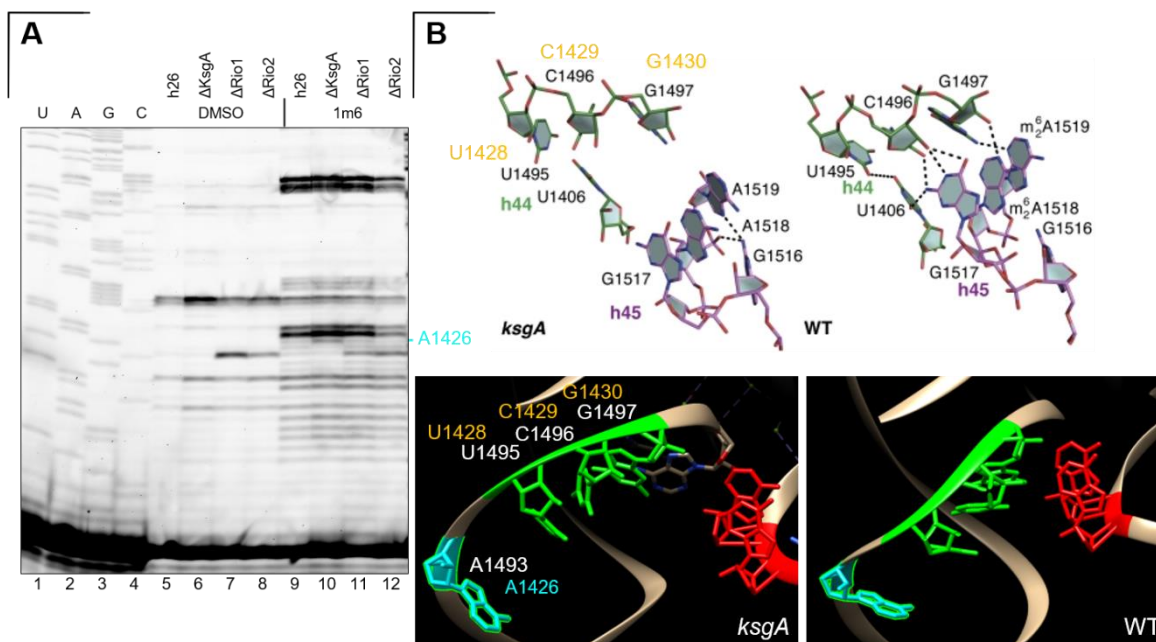


Figure 4.28 Loss of KsgA leads to increased flexibility in the proximity of h44-h45 interaction site.

[A] SHAPE profile of the 3' End of the 16S rRNA (start: 1447, same region as in Figure 4.6A), additional primer extension stop at A1426 in lane 10, $\Delta ksgA$. [B] Upper panel: Detailed interaction states between helix44 and h45 from (Demirci et al., 2010), *Haloflex volcanii* numbering added in yellow. Lower panel: Highlighting of the additional SHAPE modified nucleotide from A on both the *E. coli* structures in blue. Respective nucleotides from the upper panel H44 in green, A1518/19 of helix 45 in red. $\Delta ksgA$ (PDB 3OTO), WT (PDB: 1J5E). Images created with Chimera.

5 DISCUSSION

While bacterial and eukaryotic ribosome biogenesis have been studied for almost half a century, the kingdom of archaea lacks this detailed insight. Our results from studying putative archaeal ribosome biogenesis factors have previously shown some degree of conservation from archaea to eukaryotes with the Rio proteins (Knüppel et al., 2018). In this work I present a detailed analysis of the archaeal KsgA/Dim1 with its anomalies in *H. volcanii*. We show that (1) KsgA is dispensable in three archaeal model organisms (2) with effects on cell motility, biofilm formation and the overall translational landscape of *H. volcanii*. (3) We show that HvKsgA can methylate the 30S substrate *in vitro* and give preliminary results for the release mechanism and an outlook for a comparative factor dependent release mechanism. (4) We reveal that the highly conserved substrate shows a native abnormality in *H. volcanii*, that is associated with hypomethylation in the helix 45 of the 16S rRNA and gives further evidence for a release mechanism of KsgA independent of full methylation. Paired with establishing methods in model archaea that have previously been used in bacteria and eukarya to study ribosome biogenesis, this study lays a fruitful base for further studies in this untapped field.

5.1 Pleiotropic effects from loss of KsgA in at least one Archaeal Model organism

Strikingly, the loss of KsgA/Dim1 appears to have little effects on growth in many bacterial organisms, but still has been retained throughout evolution and is present in virtually every sequenced bacterial genome so far (Grosjean, 2009; Ng et al., 2019; Park et al., 2010). Yet many of these observations are of course made under laboratory conditions and the real-world effect would be more severe. This is mildly shown in the cold stress phenotype in *E. coli* (Connolly et al., 2008) but also in dramatic loss of virulence in *Yersinia pseudotuberculosis* (Mecsas et al., 2001). On the surface, the absence of methylation is the easily measurable difference between the wild type and the knock-out. The loss of similar rRNA modifications are also associated with a multitude of consequences. For example: loss of the RlmN (m²A2503 of the 23S rRNA) is associated with increased susceptibility to the antibiotic linezolid in *E. coli* (Toh et al., 2008), on the other hand, a single point mutation in the protein leads to resistance to the same antibiotic in *Staphylococcus aureus* (Yoshida et al., 2009). Curiously loss of RsmG (m⁷G527 in 16S rRNA) shows increased robustness towards certain stress conditions and increased streptomycin resistance compared to wild type *E. coli* and is only disadvantaged under very specific antibiotic conditions (Okamoto et al., 2007; Sergiev et al., 2012). This duality of gain and loss is similar in KsgA, i.e. loss of methylation but gain of kasugamycin resistance (in *E. coli*). These resistances depend on structural changes resulting from absence of methylation and thus impaired binding of the antibiotic (Schuwirth et al., 2006). The usage of base modifications to stabilize the structural conformation of the ribosome is a mechanisms used among all three kingdoms (Demirci et al., 2010; Sas-Chen et al., 2020; Sharma et al., 2018). The degree of rRNA modification, however varies in between kingdoms but also within the kingdoms (Decatur and Fournier, 2002; Gomes-Filho and Randau, 2019; Sloan et al., 2016).

Concluding that the nucleotide modification is not the sole purpose of these enzymes but also their respective binding position and the resulting interaction and structural change of the ribosome.

In our study we have shown that like in bacteria, KsgA is not essential for cell viability of three model archaea. Yet in comparison to *E. coli*, does not lead to (temperature dependent) growth rate defects in *H. volcanii* (*Hv*), *S. acidocaldarius* (*Saci*) and *P. furiosus* (*Pfu*) (Figure 4.20, Figure S 9 and Figure S 8 respectively). This is perhaps due to their wide temperature tolerance (30-55 °C (*Hv*), 65- 85 °C (*Saci*), 70-100 °C (*Pfu*). While we did not test a broad range of temperatures in *S. acidocaldarius* and *P. furiosus* our default was already at lower than optimal growth temperature, which did not show a defect (Figure 4.20, Figure S 8).

For *H. volcanii*, growing both strains in competition led to the wild type outcompeting Δ ksgA. The explanation for this is manifold. 1) The easiest being, that evolutionary pressure would have not retained this factor for so long if it would not benefit the cells. 2) Previous literature in bacteria has shown that loss of KsgA is often associated to a decreased translational initiation, fidelity and increased frameshifting (Kyuma et al., 2015; O'Connor et al., 1997). This is very likely due to incomplete/immature formation/folding of the SSU at the P-Site (described in 3.2.3.5.2 and 4.2.4). This is also visible in the SHAPE profile of Δ ksgA where an additional flexibility near the interaction surface of helix 44 and helix 45 (see Figure 4.28), a central element of the P- and A-site, results in additional SHAPE reactivity (also discussed later in detail). Our proteome data also support these conclusions. On a steady state level, certain proteins are less abundant in Δ ksgA. Yet some are detectable in higher abundance. In every living cell, a large variety of mRNAs compete for access to the translational machinery (Raveh et al., 2016). How and why specific mRNAs are translated inferiorly is difficult to determine. We do see that a significant part of the upregulated proteins in the knock out are mRNAs that use non-AUG as start codons (see Figure 4.26A,B and D). Interestingly, we also observe that non-AUG initiation is associated to upregulated proteins in our preliminary proteomic dataset comparing the *E. coli* WT and Δ ksgA (Figure S 14). Together, these results agree with a study showing that non-AUG translation initiation is elevated in Δ ksgA (*E.coli*) (O'Connor et al., 1997). Results from analyzing human cells deficient of Dim1 or expressing a catalytic mutant of it, show that alternative modes of translation, (e.g. via internal ribosome entry sites (Alberts, 2002, chap. 7)) were impaired due to -1 slipping of the ribosome in the 5' direction (Shen et al., 2020). Mildly downregulated proteins in the KO often have an additional non-AUG start codon within the first 10 in-frame codons on the mRNA, indicating that perhaps KsgA deficient ribosomal subunits initiate on this non-AUG start codon incorrectly and produce unstable, N-terminally shortened, proteins (Figure 4.26C). Yet in the non-AUG mRNAs, an additional non-AUG in the first 10 codons has a less significant effect on expression. However, there is no visible difference indicating towards a length bias for translation efficiency (Figure S 13), indicating that once the hurdle of translation initiation has been taken, elongation is not impeded by the loss of KsgA. Taken together this supports,

that the bulk effect on translation appears to be rather small and only a minor fraction of the proteome is leaning toward downregulation.

The loss of rRNA modifications in general is often associated to a global effect on translation (Janin et al., 2020; Sharma et al., 2018). A recent study looking at the overall effect of rRNA methyltransferase loss, shows a similar effect on translation in *E. coli* $\Delta ksgA$ (Pletnev et al., 2020). They score this by two exogeneous reporter systems (cerulean fluorescent protein and FastFT expression) as well as by looking at the overall expression by labelled 2D-SDS-PAGE overlays of wild type vs $\Delta ksgA$ (see Figure 5.1B). In all three cases, the two reporters and the 2D-SDS-PAGE, the differences are marginal but visible. They all show a very slight downregulation of the proteins in the $\Delta ksgA$ strain. Our preliminary *E. coli* WT vs $\Delta ksgA$ proteome dataset paints a similar picture to the situation in *Hv* and the data presented in Pletnev et al. (2020) (Figure S 14). Additionally, a study shows that Dim1 deficiency and a catalytic inactive mutant in human cells leads to overall decreased translation levels (Shen et al., 2020). Our initial experiments with 2D-Gel comparison of both *H. volcanii* strains revealed a very homogenous expression of proteins with some small differences (see Figure 5.1A). The differential expression of proteins based on the start codon usage in $\Delta ksgA$ in both *E. coli* and *H. volcanii* is a good basis for further studies on these proteomic dataset. Especially when considering the proposed slippage in “-1” in Dim1 deficient cells, analyzing the datasets for “-1” or even 6-frame translation (Castellana et al., 2008) (all possible peptide compositions resulting from all reading frames of the mRNAs) might reveal additional patterns of mistranslation. Yet this requires a lot of computational time and expertise.

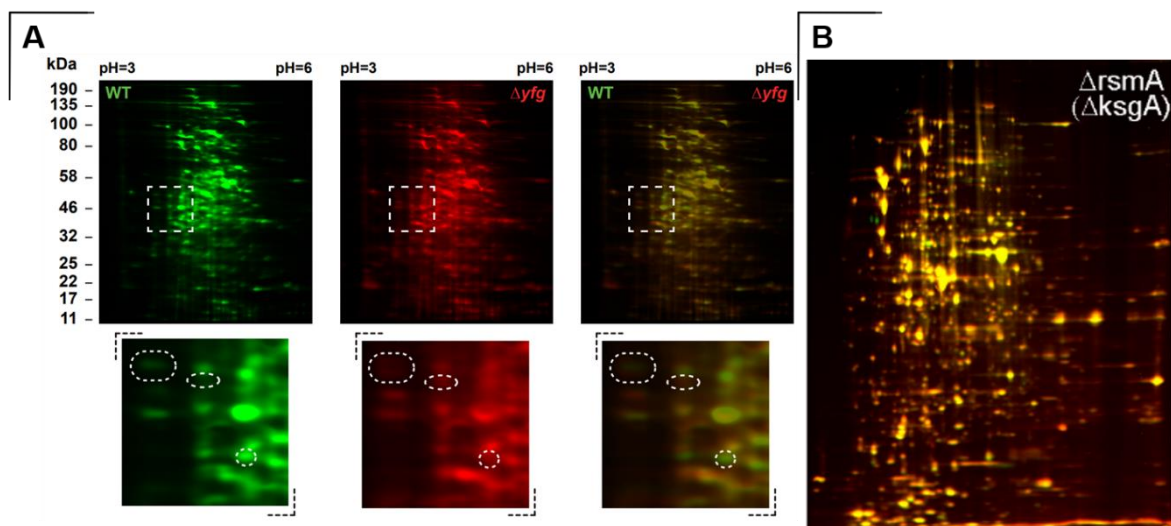


Figure 5.1 **Differential 2D gel analysis of L-AHA-labelled proteins.**

[A] Exemplary results of differentially expressed proteins. Full gel scan (upper part) for the 2D gel analysis obtained for the wildtype (Cy5.5-green) and mutant *H. volcanii* cells (WT=h26, $\Delta yfG = \Delta ksgA$) (Cy7-red) mixture are provided. Taken from (Kern and Ferreira-Cerca, submitted) [B] Merge - 2D Gel from Pletnev et al. (2020), *E. coli*: WT-Cy3 (red), $\Delta ksgA$ (green).

The proteome analysis revealed two candidates, flagellinA1 and prepilin. Both showed differential expression in the *H. volcanii* proteome data and are associated to motility (down-regulated) and

biofilm formation (up-regulated), respectively. In both cases we could validate the expression levels to a phenotype by swarming assays (or motility assays) and measuring biofilm formation at the air liquid interface of “static” cells (see Figure 4.22 and Figure 4.23 respectively). The quantitative differences in expression of the two proteins, can be seen in the two assays. The motility assays show significant results independent of media genotype and expression levels. Unfortunately, biofilm formation is only significantly elevated in $\Delta ksgA$ when using the “cloudier” enhanced Casamino Acid media. While motility assays provide a multitude of stressors for the cell: nutrient starvation and associated chemotaxis, spatial restraint in the growing colony and, if formed, dispersing from a biofilm, biofilm formation alone is very dependent on the surface and media viscosity used (Donlan, 2002).

Regarding motility, all these stressors require the cells to produce large amounts of FlgA1 (the major flagellin) to be motile and escape these unfavorable conditions (Näther-Schindler et al., 2014). With an impaired ribosome, adapting the translational program to continuous large-scale translation of the highly expressed flagellin-A1 mRNA, is perhaps severely impaired or cannot be sustained. To my knowledge there are no (or very few) studies linking ribosomal assembly/functional defects to motility defects (Fan et al., 2019, 2016) (see Figure 4.22 and Figure S 11). We tried to reproduce the technique from Legerme et al. (2016) using a flgA1-His₍₆₎ reporter to score its expression levels in the wild type and $\Delta ksgA$ but were unsuccessful (data not shown). In this experiment the flagellin is torn from the cell via centrifugation and the free flgA1-His₍₆₎ can then be detected via western blot in the supernatant. However, the method could not be reproduced by others as well (personal communication Tessa Quaxx, Uni Freiburg). Interestingly, we could also show a motility defect in *E. coli* $\Delta ksgA$, but the results were less reproducible (see Figure S 15). Both results are in accordance with the postulated requirement of intact translational fidelity and flagellar biosynthesis in bacteria (Fan et al., 2019, 2016).

Biofilm formation increased in $\Delta ksgA$ cells when using HvCa⁺-Media (Figure 4.23), that tends to have precipitated elements swimming around in the medium. This could provide additional surfaces for the cells to adhere to and improve biofilm formation. One study could link ribosomal stress to the induction of biofilm formation in *E. coli* (Boehm et al., 2009), yet we did not test biofilm formation in our *E. coli* KEIO knock out strains. An additional problem with the assay is the flat bottomed 96-well plate we used. According to the protocol established by O’Toole (2011), a round bottom well plate vastly improves biofilm formation (in bacteria) and perhaps also in *Hv*. However, the method using flat bottomed 96 well plates has been used before with *H. volcanii* (Legerme et al., 2016; Nagel et al., 2019). We could not obtain the recommended round bottomed well plates and in light of the media dependent results, comparison of two different well-plate systems would be useful.

The results from scoring the shape and length of the *ksgA* knock out show that a larger population of cells have a tendency towards an increase in length that is associated with a decreased roundness

compared to its respective parental strain (Figure 4.24B, C and Figure S 12). In our proteome data we could only detect one of the two proteins (CetZ1 [HVO_2204] and CetZ2 [HVO_0745]) known to be involved in the transition from round to rod shaped (Duggin et al., 2015). In both datasets CetZ1 showed a very slight increase in the knock out, LFQ Ratio of 1.2 and an iBAQ difference of 0.03, with a higher significance for the latter. Perhaps this is a cause for the very little increase in rod shaped cells. The comparison with the double knock out of *rio1* and *rio2* strengthen the comparably minor effect (Figure 4.24D). In addition the *rio* double knock outs show similar deficiency in motility (Figure S 11) along with a reduced doubling time (Knüppel et al., 2018) which is not the case in $\Delta ksgA$. The dramatic change of morphology might be a cause for, or a result from this growth defect. Here a look at the expression levels of CetZ1 might reveal a more dramatic effect as well. Such analyses are highly media and growth phase dependent and difficult to interpret as it only considers a very narrow window of the various growth phases of *H. volcanii*. However, while writing this thesis a preprint has shown new methods to improve the shift towards rod shaped cells at higher densities, i.e. exponential later growth phases, and also in full complex media similar to Hv-YPC (de Silva et al., 2020). Perhaps using this method, a more elaborate picture of cell morphology can be made in regard to incorrectly matured ribosomes.

Additionally, different stress factors for *H. volcanii* could be potentially tested. For example, recent findings from the Soppa Group in Frankfurt (Grünberger et al., 2020; Laass et al., 2019) suggest that lowered salt concentration leads to accumulation of incorrectly processed 16S rRNA precursors and vastly influences the transcriptome (personal communication: Felix Grünberger, Uni Regensburg). This may be a potential stress factor to test on $\Delta ksgA$ in *Hv* for doubling time, motility and biofilm formation under such conditions. Another preprint discusses the formation of liquid biofilms in *H. volcanii*, that require rapid structural rearrangements (Schiller et al., 2020). This could also be a good method to score for stress adaptation from impaired ribosomes.

Overall, we could show that KsgA can be deleted in three model archaea and shows differential effects on the *H. volcanii* proteome most likely due to impaired translation initiation. Among these effects we find that proteins involved in motility, biofilm formation and cell morphology are differentially expressed and also result in a respective phenotypic effect. While $\Delta ksgA$ is impaired in swarming in a vast array of assays it shows only an increased biofilm formation when using a very specific medium that perhaps amplifies this effect.

5.2 Structural dependency for KsgA dependent methylation

From the previous results we could observe that loss of KsgA introduces a variety of phenotypes. Along with these findings we have discovered that the composition of its substrate, helix45 of the 16S rRNA, shows a vastly diverse structure in the kingdom of archaea and in the specific case of *H. volcanii*, this results in a hypomethylated heterogenous state of methylation that is unusual for this otherwise highly conserved and well-studied enzyme.

As introduced earlier (3.2.3.5.1), the structure of the helix 45 requires defined RNP composition and of course the two adenosines in the GGAA-tetraloop to be (di-)methylated by KsgA. While many studies have introduced a variety of mutations to the helix45, discovered the versatility of this helix and tested the effects on KsgA dependent methylation (Connolly et al., 2008; Cunningham et al., 1990; Desai et al., 2011; Formenoy et al., 1994; Heus et al., 1990; Van Knippenberg, et al., 1984; Vila-Sanjurjo et al., 1999; Vila-Sanjurjo and Dahlberg, 2001) only two studies linked a sequence mutation to the large natural variety of h45 in the archaeal kingdom (Formenoy et al., 1994; Van Knippenberg, et al., 1984). Even though the sequence alone is not as important for methylation, the structure is. While the mutation introduced to the stem by Formenoy et al. (1994) results in a loss of the wobble at position 7 of the stem of h45 (U●G1523 to U-A1523, *E. coli* numbering) leads to a decreased methylation by EcKsgA *in vitro*, it appears to have no effect on the living organisms that contain such a “mutation” natively, e.g. *Thermococcus celer* (*Tce*) or *Pyrococcus furiosus* (*Pfu*) (see Figure 4.15 and Figure 5.2). Indicating that the high growth temperatures (>80 °C) of *Tce* and *Pfu* might compensate for the decreased methylation activity of KsgA at “low” temperature (37 °C) when given a suboptimal wobble-less substrate (G1523A). Our results also verify this and we cannot see an increase in unmethylated Adenosines in *Pfu* (Figure 4.10B), while introducing a *Pfu*-like rDNA (pHK-rrnC-G1523A) to *E. coli* shows decrease in methylation and longer regeneration times for plasmid shuffling (Figure 4.16B, Figure S 5 and data not shown).

The heterogeneous methylation pattern observed in helix 45 by altering the opening from a Watson-Crick to a wobble pairing (A-U or G-C to G●U, see Figure 5.2) occurs naturally in a variety of archaea, namely: Methanogens Class II, Haloarchaea and Archaeoglobales. We could verify this experimentally by primer extension on selected cell samples from these families (Figure 4.15) as well as by mimicking this loop conformation in *E. coli* (pHK-rrnC-G1520U, see Figure 4.16B). Why this single base exchange results in a significant migrational shift within the first ~10 nucleotides in a TBE-Urea Acrylamide gel on a DNA and RNA level is unclear (Figure 4.10E, Figure 4.16C and Figure 4.18D). The heterogeneous methylation pattern has been observed previously in an *E. coli* rDNA mutant (Schuwirth et al., 2006) but was left uncommented. Additionally, a U●G at the opening of h45 (U1515●G1520, *Ec* numbering) was also seen in the small ribosomal subunit of *Euglena gracilis* (*Eg*) chloroplasts (cSSU) where it leads to either no dimethylation at all or sole dimethylation of A1518 (*Ec* numbering, see Figure 5.2) (Van Buul et al., 1984).

While our data do not resolve the exact methylation pattern of which adenosines are methylated on a single strand of 16S rRNA, it does give additional support for the necessary opening/destabilization of the helix/tetraloop by introduction of methylation (Demirci et al., 2010; Rife and Moore, 1998; Van Charldorp et al., 1981). In a typical GNRA (here **GGAA**) tetraloop The first **G** and the last **A**, as well as the second **G** and the second to last **A** interact with each other as a sheared pair (see arrows Figure 5.2) (Heus and Pardi, 1991; Jucker et al., 1996). This appears to be different in a GGm₂⁶Am₂⁶A

tetraloop of h45, as NMR data shows that methylation of A1519 (last) disrupts the interaction with the first G of the GGAA tetraloop (Rife and Moore, 1998). m_2^6 A1519 stabilizes the positioning of m_2^6 A1518 by stacking the nucleobases on each other (see Figure 5.3B). The RsmJ induced methylation m_2 G1516 (Basturea et al., 2012) in *E. coli* (see Figure 5.2) appears to have no effect on tetraloop stability, regardless of KsgA dependent methylation (Rife et al., 1998) and is not present in *H. volcanii* (Grosjean et al., 2008) or *E. gracilis* chloroplast ribosomes (Van Buul et al., 1984). This destabilization and stacking of nucleobases leads to the outward rotation of GAA from the GGAA tetraloop, forming hydrogen bonding between h44 and h45 and thereby stabilizes the P- and A-site of the maturing SSU (see Figure 5.3A, C, D). In the case of *H. volcanii* ribosomes, less methylation appears to be necessary for h45 destabilization. When taking into account the previously postulated passive methylation imprint and “passive” dissociation (Boehringer et al., 2012; Connolly et al., 2008), bound HvKsgA perhaps only dimethylates one Adenosine that is in the proximity of its binding pocket, and as soon as sufficient h45 destabilization is reached, concomitant RNA structural changes contribute to KsgA dissociation and/or does not re-engage methylation.

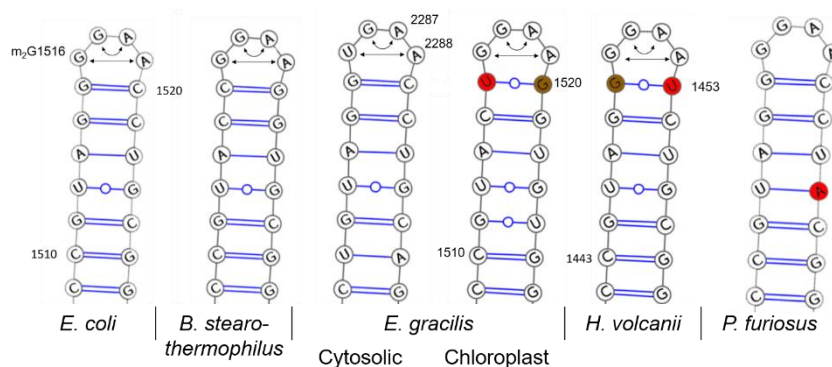


Figure 5.2 Various types of helix openings 45 in *E. coli*, *B. stearotherophilus*, *Euglena gracilis* (chloroplast), *H. volcanii* and *P. furiosus* ribosomes.

E. coli, *Euglena gracilis* and *H. volcanii* numbering, respectively. GNRA tetraloop interaction in unmethylated state marked by arrows.

While there is no obligate order of which adenosine is methylated first (O’Farrell et al., 2006), if HvKsgA, by chance, dimethylates A1452 (*Hv* numbering) first, the h45 destabilization could be enough to trigger dissociation in *H. volcanii*. However, if A1451 is methylated first, h45 destabilization could be insufficient, HvKsgA is not released and dimethylates the second adenosine. Of course, it is also possible that only the adenosine that is bound first is methylated and HvKsgA always dissociates after one round of dimethylation. Both scenarios would explain the resulting two band pattern observed in *H. volcanii* (Figure 4.10) and *E. coli* (AVS69009-pHK-rrnC-C1520U Figure 4.16) the lower stop “shows” the first of both methylated adenosines (the RT would stall on the first one) while the second shows only the second. From 76 randomly picked *Hv* methylation patterns, the majority has equal signal strength, but if one shows a stronger signal, it is mostly the first nucleotide that induces a stronger primer extension stop (Figure 5.4).

The molecular explanation why *E. gracilis* chloroplast ribosomes are methylated only at A1518 and sometimes not at all is unclear, there is no KsgA/Dim1 or KsgA-like protein found in neither the genome nor chloroplast plasmid. However, the genome is highly complex and is to date incomplete and could be missing the data for KsgA/Dim1 (Ebenezer et al., 2019). The likelihood of the almost universally conserved KsgA/Dim1 being absent is low, especially since the cytosolic SSU shows dimethylation of both adenosines in the helix 45 (Schnare and Gray, 2011).

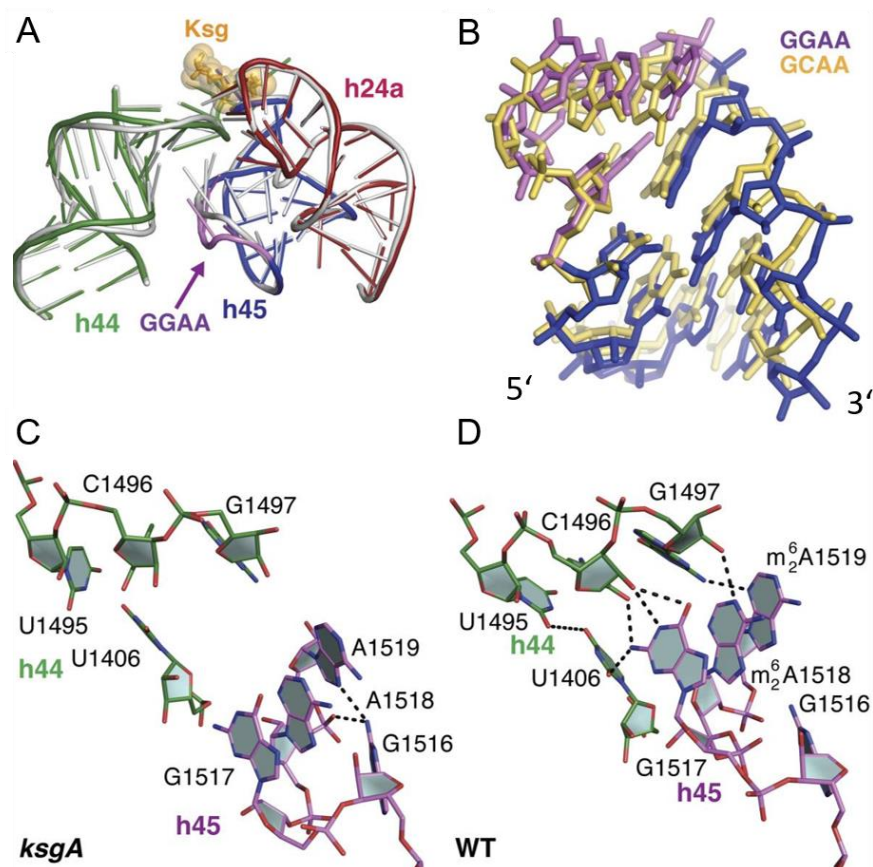


Figure 5.3 **Influence of KsgA dependent methylation on the GGAA tetraloop of helix 45 and hydrogen bonding to helix 44 in *E. coli*.**

[A] Bending of the GGAA tetraloop in the unmethylated subunit (violet) is visible. The wild-type 30S subunit structure (PDB entry 1J5E) is superimposed (gray). Kasugamycin (Ksg, orange spheres) from PDB entry 1VS5 is superimposed. [B] Comparison of the helix 45 tetraloop with typical GCAA tetraloop as observed in PDB entry 1ZIH. [C,D] The *ksgA* mutation prevents the formation of a hydrogen-bonding network between helices 45 and 44. The helix 45–44 interface in the *ksgA* mutant (e.g., 30S subunits prior to methylation) (C) and in the wild-type, fully methylated 30S subunit (D). Panels C and D are from identical viewpoints. (modified from Demirci et al., 2010)

The common feature resulting in abnormal methylation patterning is the exchange of the nucleotide following of the most 3' m_2^6A , this is not only the last nucleotide before the opening of the helix but also “the crucial turning phosphate” of the GGAA tetraloop (the phosphate where the backbone undergoes its largest change in direction, $\sim 180^\circ$) (Rife and Moore, 1998). While *Eg* chloroplast ribosomes change this turning phosphate containing nucleotide to a “larger” Guanine (*E. gracilis* cSSU G1520 vs. *E. coli* C1520), *Hv* has swapped to a similar sized nucleotide (*Hv* U1453). This difference of pyrimidine to purine at position 1520 (*Ec* numbering) might pose as a sterical restriction that prevents potential cytosolic KsgA dependent methylation or uses a different mechanism (perhaps

involving snoRNPs, like postulated for *N. equitans* (Seistrup et al., 2016)) to methylate the adjacent adenosine (1519) in *E. gracilis* chloroplast SSU biogenesis. *Bacillus stearothermophilus* (now known as *Geobacillus stearothermophilus*) also has this G1520, but contrary to the wobble base pair in *Eg* chloroplast SSUs (U1515●G1520) it is in a Watson-Crick base pair (C1515-G1520) at the opening of h45 (see Figure 5.2). This results in an increased melting temperature of the helix45 for both wild type and $\Delta ksgA$ in *B. stearothermophilus* compared to the respective genotypes in *E. coli* (Heus et al., 1990), arguing for a stability dependency of purine-pyrimidine vs purine-purine stacking 3' of the GGAA tetraloop (Rife and Moore, 1998). Nevertheless, *B. stearothermophilus* shows classical, full dimethylation of both adenosines (Buil et al., 1983) and contains the gene coding for KsgA, arguing for the issue being with the unclear methyltransferase in *E. gracilis* cSSU biogenesis.

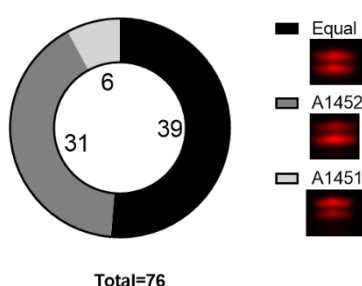


Figure 5.4 **Methylation pattern distribution of *H. volcanii*.**

76 Images were scored qualitatively. Indications to criteria given on legend. Only lanes showing two clearly distinguishable primer extension stops were used for quantification.

The stacking of the nucleotides at A1452 and U1453 might be crucial for pre-destabilization in *H.volcanii*. It could produce a conformation that is contrary to the observations in *B. stearothermophilus* where the nucleotide changes from pyrimidine to purine. While still Watson-Crick paired, this leads to an increase in melting temperature and thereby stability (see Table 2). Compared to *H. volcanii*, switching to a different pyrimidine and thus changing to a non-Watson-Crick wobble could decrease the melting temperature and thereby the stability of the loop. This could reduce the need for methylation dependent destabilization of the helix and thus to an altered methylation pattern.

Table 2 **Stability and composition of the helix 45 of *E. coli*, *B. stearothermophilus* and *H. volcanii*.**

Sequence: 5' to 3', **bold**: base paired, underlined: stacked nucleobases. t_m °C calculated with primer 3 (mM KCl).

	<i>E. coli</i>	<i>B. stearothermophilus</i>	<i>H. volcanii</i>
Sequence	CCGUAG GGGAA <u>C</u> CUGCGG	CCGUAC CGGA <u>A</u> GUGCGG	CCGUAG GGGAA <u>U</u> CUGCGG
GC %	72.2 %	70.5 %	66.6 %
Stacking	<u>Purine - pyrimidine</u>	<u>purine – purine</u>	<u>Purine - pyrimidine</u>
Basepair	Watson crick	Watson crick	Non-Watson crick (wobble)
Stability	t_m °C(52/57)	t_m °C(69.5/71)	n.D.
(t_m °C, ΔG°_{37})	ΔG°_{37} (-10.8 ±1.7 / -15.4 ±1.7)	ΔG°_{37} (-31.0 ±4.2 / -31.8±4.8)	
(Heus et al., 1990)			

(wt/ <i>ΔksgA</i>)	Medium stability	High stability	Low Stability ?
t_m °C (M KCl)	56 (50mM)	57 (50mM)	54 (50mM), 72 (2M)

Why these nucleotide exchanges have evolved is not clear. The basis for having a change in flexibility of the h45 loop from stable (unmethylated) to more flexible (methylation) underlies the passive checkpoint participation of KsgA in SSU biogenesis. The trigger for this methylation imprinting are structural rearrangements of the maturing ribosome, perhaps the nucleotide exchanges prevent that premature methylation occurs by accident which would result in premature dissociation of KsgA and inevitably letting immature SSUs enter the translational pool. Thus, the substrate is composed in such a way to compensate for innate stability changes from for example temperature or salt. High temperatures could result in a premature passive imprinting (methylation) of KsgA at high temperature due to the increased flexibility and therefore accessibility of the adenosines of h45. For *B. stearotherophilus* this more thermostable helix 45 composition could prevent such a premature methylation (and following release) of KsgA at growth temperatures of 50-65 °C (Schlegel and Zaborosch, 1992) (see Table 2). Yet in organisms growing at even higher temperatures (>90 °C) like *T. celer* or *P. furiosus*, a theoretically less thermostable “*E. coli*-like” h45 (GGGAAC) composition is used. This would result in an already very flexible (melted) immature/non-methylated h45 at these temperatures. Perhaps here the postulated less suitable substrate (Formenoy et al., 1994) (wobble-less stem at position 7, see Figure 5.2) avoids the risk of premature methylation by lowering the methylation reaction kinetics to such an extent that only if everything is in order and the substrate has a stable interaction with the binding pocket of KsgA the imprint takes place. Contrary to high temperature, high salt concentrations lead to increasing melting temperatures of structured RNA (Tan and Chen, 2011). The high intracellular salt concentration in *H. volcanii* perhaps, but unlikely, requires to compensate this by increasing the innate flexibility of the h45 loop via the wobble base pair at the opening. This however does not explain the observed heterogeneous methylation pattern in *H. volcanii* and *E. coli* (G1520U, see Figure 4.16), and why *H. volcanii* can methylate a “*E. coli*-like, more stable h45 (U1453C)” from the rDNA reporter (see Figure 4.18). Perhaps using the non-native h45 (U1453C) in *H. volcanii* results in a “sub-optimal” maturation pathway but in laboratory conditions this has no dramatic effect on viability/ fidelity. In *E. coli* (G1520U) this might lead to a slight increase in premature dissociation of KsgA due to the increased flexibility. Here testing different salt media compositions with varying salt concentration could induce an effect on methylation and perhaps on exponential growth. Yet in the end this theory does not take the other organisms into account that also display this “open” conformation and are evolutionary rooted deeper than *H. volcanii* (see Figure 3.3) and are not halophilic, e.g. *A. fulgidus* of the Methanogens Class II, and the other way around, thermophiles (\neq Thermococcales) that have a wobble in the stem, e.g. *M. kandleri* of Methanogens Class I (see Figure 4.15).

The variability of helix 45 in this otherwise highly conserved region (Domain IV of the 16S rRNA) has been recognized early on in all three kingdoms (Van Knippenberg, et al., 1984). Why archaea show such diversity is unclear (Figure 4.15) but it could be a result from the adaptation necessity discussed above. They almost universally use the conserved methyltransferase KsgA. Remarkably, the only known exception *Nanoarchaeum equitans*, has an almost identical h45 to *E. coli* (A1507-U1528 at the base of the stem are missing) but is lacking the modifying enzyme and is proposed to use sRNPs instead (Seistrup et al., 2016).

To test flexibility effects of different base compositions, the *E. coli* rDNA reporter system (Figure 4.16) offers a clean genetic background, compared to our *H. volcanii* reporter system that still has the endogenous rDNA in the background (Figure 4.18). However, *H. volcanii* offers a broad range of salt concentration and growth temperature to test for, both affecting the stability of the helix. For further testing it would be interesting to look at the effect on methylation by introducing an *E. gracilis* cSSU and *B. stearrowthermophilus* helix 45 into both rDNA reporter systems. As well as to test if *E. coli* can methylate the enlarged mutation we introduced in *H. volcanii* (G1448C, U1453C) that showed no visible effect (Figure 4.18), either because of incompatibility to KsgA or perhaps down regulation/degradation of the plasmid-encoded rRNA. Also, it could be possible that this enlarged conformation of h45 already contacts h44 at a certain point of maturation and thus does not require KsgA dependent methylation and/or leads to premature dissociation of the factor. To get a final answer on how many methylations are on a single strand of ribosomal RNA of *H. volcanii* or *E. coli* (AVS69009-pHK-rrnC-C1520U) Liquid Chromatography-Mass Spectrometry would be best (Yuan, 2017). But perhaps capillary electrophoresis can also answer this question, semi quantitatively. In regard to purine-pyrimidine vs purine-purine stacking it would be interesting to see the NMR structure of the *H. volcanii* GGAA tetraloop of the separated h45 of both wild type and Δ ksgA.

In conclusion, this analysis clearly showed how small structural changes can have a large impact on the maturation process, thus it is necessary to have tools at hand that provide the possibility to verify structural predictions. The hypomethylated state of the adenosines of h45 observed in *H. volcanii* and *E. coli* with the h45 mimicry strengthen the postulated passive dissociation by surrounding structural rearrangements of the maturing SSU (Boehringer et al., 2012; Connolly et al., 2008) instead of the requirement of full dimethylation for KsgA dissociation .

5.3 The release mechanism of KsgA remains uncertain in archaea

The hypomethylated state of h45 in *H. volcanii* gives additional support for a release mechanism that is independent of full methylation but a consequence of structural changes that occur after h45 is relaxed sufficiently to bridge with h44 as shown in previous data in *E. coli* (Demirci et al., 2010). Whereas in *E. coli* KsgA is supposed to dissociate passively after methylation has occurred by decreased affinity to the methylated substrate (Boehringer et al., 2012; Poldermans et al., 1979) or in competition for the similar binding site with RbfA (Sharma and Woodson, 2020), the release of Dim1

in yeast requires Fap7 to actively release or remove ScDim1 from the maturing ribosome (Ghalei et al., 2017). In *E. coli* this has been shown *in vitro* on purified methylation competent SSUs, in comparison to yeast where the release occurs off a 80S-like proofreading pre-ribosome (as described in the introduction 3.2.3.5.3). This puts *H. volcanii* into an interesting position as it does not contain a clear RbfA homologue, yet archaeal KsgA is clearly more homologous to *E. coli* KsgA than yeast Dim1 (Pulicherla et al., 2009). On the other hand the *H.volcanii* genome contains a homologue to Fap7 which shows typical ATPase/adenylate kinase activity (see Figure 5.5). The hypothetical advantage of *H. volcanii* over yeast (for this scientific question) is the possibility do delete the gene for KsgA, offering a good system to test the release regarding both potential mechanisms.

We were able to show that incubating a crude hv Δ ksgA cell lysate or purified Δ ksgA-SSUs with recombinant HvKsgA in the presence of excess SAM resulted in reconstitution of the methylation reaction (Figure 4.12B). This was the basis for establishing the following release assays where we incubated recombinant HvKsgA and a crude cell lysates of hv Δ ksgA cells in the presence or absence of SAM. When SAM is present methylation could occur and the recombinant hvKsgA was absent in the 30S fraction after separating the incubated lysates on a sucrose gradient (Figure 4.19). However, this did not resolve if the release occurs independently of additional factors, since everything except KsgA is present in the initial cell lysate, e.g. hvFap7. But also, it cannot exclude the release occurring from a particle similar to the 80S(70S)-like proofreading particle and/or joined LSU and a unmethylated SSU. Yet there is no evidence for such a 70S-like proofreading particle in archaea.

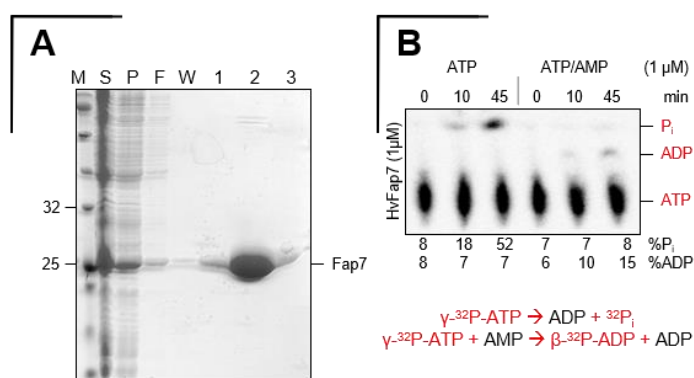


Figure 5.5 **Purification and ATPase/adenylate kinase activity of hvFap7.**

[A] Talon beads Purification of recombinant hvFap7-His₆ from 500 ml culture in K1800 buffer M: Marker, S, supernatant, P: Pellet, F: Flow Through, W: Wash, each 0.2 % of total fraction volume. 1 - 3 Elution 2.5 % of total fraction volume. **[B]** ATPase, Adenylate cyclase testing, 14 μ Ci γ -³²P-ATP per reaction. 20 % of total reaction volume per time point were stopped according to 7.2.3.4 and loaded onto TLC (as described in 7.2.3.4). Pi/ β -³²P-ADP Release percentages were calculated with Fiji.

To address this issue, a pre-bound complex consisting of an unmethylated SSU and recombinant HvKsgA would provide a system that is potentially free of additional assembly factors but remains methylation competent upon the addition of SAM. This was achieved by incubating a cell lysate of hv Δ ksgA with recombinant HvKsgA in the absence of SAM with following separation via sucrose

gradient centrifugation. The 30S fraction then contained the desired pre-bound complex and could be used for release assays using SAM or other factors such as hvFap7.

The first approach to test the release of KsgA from the bound SSU, relied on ultra-centrifugation after the addition of SAM and/or Fap7. Here, the denser SSU would migrate through either the gradient or to the pellet and the small recombinant protein would remain attached to the SSU in the absence of SAM or be detectable in the supernatant if SAM/Fap7 dependent release has occurred. Unfortunately, both rotors used for sucrose gradients the SW40 and SW60 require full loading (14 and 4.4ml respectively) and resulted in too strong dilutions and were unable to detect HvKsgA₍₆₎His. Consequently, smaller volume rotors were tested, with and without sucrose cushions but those available could not pellet the ribosomal subunits, very likely due to insufficient rotary force (TLA-55). Another method using size exclusion centrifugation using AMICON 100k filter units also revealed further issues with stickiness of the recombinant proteins in the filters (undetectable in the flow through in the protein only control). A summary of the results is shown in Figure S 16.

For this type of experiments the issue of detectability could have been avoided by testing available KsgA or Dim1 antibodies that are used for EcKsgA or ScDim1 as the protein is highly conserved and very likely detects HvKsgA on a western blot. Our approach using the His Antibody (very unspecific on *Hv* cell lysates and with low detection range) was in hindsight not the best idea when having to work at lower/limited concentrations. Our unfortunate late discovery of possible low salt purification of recombinant HvKsgA with accompanying greater and purer yields (Figure 4.12A) would have allowed to test affinity tags that offer better antibody detection and have previously been difficult or impossible to purify in high salt conditions, e.g. Streptavidin or Protein-A. Of course complementation testing and SSU binding assays would be necessary, but N-His₍₆₎-ProteinA-HvKsgA has been shown to complement *in vivo* and thus would be a good candidate (Figure 4.11). Also, being able to use higher rcf rotors, such as a TLA-100, could have likely improved separation at low volumes.

The second approach was based around single molecule methods such as total internal reflection fluorescence (TIRF-) microscopy (Thompson et al., 1981) or Fluorescence Correlation Spectroscopy (FCS) (Magde et al., 1972). Both techniques rely on fluorophores attached to the interaction partners, i.e. the SSU and HvKsgA. TIRF microscopy measures a populational change of the individual and overlapping signals. In this case, the pre-bound particles would emit mostly a merged signal, i.e. orange [SSU (green/GFP) + HvKsgA (red/Cy3[5])]. After the potential release has occurred via SAM and/or Fap7 addition, each particle would emit a solitary fluorescent signal, green and red, resulting in the average counts of orange decreasing and single green and red increasing. FCS on the other hand measures the diffusion speed of fluorescently labelled particle in a volume using a MicroTime 200 microscope. In this case a pre bound particle emits a similar speed for the red and green channel as they are bound and migrate at the same speed, after the potential release has occurred via SAM

and/or Fap7 addition the green (GFP) diffusion speed remains the same (very little change in mass) but the red signal (Cy3[5]) now has experienced a significant change in mass and should migrate at a measurable higher speed (KsgA alone).

Both techniques require a GFP labelled subunit, thus I established a GFP tagging system by creating a suitable vector backbone and tested if GFP tagged small ribosomal proteins (uS4 and uS7) can be expressed and are integrated into the SSU as well as if they emit a fluorescent signal in the microscope (see Figure S 17). The complementary fluorophore was added to the recombinant protein via either AzF labelling (integrating amber stop codons and desired sites using specific expression cells that can be labelled specifically with Dyes such as Cy3 or Cy5 (see Figure S 18A-C), described in (Willkomm et al., 2017)) or NHS ester labelling (unspecific labelling of Lysines). Both methods produced functional recombinant proteins (see Figure S 18D). The single molecule measurements were performed by Leonhard Jakob in the department of Microbiology and the initial sample preparation is described in 7.2.3.9.

Unfortunately, neither TIRF nor FCS yielded conclusive results. For TIRF microscopy, the main issue was with the immobilization step, i.e. the necessity of a biotinylated GFP antibody that is immobilized on a PEG/PEG Neutravidin slide that then immobilizes the GFP tagged ribosomal protein that is integrated in the SSU to the focal point. Unfortunately, this GFP antibody was incompatible to the high salt Buffers used in the *Hv* system (KCl 1.8 M, 50 mM MgCl₂) and resulted in no GFP signal at the focal point, i.e. no immobilization, likely due to denaturing of the antibody (data not shown). When collapsing the ribosomes by lowering the salt concentrations to ~200 mM (Gunde-Cimerman et al., 2018) a green signal appeared at the focal point, i.e. detached GFP-S7 (data not shown). To my knowledge salt stability of GFP antibodies is not well documented, very likely due to the rare application. Another issue with high salt concentration is the effect on refraction, as higher salt concentrations lead to a higher refractory index (Stupar et al., 2012), which could influence measurements on this scale, independently of the GFP antibody issue.

Similar issues arose in the FCS where we measured many different diffusion speeds in the volume and could not detect correlating speeds for the individual fluorophores or observe any differences after SAM treatment (data not shown). Here again it could be due to high salt concentration and/or impurities.

To validate if TIRF and/or FCS are suitable methods to use for this binding and release assay it would be wise to reproduce the results from previous studies in *E. coli* (Boehringer et al., 2012; Connolly et al., 2008; Poldermans et al., 1979) with these novel methods. If successful, fine tuning the reaction parameters for *Hv* could help. For example, using low salt concentrations to purify the AzF-tagged recombinant *Hv*KsgA (Figure 4.12A) might result in less impurities and better signal separation in the FCS measurements. But maybe moving to another archaeal organism with easier biochemistry, i.e. lower salt concentrations, would be best to test a Fap7 involvement in an *ΔksgA* background. The

two KsgA knock outs obtained in *P. furiosus* and *S. acidocaldarius* (Figure 4.10B), could be potential candidates, but preliminary results speak against this. 1) SaciKsgA could not be affinity purified well via N- or C-Terminal His tagging and temperature denatured clarified protein did not complement well *in vitro* (observations by practical student Michaela Bauer). 2) Preliminary complementation experiments of *P. furiosus* $\Delta ksgA$ lysates with recombinant PfuKsgA₍₆₎His or EcKsgA₍₆₎His did not work (observations by practical student Bernd Daller and myself).

Yet the main issue for both methods is the lacking comparability to the yeast system (release from 30S vs. 80S-like particle) (Connolly et al., 2008; Ghalei et al., 2017). Regarding the 80S-like scFap7 dependent release, so far, we were unable to observe any 70S fractions, mono or polysomal for *H. volcanii* in the conditions used. While writing this thesis, a protocol has been published that describes a method that inhibits 70S dissociation and reproducibly shows these 70S mono- and polysome fractions in *Hv* on a sucrose gradient (Gelsinger et al., 2020). While it is unknown if yeast-like functional proofreading 80S-like particles exist in *Haloferax volcanii*, this new technique would at least enable to purify 70S particles from *hv* $\Delta ksgA$ and see if they can be methylated by- and show KsgA release or not.

In human, Rio2 has been speculated to activate Dim1 dependent methylation via phosphorylation (Sloan et al., 2019), yet methylation was not impaired in neither *Ario1*, *Ario2* nor *Ario1Ario2* knockouts of *H. volcanii* (data not shown). Yet this of course also lacks comparability, due to the methylation taking place very early in human (nucleoplasm) vs comparably late (also, lacking cell compartmentalization) in *H. volcanii* (Grünberger et al., 2020).

Overall, both release assays need major improvements in order to test factor depended analysis of KsgA release from ribosomal subunits, but a good basis has been set for future experiments.

5.4 Most RNA structure probing chemicals are suitable for model archaea

As previously introduced, RNA structure probing has been extensively used to study the folding, context, and interaction of various RNAs. While this was mostly done in model organisms from bacteria and eukaryotes, our goal was to port and test these chemicals in our two model archaea, *Haloferax volcanii* (*Hv*) and *Sulfolobus acidocaldarius* (*Saci*). This would enable us to test 2D structure predictions in regard to ribosomal RNA. However, both grow in very specific media, so it was crucial to test suitability of these RNA probing chemicals in diverse conditions.

Luckily, all SHAPE reagents were soluble in both, the salty and acidic media up to a certain molarity (review Table 4.1). With the frequented chemical for rRNA analysis, DMS, (Hulscher et al., 2016; Swiatkowska et al., 2012) we were less lucky as its very harsh quenching conditions disrupted the *Hv* cells and could not be used, however we did not test it with *Saci* cells. CMCT is generally not taken up well by cells (Harris et al., 1995; Mitchell et al., 2019) and was just tested on lysed cells extracts, which worked well for *Hv* and ok for *Saci*. Contrary to the literature (McGinnis et al., 2015;

Takahashi et al., 2016), we had issues when using 1m6/1m7 *in vivo* with *E. coli* for a gel based read-out. This issue has also been observed by others (Lee et al., 2017; Spitale et al., 2013) and is a debated topic (Smola and Weeks, 2018). This issue stresses the importance of testing the desired chemical(s) for the target organism and to have an alternative chemical available if issues in cell uptake arise.

Both working techniques could be used to verify the structure predictions of our *Hv* helix 45 structure discussed earlier. It showed that indeed the wobble at the opening of the helix lead to SHAPE and CMCT accessible nucleotides at this position *in vitro*, *in* and *ex vivo* (Figure 4.14). In the stem the accessibility of U1445 changed in between *ex vivo* and *in vitro* when using CMCT, pointing towards the protein occlusion of this crucial wobble pair (Formenoy et al., 1994) in the RNP context. Yet, this was never accessible for the SHAPE chemicals regardless of composition. Also, we showed increased flexibility of helix 44 in *ΔksgA* (Figure 4.28), most likely due to decreased interaction of helix 44 and 45, as discussed earlier.

High throughput SHAPE read-outs (SHAPE-seq/SHAPE-Map) could offer large scale analysis of archaeal (pre-) ribosomal structures, and have been used before, for bacterial ribosomal structures (McGinnis et al., 2015; Watters et al., 2016).

The established protocol gives a good basis for future research of archaeal RNA structure and the application of the perhaps most versatile reagents (1m6/1m7/NMIA) are described in detail in (Knüppel et al., 2020) and can be implemented by laboratories working with these organisms.

5.5 4-TU labelling is working in archaea

We could implement 4TU metabolic labelling into two model archaea and in perspective of the advances that were made in the field of ribosome biogenesis over the years. During the last year, UV-cross-linking has been established for *H.volcanii* in our lab and in combination with 4TU labelling (PAR-Clip) (Hafner et al., 2010a), this might offer insights into binding interfaces of RNA and candidate proteins.

Regardless of uracil auxotrophy or prototrophy it works well for both organisms, while staying within the limitations of concentration dependent toxicity. When porting this method to other archaeal organisms, toxicity however should be evaluated as it has been associated to rRNA synthesis defects (Burger et al., 2013). With *Saci*, in the absence of 4TU, we observed unspecific labelling in the range of tRNAs (Figure 4.2) that hint toward unspecific biotinylation of these perhaps endogenously 4TU modified tRNAs. While bacteria contain 2TU and 4TU modified tRNAs (Rogers et al., 1995), the biosynthesis of 4-thiouridine remains unclear in archaea (reviewed in Čavuzić and Liu, 2017). Also compared to 4TU pulse labelling in other organisms like *S. cerevisiae* (Braun et al., 2020), we do not observe any precursor particles in short pulse times. If this is due to the small size increase of the individual archaeal pre-RNAs compared to their mature equivalents or to the faster turnover rate of these RNAs is unclear. Yet large precursors such as the archaeal large precursor equivalent to the

35S rRNA is also not visible arguing for a higher turnover rate. This might be circumvented by using the affinity purification of these particles, but adds an additional step with potential loss of RNA. Yet combining depletion analysis using CRISPRi or using plasmid-based complementation of mutants with this method, might accumulate nascently labelled precursor particles. Potential (essential) candidates that are involved in 5' and 3' processing of the (circular) pre-16S rRNA should be suitable candidates and CRISPRi constructs have already been tested and/or are in the making.

The detailed experimental setup and results have been published (Knüppel et al., 2018) and has been readily applied by others in our lab (Braun et al., 2020).

6 CONCLUSION

In this Study we were able to show the functional conservation of the highly conserved KsgA/Dim1 (di-)methyltransferase in extensive detail in *H. volcanii* and to a lesser extent in *S. acidocaldarius* and *P. furiosus*. Contrary to Yeast and higher eukaryotes but similar to bacteria, the gene for KsgA/Dim1 is not essential in our three archaeal organisms but has manifold implications for the organism. In *H. volcanii* we observed no effects on doubling time of $\Delta ksgA$ cells, but motility defects, increased biofilm formation and a light change in cell morphology. Interestingly, proteome analysis revealed that a subset of their respective genes are also differently regulated, with an overall light negative effect on translation, very likely due to impaired translation initiation from the $\Delta ksgA$ dependent immature state of the ribosome.

Functional complementation analysis revealed conserved catalytic domains with similar implications. The methylation status of the substrate in *H. volcanii* revealed an atypical heterogenous pattern that was not documented and discussed in the hitherto studied organisms and appears to be specific to a certain group of archaea and results from a single nucleotide exchange in the helix45 of the 16S rRNA. We could verify this by RNA structure probing and also by introducing the same mutation into an rDNA reporter system in *E. coli*. The evolutionary drive behind this mutation is unclear. *In vitro* reconstitution of (di-)methylation on cell lysates and purified 30S subunits were possible and were used as a basis for binding and release assays using recombinant HvKsgA. Detailed analysis regarding the release from purified 30S subunits however failed due to technical limitation and high salt incompatibilities. Yet, seeing that eukaryote like assembly factors aiding in the release of KsgA are present in *H. volcanii*, makes this binding and release assay an interesting objective for future research.

The verification of this unusual helix conformation required the establishment of methods that enable chemical structural probing. Thus, we tested various SHAPE chemicals, DMS and CMCT for the application in *H. volcanii* and *S. acidocaldarius*. Aside from DMS, CMCT and SHAPE worked well

in both organisms in varying contexts. To study the dynamics of RNA we provided proof of principle for 4-TU Pulse-/Chase labelling in *S. acidocaldarius* and *H. volcanii*.

7 MATERIAL AND METHODS

7.1 Materials

7.1.1 Chemicals

All chemicals used in this work were purchased from either Sigma-Aldrich, Merck, Fluka, Roth or J.T.Baker.

Growth Media was made from ingredients purchased from BD Biosciences (Bacto Agar, Bacto Peptone, Bacto Tryptone and Bacto Yeast Extract), Sigma-Aldrich (amino acids and uracil) and Sunrise Science Products (Yeast Nitrogen Base (YNB), amino acids and adenine). All solutions, buffers, media were prepared with purified water from an Elga Purelab Ultra. The resistivity was at a constant 18.2 M Ω -cm and a guaranteed organic content of less than five parts per billion. pH measurement was done at room temperature and adjustments were made with HCl or NaOH, unless stated otherwise. Growth media was autoclaved for 20min at 120 °C and stored depending on instructions.

7.1.2 Buffers

All buffers were stored at Room temperature unless stated otherwise

Table 7.1 Commonly used buffers

Buffer	Ingredients	Final concentration
10x PBS	NaCl KCl KH ₂ PO ₄ Na ₂ HPO ₄ pH 7.4 with NaOH	1.37 M 27 mM 18 mM 0.1 M
1x TBE	Tris boric acid EDTA pH 8.0	89 mM 89 mM 10 mM
4x Lower-Tris	Tris pH 8.8 SDS	1.5 M 0.4 %
4x Upper-Tris	Tris pH 6.8 SDS	0.5 M 0.4 %
AE	NaOAc pH 5.3 EDTA pH 8.0	50 mM 10 mM

Denhards (50x)	Ficoll (Typ400, Pharmacia) Polyvinylpyrrolidone BSA (FractionV, Sigma)	10 mg/ml 10 mg/ml 10 mg/ml
HU-Sample buffer	SDS Tris pH6.8 EDTA β -Mercaptoethanol (add fresh) Urea Bromphenolblau	5 % 200 mM 1 mM 1.5 % 8 M
<i>Hv</i> -Buffer	KCl MgCl ₂ Tris-HCl pH7.5 β -Mercaptoethanol	2.8 M 75 mM 10 mM 2 mM
K1800	Glycerol Tris HCl, pH 7.5 KCl Imidazol MgCl ₂ β -Mercaptoethanol	10 % (w/v) 20 mM 1800 mM 10 mM 50 mM 2 mM
K200	Glycerol Tris HCl, pH 7.5 KCl Imidazol MgCl ₂ β -Mercaptoethanol	10 % (w/v) 20 mM 200 mM 10 mM 5 mM 2 mM
MM (for qRT-PCR)	10x PCR-buffer (Qiagen) MgCl ₂ (Qiagen) dNTPs	2x 2 mM 0.4 mM
MOPS running Buffer (10x)	Sodium Acetat Anhydre MOPS EDTA pH 8.5 Adjust to pH 7 with NaOH store in dark RT	20 mM 0.2 M 10 mM
NaAc	NaAc * 3 H ₂ O pH 5.2 with acetic acid	3M
PBS-T	1x PBS Tween	1x 0.05 %
PeX Loading Buffer	Deionized formamide EDTA pH 8.5 Bromophenol blue	95 % 20mM 0.05 %

Prehybridization Buffer	Formamide SSC SDS Denhards	50 % 5x 0.5 % 5x
RNA Loading Buffer	Formamide Bromphenol Blue	50 % 0,05 %
SDS-Running buffer	Glycine Tris SDS	192 mM 25 mM 0,1 %
SG (for qRT-PCR)	SYBR green (Roche) in DMSO	1:400000
SSC (20x)	NaCl Natrium-Citrat Trihydrat pH 7	3M 0.3
Transfer Buffer (no SDS)	Tris Glycine MeOH	25 mM 192 mM 20%

Table 7.2 Transformation buffers

Media	ingredients	Final concentration
Buffered Spheroplasting Solution	NaCl KCl Tris-HCl pH 8.5 Sucrose Autoclave for 10 min	1 M 27 mM 50 mM 15 %
Unbuffered Spheroplasting Solution	NaCl KCl Sucrose Adjust pH to pH 7.5, Autoclave for 10 min	1 M 27 mM 15 %
Spheroplast Dilution Solution	Salt Water 30 % Sucrose Autoclave for 10 minutes. When cool add 0.75 ml of 0.5 M CaCl ₂	23 % 15 %
Regeneration Solution	Salt Water 30 % 10X YPC Sucrose	18 % 1 x 15 %
Transformant Dilution Solution	Salt Water 30 % Sucrose	18 % 15 %
Tfbl	KAc MnCl ₂	30 mM 50 mM

	KCl Glycerin adjust to pH 5.8 with 0.2 M acetic acid filtrate through a 0.22 µM filter store @ 4°C	100 mM 15 %
TfbII	MOPS CaCl ₂ KCl Glycerin adjust to pH 7 with NaOH filtrate through a 0.22 µM filter store @ 4°C	10 mM 75 mM 10 mM 15 %

7.1.3 Media

All media was stored at RT unless stated otherwise

Table 7.3 Media composition *E. coli*

Media	Ingredients	Concentration
LB	Bacto Yeast Extract Bacto Tryptone NaCl stored at 4°C	0.5% 1% 1%
Tryptone-Only	Bacto Tryptone NaCl	1 % 0.5 %
Plates	add 0,8 % Agar (w/v) to bottles before autoclaving	

Antibiotic	End concentration used
Ampicillin (Amp)	100 µg/ml
Chloramphenicol (Chl)	30 µg/ml
Gentamycin (Gen)	10 µg/ml
Kanamycin	100 µg/ml
Kasugamycin (prepare fresh)	250 µg/ml
Spectinomycin	50 µg/ml
Tetracyclin	10 µg/ml

Table 7.4 Media composition *H. volcanii*

Media	Ingredients		Concentration
Salt Water 30 %	NaCl MgCl ₂ * 6 H ₂ O MgSO ₄ * 7 H ₂ O KCl Tris-HCl pH 7.5 autoclave		4.1 M 0.15 M 0.14 M 94 mM 20 mM
10x YPC	Bacto Yeast Extract Bacto Pepton Casamino acids KOH		5 % 1 % 1 % 17 mM
10x Ca	Casamino Acids KOH Autoclave separately or filter sterilize (0.45 µm)		5 % 17 mM
Hv-YPC (complete media)	200ml Salt Water 30 % 100 ml H ₂ O 10x YPC autoclave CaCl ₂		11 % Ad. 333ml 3 mM
Hv-Ca+ (enhanced casamino acid broth)	200 ml Salt water (30 %) + 75 ml H ₂ O	autoclave	
	33 ml 10x Ca	Casamino acids Filter sterilize or autoclave seperately	51.5 mg/ml
	8.5 ml Hv-Minimal Carbon Source	Lactic acid Succinic acid Glycerol pH 7.5 with NaOH filter sterilize	10% 9% 1%
	4 ml Hv-Min Salts	NH ₄ Cl CaCl ₂ MnCl ₂ * 4 H ₂ O ZnSO ₄ * 7 H ₂ O FeSO ₄ * 7 H ₂ O CuSO ₄ * 5 H ₂ O filter sterilize	0.4 M 0.25 M 0.15 mM 0.13 mM 0.67 mM 16.7 µM
	650 µl 0.5 M KPO ₄ buffer pH 7.0	K ₂ HPO ₄ KH ₂ PO ₄ autoclave	0.3 M 0.2 M

	300 µl Thiamin & Biotin	Thiamine Biotin autoclave	0.9 mg/ml 0.1 mg/ml
Hv-Ca	200 ml Salt water (30 %) + 100 ml H ₂ O	autoclave	
	33 ml 10x Ca	Casamino acids	51.5 mg/ml
	650 µl 0.5 M KPO ₄ buffer pH 7.0	K ₂ HPO ₄ KH ₂ PO ₄ autoclave	0.3 M 0.2 M
	300 µl Thiamin & Biotin	Thiamine Biotin Filter sterilize	0.9 mg/ml 0.1 mg/ml

Table 7.5 Media composition *S. acidocaldarius*

Media	Ingredients		Concentration
Saci medium (Brock medium)	1 ml Brock I	CaCl ₂ * 2 H ₂ O autoclave	70 g/l
	10 ml Brock II	(NH ₄) ₂ SO ₄ MgSO ₄ * 7 H ₂ O H ₂ SO ₄ autoclave	130 g/l 25 g/l 1:1
	5 ml Brock III	KH ₂ PO ₄ MnCl ₂ * 4 H ₂ O Na ₂ B ₄ O ₇ * 10 H ₂ O ZnSO ₄ * 7 H ₂ O CuCl ₂ * 2 H ₂ O NaMoO ₄ * 2 H ₂ O VOSO ₄ * 2 H ₂ O CoSO ₄ * 7 H ₂ O H ₂ SO ₄ autoclave	56 g/l 0.36 g/l 0.9 g/l 44 mg/l 10 mg/l 6 mg/l 6 mg/l 2 mg/l 1:1
	1 ml Fe-solution	FeCl ₂ filter sterilize	20 g/l
	A.d. 1l H ₂ O		
	Bacto Tryptone		0.1%
	Dextrin		0.2%
	pH 3.5 with H ₂ SO ₄ autoclave Uracil		0.2 µg/ml

7.1.4 Nucleic Acids

7.1.4.1 Oligonucleotides

Oligonucleotides were ordered from MWG Operon and dissolved in ddH₂O to a concentration of 100 pmol and stored at -20 °C. The following accession numbers belong to the database of the Biochemie III chair of the University of Regensburg

Primer	5'-3'
oHv055-HvFap7-BspHI-Fw	GAGGCGTCATGAGAGTCGTCGTCACCGGC
oHv056-HvFap7-Bam-Rv	TATTATGGATCCTCATAGGTAGTCGATGAAGTC
oHv091-KOus-HvksaA-KpnI-Fw	gcatcgagGGTACCctacgcctctcggcgacg
oHv092-KOds-HvksaA-Bam-Fw	ggaacctGGATCCtccatgacgtcccccact
oHv093-KOds-HvksaA-Bam-Rv	gacgcgccGGATCCtgggagaggtatcgtgcggg
oHv094-KOds-HvksaA-XbaI-Rv	ctagccacTCTAGActcgcctcgaactctgga
oHv095-HvksaA-BspHI-Fw	GAGGCGTCATGACGAGCGACGGCAGCGA
oHv096-HvKsaA-Bam-Rv	TATTATGGATCCTTAGCGGCCGACCGACGCGG
oHv180-pTA1228seq-US	CACCGACCCGATTCGACCC
oHv181-pTA1228seq-DS	GGGAACAAAAGCTGGAGCTCC
oHv226-KsaA-us-comp-Fw	CGACTTCTACAACGACGCAC
oHv227-KsaA-us-comp-Rv	CTCGAACGACTCGAACGGTC
oHv228-KsaA-del-comp-Fw	GCGACAACGACGTGAAGTAC
oHv229-KsaA-del-comp-Rv	GAGCACCGCGGCGAGTGC GG
oHv230-KsaA-orf-comp-Fw	GACGTTCCGCCGCGCACCTGC
oHv231-KsaA-orf-comp-Rv	CTCCGAGGAGATGCCGTACG
oHv236-rDNA-Pci-3462-Rv	GCTTCGACATGTTTCGGTTGGAACC
oHv239-KsaA-E84A-Fw	CGACCGCGTGACCGTCGTCGCACAGGACCGGACGTTCCGCCG
oHv240-KsaA-E84A-Rv	GCGGCGAACGTCCGGTCTGTGCGACGACGGTCACGCGGTCCG
oHv255-16S-G468U-Fw	GACCGGTGCCAGCCGCCGCGtTAATACCGGCAGCTCAAGTG
oHv322-DY682-23Srep-Bss-Fw	ACGAGGTTTCATTCATGGGAC
oHv323-DY782-23Srep-Bss-Rv	GATAGCAGCCGACCTGTCTC
oHv324-DY682-16S-3end-Rv	AGGAGGTGATCCAGCCG
oHv325-DY782-16S ITS-5end-Rv	CGTGTGAGCCACCCCGTCCG
oHv326-DY682-Ec_16S-3end-Rv	AGGAGGTGATCCAACCG
oHv327-DY682-Sc_16S-3end-Rv	TAATGATCCTTCCGC
oHv338_16S_MS2_fw	TGATGATGATTACACATCTTTACTAGTACTCGTGGCGAAAAGCTCAG
oHv339_16S_MS2_rv	AGATGTGTAATCATCATCAAACTAGTACTCGTGCAACTAGCATGGCTA
oHv340_16S_Mango_Fw	TACGAAGGGACGGTGC GGAGAGGAGAGTAACCTCGTGGCGAAAAGCTCAG
oHv341_16S_Mango_rv	TACTCTCTCTCCGCACCGTCCCTTCGTAACCTCGTGCAACTAGCATGGC

oHv342_Nano-KsgA_Nde_Fw	ATTGCGCATATGCAGCAGCACTTCTCCAG
oHv343_Nano-KsgA_Xho_Rv	GTGGTGCTCGAGGCATGTGCCGGGCATCAACGA
oHv344_HvKsgA L128P fw	GCGTGCGTCTCGAACCCCCGTACGGCATCTC
oHv345_HvKsgA L128P rv	GAGATGCCGTACGGGGGTTTCGAGACGCACGC
oHv346_HvKsgA_RRK_A3 fw	GTTTACCCAGGCCGCAGCCACCATCAGAAACGGCATCCGC
oHv347_HvKsgA_RRK_A3 rv	TTCTGATGGTGGCTGCGGCCCTGGGTAACAGCGCCTTAC
oHv348_GE_Flag_Nde fw	ATTGCGCATATGAGAGTCCGCGTCCGCGGC
oHv349_GE_Flag_RV rv	TCATCTTTGTAGTCGATATC
oHv350_Flag_GE_Hind fw	GATAAAAAGCTTAGAGTCCGCGTCCGC
oHv351_Flag_GE_Bam rv	CTAGTGGATCCCTACCCCGACAGCGCCGACTC
oHv352_GE_D289A_fw	GCCTCCGCCGCGCTCGCCCTCGCGGAGGCGCTCTGC
oHv353_GE_D289A_rv	GCAGAGCGCCTCCGCGAGGGCGACGCCGGCGGAGGC
oHv354_GE_D338_341A_fw	CATCACGCTCGGCTCCGGCGCGGTGACGGCCCGGACCCCGAGGGAACG
oHv355_GE_D338_341A_rv	CGTTCCCTCGGGTTCGCGGGCCGTACCCGCGCCGGAGCCGAGCGTGATG
oHv356-DY682-16S-3end-long-Rv	AGGAGGTGATCCAGCCGC
oHv357-DY682-Ec_16S_long-3end-Rv	AGGAGGTGATCCAACCCGC
oHv358-DY682-Hm_16S_long-3end-Rv	AGGAGGTGATCCAGCCAC
oHv359_Hv16S_1453U-C-fw	CAAGGTAGCCGTAGGGGAACCTGCGGCTGGATCACCTCTCT
oHv360_Hv16S_1453U-C-rv	AGGAGGTGATCCAGCCGAGGTTCCCTACGGCTACCTTG
oHv361_Hv16S_1448G-A-fw	CGTAACAAGGTAGCCGTAGAGGAATCTGCGGCTGGATCACC
oHv362_Hv16S_1448G-A-rv	GGTGATCCAGCCGAGATTCTCTACGGCTACCTTGTTACG
oHv363_Hv16S_1448G-C 1453 U-C-fw	AGGAGGTGATCCAGCCGAGGTTCCGCTACGGCTACCTTGTTACGAC
oHv364_Hv16S_1448G-C 1453 U-C-rv	GTCGTAACAAGGTAGCCGTAGCGGAACCTGCGGCTGGATCACCTCTCT
oHv367_HvksgA E84A silent EcoRI_rv	GTCAGCGAATTCGCGGCGCAGGTGCGCGGCGAACGTCCGGTCTGTGCGACGACGGTC ACGCGGTCGG
oHv368_HvksgA silent EcoRI_fw	CGCCGCGCACCTGCGCCGCGAATTCGCTGACGAGGTGGAATCGGAC
oHv369_HmksgA-BspHI skip rv	AGCGTGGCGAAGTCGGCTGGTGTGAGCTTCCCGGCACGGGCGCTCATCAGGCCTTCGT CGGCGGCCTCG
oHv370_HmksgA_BamHI_rv	TATTATGGATCCTCAGGCCTCCGGCTGCCGACCTCGTACGCGAGTGTCGCCAGCGTG GCGAAGTCGGCTGGTG
oHv371-HmksgA_Bsp_Fw	GAGGCGTCATGACTACGACTGAGACAGGG
oHv380_Ec_rrnB Fw-5'-BglII	GCTCAACCTGGGAACTGCATC
oHv381_Ec_rrnB Rv-3'-XbaI	GTACGCTTAGTCGCTTAACC
oHv382_Ec_h45_GC-AU_fw	GTCGTAACAAGGTAACCGTAGAGGAATCTGCGGTTGGATCACCTCTCTTA
oHv383_Ec_h45_GC-AU_rv	TAAGGAGGTGATCCAACCGCAGATTCTCTACGGTTACCTTGTTACGAC

oHv384_Ec_h45_noW7_fw	GGTAACCGTAGGGGAACCTACGGTTGGATCACCTCCTTA
oHv385_Ec_h45_noW7_rv	TAAGGAGGTGATCCAACCGTAGGTTCCCTACGGTTACC
oHv396-DY682-16S-5end-Rv	CCCAATAGCAATGACCTCCG
oHv397-DY782-23S-5-end-Rv	CGAGCTATCCACCAGCTGGC
oHv398-T7prom-OmpA substrate Fw	TAATACGACTCACTATAGGGCCAGGGGTGCTCGGCATA
oHv399-OmpA substrate Rv	GAAACCAGCCAGTGCCACTG
oHv400-DY682-16S-m6A-Rv	AAGCCCCCTTGCGAAGCC
oHv402-Trpase_F2_RT	TTCGCGTTCCCCGGCACCGAC
oHv403-Trpase_R2	ACACCGGTTTCGAGCCGCGACG
oHv404-RibL10-H. v.-B	CCGGTCGCTGCTTGTTCTCGCG
oHv405-RibL10-H. v.-B	CCGAGGACTACCCCGTCCAGATTAGCCTG
oHv414_Hv_UTP24-Nde	GAGGCGCCATATGACCGCCACCGTAGTCGTC
oHv415_Hv_UTP24-Xho_rv	GTGGTGCTCGAGAGTTCCGTGATTGCCAGCGT
oHv416_Hv_UTP24_Bsp_pTA_fw	GAGGCGTCATGACCGCCACCGTAGTCGTCATGGACACGAACGCGCTGATGATGCCGGT CGAACTCGACGTCC
oHv417_Hv_UTP24_D9N_Bsp_pTA_fw	GAGGCGTCATGACCGCCACCGTAGTCGTCATGAACACGAACGCGCTGATGATGCCGGT CGAACTCGACGTCC
oHv418_Hv_UTP24_Bam_pTA_rv	TATTATGGATCCTTAAGGTTCCGTGATTGCCAG
oHv419_Hv_UTP24_D9E_Bsp_pTA_fw	GAGGCGTCATGACCGCCACCGTAGTCGTCATGGAGACGAACGCGCTGATGATGCCGGT CGAACTCGACGTCC
oHv426_Hv_UTP24KO_us-Kpn	GCATCGAGGGTACCAGCGGGCGACGAACCTCGAAC
oHv427_Hv_UTP24KO_ds-Xba	CTAGCCACTCTAGACCGTGAGGCCGATCTTCGAG
oHv428_Hv_UTP24KO_usds-fw	GTATCGGGACGCTCAAGTGACCGAAACTATGTACAAACGGGT
oHv429_Hv_UTP24KO_usds-rv (reversed)	GTATCGGGACGCTCAAGTGACCGAAACTATGTACAAACGGGT
oHv430_Hv_UTP24mut_usds-fw	GTATCGGGACGCTCAAGTGACGTGACCGCCACCGTAGTCGT
oHv431_Hv_UTP24mut_usds-rv	ACGACTACGGTGGCGGTACGTCACCTTGAGCGTCCCGATAC
oHv432_HvNob1 D5E_fw	ATGCGGATTCTCGAGGCGTCTGCGTTCATCC
oHv433_HvNob1 D5E_rv	GGATGAACGCAGACGCCTCGAGAATCCGCAT
oHv434_HvNob1 D5N_fw	ATGCGGATTCTCAACGCGTCTGCGTTCATCC
oHv435_HvNob1 D5N_rv	GGATGAACGCAGACGCGTTGAGAATCCGCAT
oHv441_DUF655-KO_DS-XbaI_Rv	GGCCATTCTAGAGCCGAACCTCTTTTGAAC
oHv442_DUF655-KO_US-KpnI_FW	GTTCAAGGTACCGATCAACGACGGCGCAAAGAG
oHv443_DUF655-KO_US/DS_FW-BamHi	CGAAGGCGGATCCCGGAACGGGACTTTTACCCG
oHv444_DUF655-KO_US/DS_RV-BamHi	GCCTTCGGGATCCACCAGTAGTTACGGTGAGCCG

oHv445_DUF655_BamHI_RV	AAGTCCGGATCCCTACTGTCCGTCGCGTCCGACG
oHv446_DUF655_BspHI-FW	CTACTGTCATGACACGTACGGAGAGCG
oHv446_qPCR-flgA2-fw	ACGCTCACCGTTCGTCTCGC
oHv447_qPCR-flgA2-rv	CGGAGTCGTTTCGTCCGGAG
oHv448_flgA2-rT	TTGCGGCCGTGTTCGATGGTG
oHv449_qPCR-flaI-fw	CAGCAACTGCTCACCCGCGA
oHv450_qPCR-flaI-rv	CCACGGACCTCCCCGACGAT
oHv451_flaI-rT	GGTCGCCGGTGAAACGCTGA
oHv452_qPCR-cheR-fw	TACCGCGCCTCCGAGACGAA
oHv453_qPCR-cheR-rv	CGGACCATGTTCGGTGACGGC
oHv454_cheR-rT	CTCGCGCGGTAGATGCGGAG
oHv463_GFP_Nde_Fw	ATTGCGCATATGTGCGAAAGGCGAGGAACTC
oHv464_Flag_GFP_Nde_Fw	ATTGCGCATATGGACTACAAAGATGACGACGATAAAGGGATGTGCGAAAGGCGAGGAACTC
oHv465r_GFP_Pci_Rv	GGTTCCACATGTGGCCCTGCCCTGGCCTTGCC
oHv466_KsgA_amber36_Fw	CCCGGACCACGACCAGCACTAGCTCGTCGACGACCGCGTCGTC
oHv467_KsgA_amber36_Rv	GACGACGCGGTCGTGACGAGCTAGTGTGGTCGTGGTCCGGG
oHv468_KsgA_amber97_Fw	CCGCGCACCTGCGCCGCGAGTAGGCTGACGAGGTGCAATCGGAC
oHv469_KsgA_amber97_rv	GTCCGATTGACCTCGTCAGCCTACTCGCGGCGCAGGTGCGCGG
oHv470_KsgA_amber98_Fw	CGCACCTGCGCCGCGAGTTCTAGGACGAGGTGCAATCGGACCG
oHv471_KsgA_amber98_rv	CGGTCCGATTGACCTCGTCCTAGAACTCGCGGCGCAGGTGCG
oHv472_KsgA_amber208_Fw	GTCGTCTCCGCATCACGCCGTAGGAGCCGGAGTACGAGGTGCG
oHv473_KsgA_amber208_rv	CGACCTCGTACTCCGGCTCTACGGCGTGATGCGGACGACGAC
oHv474_flgA1_Pci_Fw	GAGGCGACATGTTGAAAAACATCAACG
oHv475_flgA1_Bam_Rv	TATTATGGATCCTCAGAGCGCAATGGGGTCG
oHv494_5' Crispr_I cassette KpnI_fw	GAATTGGGTACCGAGAATCG
oHv495_3' Crispr_I cassette BamHI_rv	GCTCTAGAACTAGTGGATCCC
oHv496_crispr_5'_CrtI#a1_fw	CCGTTGATCGGTAGTTGAAGCTCTACGTCCTTACGAACGGACATGAATTCTGTCTCG
oHv497_crispr_5'_CrtI#a1_rv	GTTGCCATACCAATATCGGTCGAGACAGAATTCATGTCCGTTTCGTAAGGACGTAGA
oHv498_crispr_5'_Nob1#a1_fw	CCGTTGATCGGTAGTTGAAGCTCAATGCGGATTCTCGACGCGTCTGCGTTCATCCAC
oHv499_crispr_3'_Nob1#a1_rv	GTTGCCATACCAATATCGGTCGTGGATGAACGCAGACGCGTCGAGAATCCGCATTGA
oHv500_crispr_5'_Nob1#a2_fw	CCGTTGATCGGTAGTTGAAGCAGGATAGATTCTCAATGCGGATTCTCGACGCGTCTG
oHv501_crispr_5'_Nob1#a2_rv	GTTGCCATACCAATATCGGTCAGACGCGTCGAGAATCCGCATTGAGAATCTATCCT
oHv502_crispr_5'_Nob1#a3_fw	CCGTTGATCGGTAGTTGAAGCATCCACGAGTACCACACCGACGACGAGACGGCCTCG

oHv595_PfuKsgA_pBAD33_Fw_SmaI	ATTGCGCCCGGGATGAGAGACAACTTTTCTA
oHv596_pET24_Ec_KsgA-FW-new	TAAACACCATATGAATAATCGAGTCCACC
oHv597_pET24_Ec_ksgA_Rv	GTGGTGCTCGAGACTCTCCTGCAAAGGCGCG
oHv598_EcKsgAE66A_FW	CTGACGGTCATCGCACTTGACCGCGATC
oHv599_EcKsgAE66A_RV	GATCGCGGTCAAGTGCATGACCGTCAG
oHv600_delta 16S lig_fw	GTTAGCCCTAGTAGTTCGGTGACAGAACTACTAGGGCTAACACGG
oHv601_delta 16S lig_rv	CCGTGTTAGCCCTAGTAGTTCGTACCGAACTACTAGGGCTAAC
oHv602_recA_pBAD_FW_SmaI	ATTGCGCCCGGGATGGCTATCGACGAAAAAC
oHv603_recA_pBAD_Rv_HindIII_(reversed)	CGCAATAAGCTTTTAAAAATCTTCGTTAGTTT
oHv604	GTTTACTCGCCGTTACTAACG
oHv605-T7Prom	TAATACGACTCACTATAGGG
oHv606-pBADFW	ATGCCATAGCATTTTTATCC
oHv607-pBADrv	GATTTAATCTGTATCAGG
oHv619_hvFap7-E70A_H72A_fw	CGACTGGGACGGCATCGTCGCGAGCGCACTCGCACACCCTTCGAGG
oHv620_hvFap7-E70A_H72A_rv	CCTCGAAGTGGTGTGCGAGTGCCTCGCGACGATGCCGTCAGTCG
oHv622_DY782-23S_5-end-18nt_Rv	GCTCTCGAGCCGAGCTATCCACC
oHv623_qPCR_HVO1572_fw	TACGAAGTCGTCGACAACCTC
oHv624_qPCR_HVO1572_rv	TCGTACTGTTCTGTCGTATC
oHv625_flgA1_qPCR-fw	GGTCAGGTCGGTATCGGGACG
oHv626_flgA1_qPCR-rv	CCTTGTTACAGATTGCTG
oHv627_flgA1-II_qPCR-fw	CCTACAACGACACCGTCACC
oHv628_flgA1-II_qPCR-rv	CGGACTGCTCGTTGAGAACC
saci_025 KsgA NcoI Fw.xdna	CACGATCCATGGGAAAAGAATAAGTTAGGACAGCAC
saci_026 KsgA-NcoI Rv.xdna	GTAATAAATCTGTTATCTCCCAGGGCTTAAACTCCCTTACC
saci_027 KsgA Bam Rv.xdna	CACGATGGATCCGACAAAAGTTTATACCCATAGAATGTAATAAATCTGTTATCTC
saci_028 KsgA KO560 Bam Rv.xdna	CACGATGGATCCTAACCACATAACGATAATGCG
saci_029 KsgA KO Pst Fw.xdna	CACGATCTGCAGATGAAGAATAAGTTAGGACAG
saci_030 KsgA KOup Nde KpnI Fw.xdna	GGCAGCCATATGGGTACCATCGGCGAAGATTATTTTATG
saci_031 KsgA inFDel ovl Rv.xdna	CTGGAATATATACATCATCGTCGTAGTCTCTCAAGGTATCC
saci_032 KsgA inFDel ovl Fw.xdna	GGATACCTTGAGAGACTACGACGATGATGTATATATCCAG
saci_033 KsgA KOdw Nco Bam Rv.xdna	CACGATGGATCCATGGCAGCTCCAAACCAATTAACC
saci_034 KsgA KOtest Fw.xdna	GTACGTGGAGAGCTGAGATA
saci_035 KsgA KOtest Rv.xdna	TACTTCACTACCCTTCGCTG
saci_036 KsgA inFDel ovl Fw.xdna	GGATACCTTGAGAGACTACGATGAGCTGACCATGGGAGATAACAGATTTATTAC
saci_037 KsgA inFDel ovl Rv.xdna	GTAATAAATCTGTTATCTCCCATGGTCAGCTCATCGTAGTCTCTCAAGGTATCC

saci_041 KsgA Nde His6 Fw.xdna	ATTGCGCATATGCACCACCACCACCACCACGGAATGAAGAATAAGTTAGGACAG
saci_042 KsgA stop XhoI Rv.xdna	GTGGTGCTCGAGTCAGACAAAAGTTTATACCCATG
saci_043 KsgA E52A Fw.xdna	CTTAAACCCGATATTGCGATTGCAATAGACGTTTCTCTTATCAATC
saci_044 KsgA E52A Rv.xdna	GATTGATAAGAGAAACGTCTATTGCAATCGCAATATCGGGTTTAAG
saci_045 DY682 KsgA Me-sh-Rv.xdna	GTGATCCAGCCGCAG

7.1.4.2 Nucleotides

Nucleotides (dNTPs, 10mM each) for PCR were obtained from New England Biolabs.

Radioactively labeled γ -Phosphate³²-ATP was ordered from Merck.

ddNTP were (10mM each) were purchased from Affimetrix

7.1.4.3 Plasmids

pTA-131 (Amp ^R)	(Allers et al., 2004)
pTA-1228 (Amp ^R)	(Stroud et al., 2012)
pCRTM II-Blunt-TOPO® (Kan ^R)	Commercially available Vector/Cloning Kit from Life Technologies
pBAD33-GM	addgene.org/65098
pET15 (Amp ^R)	<i>E. coli</i> expression vector (novagen)
pET24a (Kan ^R)	<i>E. coli</i> expression vector (novagen)
pET24d (Kan ^R)	<i>E. coli</i> expression vector (novagen)
pTQ61_N-GFP_pTA1	Kind gift From Tessa Quaxx (Uni Freiburg)
pUC19 (Amp ^R)	Invitrogen-Testplasmid

7.1.4.4 Gene synthesis

Synthetic genes were ordered from MWG Operon and dissolved according to provided instructions.

7.1.5 Kits

peqGOLD Plasmid Miniprep Kit I	PeqLab
QIAEX II Gel Extraction Kit	Qiagen
QIAquick PCR Purification Kit	Qiagen
Zero Blunt® TOPO® PCR Cloning Kit	Life Technologies

7.1.6 Enzymes

All restriction enzymes were bought from New England Biolabs and used with the most suited buffer recommended by the company's double digest finder (<https://www.neb.com/tools-and-resources/interactive-tools/double-digest-finder>).

Other enzymes:

Enzyme	Manufacturer
HotStar Taq Polymerase	Qiagen
Phusion HF DNA Polymerase	New England Biolabs
M-MLV Reverse Transcriptase	Promega/NEB/Invitrogen
RadPrime DNA Labeling System	Life Technologies
RNasin	Promega
RQ1 RNase-free DNase	Promega
SuperScript III Reverse Transcriptase	Invitrogen
T4 DNA Ligase	New England Biolabs

7.1.7 Strains

Organism	Strain	Genotype
<i>Escherichia coli</i>	XL1 blue	endA1 gyrA96(nalR) thi-1 recA1 relA1 lac glnV44 F' [::Tn10 proAB+ lacIq Δ(lacZ)M15] hsdR17(rK- mK+)
<i>Escherichia coli</i>	Rosetta Star (BL21)	F- ompT hsdSB(RB- mB-) gal dcm λ(DE3 [lacI lacUV5-T7 gene 1 ind1 sam7 nin5]) pLysSRARE (CamR)
<i>Escherichia coli</i>	(BL21- AzF)	Modified pLysSRARE → pEvol-AzF described in (Willkomm et al., 2017)
<i>Escherichia coli</i>	AVS69009	Δ(rrsC-gltU-rrlC)15::cat+ilv+ (Asai et al., 1999b; Vila-Sanjurjo and Dahlberg, 2001)
<i>Haloferax volcanii</i>	h26	DS70 Derivat ΔpyrE2 (Allers et al., 2004)
<i>Haloferax volcanii</i>	H99	ΔtrpA ΔhdrB ΔpyrE2 (Allers et al., 2004)
<i>Haloferax volcanii</i>	SMHXXX	See (Knüppel et al., 2018)
<i>Haloferax volcanii</i>	H1424	DS70 DpyrE2; DhdrB; Nph-pitA; Dmrr; cdc48d-Ct
<i>Sulfolobus acidocaldarius</i>	MW001	DSM639 (https://www.dsmz.de/collection/catalogue/details/culture/DSM-639)
Biomass for various archaeal cells were a kind gift from the Archaea Center Regensburg, Thank you !		

7.1.8 Consumables

Material	Manufacturer
1 kB DNA ladder	New England Biolabs
100 bp DNA Ladder	New England Biolabs
2-log DNA ladder	New England Biolabs
96-well plates	Sarstedt
Agarose ultrapure	Invitrogen
Biosphere® Filter Tips	Sarstedt
BM Chemiluminescence Western Blotting Substrate (POD)	Roche
Cassettes 1.0 mm	Invitrogen

ColorPlus™ Prestained Protein Marker, Broad Range (7-175 kDa)	New England Biolabs
Cuvettes	Sarstedt
Extra Thick Blot Paper	Bio-Rad
Falcon tubes (15ml/50ml)	Sarstedt
Filter paper 3MM	Whatman
Gel Loading Dye (6x), blue	New England Biolabs
Glass beads (0.1 mm)	Biospec
Immun-Blot PVDF Membrane #162-0177	BioRad
PCR-Tubes and Caps	Kisker
Pipette tips (10-1000µl)	Sarstedt
Pipettes (2-50ml)	Sarstedt
Positive TM membrane	MP Biomedicals
reaction tubes (1.5ml, 2ml)	Sarstedt
SYBR Safe DNA Gel Stain	Invitrogen
Unstained Protein Ladder, Broad Range (10-250 kDa)	New England Biolabs

7.1.9 Software

Software	Producer
Fiji	Open Source
Geneious 4.8.4 Basic	Biomatters Limited.
Graphpad Prism 8.3.0	Graphpad Software, LLC
Image Reader FLA-3000 v.1.8	Fujifilm
Microsoft Office Excel 2013	Microsoft
Microsoft Office PowerPoint 2013	Microsoft
Microsoft Office Word 2013	Microsoft
MultiGauge v.3.0	Fujifilm
Photoshop CS6	Adobe
Rotor-Gene 6000	Corbett Research
SigmaPlot 12.5	Systat Software

7.2 Methods

7.2.1 Microbiology

7.2.1.1 *Escherichia Coli*

7.2.1.1.1 Making chemically competent cells

Cells were scraped from glycerol stocks and plated on a **LB**-Plate (with appropriate antibiotic) and grown over night at 37 °C. Single colonies were inoculated overnight in 50 ml **LB**-Medium (with

appropriate antibiotic) @37 °C (180 rpm). The OD₍₆₀₀₎ was measured and inoculated to a 200 ml LB₍₀₎ day culture at OD₆₀₀ ~ 0.2, and grown at same settings as before. Cells were harvested at OD₆₀₀ 0.5 into four 50 ml Falcons and centrifuged for 10min at 4 °C (4,500 rpm).

From here on out every step was rapidly done at 4 °C. The supernatant was discarded and then each cell pellet resuspended in 15 ml **TfbI** (see

Table 7.2), incubated for 20 min and then centrifuged for 10 min at 4,500 rpm. The supernatant was removed and the first of the four cell-pellets was resuspended in 4 ml **TfbII**, once resuspended it was transferred to the second cell-pellet and so on until all four pellets were resuspended in a total of 4 ml. This was then incubated for 10-20 min and subsequently divided into 50 µl cell aliquots.

Of each batch 2 dilutions of a pUC19-Vector were made to test transformation efficiency including a water control. The rest was frozen @-80 °C.

7.2.1.1.2 Transformation of Plasmids via Heat-shock

Competent cells were thawed on ice. The desired DNA (for a re-transformation, 10-40 ng of ultra-pure plasmid DNA, or half of a ligation) was added to the thawed cells, flipped briefly and then incubated for 30 min on ice.

After that the cells were heat-shocked for 1 minute at 42 °C and put back on ice for 2min. To regenerate the cells 450 µl LB-Medium was added and regenerated on a thermomixer for 30-60 min at 37 °C (700 rpm).

Retransformations were diluted 1:3 in LB-Medium and then 100 µl were plated onto LB-Plates (with appropriate Antibiotic). Ligations were completely plated onto LB-Plates (with appropriate Antibiotic).

Both were incubated over night at 37 °C.

All plasmids were amplified in XL1-Blue cells, Rosetta Star/BL21 cells were used for protein expression (see 7.2.3.1).

7.2.1.1.3 P1 Transduction

KEIO Strain *ΔksgA* J50 was grown over night in LB_(KAN) at 30 °C. 50 µl of the overnight culture was used to inoculated 4 tubes with 5 ml LB₀ (+ 0.2 % Glucose, 5 mM CaCl₂) each. Increasing concentrations of P1 Lysate (a kind gift from Markus Busch, Biochemistry II) (0/50/100/200 µl) were added to the cultures and grown for 2-6 hours at 30 °C. To each tube a few drops of Chloroform were added (use yellow tips) vortexed and put into a shaker at 37 °C for 15 min. After centrifuging the cells at 4000 rpm for 10 min at 4 °C, the supernatant was collected in a new falcon tube and after adding a few more drops of Chloroform, stored in the fridge. These P1 lysates can now be used to infect target strains and transduce *ΔksgA*.

The target strain (as a test we used BW25113) was grown over night in 5ml LB₀ (2,45 mM CaCl₂). On the next day 100 µl of the overnight culture was infected with 100 µl P1-*ΔksgA*-Lysate (various

lysate concentrations can be tested) alongside a control with 100 μ l LB₀. This was mixed and incubated without shaking at 37 °C for 30 min. The infection was stopped by adding 200 μ l 1M Na₃-Citrat and regenerated for 1 h at 37 °C in a shaker with the addition of 1 ml LB₀. After regeneration the cells were pelleted at 4000 rpm in a table top centrifuge, the supernatant was discarded and the cell pellet was resuspended in P1-Saline (145mM NaCl, 50 mM Na₃-Citrat) and in this case plated onto LB_(KAN) plates.

7.2.1.2 *Haloferax volcanii* workflow

7.2.1.2.1 Transformation of Plasmids

All steps are performed at room temperature unless stated otherwise.

This protocol is derived from (Allers et al., 2004) and aims at 4 transformations i.e. three plus one water (-) control and needs to be adjusted according to the amounts of transformations.

For buffers see (see Table 7.2)

At first 10 ml overnight culture of desired Hv-Strain were set up using Hv-YPC (+Trp 50 μ g/ml for h1424 cells, +1 mg/ml for h99). At OD₆₀₀ ~0.8 the cells were pelleted for 8 min at 6000 rpm. This was then resuspended in 2 ml buffered spheroplasting solution and transferred into a 2 ml round-bottomed tube and pelleted again at 6,000 rpm for 8 min. The pelleted was gently resuspended in 800 μ l buffered spheroplasting solution (trying to avoid air bubbles). For each transformation 200 μ l was transferred into a fresh round-bottomed tube. 20 μ l of 0.5 M EDTA pH 8.0 was added on the side of the tube and inverted to mix. The mixture was left undisturbed for 10 min to form spheroplasts. Whilst waiting, DNA was set-up for transformation: 10 μ l dam⁻ DNA (1-2 μ g) or 10 μ l Water (as control), 15 μ l unbuffered spheroplasting solution and 5 μ l 0.5 M EDTA pH 8.0. After 10 minutes the DNA was added to the spheroplasts in same manner as EDTA (see above). This was then left at RT for 5 minutes.

Meanwhile a 60% PEG 600 solution was prepared. For 4 transformation reactions 640 μ l PEG 600 and 426 μ l of unbuffered spheroplasting solution were mixed thoroughly. After 5 minutes 250 μ l of 60% PEG 600 was added to each transformation. This was added in same manner as EDTA, but the tube was shaken horizontally around 10 times to mix and left to stand at RT for 30 minutes. 1.5 ml spheroplast dilution solution was added, inverted to mix and left at RT for 2 min. The cells were pelleted at 6,000 rpm for 8 min, and the supernatant removed. Then 1 ml regeneration solution was added and was left for 1-2 h at 42 °C. After that the cells were resuspended by tapping the tubes and returned 42 °C shaker for 3-4 h. The cells were centrifuged at 6000 rpm for 8 min and resuspend in 1 ml transformant dilution solution, of which then 100 μ l (~500 μ l when transforming rDNA reporters) was plated on Hv-Ca plates and incubated at 45 °C until colonies were visible.

7.2.1.2.2 Preparation of plates

6g of Agar was dissolved in 200 ml Saltwater 30% (see Table 7.4) and 100 ml H₂O by microwaving. The salt will form a crust on the side of the bottle so either stir heavily or shake until it has dissolved again. 33 ml of 10x YPC or 33 ml of Hv-Ca⁺ broth was added before autoclaving. After the media has cooled to about 60 °C add respective additives (see Table 7.4). Pour thick plates, ~30 ml per petri-dish.

7.2.1.3 Growth rate measurements

7.2.1.3.1 H. volcanii / E. coli

An Exponentially growing culture was adjusted to a OD₆₀₀ of 0.1 and then 50 µl were used to inoculate a 96 Well plate containing 200 µl the appropriate media to a final OD₆₀₀ of 0.02. Cells were then grown at the desired temperature, while shaking for 1000s at an amplitude of 5mm before each measurement at 612nm (20 min intervals). This was repeated for 200 cycles. Evaluation as described in 7.2.6.1

7.2.1.3.2 S. acidocaldarius

Measurements were taken at the indicated time points from normal Erlmayer flasks

7.2.1.3.3 P. furiosus

P. furiosus was cultivated under anaerobic conditions in 40 ml ½ SME medium supplemented with 0.1 % yeast extract, 0.1 % peptone and 40 mM pyruvate at 85°C. For growth comparison experiments, the medium was supplemented with different CuSO₄ concentrations and each condition for MURPf52 (parental strain) and MURPf74 (Δ ksgA strain) was recorded in biological triplicates during 60 hours of incubation by measuring the turbidity changes *in situ* using a photodiode and a LED with 850 nm as light source. The recorded values were converted to cell/ml by using a calibration curve with known cell concentrations, calculated in a Thoma counting chamber (0.02-mm depth; Marienfeld, Lauda-Königshofen, Germany) using phase-contrast microscopy.

7.2.1.4 Motility Assays

Motility plates were created using the appropriate Media (Hv-YPC, -Ca, -Ca⁺, LB, Tryptone, see 7.1.3) with a reduced Agarose concentration (0.3 %). All plates (approx. 80 ml) were poured in 12cm square Petri dishes from Greiner, left to cool/dry overnight. The spotted cultures all came from exponentially growing cultures and were adjusted to equal optical densities (0.3) and 4 µl were spotted onto the agar. For *E. coli* no antibiotics were added to the plates to ensure no secondary effects. Each cell island was measured three times in “Fiji” from different angles and remeasured if the measurements differed too much. The mean of the three measurement was used for further comparisons.

7.2.1.5 Microscopy

H. volcanii cultures were grown in Hv-Ca Media for two serial dilutions over two days and imaged at low densities ($OD_{600} < 0.04$ and higher $OD_{600} > 0.06$) on 1% agarose – 18% SW pads. The cells were grown and observed on three independent occasions. The Data Analysis was done with the “MicrobeJ” Plugin for Fiji (Ducret et al., 2016) and was manually curated for outliers or false detections. Image Acquisition was done in the Lab of Sonja Albers on a Zeiss Microscope at a Magnification of 100x using PH3 setting. The parameters for MicrobeJ were the following: 100x Magnification Scale, 0.065 pixel / μm .

7.2.1.6 Biofilm

The Protocol was adapted from Esquivel et al., 2016 and O’Toole, 2011 to make it work with *Haloferax volcanii*.

Exponentially growing cells in Hv-YPC-, Ca- and Ca⁺-Media were adjusted to equal OD_{600} of 0.3 and then distributed as 150 μl aliquots (at least 3 Technical replicates) in a Standard 96 Well plate with a lid. The outer rows were not inoculated with cells and were used as media background blanks. The well plate was then incubated shaking for ~8 h and then Left in a closed box with a wet tissue at 42 °C for another 40 h. The cells were ejected in one strong motion from the plate and tapped dry multiple times into a stack of tissues (ensure that no media remains in the wells). The cells were then fixed with 200 μl of 2 % Acetic Acid in 20 % SW for 4 minutes. It is important that the volume of every Solution; Fix, Stain, Wash, Destainer is larger than the initial Culture, as the cells adhere at the air-liquid interface! Then eject the liquid into a box and the 96-well plate is tapped dry into stacks of paper. The adhering cells were then stained with 200 μl of a 0.2 % Crystal Violet solution for 10 minutes. Once this is finished, eject the stain into a box and tap the plate dry into stacks of paper. Three steps of rinsing with water preceded air drying for 1h or over night. Once fully dry, the stained cells were brought into solution with 200 μl 10 % Acetic Acid and 30 % MeOH. The final step was to shake the plate for 5 minutes in the TECAN reader to ensure good solution of the cells before measuring at 612 nm.

7.2.1.7 4TU Labelling

For 4TU pulse labelling, exponentially growing cells were transferred to fresh Hv-Ca+ medium containing the indicated amount of 4TU [typically 75% 4TU (300 μM) and 25% uracil (100 μM)].

For pulse-chase experiments, cells were first grown in presence of 4TU and transferred to Hv-Ca+ media supplemented with uracil and lacking 4TU for the indicated time.

For *Sulfolobus acidocaldarius*: 75% 4TU (135 μM) and 25% uracil (45 μM) in Brock medium.

7.2.2 DNA work

7.2.2.1 Polymerase Chain Reaction

Normal PCR was done with the Phusion polymerase from NEB. The annealing temperatures for the primers were estimated from the primer3 plugin in Geneious. Depending on the GC content either the 5x GC-Buffer (High % GC) or the 5x HF-Buffer (norm % GC) was used. Elongation time was 30 sec per 1 kb amplicon.

Setup (ad 50 µl): 10 µl 5xGC/HF-Buffer, 1.5 µl DMSO, 1 µl dNTP-mix (10mM each), 2.5 µl each primer (10 pmol), 0.5 µl Phusion polymerase, 1 µl DNA.

Colony PCRs were done with Go-Taq Polymerase from Promega in a reduced volume of 20 µl.

For further analysis part of the reactions were loaded onto an agarose gel electrophoresis and the rest if necessary was purified via QIAquick PCR purification kit (Qiagen).

7.2.2.1.1 Two-step site mutation

Two segments were amplified with one forward or reverse primer lying on the 5' or respectively 3' end of the gene and a corresponding reverse or forward primer at the site with for the desired mutation. Each amplicon was then purified and joined together (1:100 dilution) and re-amplified via PCR with just the 5' and 3' end primers.

7.2.2.1.2 Site Directed Mutagenesis

In this approach a single primer (carrying the site mutation) replicates the complete vector. Doing this in 2 separate reactions with both, either reverse or forward primers results in two complementary ssDNA vectors carrying the desired mutation. Contrary to a normal PCR the product is only linearly amplified, owing to the absent second primer. Consequently, input DNA should be high (~100 ng). The PCR products were purified and both products were annealed by cooling down from 95 °C to RT in a heating block. After this the annealed vectors were digested with 4 U DpnI to rid it from methylated, e.g. old vectors not carrying the mutation. Now only the unmethylated synthesized vectors remained to be transformed and screened for the desired mutation.

7.2.2.2 Restriction enzyme digest

DNA was digested with a large variety of restriction enzymes (purchased from NEB). Every enzyme was used as suggested by the manufacturer in the manual. The digested DNA was then separated on an agarose gel electrophoresis. PCR amplified Inserts with restriction sites for cloning were purified for ligation via QIAquick PCR purification kit (Qiagen). Digested vectors were excised from the gel with a scalpel and then extracted with QIAEX II gel extraction kit (Qiagen). Promising candidates (plasmids) were brought to GeneArt for sequencing (~350ng/7ul + 1 ul 10pmol primer).

7.2.2.3 Agarose Gel electrophoresis

Depending on the fragment size different gel concentrations were used to separate DNA. 1 % (> 2 kb), 1.5 % (0.5 - 2 kb) or 2 % (100 – 1000 bp) (w/v) agarose was dissolved by microwaving in 1x TBE buffer. Once slightly cooler SYBR safe stain (1:10000 dilution) was added and poured into form. The samples were loaded with 6x Gel loading dye (blue or violet) from NEB, as Marker a 100bp, 1 kb or 2-log Marker were available. The gel ran at around 100-180 V and was afterwards exposed on a blue light screen.

7.2.2.4 Polyacrylamide Gel electrophoresis of DNA

Polyacrylamide gels are able to separate fragments that differ by only 0.2%, hence far beyond the limits of agarose gels. Hence this was used for small fragment separation. Polyacrylamide concentration: 10 % for 30 – 1000bp, 12 % for 40 - 200 bp, 15 % for 25 bp – 150 bp.

As running buffer 1x TBE was used. To polymerize 1 % APS (20%) and 0.1% TEMED was added. Samples were loaded with 6x Gel loading dye (blue or violet) from NEB. To visualize the fragments, the Gel was stained for 10-15 min in 1x TBE with SYBR safe stain (1:10000 dilution) and then viewed on a blue light screen.

7.2.2.4.1 Crush and Soak extraction

The crush and soak method was used to extract DNA fragments from TBE-PAGE. The digested DNA was loaded onto a 1x TBE-PAGE. The gel band was excised from the gel and place into tube with 1 volume of elution buffer (i.e. Elution buffer from the QIAEX II gel extraction kit, Qiagen). This was incubated over night at 37 °C. The samples were centrifuged with full speed at RT for 10 min and the supernatant was safely recovered into a new tube. The DNA was precipitated with ice cold EtOH @-20 °C for 20 min. The pellet was re-centrifuged and resuspended in 200 µl TE, before adding 25 µl 3M NaOAc (pH 5.2) and 2 volumes of ice cold EtOH in order to precipitate for 30min. This was centrifuged and washed one last time with 70 % EtOH, before air drying the pellet. The pellet was resuspended in 10 µl TE-Buffer.

7.2.2.5 DNA Ligation

DNA ligation was done with T7-DNA ligase and the according buffer by NEB. Every ligation was done according to the NEB manual and in a volume of 10 µl. The Insert to Vector molar ratio was about three to one.

For TOPO Blunt end PCR ligation/cloning see the companies Manual (Thermofisher # 450245)

7.2.2.5.1 pTA_1228 Vector multiple cloning site

For the pTA_1228 Vector (see Figure 7.1), gene insertion with N-Terminal tag was done in frame at the PciI/NspI restriction site.

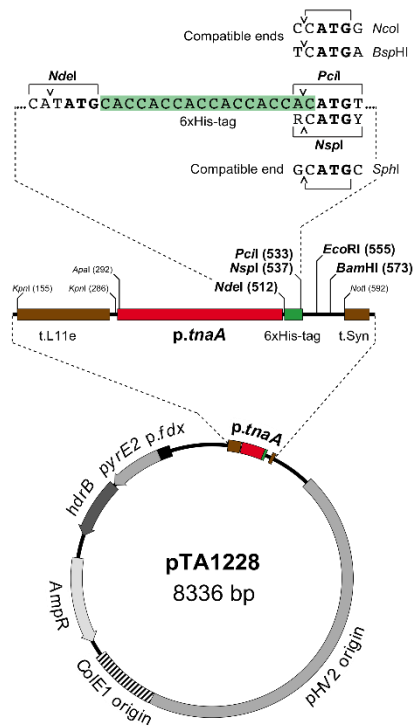


Figure 7.1 pTA1228 Vector Map, with MCS highlighted

If second codon starts with T, G, or A, pTA1228 was cut with PciI and complemented with PciI (A/CATGT), NcoI (C/CATGG) or BspHI (T/CATGA) site at 5' end of the gene, respectively. If the second codon starts with a C, the vector was cut with NspI and incorporate a SphI (GCATG/C) at the 5' site of the insert. 3' end was ligated with EcoRI/BamHI/NotI. For C-Terminal tagging the Tag has come from the 3' primer of the insert. In this case insertion was done via 5' NdeI and 3' EcoRI/BamHI/NotI.

7.2.2.6 DNA Sequencing

DNA samples (~300 ng/7 μ l + 1 μ l 10 pmol primer) were brought to GeneArt for sequencing. Depending on the sequence either our own primers were added or if suitable the companies' standard primers were used. The results were sent in as ".ab1" files and were aligned in Geneious (Kearse et al., 2012) with the databases.

7.2.2.7 DNA quantification

The Nanodrop-1000 by Peqlab was used to quantify DNA at the given presets.

7.2.2.8 cDNA Synthesis

First strand cDNA synthesis was done using the Superscript III Reverse Transcriptase. From DNase treated RNA, 1-2 μ g were added to the appropriate primers (2pmol each) and were denatured with 40mM dNTPs for 5 min at 65 $^{\circ}$ C in a total volume of 13 μ l (prepare duplicates of each samples for negative control without RT). After 5 minutes samples were put on ice and 4 μ l 5x First-strand Buffer, 1 μ l 0.1 M DTT, 1 μ l RNAsin and 1 μ l SuperScriptTM III RT (200 units/ μ l) was added or for

negative control 1 µl Water instead of RT. Incubate samples for 1 h at 50-55 °C depending on primers used, when finished heat inactivate the enzyme at 70 °C.

7.2.2.9 Quantitative real-time PCR

RNA was extracted from 4 ml logarithmically growing cells in Hv-YPC medium (OD_{600nm} = 0.5) using RNeasy Mini-Kit (Quiagen #74106) as recommended by the manufacturer instructions. Three microgram of DNase treated RNA was used for cDNA synthesis (10 min at 45°C) using QuantiNova™ Reverse Transcription Kit (Quiagen #205413) according to the manufacturer's protocol. Quantitative real-time PCR was performed on 50 ng of cDNA using the qPCR BIO SyGreen Mix Lo-ROX Kit (PCRBIOSYSTEMS) in a final volume of 10 µl in a Magnetic Induction Cycler (MIC) (Bio Molecular Systems) using the following settings: 2 min initial denaturation at 95°C following 60 cycles of 95°C 5 s and elongation for 30 s at 65°C. PCR amplification reactions targeting two regions of FlgA1 mRNA (HVO_1210, amplicon size: 139 (oHv625/626) and 126 bp (oHv627/628), and one of FlgA2 (HVO_1211, amplicon size: 142 bp oHv446/447) and Gyrase B (HVO_1572, amplicon size: 140 bp, oHv623/624) subunit were performed using the primers indicated in Supplementary Table S3. Specificity of the individual amplified product was validated by melting curve analysis. Analysis was done in technical quadruplicates. The cycle threshold (CT) values of individual amplification were determined by the accompanying dedicated software micPCR version 2.4.0 (Bio Molecular Systems).

7.2.2.10 Dideoxy chain-termination sequencing ladder

Sequencing ladders were created with Thermo Sequenase Cycle Sequencing Kit (Affimetrix) with a slightly modified protocol. Sequencing Master mix containing 1 µg template DNA (typically a Ultrapure Plasmid), 1 pmol of labelled-primer, 2 µl Reaction Buffer, and 2 µl of Thermo Sequenase DNA polymerase was completed to 17.5 µl with H₂O. 4 µl of the Master Mix was added to 4 µl of each ddNTP mix (300 µM each of dATP, dCTP, dTTP and 7-deaza-dGTP, and 3 µM of the corresponding ddNTP). Single strand synthesis was run on a PCR-Cycler with the following settings: 3min Initial Denaturation at 94°C, 55 Cycles of (30s at 94°C, 30s at 55°C and 60s at 72°C). The finished reaction was then complemented with 4 µl of Pex Loading Buffer. 3 µl were loaded per lane.

7.2.2.11 Genomic Miniprep by DNA spooling

About 1 ml of a liquid culture (OD ~0.8) was pelleted at 6000 rpm for 5min in a round bottomed tube. The pellet was resuspended in 200 µl of ST buffer (1 M NaCl, 20 mM Tris.HCl) before adding 200 µl lysis solution (100 mM EDTA pH 8.0, 0.2% SDS) and inverted to mix. The solution was covered with 1 ml EtOH to spool the DNA onto a sterile sling (white, 1 µl). The DNA was transferred into a new cup with fresh EtOH to wash the spool. To pellet the DNA, it was put in the centrifuge for 2 min at 6.000 rpm, before removing the supernatant and let the excess EtOH dry. The DNA was resuspended in 500 µl TE and left to soak for 10 min. 50 µl 3 M sodium acetate (pH 5.2) and 400 µl isopropanol were added and inverted to mix and again centrifuged at 6000 rpm for 10 min. The pellet

was washed in 1 ml 70 % EtOH and the pellet was air-dried before resuspending it in 100 µl TE. To get rid of RNA, 1 µl RNase was added and incubated (shaking) at 45 °C for 1h. Leave the DNA at 4 °C to resuspend overnight.

7.2.2.12 Southern blotting

To determine genomic fragments and their changes, i.e. deletions, southern blotting or upward capillary transfer is a simple method to screen for said changes. Overnight digested genomic DNA was separated on a large agarose gel electrophoresis. Then the gel was washed once with H₂O, then the gel was incubated two times for 15 min in Denaturing solution (0.5 M NaOH, 1.5 M NaCl). Then the gel was washed once with water before incubating it for again two times for 15 min in 1M Ammonium acetate. The transfer to the positive membrane was done overnight with 1 M Ammonium acetate. On the next day the blot was air-dried for 10 min before crosslinking the DNA to the blot on the Fluo_Link [Vilber Lourmat] at 0.3 J/cm². The blot was stored at 4 °C or used immediately.

7.2.2.12.1 Detection

The blot was pre-hybridized for 1-3 h in 25 ml hybridization buffer (0.5M Na-phosphate pH7.2, 7% SDS). While waiting the DNA probe was prepared with RadPrime DNA labeling system (GIBCO BRL). The probe was purified on a G25 spin column (Amersham) at 2,800 rpm. Salmon sperm DNA was added to the probe (final concentration of Ss-DNA in hybridization solution should be 100ug/ml). The sample was then boiled for 10 min, before they were put on ice. The probe was then added to the hybridizing buffer and left to incubate overnight rotating at 65 °C. On the next day the blot was washed with 35ml Rinse buffer (3XSSC, 0.1% SDS), following two washes with Wash Buffer #1 (0.3XSSC, 0.1% SDS) for 15 min at 65 °C. Next were two washes with Wash Buffer #2 (0.1XSSC, 0.1% SDS) for 15 min at 65 °C and one last time two washes with Wash Buffer #3 (0.1XSSC, 1.5% SDS). The blots were checked for radioactive counts and exposed to a Phosphoimager screen.

7.2.3 Protein Work

7.2.3.1 Expression of recombinant Protein in *E. coli*

7.2.3.1.1 Expression

Competent (7.2.1.1.1) BL21 cells were transformed (see 7.2.1.1.2) with the desired expression plasmids and colonies were screened via colony PCR for correct transformation using MCS flanking primers oHv605/oHv181. A 50 ml pre-culture was inoculated in LB_{Antibiotic} overnight and the OD₆₀₀ was measured the next day.

A large culture 500-1000 ml of LB-AB was inoculated to an OD₆₀₀ of 0.1 and grown for 1-2 h on a shaker @ 37 °C until OD₆₀₀ of 0.8 has been reached.

For overnight induction the culture was placed in a 20 °C shaker for 1 h to adjust temperature. To induce protein expression 0.2 mM IPTG was added to the culture and left there over night.

For daytime induction the culture was kept in the 37 °C shaker and 0.5 mM IPTG was added and incubated another 5 h on said shaker.

Either induction was pelleted at 4000 rpm for 10 min at RT.

7.2.3.1.2 Extraction and purification

To extract the protein from the cell pellet, the cells were either resuspended in K200 (*Saci/Ec/Pfu*) or K1800 (*Hv*) buffer. In all future steps these buffers are referred to as K-Buffer. All steps are performed at 4 °C unless stated otherwise.

Cell pellets were resuspended in 10 ml K-Buffer. Half the pellet volume Zirconia Beads were added and used to lyse the cells in a Precellys Evolution, with Cryolysis cooler. Three runs of 5 cycles (30s 6000 rpm 30s pause) at 4 °C were used for reproducibly good results. The lysate was centrifuged for 10 min with 4000g and the supernatant was then cleared with a second centrifugation step (15000g for 30min). The appropriate amount of Talon or Ni Beads were washed twice in the appropriate buffer (5min rotational wheel, 800g 1 min to pellet). The supernatant was added to the washed beads and incubated on a rotary wheel for 90-120 min. An aliquot of the Flow-through was taken and the beads were washed in batch 2 times for 10 min (1 min at 800g to avoid squishing the beads, take an aliquot of the first wash). The columns were equilibrated by washing with 10 ml K-Buffer. The washed beads were then loaded onto the column, washed once more and once more with 100 μ l containing a slightly higher amount of Imidazole (50 mM). Elution was performed with a total of 1 ml 250 mM Imidazole in K-Buffer, once 200 μ l then 400 μ l and the last 400 μ l to avoid Imidazole dilution from remaining K-Buffer in the column. The beads were resuspended in K-Buffer and stored. The Eluate was measured on the Nanodrop-ND1000 with according extinction coefficient and molecular weight. In order to snap freeze samples, 10 % Glycerol was added to the Elution Buffer.

To concentrate protein and wash out Imidazole the eluate was loaded onto a Amicon® Ultra-4 Centrifugal Filter Units (Merck, cut off 10 kDa) and washed once with 5 ml K-Buffer. Samples were loaded onto a SDS-PAGE (see 7.2.3.11) to verify purity, integrity and efficiency of extraction

7.2.3.1.2.1 AzF labelled Expression

Modified BL21 cells contain an additional tRNA synthase (tRNA^{Tyr}_{CUA}) under an arabinose inducible promoter (pEvol-AzF) that can incorporate para -azido- L -phenylalanine (AzF) for the Amber stop codons. Thus, induction works as follows: at OD₆₀₀ 0.3 - 0.5, 0.02% L-Arabinose is added to the AzF supplemented LB. Harvest lysis etc. is the same (7.2.3.1 in K1800), after protein binding there is one wash step followed by transferring the beads with 1 ml K1800 into a Low Bind Eppendorf tube, add 2 μ l 10 mM Dylight 650. This was then put onto a Hula wheel for 30 minutes at 42 °C in order to let the Staudinger ligation fuse the Dye to the non-canonical amino acid. In order to remove excess

Dylight Dye, two Batch washes with 1 ml K1800 were executed before loading the beads onto a column and were washed once more with 5ml K1800 before Eluting in 1 ml K1800 + 250 mM Imidazole.

7.2.3.2 Plasmid based Protein overexpression in *H. volcanii*

7.2.3.2.1 Expression

For each expression a pre-culture was inoculated. Tryptophan inducible proteins were inoculated into Hv-Ca⁺ media with 1 mM tryptophan.

7.2.3.2.2 Extraction

Procedure was the same as in 7.2.3.1.2, however only K1800 was used.

7.2.3.3 Single turnover ATPase assay

In order to quantify if, and if so, how much γ -Phosphate a Protein hydrolyses from an ATP molecule a K-Buffer with a final concentration of 50 nM ATP containing 750 nCi of γ ³²P-labeled ATP (Hartman Analytic 6000 Ci/mmol) was diluted. Both recombinant proteins (different concentrations were used) and the ATP containing buffer were pre-incubated separately at their respective temperature (*Hv*: 42 °C, *Saci*: 75 °C). To start the reaction, 1 vol of ATPase solution was added to the Protein mix and incubate at said temperatures. At each time-point 5 μ l was removed from reaction volume and stopped with 90 μ l 1M Perchloric acid and 30 μ l 3M KAc, flicked and frozen in liquid nitrogen. The samples were centrifuged at full speed for 10 min and 2 μ l of each supernatant was loaded onto a Polygram Cel 300 PEI (Macherey-Nagel) TLC plate and developed with 350 mM KH₂PO₄ buffer for 45–60 min. Plates were dried with a blow-dryer and then exposed to a PhosphorImager screen.

7.2.3.4 Adenylate cyclase reaction

The prewarmed (37°C) reaction volume of 25 μ l consisted of 1 μ M Protein, to which 2.5 μ l ATP Mix (100ul, 10 μ M pre-Mix, includes 1ul 140 μ Ci ATP) was added. At each time-point 5 μ l was removed from reaction volume and further processed as described in 7.2.3.3.

7.2.3.5 Methanol Chloroform precipitation

200 μ l protein or resuspended cell pellet were added to 480 μ l MeOH and 160 μ l CHCl₃ and vortexed. Next 640 μ l H₂O was added and vortexed again before centrifuging with full speed for 5 min at RT. The supernatant was removed but leaving a small residue behind before the liquid phase begins. 300 μ l MeOH was added before centrifuging at full speed for 30 min at 4 °C. When done the supernatant was removed and was air-dried before resuspending in 4x HU-Buffer.

7.2.3.6 TCA-precipitation

A simple method to increase the protein concentration is via TCA precipitation (not suitable for high salt conditions). To do this 1 vol of ice cold 20 % TCA in the according K-Buffer was added to the

protein sample and was left on ice for 10 min. After incubation, the samples were centrifuged at full speed for 10 min at 4 °C. The supernatant was removed carefully, and the pellet was neutralized/washed in 200 µl ice cold acetone. Centrifugation was performed as before, repeat acetone wash if necessary. The pellet was dried at 95 °C to get rid of acetone residues and was then resuspended in 4x HU buffer.

7.2.3.7 Sucrose gradient separation and fractionation

A sucrose gradient is used to fractionate ribosomal subunits from the rest of the cellular components. To generate the gradients, 5 % and 30 % Sucrose solution in Hv-Buffer were mixed using the program “SW40 LONG SUCR 5 30” of the Biocomp Gradient Master 107 IP. The cell lysate was produced as in 7.2.3.1.2. The supernatant of the lysate was then measured for its OD₂₆₀ on the Nanodrop. 15 OD₂₆₀ were loaded onto the centrifugal column and centrifuged with either with 39,000 rpm for 4 h at 4 °C or 16h at 26.000 rpm in a Beckman Coulter Optima L-80XP Ultracentrifuge in a SW40 swing-out rotor. Acceleration and brake were both set to maximum

Fraction collection (500 µl/fraction, speed: 1 ml/min) was done with the BioRad Biologic LP and data was recorded with “LP-Dataview”.

100 ul of each fractions were MeOH/CHCl₃ precipitated as shown in 7.2.3.2.2 before loading onto SDS-PAGE. Depending on the experiment the rest was pooled together or 50 µl was taken for RNA extraction as described in 7.2.5.1.

Analogously gradients for the SW60 rotor were created (Sucrose concentrations of 5 – 20 % in Hv-Buffer). These were then run with 60.000 rpm for 2 h at 4 °C in a Beckman Coulter Optima L-80XP, and then fractionated on the same setup as before but in 250 µl fractions (500 µl/min), of which 80% were used for Protein- and the rest for RNA-extraction.

7.2.3.8 *In vitro* reconstitution KsgA dependent dimethylation of *ΔksgA* cells

As a substrate for methylation whole cell cleared lysates of hv Δ ksgA cells were generated as described in 7.2.3.1.2 in a K1800 Buffer. For subunit purification the cells were lysed in Hv Buffer but as described in 7.2.3.1.2. The 30S fractions were separated on a sucrose gradient (see 7.2.3.7) concentrated and Buffer exchanged (to K1800) on an AMICON® Ultra15 -10 KDa. The RNA concentration was measured on a Nanodrop-1000. For each reaction around 50 µg of whole cell RNA/30S-Fraction was used. The recombinant protein (HvKsgA-His₍₆₎ or HvKsgA-E84A-His₍₆₎, purification described in 7.2.3.1) was added in 100 fold molar excess. The reaction was performed in a total volume of 250 µl (ad. K1800). Before adding 0.5 mM SAM (NEB: B9003S), the reaction was preincubated for 5 min at 42 °C, following 60 min reaction time with SAM. After 60 min the reactions were placed on ice and processed further: ¼ was used for protein extraction (7.2.3.5) the rest was used for RNA extraction (7.2.5.1).

7.2.3.9 Single molecule methods

Prebound particles with fluorescently labelled HvKsgA (purified as described in 7.2.3.1.2.1) was pre-bound as described in 7.2.3.8 to a crude cell lysate of *hvksgA::pTA1228-His₆-GFP-s7* (induction at 0.25 mM Trp) without the addition of SAM for 30 min and was then separated on a sucrose gradient as described in 7.2.3.7. The desired subunit was then concentrated either using an Amicon 10K filter unit according to the manufacturers protocol or to reduce cost, pelleted in a TFT 55.38 rotor at 40.900 rpm for 90 minutes at 4 °C. A fraction of the pre-bound complex was then run on a SDS-PAGE as described in 7.2.3.11, then analyzed for cy3 or cy5 signals with a Typhoon™ FLA 9500, following western blotting as described in 7.2.3.12 to check for corresponding GFP-s4/s7 signals in the 30S fraction (see Figure 7.2).

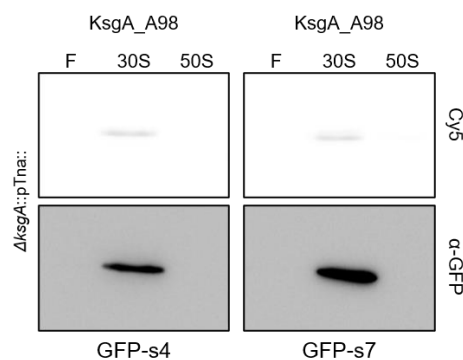


Figure 7.2 Comigration of GFP tagged small ribosomal proteins in the 30S fraction with Cy5 labelled KsgA_A98

Preparation, loading and data acquisition for the TIRF and FCS measurements were performed by Leonhard Jakob of the Microbiology department. For the FCS measurements the pre bound complex was split prior to loading onto the microscope to allow for different treatment, i.e. one aliquot without SAM to compare the aliquot with SAM.

7.2.3.10 Ribosomal subunit pelleting

200 µl of the 250 µl reaction volume (50 µg pooled 30S/KsgA-RNA + added substrates, as described in 7.2.3.8) was layered onto 250 µl sucrose cushion, the rest was used as input (RNA/Protein). For centrifugation without a cushion, the reaction (200 of 250 µl) was given into the centrifugal tube directly. This was then centrifuged 14h at 50,000 rpm in a TLA-55 rotor at 4 °C. The top 200 µl were considered as Supernatant, the next 200 µl as cushion, the remaining 50 µl were discarded, to avoid contamination with pellet. The pellet was air dried and resuspended in 250 µl K1800 Buffer by shaking on a Vibrax for 15 minutes. Of each fraction 75 % was used for protein extraction and 25 % for RNA extraction.

7.2.3.11 Polyacrylamide Gel Electrophoresis of Proteins

To separate different proteins depending on mass a SDS-PAGE is used. Depending on Size the concentration of the running gel was adjusted, Proteins >20 kDa were run on 12 % Acrylamide gels

smaller proteins were run on 15 % Acrylamide gels with 1x Lower-Tris. Stacking gels were 4 % Acrylamide with 1x Upper-Tris. All gels were polymerized with 1 % APS (20 %) and 0.1 % TEMED. To estimate the size of the proteins, Protein markers were always running with the gel, either Color prestained marker or unstained marker (see 7.1.8)

To visualize these fragments the gel was either stained with Coomassie or with a silver stain

7.2.3.11.1 Coomassie stain

The SDS-PAGE was fixed in 40 % MeOH, 10 % Acetic acid for 30-60 min while shaking. To stain the gel the fixing solution was replaced by Coomassie staining solution and microwaved for 30 s on highest power and shaken until completely blue. The gel was then de-stained with rinse buffer (40 % MeOH, 12 % acetic acid) on a shaker until only the bands remain colored.

7.2.3.11.2 Silver stain

For very low amounts of proteins a silver staining was used. The SDS-PAGE was fixed in fixing solution (50% MeOH, 12% acetic Acid, 0,02% Formaldehyde) for 1 h and then washed for 20 min in 50 % EtOH. The pre-staining was done in 1 min with 0,8mM Na₂S₂O₃, followed by three washes each 20 sec in H₂O. The gel was stained for 20 min with 12mM AgNO₃ (200mg), 0,03% Formaldehyde. Again, following two short washes of max. 20 sec each. Developing of the gel was done in 566mM Na₂CO₃ (6g), 0,02% Formaldehyde (50ul) 0,016mM Na₂S₂O₃ until bands are visible. To stop the development 1 % Acetic acid was used.

7.2.3.12 Western Blotting

The PVDF membrane was activated by washing in MeOH prior to use. Then all materials were soaked in Western blot transfer buffer setup to blot. The western blot ran in a BioRad SemiDry cell at constant 24V for 30-60 min depending on protein size. When finished the membrane was put in 1x PBS before continuing with the Antibody probing. Depending on the antibody, blocking solution was either 2% BSA in PBS-T (for #86 His Antibody) or 5 % Milk in PBS-T (for #104 anti-ProteinA Antibody and GFP antibody [Chromotek: 3H9, Rat Monoclonal]). After 20 min of blocking the Probing solution was added for another 90 min, 2% BSA in PBS-T (1:5,000 #86 His Antibody) or 1 % Milk in PBS-T (1:5,000 #104 anti-ProteinA antibody). This was then washed three times in PBS-T for 5 min. Final wash in PBS. The GFP antibody was then incubated another 2h in 5 % Milk PBS-T with the secondary antibody #81, HRP-Goat-Anti-Rat and washed again 3 times in PBS-T as before. HRP reaction was started with Roche Chemiluminescence kit (POD) and the membrane was mounted on a clear foil to view under LAS-3000 reader.

7.2.4 Mass spectrometry

7.2.4.1 Protein extraction

Cell pellets were suspended in 500µl of Extraction Buffer (150 mM NaCl, EDTA 100 mM, Tris pH 8.5 50 mM, 1 mM MgCl₂) with 1% SDS and incubated in a heating block for 13 min at 95°C. The

cell lysate was centrifuged for 10 min with max rpm to pellet cell debris, after 5 min of cooling at RT. The supernatant containing the solubilized proteins was transferred into a new 1.5 ml reaction tube. Reduction was done in the dark for 1h with 10 μ l β -Mercaptoethanol (final concentration 2 %). This was then split in two cups and precipitated with 1 ml Acetone (end concentration 80 %) at -20 °C for 2h. The precipitate was centrifuged at 4 °C with 16.000g for 10 min, the supernatant was removed and the pellet was washed twice with -20 °C Acetone and centrifuged as before. A majority of the acetone was removed but some remaining acetone was left on the samples for shipping on dry ice.

For the Mass spectrometry analysis, we did in Montreal, the pellet was additionally resuspended in 200 μ l Extraction buffer (no SDS) and Methanol Chloroform extracted (see 7.2.3.5).

The processing and the analysis of the precipitated proteins were done by PolyQuant GmbH (Bad Abbach, Germany) and are described in Schulze et al., 2020 "Dataset PXD014974". The Oeffinger Dataset was processed and analyzed by Christian Trahan of the Oeffinger Lab at the IRCM (Montreal, Canada) and the methods will be added to the publication (Knüppel et al., in preparation).

7.2.5 RNA Work

7.2.5.1 RNA extraction

Cell pellets or Eluates were resuspended in 500 μ l AE buffer and mixed with 500 μ l phenol equilibrated in AE Buffer and 50 μ l 10 % SDS. The samples then were transferred to a 65 °C thermomixer and shaken vigorously (1400 rpm) for 5min. Next, they were vortexed and cooled down on ice for 2 min. The mixture was then centrifuged at full speed and 4 °C for 2min before removing 3x 150 μ l of the aqueous layer into a fresh cup where it was vortexed with 500 μ l of phenol equilibrated in AE Buffer. Again, the samples were centrifuged as before and 3x 120 μ l of the supernatant were mixed with 500 μ l Chloroform by vortexing. Again, phase separation was done by centrifugation and 3x 100 μ l was then mixed with 2.5 vol of ice cold EtOH and 1/10 vol of 3 M NaAc pH 5.3 to precipitate the RNA. Samples were incubated at -20 °C for at least 10 min. RNA was pelleted by centrifugation for 10min at full speed and 4 °C. The pellet was air-dried and then dissolved in 50 μ l ddH₂O.

7.2.5.2 DNase digestion and RNA precipitation

To get rid of genomic DNA 1 μ l RQ1 RNase-free DNase (Promega) was added to the extraction of 50 μ l and was incubated at 37 °C for at least 1h. RNA was precipitated in 2.5 vol EtOH and 1/10 vol 3 M NaAc pH 5.3 for at least 30 min at -20 °C. The RNA was pelleted by centrifugation for 10min at full speed and 4 °C. The pellet was air-dried and then resuspended in 20 μ l Water. RNA concentration was measured on a Nanodrop-1000 at RNA settings.

7.2.5.3 RNA biotinylation

For RNA biotinylation, typically 20-100 µg total RNA was labelled in the dark in presence of 50 µg HPDP-biotin (Pierce) or 5 µg MTSEA-biotin-XX (Biotium - 90066) in 10 mM Tris-HCl pH 7.4; 1 mM EDTA pH 8 for 2 hours (HPDP-biotin) or 30 min (MTSEA-biotin-XX) (Duffy et al., 2015). Biotinylated RNAs were re-purified by hot-phenol extraction procedure (Schmitt et al., 1990).

7.2.5.4 Northern blotting and Detection of RNAs

Total RNA (typically 5-10 µg) was separated using a denaturing agarose gel. A 200 ml gel consisted of 1.3 % Agarose 20 ml 10x MOPS running buffer and 10.8 ml Formaldehyde. The Gel was run overnight in 1x MOPS running buffer and 2 % Formaldehyde at 34V. The Gel was then rinsed in 5 gel volumes of H₂O for 5 minutes on a shaker, followed by 20 min in 5 Gel volumes of 0.05M NaOH. Two steps of 20 min with 5 gel volumes of 10x SSC preceded the blotting to the washed Nylonmembran Positive™ (Qbiogen). The blotting was done analogously to the southern protocol described in 7.2.2.12, with the difference of using only thick Whatman papers and 10xSSC as transfer buffer. The transfer was done overnight. On the next day the membrane was shortly washed in 2x SSC and then airdried before Crosslinking the RNA twice in a Fluo_Link [Vilber Lourmat] at 0.3 J/cm².

7.2.5.4.1 Methylen Blue

Blots were stained with 0.02% (w/v) Methylene Blue (Sigma, 89% pure) in 0.3 M Natriumphosphate pH 5.3 until completely blue. Then washed with H₂O until bands become visible.

7.2.5.4.2 Radioactive

Blot was incubated in prehybridization buffer (see 7.1.2) for 3h at 30°C. Meanwhile the probe was prepared by mixing the following reagents, 1µl 10 µM Oligo, 1.5 µl PNK Puffer 10x NEB, 6.5 µl H₂O, 5 µl γ³²P-ATP 10 uCi/µl (50uCi), 1 µl T4 PNK NEB. This was then incubated for 45 minutes at 37 °C. and after 1 µl of 0.5 M EDTA and 50 µl H₂O was added and purified on a Microspin 6 column from Biorad. The pure probe was then added to the prehybridized blot and incubated overnight.

7.2.5.4.3 4TU labelled RNA

Labelled RNA on the Blot was first blocked for 20 min in 1x PBS pH 7.5, 1mM EDTA, 10 % SDS. After blocking IR800-Dye conjugated Streptavidin from Pierce (1:10000) was added to the blocking solution for another 20 min. The membranes were then washed twice each time in decreasing concentrations of SDS, twice in 10 %, 1 and 0.1 % respectively for 10 min. The Labelled RNAs were then visualized on a Li-COR Odyssey and quantified with Fiji.

7.2.5.5 Fluorescent Primer extension

Primer extension was done in the same way as described in 7.2.2.8 but with half the volume of the Kit and only 1 pmol (DYxxx) labeled primer. After the final denaturation step, basic RNA hydrolysis

with 1 μ l NaOH (1M) and 0.25 μ l EDTA pH8.5 (0.5 M) was performed at 60 °C for 30 minutes. The reaction was then neutralized with 1 μ l HCl (1M). An equal volume of Pex Loading Buffer was added to the finalized reaction (22.25 μ l). 50-100 ng were loaded onto either a small 14 % 1x TBE-PA gel (Novex Gel cassette, 1mm Thickness) or a medium sized very thin gel (20 cm x 17 cm, Thickness \leq 0.1 mm) with a shark tooth comb with the same ingredients. The small gels were run at 200 V until the bromophenol blue almost exited the gel. The Large gels were pre-run for 15 min at a constant 20 W and the actual run was performed at 25 W for 45 min, but the migration of the bromophenol blue was considered as an actual indicator as when to stop the run.

7.2.5.6 RNA Foot-printing

7.2.5.6.1 CMCT

CMCT was purchased from Merck (2491-17-0)

7.2.5.6.1.1 *Ex Vivo*

Prepare Stabilizing buffer the day before: 250mM Sodium Borate pH8 in K1800 buffer. Typically, 30 OD₆₀₀ of exponentially growing *Haloflex volcanii* cells were resuspended in 500 μ l K1800 Buffer and were then lysed as described in 7.2.3.1.2. The RNA concentration was measured on a Nanodrop-1000. An Input of about 10 - 15 μ g of crude RNA per 5 μ l should be used to ensure enough modified RNA for primer extension analysis. Set up the number of cups needed for no CMCT control and the concentration range that should be covered. To the 5 μ l lysate, 20 μ l Stabilizing Buffer is added and completed to 50 μ l with K1800, and incubated for 20 minutes at 20 °C. Meanwhile fresh 200mM CMCT in Water was prepared and then diluted to double the final concentrations in K1800 (i.e. 0 - 20 – 40 – 100 mM in K1800). Add 50 μ l of each CMCT dilution to the according cup and incubate further 20 minutes at 20 °C. Stop the reaction by adding 400 μ l AE Buffer and 500 μ l Phenol and proceed with RNA extraction (7.2.5.1).

7.2.5.6.1.2 *In vitro*

To CMCT modify naked RNA, 5 μ l of 4x CMCT Buffer (200 mM Borax, 20mM MgCl₂, 400 mM KCl (dissolve overnight)) and 5 μ l RNA (~3 μ g/ μ l) were incubated together for 20 min at 20 °C. Again, ensure you have proper controls and concentration gradient in mind when preparing the cups. Meanwhile 200mM CMCT was dissolved in Water. Dilutions for double the final concentrations were diluted in water and added to the reaction to end up in a final volume of 20 μ l. This was then further incubated for 20 min at 20 °C. Following addition of 480 μ l AE Buffer and 500 μ l Phenol and proceeded with RNA extraction (7.2.5.1).

7.2.5.6.2 DMS

7.2.5.6.2.1 *In vivo*

For each *in vivo* DMS foot-printing reaction, an exponentially growing *Haloferax volcanii* cells (OD ~0.6) were distributed into three aliquots of 10 ml in prewarmed 50 ml Falcons. In order to ensure reliable results, a no DMS and a Stop control were added to the experiment. To start the DMS reaction, 200 of 0.5 % of DMS in 95 % EtOH (Ratio ¼) was added to the cells and incubated shaking at 42 °C for a certain amount of time (test was 10 min). The controls were treated with Water in 95 % EtOH (Ratio ¼) and were shakend for the same amount of time. Be sure to add the stopping solutions in **order**, to ensure correct quenching of the DMS. The No DMS control was “stopped” by adding **1** - 5 ml 0.7 M β-Mercaptoethanol in 30 % SW and **2** - 5 ml of Isoamyl alcohol, Saturated with 30 % SW. the Stop control was treaded to same as the DMS control but as the final step DMS was added the same way as for a treated sample. The treated sample was treated the same way as the no DMS control after the DMS reaction of 10 min was completed. The cells were then centrifuged at 15.000g for 10 minutes at 4 °C and then washed with 2 ml of ice cold 23% SW containing 0.7 M β-Mercaptoethanol, centrifuged again and repeated. If cells have survived the harsh treatment, proceed with RNA extraction (7.2.5.1). The Haloferax cells however did not survive the Isoamyl alcohol and immediately burst once exposed to it.

7.2.5.6.2.2 *Ex vivo*

In vitro DMS foot-printing worked the same way as *in vivo* but with lower volumes. Typically, 50 µg of RNA was resuspended in 200 µl K1800 Buffer and then processed the same way as before: No DMS, Stop control, DMS Sample. The volumes for the β-Mercaptoethanol Mix and the Isoamyl Mix were 150 µl instead of 5 ml. The DMS mix was added to a final concentration of 2 %. After treatment the samples were used for RNA extraction (7.2.5.1). But with major losses in the extraction due to the density of the Samples compared with Phenol, resulting in no supernatant.

7.2.5.6.3 SHAPE

Was performed as described in detail in (Knüppel et al., 2020)

7.2.5.7 **RNA Affinity purification**

7.2.5.7.1 MS2 Aptamer purification

Mobicol columns were equilibrated in the desired buffer (here K200 + 15mM Imidazole) and 20 µl Ni NTA Agarose beads (slurry) were washed 2 times in the respective buffer (by centrifugation 0.2 g at 4 °C, all following wash/centrifugation steps use this setting if not stated otherwise.). Add ~200 µg recombinant MS2 (purification in K200 buffer, 0.2m mM IPTG for 5h at 37 °C, rest as described in 7.2.3.1) and incubate for 90 min at 4 °C on a rotating wheel in a total volume of 400 µl (add final concentration of 10 mM Imidazole). Then wash bound MS2-Ni-NTA once with K200 Buffer. Block MS2 Ni-NTA complex with 50 µg of yeast tRNA and incubate for 15 min at 4 °C on a rotating

wheel. Normally 10-20 µg of RNA (~10 fold less than MS2) was added to the blocked complex and let incubate for another 2h at the same conditions as before, alongside 20U RNasin. After RNA binding the flow through was collected via centrifugation, and washed three times for 5 minutes in batch on the rotating wheel at 4 °C with the according buffers tested (200/500/750/1000 mM KCl; 20 mM Tris/HCl pH 7,5; 10 mM MgCl₂; 10 mM Imidazole), washes were collected as well. Elution was done with an increased Imidazole concentration of 250 mM in 500 µl Buffer (500 mM KCl; 20 mM Tris/HCl pH 7,5; 10 mM MgCl₂). Further processing as described in 7.2.2.1, 7.2.2.8, 7.2.2.4 (10 % Gels) and 7.2.5.1.

7.2.5.7.2 Biotinylated RNA purification

Total RNA was extracted as described in 7.2.5.1. Residual genomic DNA was digested in presence of RQ1 DNase (Promega) and RNasin (Promega) as recommended by the manufacturer. The RNA was purified by hot-phenol extraction and biotinylated as described in 7.2.5.3. Purified RNA (25 µg) was resuspended in binding Buffer (20mM Tris–HCl pH 7.6, 150 mM NaCl, 5 mM MgCl₂, 1 mM DTT) (Nielsen et al., 2011) and incubated for 2 h on a rotating wheel at 4 °C with high-capacity Streptavidin agarose beads (Pierce) in a total volume of 800 ml binding buffer. Immobilized RNA was washed three times for 10 min on a rotating wheel at 4 °C with 800 ml the binding buffer. Competitive RNA elution was performed twice in batches using 500 ml buffer B supplemented with 2.5 mM Desthiobiotin (IBA) at 4 and 23 °C, respectively. RNA was purified using hot-phenol extraction as described 7.2.5.1 and 1 % of the extracted affinity purified RNA was used for qPCR and 20 % for primer extension analysis as described in 7.2.2.8 and 7.2.2.9.

7.2.6 Miscellaneous

7.2.6.1 TECAN-Reader

Values were normalized against mean values of Hv-YPC only wells, respectively for Hv-YPC(+trp).

Doubling times from TECAN reader were calculated with the following formula:

$$\text{Doubling time} = (t(1) - t(0)) * \log_2\left(\frac{OD(t = 1)}{OD(t = 0)}\right)$$

The time range chosen, was in the exponential grown phase according to the growth curves.

7.3 Statistics

Statistical tests were done in Graphpad or Excel using an unpaired t-test and the P-values are indicated below the figures.

8 LIST OF FIGURES

Figure 3.1 Three Domains of life tree	3
Figure 3.2 Eukaryo-archaeal ancestry	4
Figure 3.3 Archaeal groups with representative species	5
Figure 3.4 Electron micrographs of <i>Haloferox volcanii</i> and <i>Sulfolobus acidocaldarius</i>	6
Figure 3.5 Structural comparison of the bacterial and Eukaryotic ribosome	8
Figure 3.6 Comparison of the individual subunits from bacteria and eukarya	9
Figure 3.7 Venn diagram of shared ribosomal proteins of all three kingdoms	10
Figure 3.8 Assembly maps of the 30S and 50S subunits, reinterpreted from Nomura and Nierhaus	11
Figure 3.9 Schematic drawing of the <i>rrnB</i> operon	12
Figure 3.10 Schematic representation of the yeast rDNA locus	13
Figure 3.11 Schematic representation of the pre-rRNA processing pathways in <i>S. cerevisiae</i>	15
Figure 3.12 Ribosome assembly and maturation pathway	16
Figure 3.13 Polycistronic organization of two representative archaeal rDNA loci	17
Figure 3.14 Methylation reaction and 2D-Structure of 16S rRNA in <i>E. coli</i>	23
Figure 3.15 T-Coffee multiple sequence alignment of KsgA from four representative organisms and two other methyltransferases	24
Figure 3.16 Binding Sites and Structure of KsgA/Dim1	25
Figure 3.17 Proximity of Era to RbfA and KsgA on the SSU	27
Figure 3.18 Schematic interpretation of the late biogenesis events in <i>E. coli</i> based on my interpretation of the presented literature	28
Figure 3.19 Biotinylation of 4SU [A] “old” reagent [B] New and improved reagent (modified from (Duffy et al., 2015))	31
Figure 3.20 Selection of RNA probing chemicals	33
Figure 4.1 <i>In vivo</i> incorporation of 4TU in model archaea	36
Figure 4.2 Steady state and concentration dependent labelling of 4TU in model archaea	36
Figure 4.3 Pulse chase comparison between two model archaea	37
Figure 4.4 Influence of pyrimidine <i>de novo</i> synthesis on overall 4TU incorporation	38
Figure 4.5 Analysis of the transcriptionally regulated tryptophanase mRNA with 4TU	39
Figure 4.6 Exemplary <i>in vivo</i> SHAPE analysis of <i>H. volcanii</i> RNA using three different SHAPE reagents	41
Figure 4.7 Exemplary <i>in vivo</i> SHAPE modification of WT <i>S. acidocaldarius</i> cells	42
Figure 4.8 Scheme for <i>ksgA</i> knock out cassette	43
Figure 4.9 Southern Blot and PCR Verification of Knockouts in <i>Haloferox volcanii</i> and <i>Sulfolobus acidocaldarius</i>	43

Figure 4.10 Primer extension analysis of Knock out and Wild type constructs in four Organisms.	45
Figure 4.11 Overexpression and complementation lead to similar results as the wild type.	46
Figure 4.12 Exemplary purification and <i>in vitro</i> reconstitution assay.	48
Figure 4.13 Alignment and RNA fold prediction of helix45 of the 16S rRNA.	49
Figure 4.14 RNA foot-printing and mapping to 2D structure prediction.	50
Figure 4.15 Phylogenetic tree of helix45 sequences shows high variance in the archaeal kingdom.	52
Figure 4.16 <i>E. coli</i> rDNA mutants produce predicted methylation pattern.	54
Figure 4.17 Kasugamycin induced KsgA deficiency.	55
Figure 4.18 Reporter rDNA can be methylated <i>in vivo</i>.	56
Figure 4.19 KsgA is not detectable on the 30S fraction after adding SAM to a whole cell reconstitution.	57
Figure 4.20 No negative growth effect of <i>ΔksgA</i> but fitness advantage in competition.	58
Figure 4.21 Archaeum structure and exemplary Motility assays.	60
Figure 4.22 Absence of KsgA significantly decreases motility.	61
Figure 4.23 <i>ΔksgA</i> cells adhere significantly better in Hv-Ca⁺ Media.	62
Figure 4.24 Loss of KsgA does not lead to a significant change in cell morphology.	64
Figure 4.25 Flagellin A1 is less abundant in KsgA Knock out cells.	65
Figure 4.26 Violin Plots of AUG vs non-AUG initiation codons usage indicate increased upregulated non-AUG initiation in <i>ΔksgA</i> in <i>H. volcanii</i>.	66
Figure 4.27 ArCOG (GO-Term) Analysis of two Proteome Data sets and distribution effect of KsgA deficiency.	67
Figure 4.28 Loss of KsgA leads to increased flexibility in the proximity of h44-h45 interaction site.	68
Figure 5.1 Differential 2D gel analysis of L-AHA-labelled proteins.	71
Figure 5.2 Various types of helix openings 45 in <i>E. coli</i>, <i>B. stearotherophilus</i>, <i>Euglena gracilis</i> (chloroplast), <i>H. volcanii</i> and <i>P. furiosus</i> ribosomes.	75
Figure 5.3 Influence of KsgA dependent methylation on the GGAA tetraloop of helix 45 and hydrogen bonding to helix 44 in <i>E. coli</i>.	76
Figure 5.4 Methylation pattern distribution of <i>H. volcanii</i>.	77
Figure 5.5 Purification and ATPase/adenylate kinase activity of hvFap7.	80
Figure 7.1 pTA1228 Vector Map, with MCS highlighted	108
Figure 7.2 Comigration of GFP tagged small ribosomal proteins in the 30S fraction with Cy5 labelled KsgA_A98.	114

9 LIST OF TABLES

Table 3.1 Ribosome composition in the three domains of life.....	9
Table 4.1 SHAPE reagent solubility in different cultivation medium.	40
Table 2 Stability and composition of the helix 45 of <i>E. coli</i> , <i>B. stearothermophilus</i> and <i>H. volcanii</i>	77
Table 7.1 Commonly used buffers	87
Table 7.2 Transformation buffers.....	89
Table 7.3 Media composition <i>E. coli</i>	90
Table 7.4 Media composition <i>H. volcanii</i>	90
Table 7.5 Media composition <i>S. acidocaldarius</i>	92

10 SUPPLEMENTS

10.1 Identifiers for ArCOGs:

PolyQuant (used Uniprot Identifiers):

Down:

D4GU63;D4GTL4;D4GVY6;D4GX95;D4GVL3;D4GVY7;D4GW38;D4GP73;D4GU40;D4GWL4;D4GTW6;P18284;D4GRY8;D4GX13;D4GUC8;D4GZR5;D4GVY1;D4GY13;D4GPP7;D4GR95;D4GUH6;D4GYD7;D4GVQ0;D4GZT2;D4GWH1;D4GWS7;D4GVA8;D4GVG8;D4GSI6;D4H080;D4GY14;D4GTZ7;D4GW56;D4GZR9;D4GWP2;D4H052;D4GYG6;D4GVC2;D4GT98;D4GTX5;D4GV87;D4GXW2;D4GYW5;D4GWR0;D4GQU5;D4GV10;D4GW28;D4GXM6;D4GWR3;D4GQN4;D4GYU8;D4GPF0;D4GQU9;D4GXK2;D4GR47;D4GYP7;D4GZM2;D4GP72;D4GUM9;D4GTB9;D4GXG7;D4GRG5;D4GU83;D4GVC1;D4GV91;D4GXB4;D4GYG7;D4GQ28;D4GX36;D4GX92;D4GUS8;D4GTS8;D4GSH7;D4GVU1;D4GRD7;D4GVY5;D4GSM9;D4GVR7;D4GU66;D4GU72;D4GPF6;D4GP81;D4GR46;D4GV57;D4GW78;D4GW15;D4GU71;D4GUL4;D4GV93;D4GZA2;D4GVX2;D4GVY2;D4GTD0;D4GVT4;D4GRV5;D4GUA4;D4GQ44;D4GVK4;D4GVM4;D4H025

Up:

D4GXB9;D4GS66;D4GWS1;D4GXY9;D4GYI2;D4GZS0;D4GRB6;D4GVS7;D4GS20;D4GS45;D4GP49;D4GQ18;D4GYI3;D4GZN7;D4GSM4;D4GY89;O07118;D4GYT2;D4GZP2;D4GW15;Q48328;D4GS83;D4GQE6;D4GY63;D4GZ3;D4GTN2;D4GY76;D4GWM3;D4GU45;D4GTS2;D4GPI3;D4GXT2;D4GUL3;D4GXL4;D4GY62;D4GXY7;D4GTB1;D4GYL4;D4GP57;D4GSF6;D4GYE3;D4GTT7;D4GSX7;D4GZ05;D4GZ55;D4GX08;D4GW82;D4H061;Q03301;D4GZF4;L9VGF7;D4GYM0;D4GZN4;D4GXS5;D4GQG9;D4GXG1;D4GYN6;D4GSE4;D4GZI9;D4GZY5;D4GQ21;D4GTF7;D4GSG0;D4GUG5;D4GSF3;D4GWY0;D4GXW4;D4GYR6;D4GRU8;D4GSG2;D4GS15;D4GXP5;D4GZ79;D4GS63

Öffinger (used Hvo Identifiers):

Up

HVO_A0087;HVO_A0021;HVO_0569;HVO_2746;HVO_A0048;HVO_1848_A;HVO_0172;HVO_A0047;HVO_1749;HVO_0202;HVO_1011;HVO_2962;HVO_0653;HVO_0978;HVO_0834;HVO_0632;HVO_0013;HVO_A0049;HVO_A

0092;HVO_2024;HVO_2751;HVO_0821;HVO_1889;HVO_0420;HVO_2094;HVO_1583;HVO_0844;HVO_0241;HVO_B0041;HVO_A0289;HVO_A0084;HVO_B0072;HVO_0098;HVO_2979;HVO_B0130;HVO_1248;HVO_0939;HVO_B0044;HVO_B0353;HVO_0597;HVO_A0555;HVO_B0017;HVO_B0199;HVO_2276;HVO_0266;HVO_2014;HVO_A0329;HVO_1153;HVO_0143;HVO_0910;HVO_1476;HVO_2505;HVO_1210;HVO_2590;HVO_2151;HVO_0958;HVO_B0381;HVO_0252;HVO_0071;HVO_B0305;HVO_A0474;HVO_1607;HVO_1549;HVO_0818;HVO_B0295;HVO_0735;HVO_2655;HVO_A0083;HVO_B0382;HVO_1908;HVO_A0369;HVO_0320;HVO_0505;HVO_0386;HVO_0690;HVO_B0380;HVO_0219;HVO_A0064;HVO_2946;HVO_1584;HVO_2621A;HVO_0438;HVO_0090;HVO_0221;HVO_0965;HVO_A0082;"HVO_A0138;HVO_A0101";HVO_0041;HVO_1739;HVO_2682;HVO_C0060;HVO_2897;HVO_0724;HVO_B0084;HVO_1438;HVO_2689;HVO_0265;HVO_1810;HVO_C0080;HVO_2900;HVO_0669;HVO_B0031;HVO_0565;HVO_1359;HVO_1484;HVO_0564;HVO_0848;HVO_1633;HVO_A0160;HVO_0235;HVO_0852;HVO_0786;HVO_0825;HVO_1512;HVO_0201;HVO_1753;HVO_1888_A;HVO_C0051;HVO_A0045;HVO_1443;HVO_2919;HVO_0110;HVO_0819;HVO_C0007;HVO_B0085;HVO_1869;HVO_0676;HVO_0696;HVO_1325;HVO_A0115;HVO_B0138;HVO_1755;HVO_A0611;HVO_1358;HVO_0101;HVO_0486;HVO_1451;HVO_2064;HVO_1905;HVO_1742;HVO_0253;HVO_1587;HVO_B0004;HVO_1787;HVO_0954;HVO_0435;HVO_0391;HVO_A0488;HVO_0428;HVO_0107;"HVO_A0415;HVO_A0119";HVO_1593;HVO_A0243;HVO_1693;HVO_B0347;HVO_0802;HVO_B0053;HVO_1440;HVO_2992;HVO_2892_A;HVO_A0368;

Down:

HVO_1124;HVO_2684;HVO_C0075;HVO_1016;HVO_3006;HVO_0788;HVO_2299;HVO_1398;HVO_2659;HVO_1694;HVO_0231;HVO_1034;HVO_A0522;HVO_2977;HVO_1040;HVO_0283;"HVO_A0009;HVO_A0434";HVO_B0257;HVO_A0417;HVO_1424;HVO_2694;HVO_2269;HVO_1762;HVO_2681;HVO_0162;HVO_A0466;HVO_2229;HVO_B0186;HVO_B0136;HVO_1528;HVO_0865;HVO_0506;HVO_2079;HVO_0652;HVO_B0045;HVO_2318;HVO_2069;HVO_2528;HVO_2271;HVO_2101;HVO_B0071;HVO_1602;HVO_A0587;HVO_0193;HVO_B0146;"HVO_0330;HVO_A0038";HVO_A0279_A;HVO_2576;HVO_1200;HVO_0803;HVO_1138;HVO_1567;HVO_2046;HVO_0588;HVO_0772A;HVO_A0267;HVO_0789;HVO_2165;HVO_0479;HVO_A0451;HVO_1171;HVO_2270;HVO_0596;HVO_1098;HVO_1346;HVO_2909;HVO_1126;HVO_C0077;HVO_2033;HVO_2993;HVO_2767;HVO_0855;HVO_2760;HVO_1264;HVO_0734;HVO_1351;HVO_1394;HVO_2365;HVO_0039;HVO_A0296;HVO_A0141;HVO_0532;HVO_1033;HVO_2905;HVO_1477;HVO_1227;HVO_2084;HVO_2172;HVO_2667;HVO_2881;HVO_2049;HVO_2111;HVO_1859;HVO_1281;HVO_1074;HVO_0984;HVO_1548;HVO_0414;HVO_1441;HVO_0770;HVO_2186;HVO_1021;HVO_A0428;HVO_0948;HVO_A0432;HVO_1283;HVO_1066;HVO_0945;HVO_1610;HVO_1274;HVO_2811;HVO_1923;HVO_1318;HVO_2171;HVO_0722;HVO_2048;HVO_1461;HVO_A0464;HVO_1499;HVO_2047;HVO_1988;HVO_A0276;HVO_0643;HVO_0989;HVO_2451;HVO_A0430;HVO_2021;HVO_A0429_A;HVO_A0275;HVO_2787;HVO_A0320

10.2 Supplementary Figures

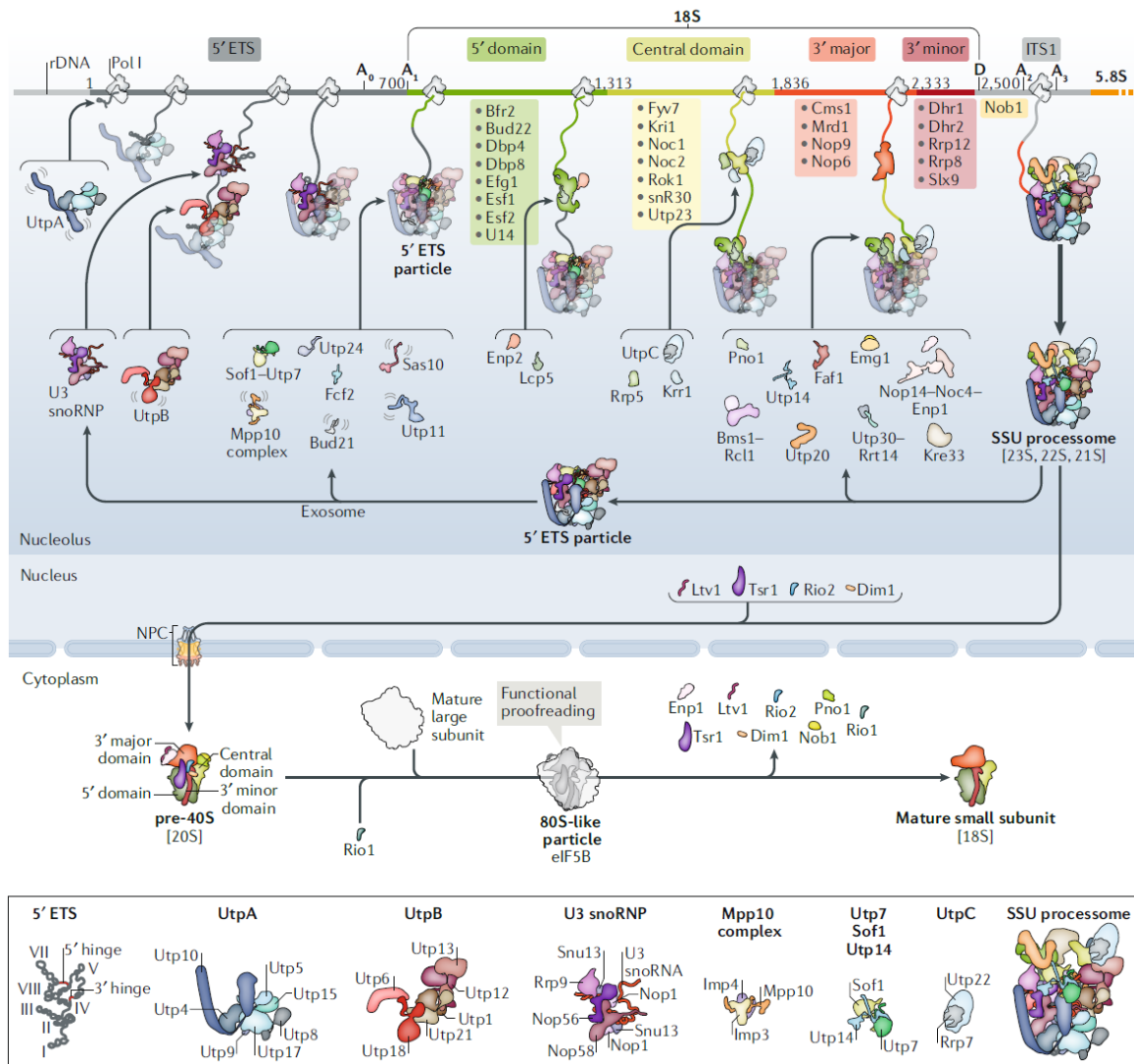


Figure S1 “Assembly of the small ribosomal subunit. Consecutive stages in the maturation of the small ribosomal subunit (40S) are shown, beginning with the earliest co-transcriptional steps in the nucleolus, the formation of the small-subunit-specific portions of ribosomal DNA (rDNA) are depicted with colour-coding of the 5' external transcribed spacer (5' ETS); the 5', central, major and 3' minor domains of the 18S ribosomal RNA (rRNA); and the internal transcribed spacer 1 (ITS1). The pre-rRNA cleavage sites A⁰, A¹, D and A² are indicated. Three ribosome particle intermediates are shown: the 5' ETS particle, SSU processome and the pre-40S particle. Pre-rRNA intermediates present in each particle are indicated in square parentheses beneath each particle. There are likely additional assembly intermediates not yet identified. Sequential association and dissociation of assembly factors and complexes of assembly factors are shown. Assembly factors and complexes for which structures have been determined are depicted in cartoon form, whereas those for which no structures are known are indicated only with text. The 5' ETS particle was inferred from purification of complexes assembled on 3' truncated pre-rRNAs. The earliest assembly intermediate for which cryo-electron microscopy structures were obtained is the SSU processome. Endonucleolytic cleavage at the A⁰, A¹ and A² sites and major structural remodelling (not shown) result in the release of assembly factors and the 5' ETS particle from the SSU processome. The resulting pre-40S particle assembles in the nucleus with a set of export factors and is rapidly exported to the cytoplasm, where the pre-40S particles engage in functional proofreading by joining with mature 60S subunits. The last assembly factors are released and the D site is cleaved to generate mature subunits containing 18S rRNA. Proteins that joined the growing SSU processome at an earlier stage are shown as transparent to highlight new components (not transparent). The ‘wiggling’ signs highlight components that are flexible in isolation. NPC, nuclear pore complex; Pol I, RNA polymerase I; snoRNP, small nucleolar ribonucleoprotein. Adapted with permission from “...”, Elsevier.“ (taken from Klinge and Woolford, 2019)

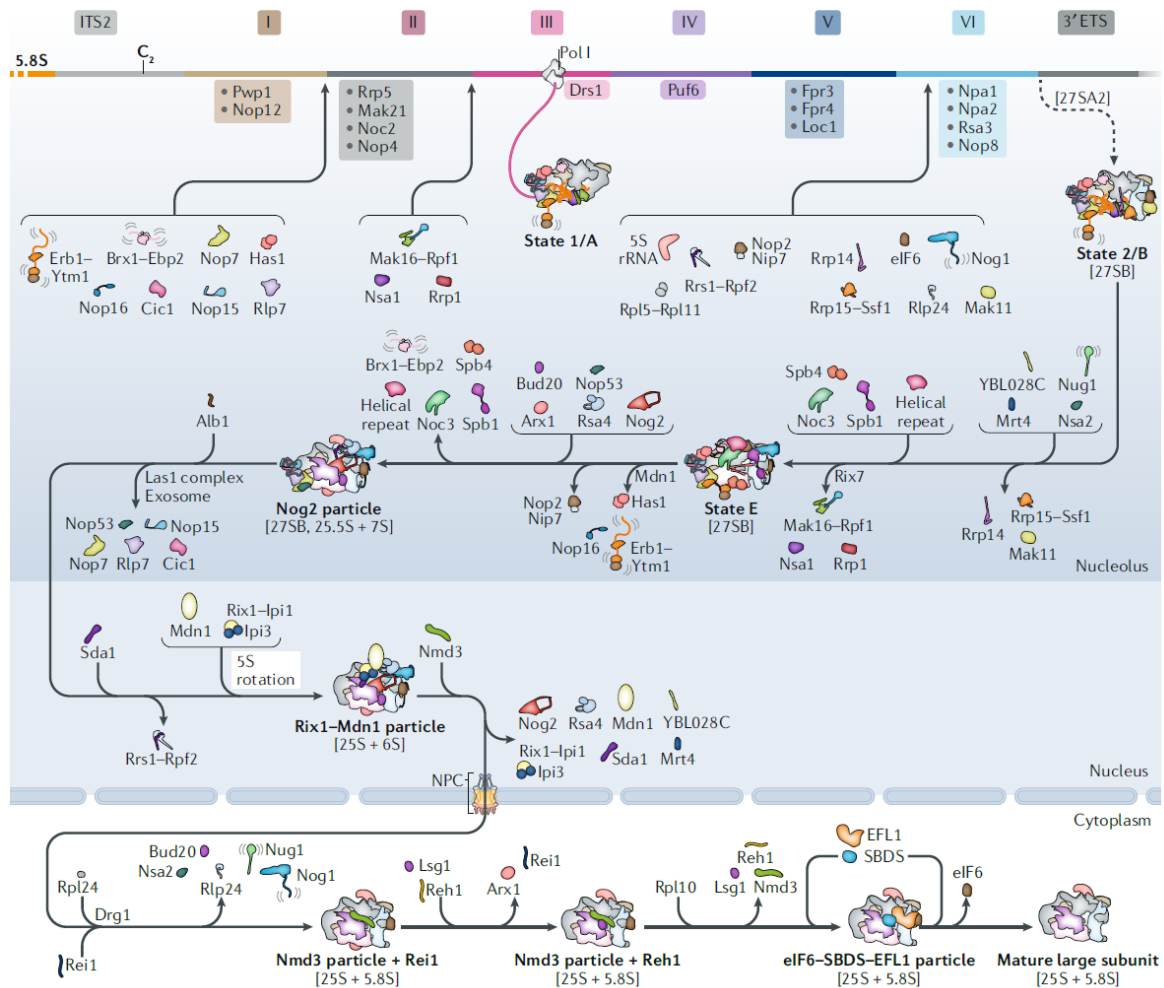


Figure S 2 “**Assembly of the large ribosomal subunit.** Consecutive stages in the maturation of the large ribosomal subunit (60S) are shown, from the earliest stages in the nucleolus, through stages in the nucleoplasm and finally in the cytoplasm. Large- subunit-specific portions of ribosomal DNA (rDNA) are depicted with colour- coding of the 5.8S ribosomal RNA (rRNA), the internal transcribed spacer 2 (ITS2), the 25S rRNA domains I–VI and the 3’ external transcribed spacer (3’ ETS). Six assembly intermediates for which cryoelectron microscopy (cryo- EM) structures have been determined are shown: state 1 or state A (state 1/A), state 2/B, state E, Nog2, Rix1–Mdn1 and Nmd3 particles. Pre- rRNA intermediates present in each particle are indicated in square brackets, and rRNA domains that have assembled into stable visible domains are depicted using the same colours of the rDNA. Note that some of the different particles contain the same pre- rRNAs but differ in structure and protein content (for example, state 1/A and state 2/B). There are likely additional assembly intermediates to be discovered. The association and dissociation of assembly factors is shown. Assembly factors for which structural information is available are depicted in cartoon form; those for which no structures are known are indicated with text only. The earliest preribosomal particles present before state 1/A particles are formed cotranscriptionally and have not been visualized by electron microscopy. In the state 1/A and state 2/B particles, 25S rRNA domains I, II and VI and the 5.8S rRNA and ITS2 have begun to form and become stable, visible conformations. The transition from state 2/B to states C and D (which are not shown as particles), and then to state E, involves assembly of domains III, IV and V and includes early steps in the formation of the peptidyl transferase centre and polypeptide exit tunnel functional centres. Major structural remodelling occurs to form Nog2 particles, which translocate from the nucleolus to the nucleoplasm, where additional restructuring as well as quality control checkpoints are carried out to prepare particles for nuclear export. Upon entry into the cytoplasm, the remaining assembly factors are released, as the assembly and surveillance of functional centres is completed. The ‘wiggling’ signs highlight components that are flexible. NPC, nuclear pore complex.” (taken from Klinge and Woolford, 2019)

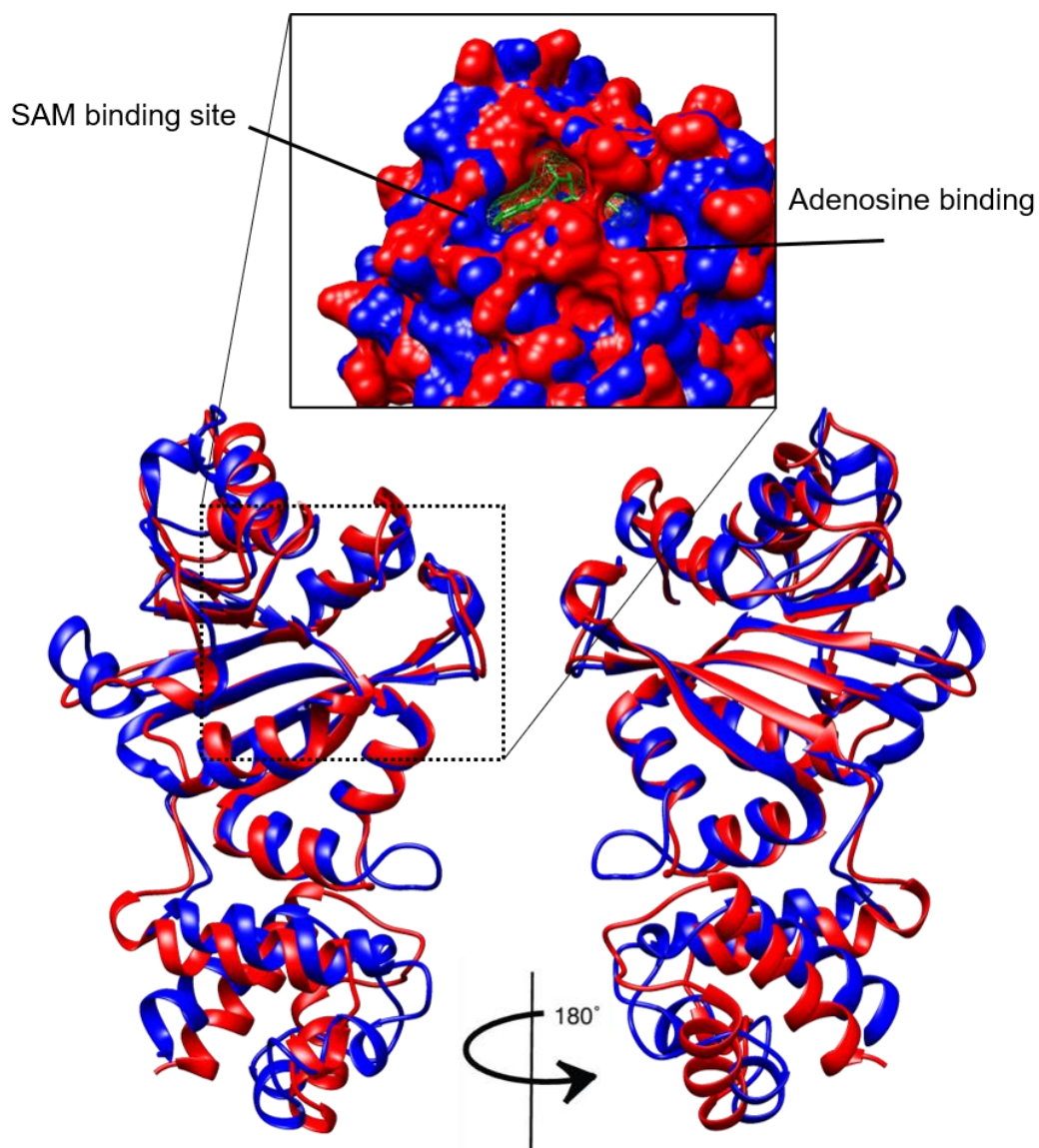


Figure S 3 Match of *Bs_ermC'* (Red:1QAO) and *Ec_KsgA* (Blue:1QYR) crystal structures. Close up shows surface with binding pockets with SAM bound to the binding pocket of *ermC* (green).

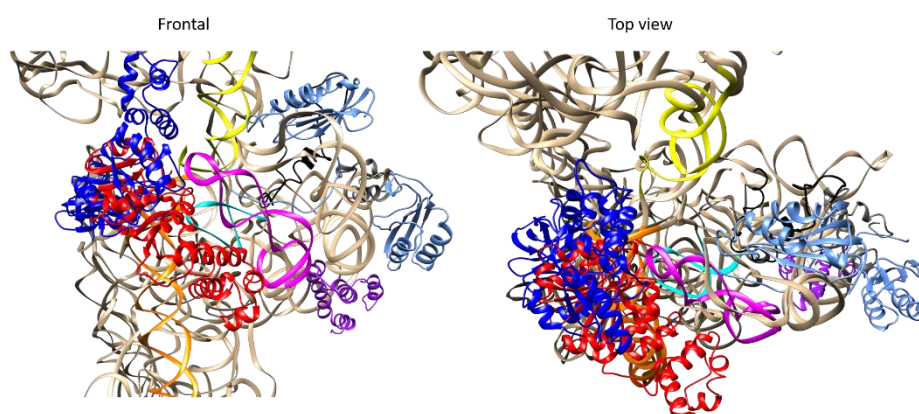


Figure S 4 Superimposition of 30S+RsgA (PDB 2YKR) and 30S+KsgA (PDB 4ADV). S6 cornflower blue, S11 - medium blue, S15 - purple, S18 - dark grey, S21 - black, h24 pink, h44 orange, h45 cyan, h28 yellow, KsgA - Red, RfbA - blue. Created using Chimera

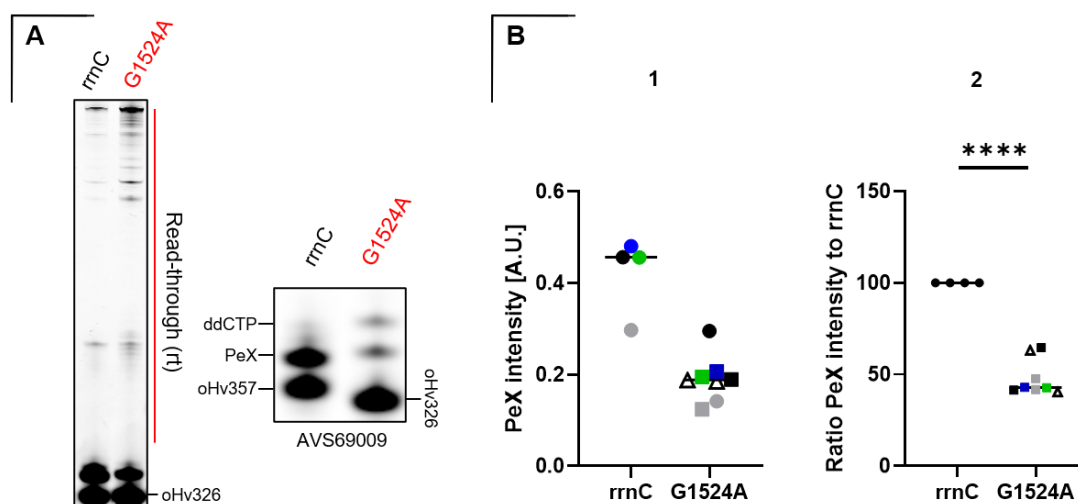


Figure S 5 **Decreased methylation of G1523A helix45 conformation in *E. coli* in vivo.** [A] Primer extension reaction of AVS69009::pHK with the indicated mutations. Left normal primer extension using dNTP showing increased readthrough of G1523A. Right primer extension using ddCTP showing increased ddCTP readthrough of G1523A. Note the different primers, due to the G1523A mutation the shortened primer oHv357 is not needed, for ddCTP. Using oHv357 on AVS69009::pHKG1523A often caused issues during primer extension and using different primers lacks comparability. Thus, using the same primer for all runs (oHv 326 with dNTPs) the signal intensities of: Primer extension stops (Pex) and oligo (oHv) were measured with Fiji. The data is shown in [B] The left graph shows the raw measurements of intensity for both strains. The calculation was done as follows: $[Pex/(Pex+oHv)]$. Each experiment (primer extension) is indicated by color, each biological replicate by shape (individual clones) the right graph was only done for 2 biological replicates. Cells were harvested at OD ~0.4. Statistical testing is difficult as paired t-test is necessary, using ratio pairing $p=0.0051$, Wilcoxon t-test (paired) $p=0.1250$. Due to the difficulty in comparison I calculated the differences between rrnC and 1523 from Graph 1 of each experiment (color) Ratio Values from PeX intensity of rrnC are shown in Graph 2. Biological replicates remain the same. Unpaired t-test $p<0.0001$.

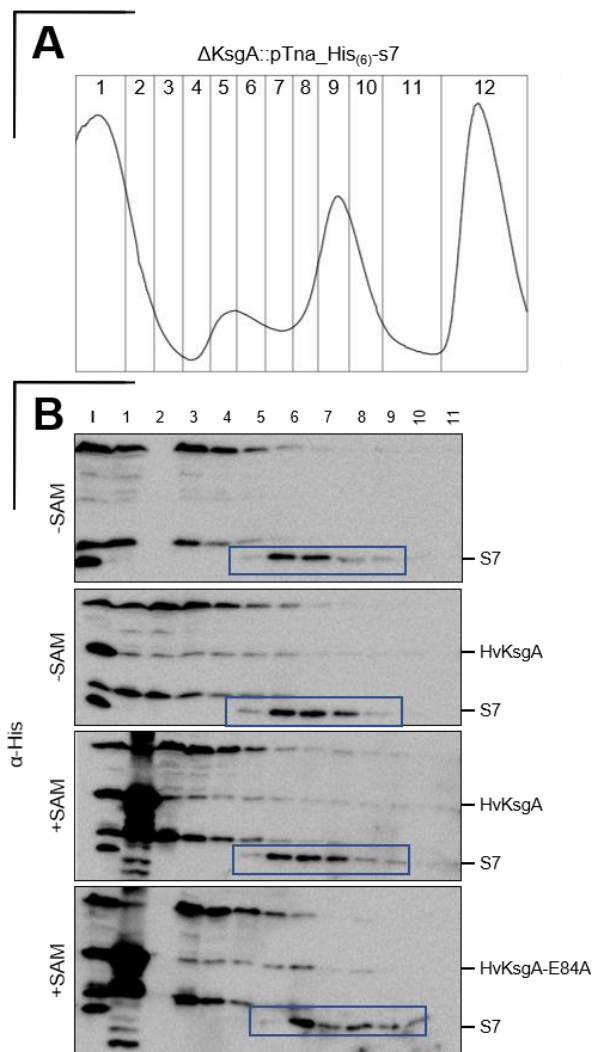


Figure S 6 **Initial binding and release experiment.** One representative sucrose gradient profile is depicted. Blots were acquired individually and have different exposure times to detect the slightest signals. Fractions (blue) according to s7 signals were pooled for blot in Figure 4.19. 50S are those following the last blue fraction. Fraction 2 of the first gel was somehow lost during extraction. 200 μ l of each 500 μ l fraction was extracted and loaded completely. Pooled fraction were re-extracted, i.e. 40 μ l of each fraction and pooled into one extraction (200 μ l total). Extraction as described in 7.2.3.5.

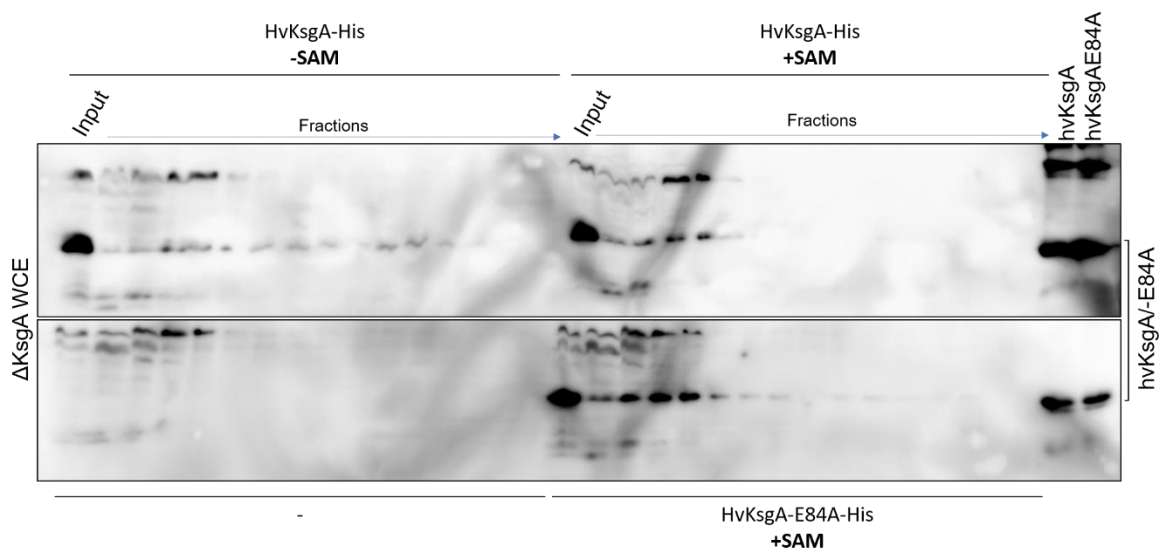


Figure S 7 **Repetition of binding and release experiment.** Fractions 1-15 of the SW40 5-30% sucrose gradient are shown for the indicated experiments. All experiments used the basic $\Delta ksgA$ K4 strain as substrate. Excess of recombinant protein is loaded on the right of each blot. Detection of His Antibody with Thermo Scientific™ SuperSignal™ West Femto Chemilumineszenz-Substrate

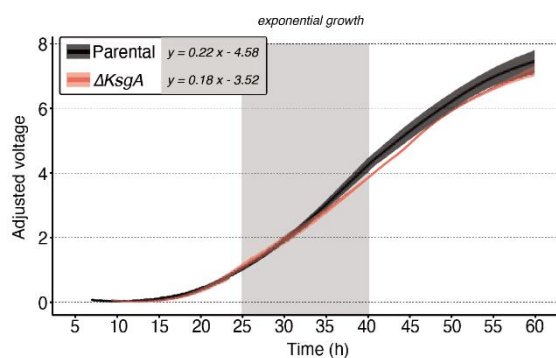


Figure S 8 **No significant differences in growth rate in *P. furiosus*.** Preliminary data needs to be re-evaluated. Analysis was done by Winfried Hausner and Felix Grünberger of the Microbiology department. Method is described in 7.2.1.3.3

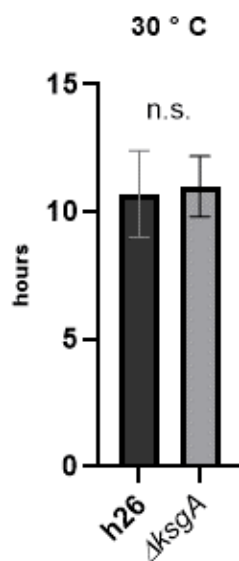


Figure S 9 **TECAN doubling times of h26 and $\Delta ksgA$** . Three biological replicates for $\Delta ksgA$ and two independent cultures of h26. All were run in technical duplicates. Unpaired t-test ($p=0.7494$)

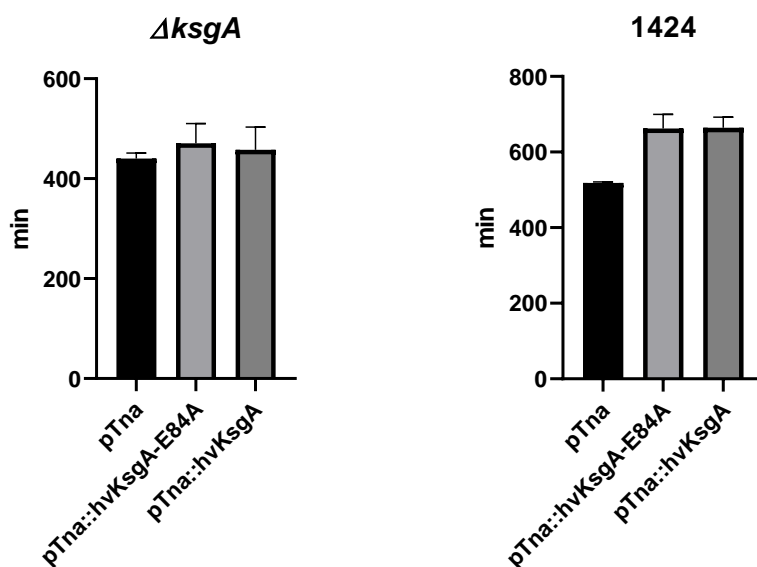


Figure S 10 **TECAN doubling times of complementation and overexpression constructs**. 2 Biological and three technical replicates were grown in a 96 well plate in a TECAN reader at 41.5 °C. Doubling time was calculated between timepoints of exponential growth. Hv cells grow very slowly in a TECAN reader but are intrinsically comparable, doubling time of WT or $\Delta ksgA$ cells in flask ~240 min

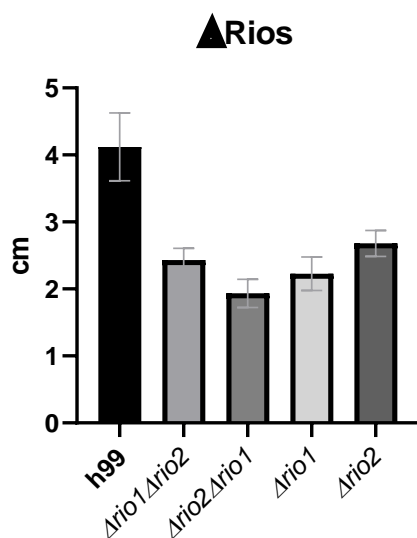


Figure S 11 **Motilities of various Rio knock outs**. Strains from Knüppel et al., 2018, Biological replicates: 1, technical 3. Grown as described in 7.2.1.3

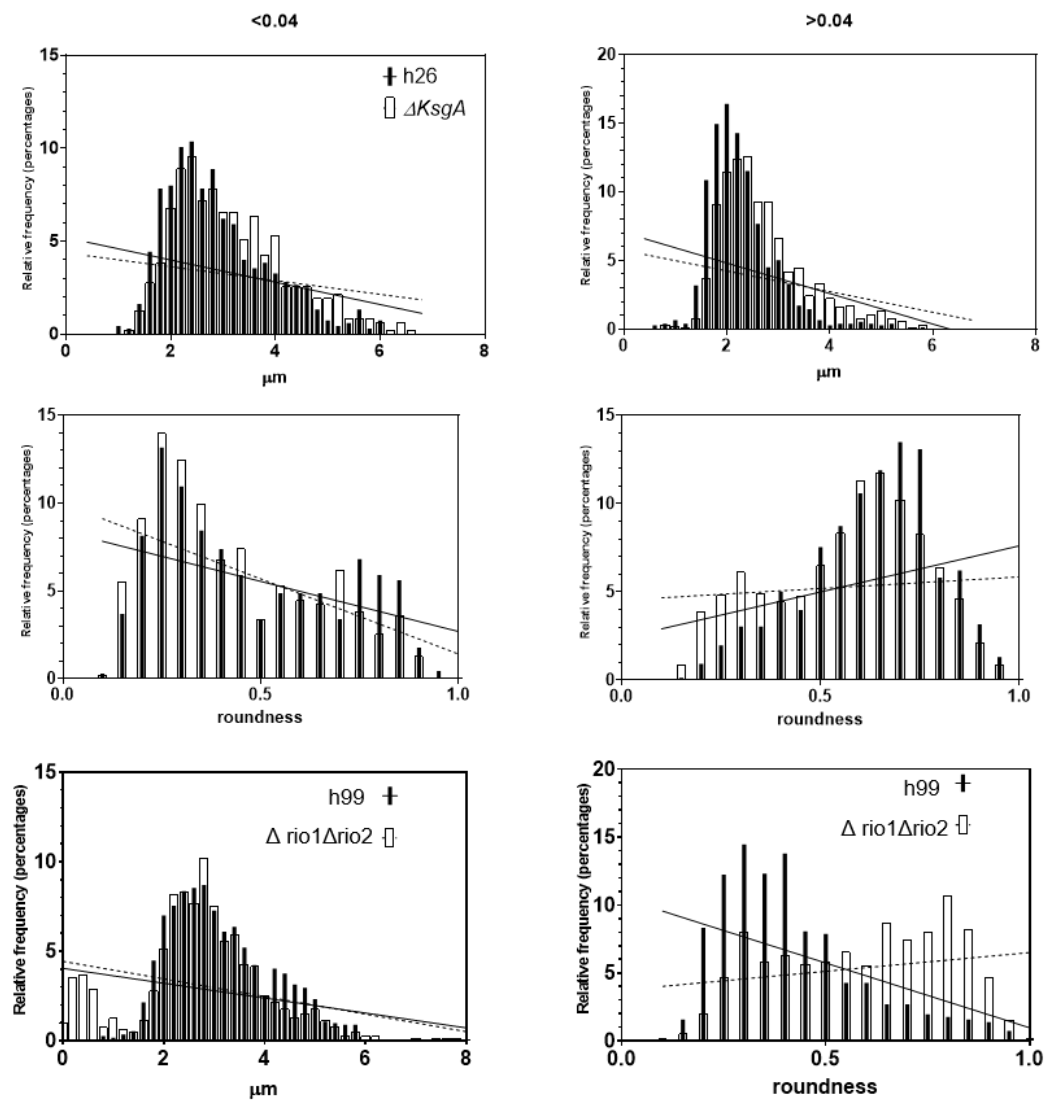


Figure S 12 **Relative frequency shows trend towards increased length and rod shape of $\Delta ksgA$.** Data from Figure 4.24 averaged for the relative frequency (percentage of total cell number) of each strain. Histogram with Binning size of $0.2 \mu\text{m}$ and 0.05 roundness is depicted. Wild type in black and knock out underlaid in white. Linear regression for wild type in black and dotted for knock out.

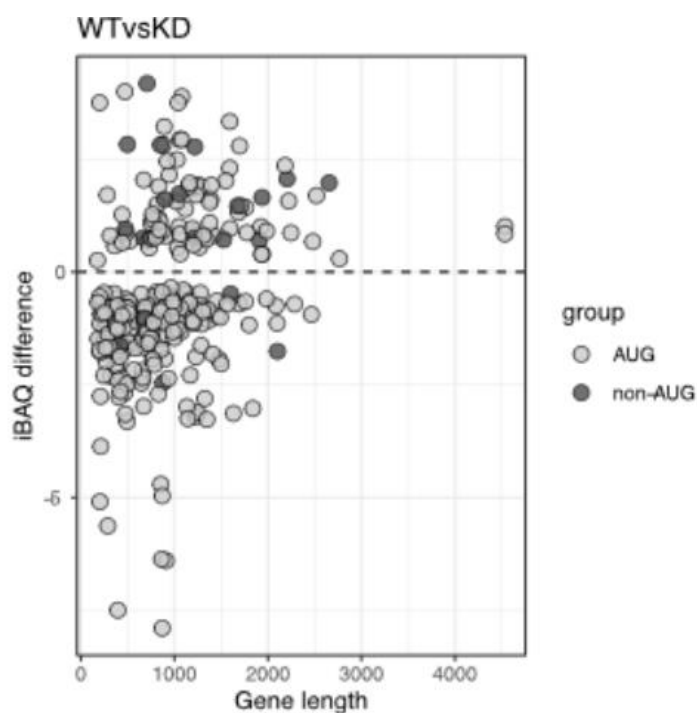


Figure S 13 **No length bias form regarding steady state expression levels in *ΔksgA***. Data from Figure 4.26A filtered for mRNA length and plotted against iBAQ differences. Data analysis by Felix Grünberger

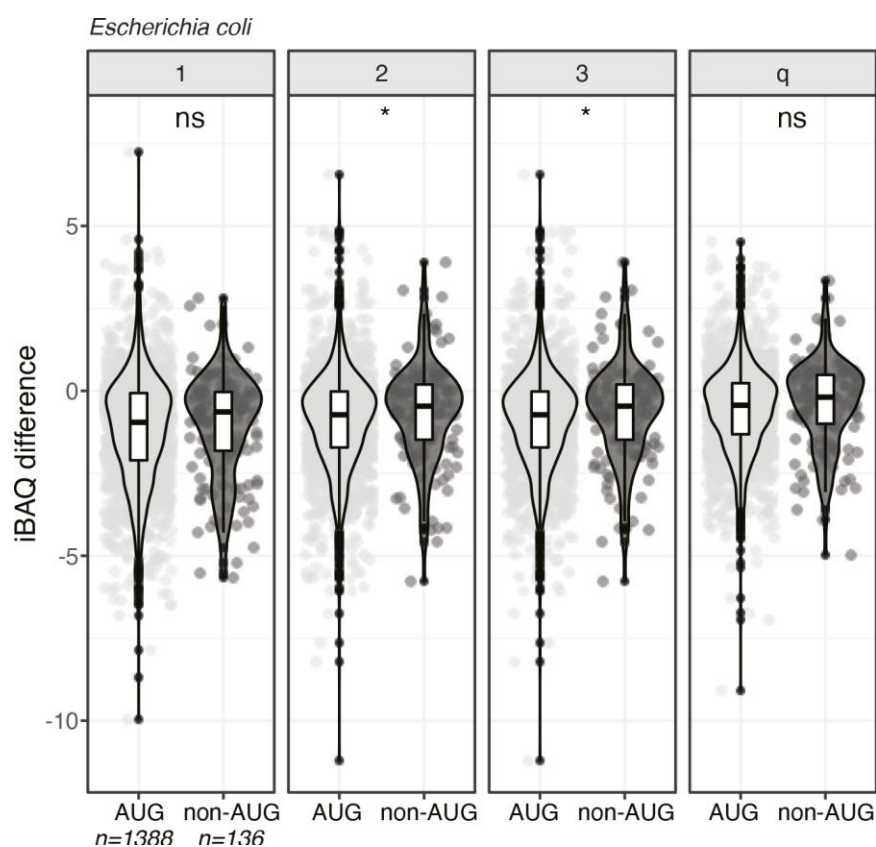


Figure S 14 **Non-AUG initiation is also associated to upregulated proteins**. Mass spectrometry by Öffinger Lab. Data Analysis by Felix Grünberg. Strains KEIO WT (BW25113) and *ΔksgA* (J50 and J49). High biological variance in between the knock out cells reduce statistical significance of the MaxQuant analysis. 1, 2, 3 and q are 4 differently composed MaxQuant Datasets, e.g. WT biological replicate 1 with J50 1 excluding J49 and other way around.

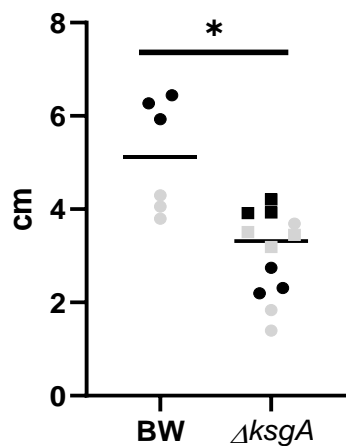


Figure S 15 Motility of Wild type (BW) and $\Delta ksgA$ (KEIO collection strain J50 rectangular and J49, round) in *E. coli*. Cells were grown over roughly 14h at 37°C on LB 0.3% Agar plates. Colors indicate technical replicate groups.

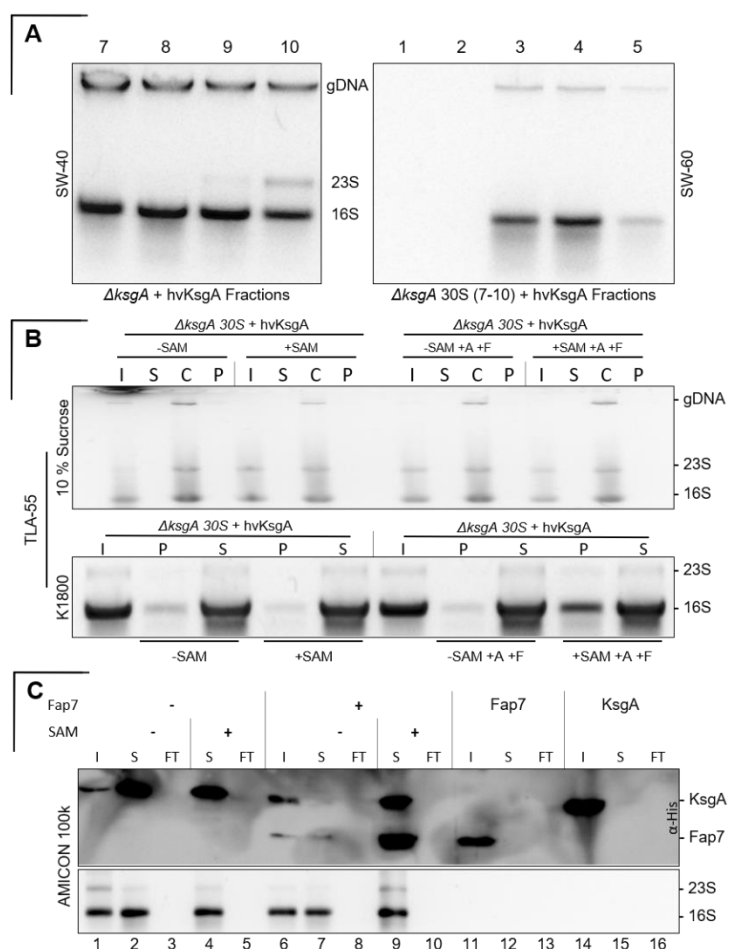


Figure S 16 Following the 30S through different types of centrifugation. **[A]** Sybr safe gels showing: SW-40 Fractions 7-10 containing the 30S subunits from a run of $\Delta ksgA$ cells + recombinant HvKsgA of a 5-30 % sucrose gradient. These were concentrated on an AMICON 10k filter unit (while also washing out sucrose) and then loaded onto a SW-60 rotor and separated via centrifugation. The resulting fractions 1-5 are shown in the left panel. **[B]** TLA-55 centrifugation as described in 7.2.3.10. Upper panel: Sybr Safe gel of pooled pre-bound $\Delta ksgA$ 30S subunit + HvKsgA complex with their respective added substrates after centrifugation through a 10 % Sucrose cushion in K1800 Buffer. Lower panel: Sybr Safe gel of pooled pre-bound $\Delta ksgA$ 30S subunit + HvKsgA complex with their respective added substrates after centrifugation

without sucrose. A: ATP/AMP (1 μ M), SAM (1 μ M), F: hvFap7 (1 μ M), I: Input, S, Supernatant, C: cushion, P: Pellet. [C] Western blot and Sybr Safe gel of pre-bound complex with respective additions centrifugation through AMICON 100k filter units. Pre-bound complexes were purified using the TFT-55.38 rotor and the reaction was setup as in **B**, the according Substrates were added and adjusted to a total volume of 500 μ l in K1800 buffer. The complexes were then centrifuged through the filter unit at 14,000 g at 4 $^{\circ}$ C while checking the units every 30s to estimate the remaining volume. At half volume the flow through was collected (250 μ l), the filter unit was filled once more with 250 μ l K1800 buffer and centrifuged further until only 250 μ l remained in the filter. The flow through was added to the already collected flow through, the filter was washed with an additional 250 μ l of K1800 buffer and the total volume of 500 μ l was considered as the supernatant and collected in a new cup. 50% was used for RNA extraction and the other 50% for Protein extraction. I: Input (5%), S: supernatant (70%), FT: Flow through (66 %). Lanes 11-16 are the recombinant proteins only with no substrate.

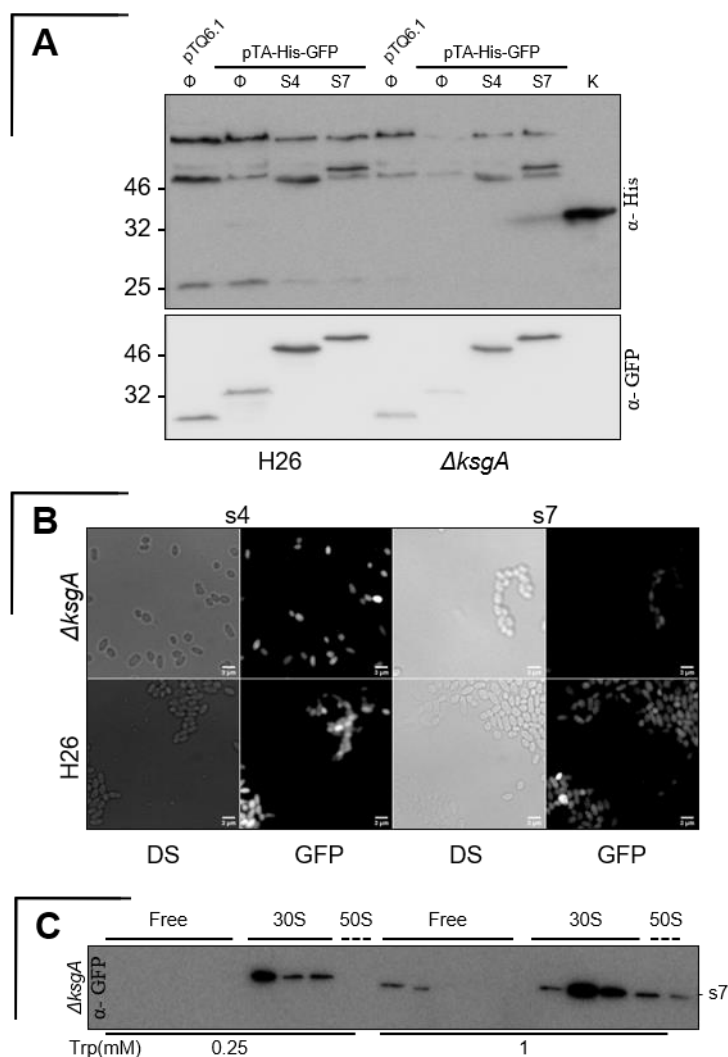


Figure S 17 **Verification of GFP tagged small ribosomal proteins.** [A] Western blot of His-GFP constructs: pTQ6.1 (GFP plasmid from Tessa Quaxx, Uni Freiburg), with both anti His and GFP antibody (same blot). Size difference of empty (Φ) results from different codons before reaching a STOP after GFP in the plasmid. K: recombinant HvKsgA (32 kDa) as control. [B] Light field (DS) and GFP signals at with 60x lens of the same constructs as in A, empty plasmids did not show any GFP signals (data not shown), possibly due to the prolonged readthrough (kDa difference of Φ in A). Scale bar 3 μ m. H26 s4 DS/GFP slightly misaligned at acquisition. [C] Sucrose gradients of $\Delta ksgA::pTna-His_{(6)}-GFP-s7$ at different molarities of Tryptophan.

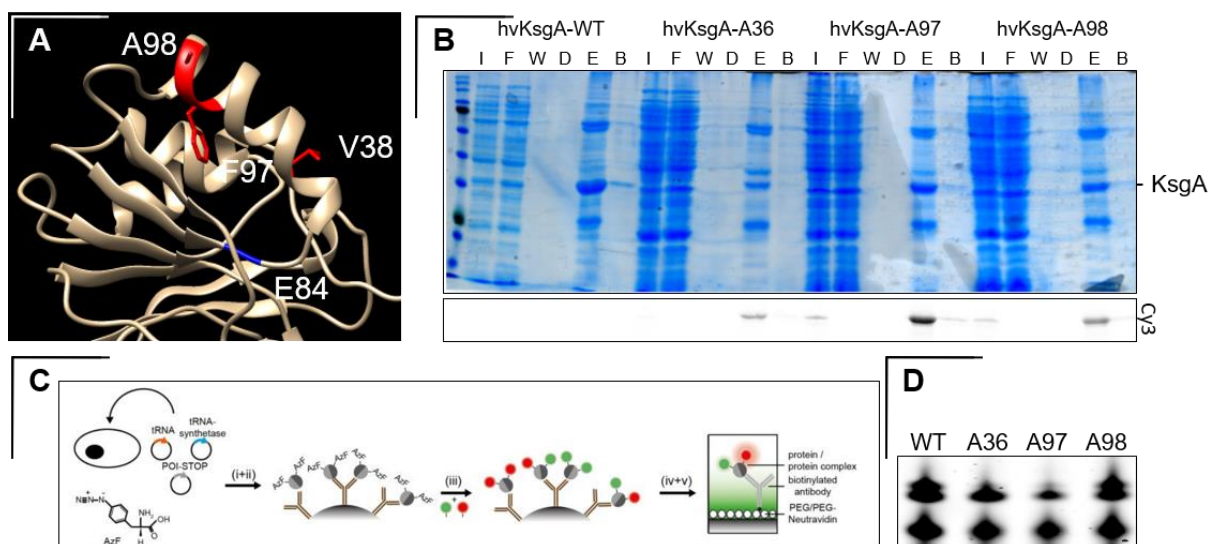


Figure S 18 **AzF** labelled recombinant **HvKsgA** **[A]** Cutout of Phyre2 Model of HvKsgA (mapped to 3GRV) with the AzF exchanged amino acid (red) and the active center (blue). Mutations were introduced via PCR with primers oHv466-oHv473 with the respective upstream and downstream primer oHv095 and 096. **[B]** Exemplary purification of 3 Amber (described in 7.2.3.1.2.1) and one wild type HvKsgA-His₆ construct with the appropriate Cy3 signal. I: Input, F: Flowthrough, W: Wash, D: Wash after Dylight, E: Elution, B: Beads. Cy3 signal in Input lanes are possibly inaccurate loading/spillover. **[C]** Scheme of Purification of labeled protein of interest (POI). In this purification only one Amber and dye were used per construct (modified from (Gust et al., 2018)) **[D]** Primer extension of *in vitro* reconstituted $\Delta ksgA$ whole cell lysate with Amber stop codon Dylight labelled HvKsgA.

11 REFERENCES

- Adler, J., Templeton, B., 1967. The Effect of Environmental Conditions on the Motility of *Escherichia coli*. *Journal of General Microbiology* 46, 175–184. <https://doi.org/10.1099/00221287-46-2-175>
- Albers, S.-V., Forterre, P., Prangishvili, D., Schleper, C., 2013. The legacy of Carl Woese and Wolfram Zillig: from phylogeny to landmark discoveries. *Nat Rev Microbiol* 11, 713–719. <https://doi.org/10.1038/nrmicro3124>
- Albers, S.-V., Jarrell, K.F., 2015. The archaeum: how archaea swim. *Front. Microbiol.* 6. <https://doi.org/10.3389/fmicb.2015.00023>
- Alberts, B. (Ed.), 2002. *Molecular biology of the cell*, 4th ed. ed. Garland Science, New York.
- Allers, T., Barak, S., Liddell, S., Wardell, K., Mevarech, M., 2010. Improved Strains and Plasmid Vectors for Conditional Overexpression of His-Tagged Proteins in *Haloferax volcanii*. *Appl Environ Microbiol* 76, 1759–1769. <https://doi.org/10.1128/AEM.02670-09>
- Allers, T., Ngo, H.-P., Mevarech, M., Lloyd, R.G., 2004. Development of Additional Selectable Markers for the Halophilic Archaeon *Haloferax volcanii* Based on the *leuB* and *trpA* Genes. *Appl. Environ. Microbiol.* 70, 943–953. <https://doi.org/10.1128/AEM.70.2.943-953.2004>
- Allmang, C., Tollervey, D., 1998. The role of the 3' external transcribed spacer in yeast pre-rRNA processing. *J. Mol. Biol.* 278, 67–78. <https://doi.org/10.1006/jmbi.1998.1693>
- Ameismeier, M., Cheng, J., Berninghausen, O., Beckmann, R., 2018. Visualizing late states of human 40S ribosomal subunit maturation. *Nature* 558, 249–253. <https://doi.org/10.1038/s41586-018-0193-0>
- Amsler, C.D., Cho, M., Matsumura, P., 1993. Multiple factors underlying the maximum motility of *Escherichia coli* as cultures enter post-exponential growth. *J. Bacteriol.* 175, 6238–6244. <https://doi.org/10.1128/jb.175.19.6238-6244.1993>
- Anantharaman, V., Aravind, L., 2002. The PRC-barrel: a widespread, conserved domain shared by photosynthetic reaction center subunits and proteins of RNA metabolism. *Genome Biol.* 3, RESEARCH0061. <https://doi.org/10.1186/gb-2002-3-11-research0061>
- Antal, M., Boros, E., Solymosy, F., Kiss, T., 2002. Analysis of the structure of human telomerase RNA in vivo. *Nucleic Acids Res.* 30, 912–920. <https://doi.org/10.1093/nar/30.4.912>
- Armache, J.-P., Anger, A.M., Márquez, V., Franckenberg, S., Fröhlich, T., Villa, E., Berninghausen, O., Thomm, M., Arnold, G.J., Beckmann, R., Wilson, D.N., 2013. Promiscuous behaviour of archaeal ribosomal proteins: Implications for eukaryotic ribosome evolution. *Nucleic Acids Research* 41, 1284–1293. <https://doi.org/10.1093/nar/gks1259>
- Asai, T., Condon, C., Voulgaris, J., Zaporojets, D., Shen, B., Al-Omar, M., Squires, C., Squires, C.L., 1999a. Construction and initial characterization of *Escherichia coli* strains with few or no intact chromosomal rRNA operons. *J. Bacteriol.* 181, 3803–3809.
- Asai, T., Zaporojets, D., Squires, C., Squires, C.L., 1999b. An *Escherichia coli* strain with all chromosomal rRNA operons inactivated: complete exchange of rRNA genes between bacteria. *Proc. Natl. Acad. Sci. U.S.A.* 96, 1971–1976.
- Ausiannikava, D., Allers, T., 2017. Diversity of DNA Replication in the Archaea. *Genes* 8, 56. <https://doi.org/10.3390/genes8020056>
- Baba, T., Ara, T., Hasegawa, M., Takai, Y., Okumura, Y., Baba, M., Datsenko, K.A., Tomita, M., Wanner, B.L., Mori, H., 2006. Construction of *Escherichia coli* K-12 in-frame, single-gene knockout mutants: the Keio collection. *Mol. Syst. Biol.* 2, 2006.0008. <https://doi.org/10.1038/msb4100050>
- Balter, M., 2004. PALEOANTHROPOLOGY: Skeptics Question Whether Flores Hominid Is a New Species. *Science* 306, 1116a–1116a. <https://doi.org/10.1126/science.306.5699.1116a>
- Ban, N., Beckmann, R., Cate, J.H., Dinman, J.D., Dragon, F., Ellis, S.R., Lafontaine, D.L., Lindahl, L., Liljas, A., Lipton, J.M., McAlear, M.A., Moore, P.B., Noller, H.F., Ortega, J., Panse, V.G., Ramakrishnan, V., Spahn, C.M., Steitz, T.A., Tchorzewski, M., Tollervey, D., Warren, A.J., Williamson, J.R., Wilson, D., Yonath, A., Yusupov, M., 2014. A new system for naming ribosomal proteins. *Current Opinion in Structural Biology* 24, 165–169. <https://doi.org/10.1016/j.sbi.2014.01.002>

- Barandun, J., Chaker-Margot, M., Hunziker, M., Molloy, K.R., Chait, B.T., Klinge, S., 2017. The complete structure of the small-subunit processome. *Nat. Struct. Mol. Biol.* 24, 944–953. <https://doi.org/10.1038/nsmb.3472>
- Barandun, J., Hunziker, M., Klinge, S., 2018. Assembly and structure of the SSU processome—a nucleolar precursor of the small ribosomal subunit. *Curr. Opin. Struct. Biol.* 49, 85–93. <https://doi.org/10.1016/j.sbi.2018.01.008>
- Basturea, G.N., Dague, D.R., Deutscher, M.P., Rudd, K.E., 2012. YhiQ is RsmJ, the methyltransferase responsible for methylation of G1516 in 16S rRNA of *E. coli*. *J. Mol. Biol.* 415, 16–21. <https://doi.org/10.1016/j.jmb.2011.10.044>
- Baumas, K., Soudet, J., Caizergues-Ferrer, M., Faublader, M., Henry, Y., Mouglin, A., 2012. Human RioK3 is a novel component of cytoplasmic pre-40S pre-ribosomal particles. *RNA Biol* 9, 162–174. <https://doi.org/10.4161/rna.18810>
- Beltrame, M., Henry, Y., Tollervey, D., 1994. Mutational analysis of an essential binding site for the U3 snoRNA in the 5' external transcribed spacer of yeast pre-rRNA. *Nucleic Acids Res.* 22, 4057–4065. <https://doi.org/10.1093/nar/22.20.4057>
- Beltrame, M., Tollervey, D., 1992. Identification and functional analysis of two U3 binding sites on yeast pre-ribosomal RNA. *EMBO J.* 11, 1531–1542.
- Benelli, D., La Teana, A., Londei, P., 2017. Translation Regulation: The Archaea-Eukaryal Connection, in: Clouet-d'Orval, B. (Ed.), *RNA Metabolism and Gene Expression in Archaea, Nucleic Acids and Molecular Biology*. Springer International Publishing, Cham, pp. 71–88. https://doi.org/10.1007/978-3-319-65795-0_3
- Benelli, D., La Teana, A., Londei, P., 2016. Evolution of Translational Initiation: From Archaea to Eukarya, in: Hernández, G., Jagus, R. (Eds.), *Evolution of the Protein Synthesis Machinery and Its Regulation*. Springer International Publishing, Cham, pp. 61–79. https://doi.org/10.1007/978-3-319-39468-8_4
- Benelli, D., Londei, P., 2011. Translation initiation in Archaea: conserved and domain-specific features. *Biochem Soc Trans* 39, 89–93. <https://doi.org/10.1042/BST0390089>
- Benelli, D., Londei, P., 2009. Begin at the beginning: evolution of translational initiation. *Research in Microbiology, Special issue on the origin of life and microbiology* 160, 493–501. <https://doi.org/10.1016/j.resmic.2009.06.003>
- Ben-Shem, A., Garreau de Loubresse, N., Melnikov, S., Jenner, L., Yusupova, G., Yusupov, M., 2011. The structure of the eukaryotic ribosome at 3.0 Å resolution. *Science* 334, 1524–1529. <https://doi.org/10.1126/science.1212642>
- Bernier, C.R., Petrov, A.S., Waterbury, C.C., Jett, J., Li, F., Freil, L.E., Xiong, X., Wang, L., Migliozzi, B.L.R., Hershkovits, E., Xue, Y., Hsiao, C., Bowman, J.C., Harvey, S.C., Grover, M.A., Wartell, Z.J., Williams, L.D., 2014. RiboVision suite for visualization and analysis of ribosomes. *Faraday Discuss.* 169, 195–207. <https://doi.org/10.1039/C3FD00126A>
- Boehm, A., Steiner, S., Zaehring, F., Casanova, A., Hamburger, F., Ritz, D., Keck, W., Ackermann, M., Schirmer, T., Jenal, U., 2009. Second messenger signalling governs *Escherichia coli* biofilm induction upon ribosomal stress. *Molecular Microbiology* 72, 1500–1516. <https://doi.org/10.1111/j.1365-2958.2009.06739.x>
- Boehringer, D., O'Farrell, H.C., Rife, J.P., Ban, N., 2012. Structural Insights into Methyltransferase KsgA Function in 30S Ribosomal Subunit Biogenesis. *J Biol Chem* 287, 10453–10459. <https://doi.org/10.1074/jbc.M111.318121>
- Bonawitz, N.D., Clayton, D.A., Shadel, G.S., 2006. Initiation and beyond: multiple functions of the human mitochondrial transcription machinery. *Mol. Cell* 24, 813–825. <https://doi.org/10.1016/j.molcel.2006.11.024>
- Boone, D.R., 2001. *Bergey's Manual® of Systematic Bacteriology*. Springer New York, New York, NY.
- Bowers, K.J., Wiegel, J., 2011. Temperature and pH optima of extremely halophilic archaea: a mini-review. *Extremophiles* 15, 119–128. <https://doi.org/10.1007/s00792-010-0347-y>
- Brand, R.C., Klootwijk, J., Van Steenberg, T.J., De Kok, A.J., Planta, R.J., 1977. Secondary methylation of yeast ribosomal precursor RNA. *Eur. J. Biochem.* 75, 311–318. <https://doi.org/10.1111/j.1432-1033.1977.tb11531.x>
- Braun, C.M., Hackert, P., Schmid, C.E., Bohnsack, M.T., Bohnsack, K.E., Perez-Fernandez, J., 2020. Pol5 is required for recycling of small subunit biogenesis factors and for formation of the

- peptide exit tunnel of the large ribosomal subunit. *Nucleic Acids Res.* 48, 405–420. <https://doi.org/10.1093/nar/gkz1079>
- Breithaupt, H., 2001. The hunt for living gold: The search for organisms in extreme environments yields useful enzymes for industry. *EMBO Rep* 2, 968–971. <https://doi.org/10.1093/embo-reports/kve238>
- Breuert, S., Allers, T., Spohn, G., Soppa, J., 2006. Regulated Polyploidy in Halophilic Archaea. *PLoS ONE* 1, e92. <https://doi.org/10.1371/journal.pone.0000092>
- Britton, R.A., 2009. Role of GTPases in bacterial ribosome assembly. *Annu. Rev. Microbiol.* 63, 155–176. <https://doi.org/10.1146/annurev.micro.091208.073225>
- Britton, R.A., Wen, T., Schaefer, L., Pellegrini, O., Uicker, W.C., Mathy, N., Tobin, C., Daou, R., Szyk, J., Condon, C., 2007. Maturation of the 5' end of *Bacillus subtilis* 16S rRNA by the essential ribonuclease YkqC/RNase J1. *Mol Microbiol* 63, 127–138. <https://doi.org/10.1111/j.1365-2958.2006.05499.x>
- Brock, T.D., Brock, K.M., Belly, R.T., Weiss, R.L., 1972. *Sulfolobus*: A new genus of sulfur-oxidizing bacteria living at low pH and high temperature. *Archiv. Mikrobiol.* 84, 54–68. <https://doi.org/10.1007/BF00408082>
- Bubunenko, M., Court, D.L., Al Refaii, A., Saxena, S., Korepanov, A., Friedman, D.I., Gottesman, M.E., Alix, J.-H., 2013. Nus transcription elongation factors and RNase III modulate small ribosome subunit biogenesis in *Escherichia coli*: *E. coli* Nus factors and ribosome genesis. *Molecular Microbiology* 87, 382–393. <https://doi.org/10.1111/mmi.12105>
- Bubunenko, M., Korepanov, A., Court, D.L., Jagannathan, I., Dickinson, D., Chaudhuri, B.R., Garber, M.B., Culver, G.M., 2006. 30S ribosomal subunits can be assembled in vivo without primary binding ribosomal protein S15. *RNA* 12, 1229–1239. <https://doi.org/10.1261/rna.2262106>
- Burger, K., Mühl, B., Kellner, M., Rohmoser, M., Gruber-Eber, A., Windhager, L., Friedel, C.C., Dölken, L., Eick, D., 2013. 4-thiouridine inhibits rRNA synthesis and causes a nucleolar stress response. *RNA Biology* 10, 1623–1630. <https://doi.org/10.4161/rna.26214>
- Buul, C.P.J.J.V., Damm, J.B.L., Knippenberg, P.H.V., 1983. Kasugamycin resistant mutants of *Bacillus stearothermophilus* lacking the enzyme for the methylation of two adjacent adenosines in 16S ribosomal RNA. *Molec. Gen. Genet.* 189, 475–478. <https://doi.org/10.1007/BF00325912>
- Bylund, G.O., Lövgren, J.M., Wikström, P.M., 2001. Characterization of Mutations in the *metY-nusA-infB* Operon That Suppress the Slow Growth of a Δ rimM Mutant. *J. Bacteriol.* 183, 6095–6106. <https://doi.org/10.1128/JB.183.20.6095-6106.2001>
- Bylund, G.O., Wipemo, L.C., Lundberg, L.A.C., Wikström, P.M., 1998. RimM and RbfA Are Essential for Efficient Processing of 16S rRNA in *Escherichia coli*. *Journal of Bacteriology* 180, 73–82.
- Byrgazov, K., Grishkovskaya, I., Arenz, S., Coudeville, N., Temmel, H., Wilson, D.N., Djinovic-Carugo, K., Moll, I., 2015. Structural basis for the interaction of protein S1 with the *Escherichia coli* ribosome. *Nucleic Acids Res.* 43, 661–673. <https://doi.org/10.1093/nar/gku1314>
- Cannone, J.J., Subramanian, S., Schnare, M.N., Collett, J.R., D'Souza, L.M., Du, Y., Feng, B., Lin, N., Madabusi, L.V., Müller, K.M., Pande, N., Shang, Z., Yu, N., Gutell, R.R., 2002. The comparative RNA web (CRW) site: an online database of comparative sequence and structure information for ribosomal, intron, and other RNAs. *BMC Bioinformatics* 3, 2. <https://doi.org/10.1186/1471-2105-3-2>
- Carlson, M., 1987. Regulation of sugar utilization in *Saccharomyces* species. *Journal of Bacteriology* 169, 4873–4877. <https://doi.org/10.1128/JB.169.11.4873-4877.1987>
- Castellana, N.E., Payne, S.H., Shen, Z., Stanke, M., Bafna, V., Briggs, S.P., 2008. Discovery and revision of *Arabidopsis* genes by proteogenomics. *Proceedings of the National Academy of Sciences* 105, 21034–21038. <https://doi.org/10.1073/pnas.0811066106>
- Čavuzić, M., Liu, Y., 2017. Biosynthesis of Sulfur-Containing tRNA Modifications: A Comparison of Bacterial, Archaeal, and Eukaryotic Pathways. *Biomolecules* 7. <https://doi.org/10.3390/biom7010027>
- Chaker-Margot, M., Barandun, J., Hunziker, M., Klinge, S., 2017. Architecture of the yeast small subunit processome. *Science* 355. <https://doi.org/10.1126/science.aal1880>

- Chaker-Margot, M., Klinge, S., 2019. Assembly and early maturation of large subunit precursors. *RNA* 25, 465–471. <https://doi.org/10.1261/rna.069799.118>
- Champney, W.S., Chittum, H.S., Tober, C.L., 2003. A 50S Ribosomal Subunit Precursor Particle Is a Substrate for the ErmC Methyltransferase in *Staphylococcus aureus* Cells. *Current Microbiology* 46, 453–460. <https://doi.org/10.1007/s00284-002-3901-8>
- Chen, L., Brügger, K., Skovgaard, M., Redder, P., She, Q., Torarinsson, E., Greve, B., Awayez, M., Zibat, A., Klenk, H.-P., Garrett, R.A., 2005. The Genome of *Sulfolobus acidocaldarius*, a Model Organism of the Crenarchaeota. *J Bacteriol* 187, 4992–4999. <https://doi.org/10.1128/JB.187.14.4992-4999.2005>
- Chen, W., Xie, Z., Yang, F., Ye, K., 2017. Stepwise assembly of the earliest precursors of large ribosomal subunits in yeast. *Nucleic Acids Res.* 45, 6837–6847. <https://doi.org/10.1093/nar/gkx254>
- Chen, X., Court, D.L., Ji, X., 1999. Crystal structure of ERA: A GTPase-dependent cell cycle regulator containing an RNA binding motif. *Proceedings of the National Academy of Sciences* 96, 8396–8401. <https://doi.org/10.1073/pnas.96.15.8396>
- Cheng, J., Kellner, N., Berninghausen, O., Hurt, E., Beckmann, R., 2017. 3.2-Å-resolution structure of the 90S preribosome before A1 pre-rRNA cleavage. *Nat. Struct. Mol. Biol.* 24, 954–964. <https://doi.org/10.1038/nsmb.3476>
- Cheng, X., 1995. Structure and Function of DNA Methyltransferases. *Annu. Rev. Biophys. Biomol. Struct.* 24, 293–318. <https://doi.org/10.1146/annurev.bb.24.060195.001453>
- Chien, A., Edgar, D.B., Trela, J.M., 1976. Deoxyribonucleic acid polymerase from the extreme thermophile *Thermus aquaticus*. *J. Bacteriol.* 127, 1550–1557.
- Chimileski, S., Franklin, M.J., Papke, R.T., 2014. Biofilms formed by the archaeon *Haloferax volcanii* exhibit cellular differentiation and social motility, and facilitate horizontal gene transfer. *BMC Biol.* 12, 65. <https://doi.org/10.1186/s12915-014-0065-5>
- Chow, C.S., Lamichhane, T.N., Mahto, S.K., 2007. Expanding the nucleotide repertoire of the ribosome with post-transcriptional modifications. *ACS Chem. Biol.* 2, 610–619. <https://doi.org/10.1021/cb7001494>
- Clatterbuck Soper, S.F., Dator, R.P., Limbach, P.A., Woodson, S.A., 2013. In vivo X-ray footprinting of pre-30S ribosomes reveals chaperone-dependent remodeling of late assembly intermediates. *Mol. Cell* 52, 506–516. <https://doi.org/10.1016/j.molcel.2013.09.020>
- Cline, S.W., Schalkwyk, L.C., Doolittle, W.F., 1989. Transformation of the archaeobacterium *Halobacterium volcanii* with genomic DNA. *J. Bacteriol.* 171, 4987–4991. <https://doi.org/10.1128/jb.171.9.4987-4991.1989>
- Clouet-d'Orval, B., Batista, M., Bouvier, M., Quentin, Y., Fichant, G., Marchfelder, A., Maier, L.-K., 2018. Insights into RNA-processing pathways and associated RNA-degrading enzymes in Archaea. *FEMS Microbiology Reviews* 42, 579–613. <https://doi.org/10.1093/femsre/fuy016>
- Collins, J.C., Ghalei, H., Doherty, J.R., Huang, H., Culver, R.N., Karbstein, K., 2018. Ribosome biogenesis factor Ltv1 chaperones the assembly of the small subunit head. *J. Cell Biol.* 217, 4141–4154. <https://doi.org/10.1083/jcb.201804163>
- Connolly, K., Culver, G., 2013. Overexpression of RbfA in the absence of the KsgA checkpoint results in impaired translation initiation. *Mol Microbiol* 87, 968–981. <https://doi.org/10.1111/mmi.12145>
- Connolly, K., Rife, J.P., Culver, G., 2008. Mechanistic insight into the ribosome biogenesis functions of the ancient protein KsgA. *Mol Microbiol* 70, 1062–1075. <https://doi.org/10.1111/j.1365-2958.2008.06485.x>
- Cotney, J., McKay, S.E., Shadel, G.S., 2009. Elucidation of separate, but collaborative functions of the rRNA methyltransferase-related human mitochondrial transcription factors B1 and B2 in mitochondrial biogenesis reveals new insight into maternally inherited deafness. *Hum. Mol. Genet.* 18, 2670–2682. <https://doi.org/10.1093/hmg/ddp208>
- Cotney, J., Wang, Z., Shadel, G.S., 2007. Relative abundance of the human mitochondrial transcription system and distinct roles for h-mtTFB1 and h-mtTFB2 in mitochondrial biogenesis and gene expression. *Nucleic Acids Res.* 35, 4042–4054. <https://doi.org/10.1093/nar/gkm424>

- Cox, J., Hein, M.Y., Lubner, C.A., Paron, I., Nagaraj, N., Mann, M., 2014. Accurate proteome-wide label-free quantification by delayed normalization and maximal peptide ratio extraction, termed MaxLFQ. *Mol. Cell Proteomics* 13, 2513–2526. <https://doi.org/10.1074/mcp.M113.031591>
- Cruz, J.A., Westhof, E., 2009. The Dynamic Landscapes of RNA Architecture. *Cell* 136, 604–609. <https://doi.org/10.1016/j.cell.2009.02.003>
- Cunningham, P.R., Weitzmann, C.J., Nurse, K., Masurel, R., Van Knippenberg, P.H., Ofengand, J., 1990. Site-specific mutation of the conserved m62 A m62 A residues of E. coli 16S ribosomal RNA. Effects on ribosome function and activity of the ksgA methyltransferase. *Biochimica et Biophysica Acta (BBA) - Gene Structure and Expression* 1050, 18–26. [https://doi.org/10.1016/0167-4781\(90\)90135-O](https://doi.org/10.1016/0167-4781(90)90135-O)
- Da Cunha, V., Gaia, M., Nasir, A., Forterre, P., 2018. Asgard archaea do not close the debate about the universal tree of life topology. *PLoS Genet* 14, e1007215. <https://doi.org/10.1371/journal.pgen.1007215>
- Dammel, C.S., Noller, H.F., 1995. Suppression of a cold-sensitive mutation in 16S rRNA by overexpression of a novel ribosome-binding factor, RbfA. *Genes Dev.* 9, 626–637. <https://doi.org/10.1101/gad.9.5.626>
- Danan, M., Schwartz, S., Edelheit, S., Sorek, R., 2012. Transcriptome-wide discovery of circular RNAs in Archaea. *Nucleic Acids Research* 40, 3131–3142. <https://doi.org/10.1093/nar/gkr1009>
- Darzacq, X., Jády, B.E., Verheggen, C., Kiss, A.M., Bertrand, E., Kiss, T., 2002. Cajal body-specific small nuclear RNAs: a novel class of 2'-O-methylation and pseudouridylation guide RNAs. *EMBO J.* 21, 2746–2756. <https://doi.org/10.1093/emboj/21.11.2746>
- DasSarma, S., 2006. Extreme halophiles are models for astrobiology. *MICROBE-AMERICAN SOCIETY FOR MICROBIOLOGY* 1, 120.
- Datta, P.P., Wilson, D.N., Kawazoe, M., Swami, N.K., Kaminishi, T., Sharma, M.R., Booth, T.M., Takemoto, C., Fucini, P., Yokoyama, S., Agrawal, R.K., 2007. Structural aspects of RbfA action during small ribosomal subunit assembly. *Mol. Cell* 28, 434–445. <https://doi.org/10.1016/j.molcel.2007.08.026>
- Davis, J.H., Tan, Y.Z., Carragher, B., Potter, C.S., Lyumkis, D., Williamson, J.R., 2016. Modular Assembly of the Bacterial Large Ribosomal Subunit. *Cell* 167, 1610–1622.e15. <https://doi.org/10.1016/j.cell.2016.11.020>
- Davis, J.H., Williamson, J.R., 2017. Structure and dynamics of bacterial ribosome biogenesis. *Phil. Trans. R. Soc. B* 372, 20160181. <https://doi.org/10.1098/rstb.2016.0181>
- de la Cruz, J., Lacombe, T., Deloche, O., Linder, P., Kressler, D., 2004. The putative RNA helicase Dbp6p functionally interacts with Rpl3p, Nop8p and the novel trans-acting Factor Rsa3p during biogenesis of 60S ribosomal subunits in *Saccharomyces cerevisiae*. *Genetics* 166, 1687–1699. <https://doi.org/10.1534/genetics.166.4.1687>
- de Silva, R.T., Abdul-Halim, M.F., Pittrich, D.A., Brown, H.J., Pohlschroder, M., Duggin, I.G., 2020. Improved growth and morphological plasticity of *Haloferax volcanii* (preprint). *Microbiology*. <https://doi.org/10.1101/2020.05.04.078048>
- Decatur, W.A., Fournier, M.J., 2002. rRNA modifications and ribosome function. *Trends Biochem. Sci.* 27, 344–351.
- DeLong, E.F., Pace, N.R., 2001. Environmental Diversity of Bacteria and Archaea. *Systematic Biology* 50, 470–478. <https://doi.org/10.1080/106351501750435040>
- Demirci, H., Murphy, F., Belardinelli, R., Kelley, A.C., Ramakrishnan, V., Gregory, S.T., Dahlberg, A.E., Jögl, G., 2010. Modification of 16S ribosomal RNA by the KsgA methyltransferase restructures the 30S subunit to optimize ribosome function. *RNA* 16, 2319–2324. <https://doi.org/10.1261/rna.2357210>
- Dennis, P.P., Tripp, V., Lui, L., Lowe, T., Randau, L., 2015. C/D box sRNA-guided 2'-O-methylation patterns of archaeal rRNA molecules. *BMC Genomics* 16, 632. <https://doi.org/10.1186/s12864-015-1839-z>
- Denoya, C., Dubnau, D., 1989. Mono- and dimethylating activities and kinetic studies of the ermC 23 S rRNA methyltransferase. *J. Biol. Chem.* 264, 2615–2624.

- Desai, P.M., Culver, G.M., Rife, J.P., 2011. Site-Directed Mutants of 16S rRNA Reveal Important RNA Domains for KsgA Function and 30S Subunit Assembly. *Biochemistry* 50, 854–863. <https://doi.org/10.1021/bi101005r>
- Desai, P.M., Rife, J.P., 2006. The adenosine dimethyltransferase KsgA recognizes a specific conformational state of the 30S ribosomal subunit. *Arch. Biochem. Biophys.* 449, 57–63. <https://doi.org/10.1016/j.abb.2006.02.028>
- Dolken, L., Ruzsics, Z., Radle, B., Friedel, C.C., Zimmer, R., Mages, J., Hoffmann, R., Dickinson, P., Forster, T., Ghazal, P., Koszinowski, U.H., 2008. High-resolution gene expression profiling for simultaneous kinetic parameter analysis of RNA synthesis and decay. *RNA* 14, 1959–1972. <https://doi.org/10.1261/rna.1136108>
- Dombrowski, N., Lee, J.-H., Williams, T.A., Offre, P., Spang, A., 2019. Genomic diversity, lifestyles and evolutionary origins of DPANN archaea. *FEMS Microbiol. Lett.* 366. <https://doi.org/10.1093/femsle/fnz008>
- Donlan, R.M., 2002. Biofilms: microbial life on surfaces. *Emerging Infect. Dis.* 8, 881–890. <https://doi.org/10.3201/eid0809.020063>
- Donlan, R.M., 2001. Biofilm Formation: A Clinically Relevant Microbiological Process. *CLIN INFECT DIS* 33, 1387–1392. <https://doi.org/10.1086/322972>
- Dragon, F., Gallagher, J.E.G., Compagnone-Post, P.A., Mitchell, B.M., Porwancher, K.A., Wehner, K.A., Wormsley, S., Settlege, R.E., Shabanowitz, J., Osheim, Y., Beyer, A.L., Hunt, D.F., Baserga, S.J., 2002. A large nucleolar U3 ribonucleoprotein required for 18S ribosomal RNA biogenesis. *Nature* 417, 967–970. <https://doi.org/10.1038/nature00769>
- Ducret, A., Quardokus, E.M., Brun, Y.V., 2016. MicrobeJ, a tool for high throughput bacterial cell detection and quantitative analysis. *Nat Microbiol* 1, 16077. <https://doi.org/10.1038/nmicrobiol.2016.77>
- Duffy, E.E., Rutenberg-Schoenberg, M., Stark, C.D., Kitchen, R.R., Gerstein, M.B., Simon, M.D., 2015. Tracking Distinct RNA Populations Using Efficient and Reversible Covalent Chemistry. *Mol. Cell* 59, 858–866. <https://doi.org/10.1016/j.molcel.2015.07.023>
- Duffy, E.E., Schofield, J.A., Simon, M.D., 2019. Gaining insight into transcriptome-wide RNA population dynamics through the chemistry of 4-thiouridine. *WIREs RNA* 10, e1513. <https://doi.org/10.1002/wrna.1513>
- Duggin, I.G., Aylett, C.H.S., Walsh, J.C., Michie, K.A., Wang, Q., Turnbull, L., Dawson, E.M., Harry, E.J., Whitchurch, C.B., Amos, L.A., Löwe, J., 2015. CetZ tubulin-like proteins control archaeal cell shape. *Nature* 519, 362–365. <https://doi.org/10.1038/nature13983>
- Durovic, P., Dennis, P.P., 1994. Separate pathways for excision and processing of 16S and 23S rRNA from the primary rRNA operon transcript from the hyperthermophilic archaeobacterium *Sulfolobus acidocaldarius*: similarities to eukaryotic rRNA processing. *Molecular Microbiology* 13, 229–242. <https://doi.org/10.1111/j.1365-2958.1994.tb00418.x>
- Duss, O., Stepanyuk, G.A., Puglisi, J.D., Williamson, J.R., 2019. Transient Protein-RNA Interactions Guide Nascent Ribosomal RNA Folding. *Cell* 179, 1357–1369.e16. <https://doi.org/10.1016/j.cell.2019.10.035>
- Dutca, L.M., Gallagher, J.E.G., Baserga, S.J., 2011. The initial U3 snoRNA:pre-rRNA base pairing interaction required for pre-18S rRNA folding revealed by in vivo chemical probing. *Nucleic Acids Research* 39, 5164–5180. <https://doi.org/10.1093/nar/gkr044>
- Ebenezer, T.E., Zoltner, M., Burrell, A., Nenarokova, A., Novák Vanclová, A.M.G., Prasad, B., Soukal, P., Santana-Molina, C., O'Neill, E., Nankissoor, N.N., Vadakedath, N., Daiker, V., Obado, S., Silva-Pereira, S., Jackson, A.P., Devos, D.P., Lukeš, J., Lebert, M., Vaughan, S., Hampl, V., Carrington, M., Ginger, M.L., Dacks, J.B., Kelly, S., Field, M.C., 2019. Transcriptome, proteome and draft genome of *Euglena gracilis*. *BMC Biol* 17, 11. <https://doi.org/10.1186/s12915-019-0626-8>
- Ebersberger, I., Simm, S., Leisegang, M.S., Schmitzberger, P., Mirus, O., Haeseler, A. von, Bohnsack, M.T., Schleiff, E., 2014. The evolution of the ribosome biogenesis pathway from a yeast perspective. *Nucl. Acids Res.* 42, 1509–1523. <https://doi.org/10.1093/nar/gkt1137>
- Elazari-Volcani, B., 1943. Bacteria in the Bottom Sediments of the Dead Sea. *Nature* 152, 274–275. <https://doi.org/10.1038/152274c0>
- Elkins, J.G., Podar, M., Graham, D.E., Makarova, K.S., Wolf, Y., Randau, L., Hedlund, B.P., Brochier-Armanet, C., Kunin, V., Anderson, I., Lapidus, A., Goltsman, E., Barry, K.,

- Koonin, E.V., Hugenholtz, P., Kyrpides, N., Wanner, G., Richardson, P., Keller, M., Stetter, K.O., 2008. A korarchaeal genome reveals insights into the evolution of the Archaea. *Proc. Natl. Acad. Sci. U.S.A.* 105, 8102–8107. <https://doi.org/10.1073/pnas.0801980105>
- Esquivel, R.N., Schulze, S., Xu, R., Hippler, M., Pohlschroder, M., 2016. Identification of Haloferax volcanii Pilin N-Glycans with Diverse Roles in Pilus Biosynthesis, Adhesion, and Microcolony Formation. *J Biol Chem* 291, 10602–10614. <https://doi.org/10.1074/jbc.M115.693556>
- Esser, D., Siebers, B., 2013. Atypical protein kinases of the RIO family in archaea. *Biochemical Society Transactions* 41, 399–404. <https://doi.org/10.1042/BST20120317>
- Fan, Y., Evans, C.R., Ling, J., 2016. Reduced Protein Synthesis Fidelity Inhibits Flagellar Biosynthesis and Motility. *Sci Rep* 6, 30960. <https://doi.org/10.1038/srep30960>
- Fan, Y., Thompson, L., Lyu, Z., Cameron, T.A., De Lay, N.R., Krachler, A.M., Ling, J., 2019. Optimal translational fidelity is critical for Salmonella virulence and host interactions. *Nucleic Acids Res.* 47, 5356–5367. <https://doi.org/10.1093/nar/gkz229>
- Fatica, A., Oeffinger, M., Dlakic, M., Tollervey, D., 2003. Nob1p Is Required for Cleavage of the 3' End of 18S rRNA. *Molecular and Cellular Biology* 23, 1798–1807. <https://doi.org/10.1128/mcb.23.5.1798-1807.2003>
- Favre, A., Bezerra, R., Hajnsdorf, E., Lemaigre Dubreuil, Y., Expert-Bezançon, A., 1986. Substitution of uridine in vivo by the intrinsic photoactivable probe 4-thiouridine in Escherichia coli RNA. Its use for E. coli ribosome structural analysis. *Eur. J. Biochem.* 160, 441–449. <https://doi.org/10.1111/j.1432-1033.1986.tb10060.x>
- Ferreira-Cerca, S., 2017. Life and Death of Ribosomes in Archaea, in: Clouet-d'Orval, B. (Ed.), *RNA Metabolism and Gene Expression in Archaea*, *Nucleic Acids and Molecular Biology*. Springer International Publishing, Cham, pp. 129–158. https://doi.org/10.1007/978-3-319-65795-0_6
- Ferreira-Cerca, S., Kiburu, I., Thomson, E., LaRonde, N., Hurt, E., 2014. Dominant Rio1 kinase/ATPase catalytic mutant induces trapping of late pre-40S biogenesis factors in 80S-like ribosomes. *Nucleic Acids Res.* 42, 8635–8647. <https://doi.org/10.1093/nar/gku542>
- Ferreira-Cerca, S., Pöll, G., Gleizes, P.-E., Tschochner, H., Milkereit, P., 2005. Roles of eukaryotic ribosomal proteins in maturation and transport of pre-18S rRNA and ribosome function. *Mol. Cell* 20, 263–275. <https://doi.org/10.1016/j.molcel.2005.09.005>
- Ferreira-Cerca, S., Pöll, G., Kühn, H., Neueder, A., Jakob, S., Tschochner, H., Milkereit, P., 2007. Analysis of the in vivo assembly pathway of eukaryotic 40S ribosomal proteins. *Mol. Cell* 28, 446–457. <https://doi.org/10.1016/j.molcel.2007.09.029>
- Ferreira-Cerca, S., Sagar, V., Schäfer, T., Diop, M., Wesseling, A.-M., Lu, H., Chai, E., Hurt, E., LaRonde-LeBlanc, N., 2012. ATPase-dependent role of the atypical kinase Rio2 on the evolving pre-40S ribosomal subunit. *Nat. Struct. Mol. Biol.* 19, 1316–1323. <https://doi.org/10.1038/nsmb.2403>
- Fiala, G., Stetter, K.O., 1986. *Pyrococcus furiosus* sp. nov. represents a novel genus of marine heterotrophic archaeobacteria growing optimally at 100°C. *Arch. Microbiol.* 145, 56–61. <https://doi.org/10.1007/BF00413027>
- Formenoy, L.J., Cunningham, P.R., Nurse, K., Pleij, C.W., Ofengand, J., 1994. Methylation of the conserved A1518-A1519 in Escherichia coli 16S ribosomal RNA by the ksgA methyltransferase is influenced by methylations around the similarly conserved U1512.G1523 base pair in the 3' terminal hairpin. *Biochimie* 76, 1123–1128.
- Fowlie, A., Bardsley, M.H., 2016. Superplot: a graphical interface for plotting and analysing MultiNest output. *Eur. Phys. J. Plus* 131, 391. <https://doi.org/10.1140/epjp/i2016-16391-0>
- Fox, G.E., 2010. Origin and evolution of the ribosome. *Cold Spring Harb Perspect Biol* 2, a003483. <https://doi.org/10.1101/cshperspect.a003483>
- Fox, G.E., Magrum, L.J., Balch, W.E., Wolfe, R.S., Woese, C.R., 1977. Classification of methanogenic bacteria by 16S ribosomal RNA characterization. *Proceedings of the National Academy of Sciences of the United States of America* 74, 4537.
- Frank, D.N., Pace, N.R., 1998. RIBONUCLEASE P: Unity and Diversity in a tRNA Processing Ribozyme. *Annu. Rev. Biochem.* 67, 153–180. <https://doi.org/10.1146/annurev.biochem.67.1.153>

- Fristedt, R., Scharff, L.B., Clarke, C.A., Wang, Q., Lin, C., Merchant, S.S., Bock, R., 2014. RBF1, a Plant Homolog of the Bacterial Ribosome-Binding Factor RbfA, Acts in Processing of the Chloroplast 16S Ribosomal RNA. *PLANT PHYSIOLOGY* 164, 201–215. <https://doi.org/10.1104/pp.113.228338>
- Fujii, K., Susanto, T.T., Saurabh, S., Barna, M., 2018. Decoding the Function of Expansion Segments in Ribosomes. *Molecular Cell* 72, 1013–1020.e6. <https://doi.org/10.1016/j.molcel.2018.11.023>
- Fuller-Pace, F.V., Nicol, S.M., Reid, A.D., Lane, D.P., 1993. DbpA: a DEAD box protein specifically activated by 23s rRNA. *EMBO J.* 12, 3619–3626.
- Gallagher, J.E.G., Dunbar, D.A., Granneman, S., Mitchell, B.M., Osheim, Y., Beyer, A.L., Baserga, S.J., 2004. RNA polymerase I transcription and pre-rRNA processing are linked by specific SSU processome components. *Genes Dev.* 18, 2506–2517. <https://doi.org/10.1101/gad.1226604>
- Ganser, L.R., Kelly, M.L., Herschlag, D., Al-Hashimi, H.M., 2019. The roles of structural dynamics in the cellular functions of RNAs. *Nat Rev Mol Cell Biol* 20, 474–489. <https://doi.org/10.1038/s41580-019-0136-0>
- García-Gómez, J.J., Fernández-Pevida, A., Lebaron, S., Rosado, I.V., Tollervey, D., Kressler, D., de la Cruz, J., 2014. Final pre-40S maturation depends on the functional integrity of the 60S subunit ribosomal protein L3. *PLoS Genet.* 10, e1004205. <https://doi.org/10.1371/journal.pgen.1004205>
- Gartmann, M., Blau, M., Armache, J.-P., Mielke, T., Topf, M., Beckmann, R., 2010. Mechanism of eIF6-mediated Inhibition of Ribosomal Subunit Joining. *J. Biol. Chem.* 285, 14848–14851. <https://doi.org/10.1074/jbc.C109.096057>
- Gaspin, C., Cavailié, J., Erauso, G., Bachellerie, J.P., 2000. Archaeal homologs of eukaryotic methylation guide small nucleolar RNAs: lessons from the *Pyrococcus* genomes. *J. Mol. Biol.* 297, 895–906. <https://doi.org/10.1006/jmbi.2000.3593>
- Gelsinger, D.R., Dallon, E., Reddy, R., Mohammad, F., Buskirk, A.R., DiRuggiero, J., 2020. Ribosome profiling in archaea reveals leaderless translation, novel translational initiation sites, and ribosome pausing at single codon resolution. *Nucleic Acids Research* gkaa304. <https://doi.org/10.1093/nar/gkaa304>
- Ghalei, H., Trepreau, J., Collins, J.C., Bhaskaran, H., Strunk, B.S., Karbstein, K., 2017. The ATPase Fap7 Tests the Ability to Carry Out Translocation-Like Conformational Changes and Releases Dim1 During 40S Ribosome Maturation. *Mol Cell* 67, 990–1000.e3. <https://doi.org/10.1016/j.molcel.2017.08.007>
- Ghosal, A., Babu, V.M.P., Walker, G.C., 2018. Elevated Levels of Era GTPase Improve Growth, 16S rRNA Processing, and 70S Ribosome Assembly of *Escherichia coli* Lacking Highly Conserved Multifunctional YbeY Endoribonuclease. *J Bacteriol* 200. <https://doi.org/10.1128/JB.00278-18>
- Gilbert, W., 1986. Origin of life: The RNA world. *Nature* 319, 618–618. <https://doi.org/10.1038/319618a0>
- Gilbert, W.V., 2011. Functional specialization of ribosomes? *Trends Biochem. Sci.* 36, 127–132. <https://doi.org/10.1016/j.tibs.2010.12.002>
- Gill, E.E., Brinkman, F.S.L., 2011. The proportional lack of archaeal pathogens: Do viruses/phages hold the key? *Bioessays* 33, 248–254. <https://doi.org/10.1002/bies.201000091>
- Gomes-Filho, J.V., Randau, L., 2019. RNA stabilization in hyperthermophilic archaea. *Ann. N.Y. Acad. Sci.* 1447, 88–96. <https://doi.org/10.1111/nyas.14060>
- Goto, S., Kato, S., Kimura, T., Muto, A., Himeno, H., 2011. RsgA releases RbfA from 30S ribosome during a late stage of ribosome biosynthesis. *EMBO J.* 30, 104–114. <https://doi.org/10.1038/emboj.2010.291>
- Grandi, P., Rybin, V., Baßler, J., Petfalski, E., Strauß, D., Marzioch, M., Schäfer, T., Kuster, B., Tschochner, H., Tollervey, D., Gavin, A.-C., Hurt, E., 2002. 90S Pre-Ribosomes Include the 35S Pre-rRNA, the U3 snoRNP, and 40S Subunit Processing Factors but Predominantly Lack 60S Synthesis Factors. *Molecular Cell* 10, 105–115. [https://doi.org/10.1016/S1097-2765\(02\)00579-8](https://doi.org/10.1016/S1097-2765(02)00579-8)

- Granneman, S., Petfalski, E., Swiatkowska, A., Tollervey, D., 2010. Cracking pre-40S ribosomal subunit structure by systematic analyses of RNA-protein cross-linking. *EMBO J.* 29, 2026–2036. <https://doi.org/10.1038/emboj.2010.86>
- Greber, B.J., Boehringer, D., Godinic-Mikulcic, V., Crnkovic, A., Ibba, M., Weygand-Durasevic, I., Ban, N., 2012. Cryo-EM structure of the archaeal 50S ribosomal subunit in complex with initiation factor 6 and implications for ribosome evolution. *J. Mol. Biol.* 418, 145–160. <https://doi.org/10.1016/j.jmb.2012.01.018>
- Gregor, D., Pfeifer, F., 2005. In vivo analyses of constitutive and regulated promoters in halophilic archaea. *Microbiology* 151, 25–33. <https://doi.org/10.1099/mic.0.27541-0>
- Gregory, B., Rahman, N., Bommakanti, A., Shamsuzzaman, M., Thapa, M., Lescure, A., Zengel, J.M., Lindahl, L., 2019. The small and large ribosomal subunits depend on each other for stability and accumulation. *Life Sci Alliance* 2. <https://doi.org/10.26508/lsa.201800150>
- Grogan, D.W., 1989. Phenotypic characterization of the archaeobacterial genus *Sulfolobus*: comparison of five wild-type strains. *J Bacteriol* 171, 6710–6719.
- Grosjean, H. (Ed.), 2009. DNA and RNA modification enzymes: structure, mechanism, function and evolution, Molecular biology intelligence unit. Landes Bioscience, Austin, Tex.
- Grosjean, H., Gaspin, C., Marck, C., Decatur, W.A., de Crécy-Lagard, V., 2008. RNomics and Modomics in the halophilic archaea *Haloferax volcanii*: identification of RNA modification genes. *BMC Genomics* 9, 470. <https://doi.org/10.1186/1471-2164-9-470>
- Grünberger, F., Knüppel, R., Jüttner, M., Fenk, M., Borst, A., Reichelt, R., Hausner, W., Soppa, J., Ferreira-Cerca, S., Grohmann, D., 2020. Exploring prokaryotic transcription, operon structures, rRNA maturation and modifications using Nanopore-based native RNA sequencing (preprint). *Microbiology*. <https://doi.org/10.1101/2019.12.18.880849>
- Gunde-Cimerman, N., Plemenitaš, A., Oren, A., 2018. Strategies of adaptation of microorganisms of the three domains of life to high salt concentrations. *FEMS Microbiology Reviews* 42, 353–375. <https://doi.org/10.1093/femsre/fuy009>
- Gunderson, J.H., Sogin, M.L., Wollett, G., Hollingdale, M., de la Cruz, V.F., Waters, A.P., McCutchan, T.F., 1987. Structurally distinct, stage-specific ribosomes occur in *Plasmodium*. *Science* 238, 933–937. <https://doi.org/10.1126/science.3672135>
- Guo, Q., Goto, S., Chen, Y., Feng, B., Xu, Y., Muto, A., Himeno, H., Deng, H., Lei, J., Gao, N., 2013. Dissecting the in vivo assembly of the 30S ribosomal subunit reveals the role of RimM and general features of the assembly process. *Nucleic Acids Res.* 41, 2609–2620. <https://doi.org/10.1093/nar/gks1256>
- Gupta, N., Culver, G.M., 2014. Multiple in vivo pathways for *Escherichia coli* small ribosomal subunit assembly occur on one pre-rRNA. *Nat. Struct. Mol. Biol.* 21, 937–943. <https://doi.org/10.1038/nsmb.2887>
- Gust, A., Jakob, L., Zeitler, D.M., Bruckmann, A., Kramm, K., Willkomm, S., Tinnefeld, P., Meister, G., Grohmann, D., 2018. Site-Specific Labelling of Native Mammalian Proteins for Single-Molecule FRET Measurements. *Chembiochem* 19, 780–783. <https://doi.org/10.1002/cbic.201700696>
- Guy, L., Ettema, T.J.G., 2011. The archaeal “TACK” superphylum and the origin of eukaryotes. *Trends Microbiol.* 19, 580–587. <https://doi.org/10.1016/j.tim.2011.09.002>
- Hafner, M., Landthaler, M., Burger, L., Khorshid, M., Hausser, J., Berninger, P., Rothballer, A., Ascano, M., Jungkamp, A.-C., Munschauer, M., Ulrich, A., Wardle, G.S., Dewell, S., Zavolan, M., Tuschl, T., 2010a. PAR-CLIP—a method to identify transcriptome-wide the binding sites of RNA binding proteins. *J Vis Exp*. <https://doi.org/10.3791/2034>
- Hafner, M., Landthaler, M., Burger, L., Khorshid, M., Hausser, J., Berninger, P., Rothballer, A., Ascano, M., Jungkamp, A.-C., Munschauer, M., Ulrich, A., Wardle, G.S., Dewell, S., Zavolan, M., Tuschl, T., 2010b. Transcriptome-wide identification of RNA-binding protein and microRNA target sites by PAR-CLIP. *Cell* 141, 129–141. <https://doi.org/10.1016/j.cell.2010.03.009>
- Hage, A.E., Tollervey, D., 2004. A Surfeit of Factors: Why is Ribosome Assembly So Much More Complicated in Eukaryotes than Bacteria? *RNA Biology* 1, 9–14. <https://doi.org/10.4161/rna.1.1.932>
- Hallam, S.J., Konstantinidis, K.T., Putnam, N., Schleper, C., Watanabe, Y., Sugahara, J., Preston, C., de la Torre, J., Richardson, P.M., DeLong, E.F., 2006. Genomic analysis of the

- uncultivated marine crenarchaeote *Cenarchaeum symbiosum*. *Proc. Natl. Acad. Sci. U.S.A.* 103, 18296–18301. <https://doi.org/10.1073/pnas.0608549103>
- Harcourt, E.M., Ehrenschrwender, T., Batista, P.J., Chang, H.Y., Kool, E.T., 2013. Identification of a Selective Polymerase Enables Detection of N⁶-Methyladenosine in RNA. *J. Am. Chem. Soc.* 135, 19079–19082. <https://doi.org/10.1021/ja4105792>
- Harnpicharnchai, P., Jakovljevic, J., Horsey, E., Miles, T., Roman, J., Rout, M., Meagher, D., Imai, B., Guo, Y., Brame, C.J., Shabanowitz, J., Hunt, D.F., Woolford, J.L., 2001. Composition and functional characterization of yeast 66S ribosome assembly intermediates. *Mol. Cell* 8, 505–515.
- Harris, J.K., Kelley, S.T., Spiegelman, G.B., Pace, N.R., 2003. The genetic core of the universal ancestor. *Genome Res.* 13, 407–412. <https://doi.org/10.1101/gr.652803>
- Harris, K.A., Crothers, D.M., Ullu, E., 1995. In vivo structural analysis of spliced leader RNAs in *Trypanosoma brucei* and *Leptomonas collosoma*: a flexible structure that is independent of cap4 methylations. *RNA* 1, 351–362.
- Hartman, A.L., Norais, C., Badger, J.H., Delmas, S., Haldenby, S., Madupu, R., Robinson, J., Khouri, H., Ren, Q., Lowe, T.M., Maupin-Furlow, J., Pohlschroder, M., Daniels, C., Pfeiffer, F., Allers, T., Eisen, J.A., 2010. The Complete Genome Sequence of *Haloferax volcanii* DS2, a Model Archaeon. *PLoS One* 5. <https://doi.org/10.1371/journal.pone.0009605>
- Hartmann, R.K., Bindereif, A., Schön, A., Westhof, E. (Eds.), 2014. *Handbook of RNA Biochemistry: Second, Completely Revised and Enlarged Edition*. Wiley-VCH Verlag GmbH & Co. KGaA, Weinheim, Germany. <https://doi.org/10.1002/9783527647064>
- Held, W.A., Ballou, B., Mizushima, S., Nomura, M., 1974a. Assembly Mapping of 30 S Ribosomal Proteins from *Escherichia coli* FURTHER STUDIES. *J. Biol. Chem.* 249, 3103–3111.
- Held, W.A., Nomura, M., Hershey, J.W.B., 1974b. Ribosomal protein S21 is required for full activity in the initiation of protein synthesis. *Molec. Gen. Genet.* 128, 11–22. <https://doi.org/10.1007/BF00267291>
- Helser, T.L., Davies, J.E., Dahlberg, J.E., 1972. Mechanism of Kasugamycin Resistance in *Escherichia coli*. *Nature New Biology* 235, 6–9. <https://doi.org/10.1038/newbio235006a0>
- Henras, A.K., Plisson-Chastang, C., O’Donohue, M.-F., Chakraborty, A., Gleizes, P.-E., 2015. An overview of pre-ribosomal RNA processing in eukaryotes. *Wiley Interdiscip Rev RNA* 6, 225–242. <https://doi.org/10.1002/wrna.1269>
- Herman, R.C., Penman, S., 1977. Multiple decay rates of heterogeneous nuclear RNA in HeLa cells. *Biochemistry* 16, 3460–3465. <https://doi.org/10.1021/bi00634a026>
- Herold, M., Nierhaus, K.H., 1987. Incorporation of six additional proteins to complete the assembly map of the 50 S subunit from *Escherichia coli* ribosomes. *J. Biol. Chem.* 262, 8826–8833.
- Herzog, V.A., Reichholf, B., Neumann, T., Rescheneder, P., Bhat, P., Burkard, T.R., Wlotzka, W., von Haeseler, A., Zuber, J., Ameres, S.L., 2017. Thiol-linked alkylation of RNA to assess expression dynamics. *Nat Methods* 14, 1198–1204. <https://doi.org/10.1038/nmeth.4435>
- Heuer, A., Thomson, E., Schmidt, C., Berninghausen, O., Becker, T., Hurt, E., Beckmann, R., 2017. Cryo-EM structure of a late pre-40S ribosomal subunit from *Saccharomyces cerevisiae*. *eLife* 6, e30189. <https://doi.org/10.7554/eLife.30189>
- Heus, H.A., Formenoy, L.J., Knippenberg, P.H., 1990. Conformational and thermodynamic effects of naturally occurring base methylations in a ribosomal RNA hairpin of *Bacillus stearothermophilus*. *Eur J Biochem* 188, 275–281. <https://doi.org/10.1111/j.1432-1033.1990.tb15400.x>
- Heus, H.A., Pardi, A., 1991. Structural features that give rise to the unusual stability of RNA hairpins containing GNRA loops. *Science* 253, 191–194. <https://doi.org/10.1126/science.1712983>
- Hierlmeier, T., Merl, J., Sauert, M., Perez-Fernandez, J., Schultz, P., Bruckmann, A., Hamperl, S., Ohmayer, U., Rachel, R., Jacob, A., Hergert, K., Deutzmann, R., Griesenbeck, J., Hurt, E., Milkereit, P., Baßler, J., Tschochner, H., 2013. Rrp5p, Noc1p and Noc2p form a protein module which is part of early large ribosomal subunit precursors in *S. cerevisiae*. *Nucleic Acids Res.* 41, 1191–1210. <https://doi.org/10.1093/nar/gks1056>
- Hileman, T.H., Santangelo, T.J., 2012. Genetics Techniques for *Thermococcus kodakarensis*. *Front. Microbio.* 3. <https://doi.org/10.3389/fmicb.2012.00195>
- Hinnebusch, A.G., 2014. The scanning mechanism of eukaryotic translation initiation. *Annu. Rev. Biochem.* 83, 779–812. <https://doi.org/10.1146/annurev-biochem-060713-035802>

- Ho, J.H.-N., Kallstrom, G., Johnson, A.W., 2000. Nmd3p Is a Crm1p-Dependent Adapter Protein for Nuclear Export of the Large Ribosomal Subunit. *The Journal of Cell Biology* 151, 1057–1066. <https://doi.org/10.1083/jcb.151.5.1057>
- Hölzle, A., Fischer, S., Heyer, R., Schütz, S., Zacharias, M., Walther, P., Allers, T., Marchfelder, A., 2008. Maturation of the 5S rRNA 5' end is catalyzed in vitro by the endonuclease tRNase Z in the archaeon *H. volcanii*. *RNA* 14, 928–937. <https://doi.org/10.1261/rna.933208>
- Huber, H., Hohn, M.J., Rachel, R., Fuchs, T., Wimmer, V.C., Stetter, K.O., 2002. A new phylum of Archaea represented by a nanosized hyperthermophilic symbiont. *Nature* 417, 63–67. <https://doi.org/10.1038/417063a>
- Hulscher, R.M., Bohon, J., Rappé, M.C., Gupta, S., D'Mello, R., Sullivan, M., Ralston, C.Y., Chance, M.R., Woodson, S.A., 2016. Probing the structure of ribosome assembly intermediates in vivo using DMS and hydroxyl radical footprinting. *Methods* 103, 49–56. <https://doi.org/10.1016/j.ymeth.2016.03.012>
- Hunziker, M., Barandun, J., Petfalski, E., Tan, D., Delan-Forino, C., Molloy, K.R., Kim, K.H., Dunn-Davies, H., Shi, Y., Chaker-Margot, M., Chait, B.T., Walz, T., Tollervey, D., Klinge, S., 2016. UtpA and UtpB chaperone nascent pre-ribosomal RNA and U3 snoRNA to initiate eukaryotic ribosome assembly. *Nat Commun* 7, 12090. <https://doi.org/10.1038/ncomms12090>
- Ikeda, Y., Okada, Y., Sato, A., Kanai, T., Tomita, M., Atomi, H., Kanai, A., 2017. An archaeal RNA binding protein, FAU-1, is a novel ribonuclease related to rRNA stability in *Pyrococcus* and *Thermococcus*. *Sci Rep* 7, 12674. <https://doi.org/10.1038/s41598-017-13062-3>
- Ikegami, K., Lieb, J.D., 2013. Integral nuclear pore proteins bind to Pol III-transcribed genes and are required for Pol III transcript processing in *C. elegans*. *Mol. Cell* 51, 840–849. <https://doi.org/10.1016/j.molcel.2013.08.001>
- Imachi, H., Nobu, M.K., Nakahara, N., Morono, Y., Ogawara, M., Takaki, Y., Takano, Y., Uematsu, K., Ikuta, T., Ito, M., Matsui, Y., Miyazaki, M., Murata, K., Saito, Y., Sakai, S., Song, C., Tasumi, E., Yamanaka, Y., Yamaguchi, T., Kamagata, Y., Tamaki, H., Takai, K., 2020. Isolation of an archaeon at the prokaryote–eukaryote interface. *Nature* 577, 519–525. <https://doi.org/10.1038/s41586-019-1916-6>
- Inoue, K., Alsina, J., Chen, J., Inouye, M., 2003. Suppression of defective ribosome assembly in a rbfA deletion mutant by overexpression of Era, an essential GTPase in *Escherichia coli*. *Mol. Microbiol.* 48, 1005–1016. <https://doi.org/10.1046/j.1365-2958.2003.03475.x>
- Inoue, K., Basu, S., Inouye, M., 2007. Dissection of 16S rRNA Methyltransferase (KsgA) Function in *Escherichia coli*. *J Bacteriol* 189, 8510–8518. <https://doi.org/10.1128/JB.01259-07>
- Inoue, K., Chen, J., Tan, Q., Inouye, M., 2006. Era and RbfA have overlapping function in ribosome biogenesis in *Escherichia coli*. *J. Mol. Microbiol. Biotechnol.* 11, 41–52. <https://doi.org/10.1159/000092818>
- Jacob, A.I., Köhrer, C., Davies, B.W., RajBhandary, U.L., Walker, G.C., 2013. Conserved bacterial RNase YbeY plays key roles in 70S ribosome quality control and 16S rRNA maturation. *Mol. Cell* 49, 427–438. <https://doi.org/10.1016/j.molcel.2012.11.025>
- Jacob, F., Monod, J., 1961. Genetic regulatory mechanisms in the synthesis of proteins. *Journal of Molecular Biology* 3, 318–356. [https://doi.org/10.1016/S0022-2836\(61\)80072-7](https://doi.org/10.1016/S0022-2836(61)80072-7)
- Jain, C., 2020. RNase AM, a 5' to 3' exonuclease, matures the 5' end of all three ribosomal RNAs in *E. coli*. *Nucleic Acids Research* 48, 5616–5623. <https://doi.org/10.1093/nar/gkaa260>
- Janin, M., Coll-SanMartin, L., Esteller, M., 2020. Disruption of the RNA modifications that target the ribosome translation machinery in human cancer. *Mol Cancer* 19, 70. <https://doi.org/10.1186/s12943-020-01192-8>
- Jarrell, K.F., McBride, M.J., 2008. The surprisingly diverse ways that prokaryotes move. *Nat Rev Microbiol* 6, 466–476. <https://doi.org/10.1038/nrmicro1900>
- Jeganathan, A., Razi, A., Thurlow, B., Ortega, J., 2015. The C-terminal helix in the YjeQ zinc-finger domain catalyzes the release of RbfA during 30S ribosome subunit assembly. *RNA* 21, 1203–1216. <https://doi.org/10.1261/rna.049171.114>
- Jenney Jr, F.E., Adams, M.W.W., 2008. The impact of extremophiles on structural genomics (and vice versa). *Extremophiles* 12, 39–50. <https://doi.org/10.1007/s00792-007-0087-9>

- Jia, M.Z., Horita, S., Nagata, K., Tanokura, M., 2010. An archaeal Dim2-like protein, aDim2p, forms a ternary complex with a/eIF2 alpha and the 3' end fragment of 16S rRNA. *J. Mol. Biol.* 398, 774–785. <https://doi.org/10.1016/j.jmb.2010.03.055>
- Johnson, M.C., Ghalei, H., Doxtader, K.A., Karbstein, K., Stroupe, M.E., 2017. Structural Heterogeneity in Pre-40S Ribosomes. *Structure* 25, 329–340. <https://doi.org/10.1016/j.str.2016.12.011>
- Jolley, K.A., Rapaport, E., Hough, D.W., Danson, M.J., Woods, W.G., Dyall-Smith, M.L., 1996. Dihydrolipoamide dehydrogenase from the halophilic archaeon *Haloferax volcanii*: homologous overexpression of the cloned gene. *Journal of Bacteriology* 178, 3044–3048.
- Jucker, F.M., Heus, H.A., Yip, P.F., Moors, E.H., Pardi, A., 1996. A network of heterogeneous hydrogen bonds in GNRA tetraloops. *J. Mol. Biol.* 264, 968–980. <https://doi.org/10.1006/jmbi.1996.0690>
- Juhnke, H., Charizanis, C., Latifi, F., Krems, B., Entian, K.D., 2000. The essential protein fap7 is involved in the oxidative stress response of *Saccharomyces cerevisiae*. *Mol. Microbiol.* 35, 936–948. <https://doi.org/10.1046/j.1365-2958.2000.01768.x>
- Jüttner, M., Weiß, M., Ostheimer, N., Reglin, C., Kern, M., Knüppel, R., Ferreira-Cerca, S., 2020. A versatile cis-acting element reporter system to study the function, maturation and stability of ribosomal RNA mutants in archaea. *Nucleic Acids Res.* 48, 2073–2090. <https://doi.org/10.1093/nar/gkz1156>
- Kaczanowska, M., Rydén-Aulin, M., 2007. Ribosome biogenesis and the translation process in *Escherichia coli*. *Microbiol. Mol. Biol. Rev.* 71, 477–494. <https://doi.org/10.1128/MMBR.00013-07>
- Kaledhonkar, S., Fu, Z., Caban, K., Li, W., Chen, B., Sun, M., Gonzalez, R.L., Frank, J., 2019. Late steps in bacterial translation initiation visualized using time-resolved cryo-EM. *Nature* 570, 400–404. <https://doi.org/10.1038/s41586-019-1249-5>
- Kanehisa, M., Sato, Y., Kawashima, M., Furumichi, M., Tanabe, M., 2016. KEGG as a reference resource for gene and protein annotation. *Nucleic Acids Res.* 44, D457–462. <https://doi.org/10.1093/nar/gkv1070>
- Karbstein, K., 2013. Quality control mechanisms during ribosome maturation. *Trends Cell Biol.* 23, 242–250. <https://doi.org/10.1016/j.tcb.2013.01.004>
- Kater, L., Thoms, M., Barrio-Garcia, C., Cheng, J., Ismail, S., Ahmed, Y.L., Bange, G., Kressler, D., Berninghausen, O., Sinning, I., Hurt, E., Beckmann, R., 2017. Visualizing the Assembly Pathway of Nucleolar Pre-60S Ribosomes. *Cell* 171, 1599–1610.e14. <https://doi.org/10.1016/j.cell.2017.11.039>
- Kearns, D.B., 2010. A field guide to bacterial swarming motility. *Nat. Rev. Microbiol.* 8, 634–644. <https://doi.org/10.1038/nrmicro2405>
- Kearse, M., Moir, R., Wilson, A., Stones-Havas, S., Cheung, M., Sturrock, S., Buxton, S., Cooper, A., Markowitz, S., Duran, C., Thierer, T., Ashton, B., Meintjes, P., Drummond, A., 2012. Geneious Basic: an integrated and extendable desktop software platform for the organization and analysis of sequence data. *Bioinformatics* 28, 1647–1649. <https://doi.org/10.1093/bioinformatics/bts199>
- Kenzelmann, M., Maertens, S., Hergenahn, M., Kueffer, S., Hotz-Wagenblatt, A., Li, L., Wang, S., Ittrich, C., Lemberger, T., Arribas, R., Jonnakuty, S., Hollstein, M.C., Schmid, W., Gretz, N., Gröne, H.J., Schütz, G., 2007. Microarray analysis of newly synthesized RNA in cells and animals. *Proc. Natl. Acad. Sci. U.S.A.* 104, 6164–6169. <https://doi.org/10.1073/pnas.0610439104>
- Kiss, T., 2002. Small Nucleolar RNAs. *Cell* 109, 145–148. [https://doi.org/10.1016/S0092-8674\(02\)00718-3](https://doi.org/10.1016/S0092-8674(02)00718-3)
- Kiss-László, Z., Henry, Y., Bachellerie, J.P., Caizergues-Ferrer, M., Kiss, T., 1996. Site-specific ribose methylation of preribosomal RNA: a novel function for small nucleolar RNAs. *Cell* 85, 1077–1088. [https://doi.org/10.1016/s0092-8674\(00\)81308-2](https://doi.org/10.1016/s0092-8674(00)81308-2)
- Klinge, S., Voigts-Hoffmann, F., Leibundgut, M., Arpagaus, S., Ban, N., 2011. Crystal structure of the eukaryotic 60S ribosomal subunit in complex with initiation factor 6. *Science* 334, 941–948. <https://doi.org/10.1126/science.1211204>
- Klinge, S., Woolford, J.L., 2019. Ribosome assembly coming into focus. *Nat Rev Mol Cell Biol* 20, 116–131. <https://doi.org/10.1038/s41580-018-0078-y>

- Klootwijk, J., Klein, I., Grivell, L.A., 1975. Minimal post-transcriptional modification of yeast mitochondrial ribosomal RNA. *Journal of Molecular Biology* 97, 337–350. [https://doi.org/10.1016/S0022-2836\(75\)80044-1](https://doi.org/10.1016/S0022-2836(75)80044-1)
- Knüppel, R., Christensen, R.H., Gray, F.C., Esser, D., Strauß, D., Medenbach, J., Siebers, B., MacNeill, S.A., LaRonde, N., Ferreira-Cerca, S., 2018. Insights into the evolutionary conserved regulation of Rio ATPase activity. *Nucleic Acids Res.* 46, 1441–1456. <https://doi.org/10.1093/nar/gkx1236>
- Knüppel, R., Fenk, M., Jüttner, M., Ferreira-Cerca, S., 2020. In Vivo RNA Chemical Footprinting Analysis in Archaea, in: Heise, T. (Ed.), *RNA Chaperones, Methods in Molecular Biology*. Springer US, New York, NY, pp. 193–208. https://doi.org/10.1007/978-1-0716-0231-7_12
- Knüppel, R., Kuttenger, C., Ferreira-Cerca, S., 2017. Toward Time-Resolved Analysis of RNA Metabolism in Archaea Using 4-Thiouracil. *Front. Microbiol.* 8. <https://doi.org/10.3389/fmicb.2017.00286>
- Konikkat, S., Woolford, J.L., 2017. Principles of 60S ribosomal subunit assembly emerging from recent studies in yeast. *Biochem. J.* 474, 195–214. <https://doi.org/10.1042/BCJ20160516>
- Kontziampasis, D., Klebl, D.P., Iadanza, M.G., Scarff, C.A., Kopf, F., Sobott, F., Monteiro, D.C.F., Trebbin, M., Muench, S.P., White, H.D., 2019. A cryo-EM grid preparation device for time-resolved structural studies. *IUCrJ* 6, 1024–1031. <https://doi.org/10.1107/S2052252519011345>
- Kornprobst, M., Turk, M., Kellner, N., Cheng, J., Flemming, D., Koš-Braun, I., Koš, M., Thoms, M., Berninghausen, O., Beckmann, R., Hurt, E., 2016. Architecture of the 90S Pre-ribosome: A Structural View on the Birth of the Eukaryotic Ribosome. *Cell* 166, 380–393. <https://doi.org/10.1016/j.cell.2016.06.014>
- Kos, M., Tollervey, D., 2010. Yeast pre-rRNA processing and modification occur cotranscriptionally. *Mol. Cell* 37, 809–820. <https://doi.org/10.1016/j.molcel.2010.02.024>
- Koskinen, K., Pausan, M.R., Perras, A.K., Beck, M., Bang, C., Mora, M., Schilhabel, A., Schmitz, R., Moissl-Eichinger, C., 2017. First Insights into the Diverse Human Archaeome: Specific Detection of Archaea in the Gastrointestinal Tract, Lung, and Nose and on Skin. *mBio* 8. <https://doi.org/10.1128/mBio.00824-17>
- Kramer, P., Gäbel, K., Pfeiffer, F., Soppa, J., 2014. *Haloferax volcanii*, a prokaryotic species that does not use the Shine Dalgarno mechanism for translation initiation at 5'-UTRs. *PLoS ONE* 9, e94979. <https://doi.org/10.1371/journal.pone.0094979>
- Kressler, D., Hurt, E., Bergler, H., Bassler, J., 2012. The power of AAA-ATPases on the road of pre-60S ribosome maturation--molecular machines that strip pre-ribosomal particles. *Biochim. Biophys. Acta* 1823, 92–100. <https://doi.org/10.1016/j.bbamcr.2011.06.017>
- Kressler, D., Roser, D., Pertschy, B., Hurt, E., 2008. The AAA ATPase Rix7 powers progression of ribosome biogenesis by stripping Nsa1 from pre-60S particles. *J. Cell Biol.* 181, 935–944. <https://doi.org/10.1083/jcb.200801181>
- Kreuzer, M., Schmutzler, K., Waege, I., Thomm, M., Hausner, W., 2013. Genetic engineering of *Pyrococcus furiosus* to use chitin as a carbon source. *BMC Biotechnol* 13, 9. <https://doi.org/10.1186/1472-6750-13-9>
- Kufel, J., Dichtl, B., Tollervey, D., 1999. Yeast Rnt1p is required for cleavage of the pre-ribosomal RNA in the 3' ETS but not the 5' ETS. *RNA* 5, 909–917. <https://doi.org/10.1017/s135583829999026x>
- Kyuma, T., Kizaki, H., Ryuno, H., Sekimizu, K., Kaito, C., 2015. 16S rRNA methyltransferase KsgA contributes to oxidative stress resistance and virulence in *Staphylococcus aureus*. *Biochimie* 119, 166–174. <https://doi.org/10.1016/j.biochi.2015.10.027>
- Laass, S., Monzon, V.A., Kliemt, J., Hammelmann, M., Pfeiffer, F., Förstner, K.U., Soppa, J., 2019. Characterization of the transcriptome of *Haloferax volcanii*, grown under four different conditions, with mixed RNA-Seq. *PLoS ONE* 14, e0215986. <https://doi.org/10.1371/journal.pone.0215986>
- Lafontaine, D., Delcour, J., Glasser, A.L., Desgrès, J., Vandenhoute, J., 1994. The DIM1 gene responsible for the conserved m(6)Am(6)A dimethylation in the 3'-terminal loop of 18 S rRNA is essential in yeast. *J. Mol. Biol.* 241, 492–497. <https://doi.org/10.1006/jmbi.1994.1525>

- Lafontaine, D., Vandenhaute, J., Tollervey, D., 1995. The 18S rRNA dimethylase Dim1p is required for pre-ribosomal RNA processing in yeast. *Genes Dev.* 9, 2470–2481.
- Lafontaine, D.L., Preiss, T., Tollervey, D., 1998. Yeast 18S rRNA dimethylase Dim1p: a quality control mechanism in ribosome synthesis? *Mol. Cell. Biol.* 18, 2360–2370. <https://doi.org/10.1128/mcb.18.4.2360>
- Lafontaine, D.L.J., Tollervey, D., 1998. Birth of the snoRNPs: the evolution of the modification-guide snoRNAs. *Trends in Biochemical Sciences* 23, 383–388. [https://doi.org/10.1016/S0968-0004\(98\)01260-2](https://doi.org/10.1016/S0968-0004(98)01260-2)
- Lake, J.A., Henderson, E., Oakes, M., Clark, M.W., 1984. Eocytes: a new ribosome structure indicates a kingdom with a close relationship to eukaryotes. *Proceedings of the National Academy of Sciences* 81, 3786–3790. <https://doi.org/10.1073/pnas.81.12.3786>
- Lam, W.L., Doolittle, W.F., 1989. Shuttle vectors for the archaeobacterium *Halobacterium volcanii*. *Proceedings of the National Academy of Sciences* 86, 5478–5482. <https://doi.org/10.1073/pnas.86.14.5478>
- Lamanna, A.C., Karbstein, K., 2011. An RNA conformational switch regulates pre-18S rRNA cleavage. *J. Mol. Biol.* 405, 3–17. <https://doi.org/10.1016/j.jmb.2010.09.064>
- Lamanna, A.C., Karbstein, K., 2009. Nob1 binds the single-stranded cleavage site D at the 3'-end of 18S rRNA with its PIN domain. *Proc. Natl. Acad. Sci. U.S.A.* 106, 14259–14264. <https://doi.org/10.1073/pnas.0905403106>
- Large, A., Stamme, C., Lange, C., Duan, Z., Allers, T., Soppa, J., Lund, P.A., 2007. Characterization of a tightly controlled promoter of the halophilic archaeon *Haloferax volcanii* and its use in the analysis of the essential *cct1* gene. *Molecular Microbiology* 66, 1092–1106. <https://doi.org/10.1111/j.1365-2958.2007.05980.x>
- LaRonde, N.A., 2014. The ancient microbial RIO kinases. *J. Biol. Chem.* 289, 9488–9492. <https://doi.org/10.1074/jbc.R113.538090>
- LaRonde-LeBlanc, N., Wlodawer, A., 2005. A Family Portrait of the RIO Kinases. *J. Biol. Chem.* 280, 37297–37300. <https://doi.org/10.1074/jbc.R500013200>
- Latham, J., Cech, T., 1989. Defining the inside and outside of a catalytic RNA molecule. *Science* 245, 276–282. <https://doi.org/10.1126/science.2501870>
- Laurentii Salvii., Linné, C. von, 1753. *Caroli Linnaei ... Species plantarum :exhibentes plantas rite cognitatas, ad genera relatas, cum differentiis specificis, nominibus trivialibus, synonymis selectis, locis natalibus, secundum systema sexuale digestas... Impensis Laurentii Salvii, Holmiae :* <https://doi.org/10.5962/bhl.title.669>
- Lebaron, S., Schneider, C., van Nues, R.W., Swiatkowska, A., Walsh, D., Böttcher, B., Granneman, S., Watkins, N.J., Tollervey, D., 2012. Proofreading of pre-40S ribosome maturation by a translation initiation factor and 60S subunits. *Nat. Struct. Mol. Biol.* 19, 744–753. <https://doi.org/10.1038/nsmb.2308>
- Lecompte, O., Ripp, R., Thierry, J.-C., Moras, D., Poch, O., 2002. Comparative analysis of ribosomal proteins in complete genomes: an example of reductive evolution at the domain scale. *Nucleic Acids Res.* 30, 5382–5390.
- Lee, B., Flynn, R.A., Kadina, A., Guo, J.K., Kool, E.T., Chang, H.Y., 2017. Comparison of SHAPE reagents for mapping RNA structures inside living cells. *RNA* 23, 169–174. <https://doi.org/10.1261/rna.058784.116>
- Legerme, G., Yang, E., Esquivel, R.N., Kiljunen, S., Savilahti, H., Pohlschroder, M., 2016. Screening of a *Haloferax volcanii* Transposon Library Reveals Novel Motility and Adhesion Mutants. *Life (Basel)* 6. <https://doi.org/10.3390/life6040041>
- Leigh, J.A., Albers, S.-V., Atomi, H., Allers, T., 2011. Model organisms for genetics in the domain Archaea: methanogens, halophiles, Thermococcales and Sulfolobales. *FEMS Microbiology Reviews* 35, 577–608. <https://doi.org/10.1111/j.1574-6976.2011.00265.x>
- Lesnyak, D.V., Sergiev, P.V., Bogdanov, A.A., Dontsova, O.A., 2006. Identification of *Escherichia coli* m2G methyltransferases: I. the *ycbY* gene encodes a methyltransferase specific for G2445 of the 23 S rRNA. *J. Mol. Biol.* 364, 20–25. <https://doi.org/10.1016/j.jmb.2006.09.009>
- Li, G.-W., Burkhardt, D., Gross, C., Weissman, J.S., 2014. Quantifying absolute protein synthesis rates reveals principles underlying allocation of cellular resources. *Cell* 157, 624–635. <https://doi.org/10.1016/j.cell.2014.02.033>

- Li, Z., Deutscher, M.P., 1995. The tRNA processing enzyme RNase T is essential for maturation of 5S RNA. *Proc. Natl. Acad. Sci. U.S.A.* 92, 6883–6886.
- Li, Z., Kinoshita, Y., Rodriguez-Franco, M., Nußbaum, P., Braun, F., Delpesch, F., Quax, T.E.F., Albers, S.-V., 2019. Positioning of the Motility Machinery in Halophilic Archaea. *mBio* 10, e00377-19, /mbio/10/3/mBio.00377-19.atom. <https://doi.org/10.1128/mBio.00377-19>
- Li, Zhongwei, Pandit, S., Deutscher, M.P., 1999. RNase G (CafA protein) and RNase E are both required for the 5' maturation of 16S ribosomal RNA. *The EMBO Journal* 18, 2878–2885. <https://doi.org/10.1093/emboj/18.10.2878>
- Li, Z., Pandit, S., Deutscher, M.P., 1999. Maturation of 23S ribosomal RNA requires the exoribonuclease RNase T. *RNA* 5, 139–146.
- Liu, Y., Zhou, Z., Pan, J., Baker, B.J., Gu, J.-D., Li, M., 2018. Comparative genomic inference suggests mixotrophic lifestyle for Thorarchaeota. *ISME J* 12, 1021–1031. <https://doi.org/10.1038/s41396-018-0060-x>
- Lo, K.-Y., Li, Z., Bussiere, C., Bresson, S., Marcotte, E.M., Johnson, A.W., 2010. Defining the pathway of cytoplasmic maturation of the 60S ribosomal subunit. *Mol. Cell* 39, 196–208. <https://doi.org/10.1016/j.molcel.2010.06.018>
- Loc'h, J., Blaud, M., Réty, S., Lebaron, S., Deschamps, P., Bareille, J., Jombart, J., Robert-Paganin, J., Delbos, L., Chardon, F., Zhang, E., Charenton, C., Tollervey, D., Leulliot, N., 2014. RNA Mimicry by the Fap7 Adenylate Kinase in Ribosome Biogenesis. *PLoS Biol* 12. <https://doi.org/10.1371/journal.pbio.1001860>
- López-Alonso, J.P., Kaminishi, T., Kikuchi, T., Hirata, Y., Iturrioz, I., Dhimole, N., Schedlbauer, A., Hase, Y., Goto, S., Kurita, D., Muto, A., Zhou, S., Naoe, C., Mills, D.J., Gil-Carton, D., Takemoto, C., Himeno, H., Fucini, P., Connell, S.R., 2017. RsgA couples the maturation state of the 30S ribosomal decoding center to activation of its GTPase pocket. *Nucleic Acids Res.* 45, 6945–6959. <https://doi.org/10.1093/nar/gkx324>
- López-García, P., Moreira, D., 2020. Cultured Asgard Archaea Shed Light on Eukaryogenesis. *Cell* 181, 232–235. <https://doi.org/10.1016/j.cell.2020.03.058>
- Lövgren, J.M., Bylund, G.O., Srivastava, M.K., Lundberg, L.A.C., Persson, O.P., Wingsle, G., Wikström, P.M., 2004. The PRC-barrel domain of the ribosome maturation protein RimM mediates binding to ribosomal protein S19 in the 30S ribosomal subunits. *RNA* 10, 1798–1812. <https://doi.org/10.1261/rna.7720204>
- Lu, Q., Inouye, M., 1998. The gene for 16S rRNA methyltransferase (ksgA) functions as a multicopy suppressor for a cold-sensitive mutant of era, an essential RAS-like GTP-binding protein in *Escherichia coli*. *J. Bacteriol.* 180, 5243–5246.
- Lucks, J.B., Mortimer, S.A., Trapnell, C., Luo, S., Aviran, S., Schroth, G.P., Pachter, L., Doudna, J.A., Arkin, A.P., 2011. Multiplexed RNA structure characterization with selective 2'-hydroxyl acylation analyzed by primer extension sequencing (SHAPE-Seq). *Proc. Natl. Acad. Sci. U.S.A.* 108, 11063–11068. <https://doi.org/10.1073/pnas.1106501108>
- Lugowski, A., Nicholson, B., Rissland, O.S., 2018. Determining mRNA half-lives on a transcriptome-wide scale. *Methods* 137, 90–98. <https://doi.org/10.1016/j.ymeth.2017.12.006>
- Ma, C., Wu, S., Li, N., Chen, Y., Yan, K., Li, Z., Zheng, L., Lei, J., Woolford, J.L., Gao, N., 2017. Structural snapshot of cytoplasmic pre-60S ribosomal particles bound by Nmd3, Lsg1, Tif6 and Reh1. *Nat. Struct. Mol. Biol.* 24, 214–220. <https://doi.org/10.1038/nsmb.3364>
- MacLeod, F., S. Kindler, G., Lun Wong, H., Chen, R., P. Burns, B., 1 School of Biotechnology and Biomolecular Sciences, The University of New South Wales, Sydney, Australia, 2 Australian Centre for Astrobiology, The University of New South Wales, Sydney, Australia, 2019. Asgard archaea: Diversity, function, and evolutionary implications in a range of microbiomes. *AIMS Microbiology* 5, 48–61. <https://doi.org/10.3934/microbiol.2019.1.48>
- Magde, D., Elson, E., Webb, W.W., 1972. Thermodynamic Fluctuations in a Reacting System—Measurement by Fluorescence Correlation Spectroscopy. *Phys. Rev. Lett.* 29, 705–708. <https://doi.org/10.1103/PhysRevLett.29.705>
- Mailler, E., Paillart, J.-C., Marquet, R., Smyth, R.P., Vivet-Boudou, V., 2019. The evolution of RNA structural probing methods: From gels to next-generation sequencing. *WIREs RNA* 10, e1518. <https://doi.org/10.1002/wrna.1518>

- Makarova, K.S., Wolf, Y.I., Koonin, E.V., 2015. Archaeal Clusters of Orthologous Genes (arCOGs): An Update and Application for Analysis of Shared Features between Thermococcales, Methanococcales, and Methanobacteriales. *Life (Basel)* 5, 818–840. <https://doi.org/10.3390/life5010818>
- Makosky, P.C., Dahlberg, A.E., 1987. Spectinomycin resistance at site 1192 in 16S ribosomal RNA of *E. coli*: an analysis of three mutants. *Biochimie* 69, 885–889. [https://doi.org/10.1016/0300-9084\(87\)90216-1](https://doi.org/10.1016/0300-9084(87)90216-1)
- Mancinelli, R.L., Fahlen, T.F., Landheim, R., Klovstad, M.R., 2004. Brines and evaporites: analogs for Martian life. *Advances in Space Research* 33, 1244–1246. <https://doi.org/10.1016/j.asr.2003.08.034>
- Marmier-Gourrier, N., Cléry, A., Schlotter, F., Senty-Ségault, V., Branlant, C., 2011. A second base pair interaction between U3 small nucleolar RNA and the 5'-ETS region is required for early cleavage of the yeast pre-ribosomal RNA. *Nucleic Acids Res.* 39, 9731–9745. <https://doi.org/10.1093/nar/gkr675>
- Marteinsson, V.T., Birrien, J.L., Reysenbach, A.L., Vernet, M., Marie, D., Gambacorta, A., Messner, P., Sleytr, U.B., Prieur, D., 1999. *Thermococcus barophilus* sp. nov., a new barophilic and hyperthermophilic archaeon isolated under high hydrostatic pressure from a deep-sea hydrothermal vent. *Int. J. Syst. Bacteriol.* 49 Pt 2, 351–359. <https://doi.org/10.1099/00207713-49-2-351>
- Maurer, L.M., Yohannes, E., Bondurant, S.S., Radmacher, M., Slonczewski, J.L., 2005. pH regulates genes for flagellar motility, catabolism, and oxidative stress in *Escherichia coli* K-12. *J. Bacteriol.* 187, 304–319. <https://doi.org/10.1128/JB.187.1.304-319.2005>
- McGinnis, J.L., Liu, Q., Lavender, C.A., Devaraj, A., McClory, S.P., Fredrick, K., Weeks, K.M., 2015. In-cell SHAPE reveals that free 30S ribosome subunits are in the inactive state. *Proc. Natl. Acad. Sci. U.S.A.* 112, 2425–2430. <https://doi.org/10.1073/pnas.1411514112>
- McIntosh, K.B., Warner, J.R., 2007. Yeast Ribosomes: Variety Is the Spice of Life. *Cell* 131, 450–451. <https://doi.org/10.1016/j.cell.2007.10.028>
- Mecas, J., Bilis, I., Falkow, S., 2001. Identification of attenuated *Yersinia pseudotuberculosis* strains and characterization of an orogastric infection in BALB/c mice on day 5 postinfection by signature-tagged mutagenesis. *Infect. Immun.* 69, 2779–2787. <https://doi.org/10.1128/IAI.67.5.2779-2787.2001>
- Melnikov, S., Ben-Shem, A., Garreau de Loubresse, N., Jenner, L., Yusupova, G., Yusupov, M., 2012. One core, two shells: bacterial and eukaryotic ribosomes. *Nat. Struct. Mol. Biol.* 19, 560–567. <https://doi.org/10.1038/nsmb.2313>
- Melvin, W.T., Milne, H.B., Slater, A.A., Allen, H.J., Keir, H.M., 1978. Incorporation of 6-Thioguanosine and 4-Thiouridine into RNA. Application to Isolation of Newly Synthesised RNA by Affinity Chromatography. *Eur J Biochem* 92, 373–379. <https://doi.org/10.1111/j.1432-1033.1978.tb12756.x>
- Merino, E.J., Wilkinson, K.A., Coughlan, J.L., Weeks, K.M., 2005. RNA Structure Analysis at Single Nucleotide Resolution by Selective 2'-Hydroxyl Acylation and Primer Extension (SHAPE). *J. Am. Chem. Soc.* 127, 4223–4231. <https://doi.org/10.1021/ja043822v>
- Merino, N., Aronson, H.S., Bojanova, D.P., Feyhl-Buska, J., Wong, M.L., Zhang, S., Giovannelli, D., 2019. Living at the Extremes: Extremophiles and the Limits of Life in a Planetary Context. *Front. Microbiol.* 10, 780. <https://doi.org/10.3389/fmicb.2019.00780>
- Milkereit, P., Gadal, O., Podtelejnikov, A., Trumtel, S., Gas, N., Petfalski, E., Tollervey, D., Mann, M., Hurt, E., Tschochner, H., 2001. Maturation and intranuclear transport of pre-ribosomes requires Noc proteins. *Cell* 105, 499–509. [https://doi.org/10.1016/s0092-8674\(01\)00358-0](https://doi.org/10.1016/s0092-8674(01)00358-0)
- Miller, M.R., Robinson, K.J., Cleary, M.D., Doe, C.Q., 2009. TU-tagging: cell type-specific RNA isolation from intact complex tissues. *Nat Methods* 6, 439–441. <https://doi.org/10.1038/nmeth.1329>
- Misra, T.K., Apirion, D., 1979. RNase E, an RNA processing enzyme from *Escherichia coli*. *J. Biol. Chem.* 254, 11154–11159.
- Mitchell, D., Renda, A.J., Douds, C.A., Babitzke, P., Assmann, S.M., Bevilacqua, P.C., 2019. In vivo RNA structural probing of uracil and guanine base-pairing by 1-ethyl-3-(3-dimethylaminopropyl)carbodiimide (EDC). *RNA* 25, 147–157. <https://doi.org/10.1261/rna.067868.118>

- Mitra, S., Shcherbakova, I.V., Altman, R.B., Brenowitz, M., Laederach, A., 2008. High-throughput single-nucleotide structural mapping by capillary automated footprinting analysis. *Nucleic Acids Research* 36, e63–e63. <https://doi.org/10.1093/nar/gkn267>
- Mitterer, V., Shayan, R., Ferreira-Cerca, S., Murat, G., Enne, T., Rinaldi, D., Weigl, S., Omanic, H., Gleizes, P.-E., Kressler, D., Plisson-Chastang, C., Pertschy, B., 2019. Conformational proofreading of distant 40S ribosomal subunit maturation events by a long-range communication mechanism. *Nat Commun* 10, 2754. <https://doi.org/10.1038/s41467-019-10678-z>
- Mizushima, S., Nomura, M., 1970. Assembly Mapping of 30S Ribosomal Proteins from *E. coli*. *Nature* 226, 1214. <https://doi.org/10.1038/2261214a0>
- Moazed, D., Robertson, J.M., Noller, H.F., 1988. Interaction of elongation factors EF-G and EF-Tu with a conserved loop in 23S RNA. *Nature* 334, 362–364. <https://doi.org/10.1038/334362a0>
- Moazed, D., Stern, S., Noller, H.F., 1986. Rapid chemical probing of conformation in 16 S ribosomal RNA and 30 S ribosomal subunits using primer extension. *J. Mol. Biol.* 187, 399–416. [https://doi.org/10.1016/0022-2836\(86\)90441-9](https://doi.org/10.1016/0022-2836(86)90441-9)
- Moissl-Eichinger, C., Pausan, M., Taffner, J., Berg, G., Bang, C., Schmitz, R.A., 2018. Archaea Are Interactive Components of Complex Microbiomes. *Trends in Microbiology* 26, 70–85. <https://doi.org/10.1016/j.tim.2017.07.004>
- Moissl-Eichinger, C., Rettberg, P., Pukall, R., 2012. The first collection of spacecraft-associated microorganisms: a public source for extremotolerant microorganisms from spacecraft assembly clean rooms. *Astrobiology* 12, 1024–1034. <https://doi.org/10.1089/ast.2012.0906>
- Moore, P.B., 2003. After the ribosome structures: How does peptidyl transferase work? *RNA* 9, 155–159. <https://doi.org/10.1261/rna.2127103>
- Moriggi, G., Nieto, B., Dosil, M., 2014. Rrp12 and the Exportin Crm1 Participate in Late Assembly Events in the Nucleolus during 40S Ribosomal Subunit Biogenesis. *PLoS Genet* 10, e1004836. <https://doi.org/10.1371/journal.pgen.1004836>
- Mulder, A.M., Yoshioka, C., Beck, A.H., Bunner, A.E., Milligan, R.A., Potter, C.S., Carragher, B., Williamson, J.R., 2010. Visualizing ribosome biogenesis: parallel assembly pathways for the 30S subunit. *Science* 330, 673–677. <https://doi.org/10.1126/science.1193220>
- Nagel, C., Machulla, A., Zahn, S., Soppa, J., 2019. Several One-Domain Zinc Finger μ -Proteins of *Haloferax Volcanii* Are Important for Stress Adaptation, Biofilm Formation, and Swarming. *Genes* 10, 361. <https://doi.org/10.3390/genes10050361>
- Nakhoul, H., Ke, J., Zhou, X., Liao, W., Zeng, S.X., Lu, H., 2014. Ribosomopathies: mechanisms of disease. *Clin Med Insights Blood Disord* 7, 7–16. <https://doi.org/10.4137/CMBD.S16952>
- Näther-Schindler, D.J., Schopf, S., Bellack, A., Rachel, R., Wirth, R., 2014. *Pyrococcus furiosus* flagella: biochemical and transcriptional analyses identify the newly detected flaB0 gene to encode the major flagellin. *Front. Microbiol.* 5. <https://doi.org/10.3389/fmicb.2014.00695>
- Ng, C., Tan, B., Jiang, X.-T., Gu, X., Chen, H., Schmitz, B.W., Haller, L., Charles, F.R., Zhang, T., Gin, K., 2019. Metagenomic and Resistome Analysis of a Full-Scale Municipal Wastewater Treatment Plant in Singapore Containing Membrane Bioreactors. *Front. Microbiol.* 10, 172. <https://doi.org/10.3389/fmicb.2019.00172>
- Ni, J., Tien, A.L., Fournier, M.J., 1997. Small nucleolar RNAs direct site-specific synthesis of pseudouridine in ribosomal RNA. *Cell* 89, 565–573. [https://doi.org/10.1016/s0092-8674\(00\)80238-x](https://doi.org/10.1016/s0092-8674(00)80238-x)
- Nierhaus, K.H., 1991. The assembly of prokaryotic ribosomes. *Biochimie* 73, 739–755.
- Nierhaus, K.H., 1980. The assembly of the prokaryotic ribosome. *Biosystems* 12, 273–282. [https://doi.org/10.1016/0303-2647\(80\)90024-6](https://doi.org/10.1016/0303-2647(80)90024-6)
- Nierhaus, K.H., Dohme, F., 1974. Total reconstitution of functionally active 50S ribosomal subunits from *Escherichia coli*. *Proc. Natl. Acad. Sci. U.S.A.* 71, 4713–4717.
- Nierhaus, K.H., Wilson, D.N., 2004. Protein synthesis and ribosome structure: translating the genome. Wiley-VCH, Weinheim.
- Nissan, T.A., Baßler, J., Petfalski, E., Tollervey, D., Hurt, E., 2002. 60S pre-ribosome formation viewed from assembly in the nucleolus until export to the cytoplasm. *The EMBO Journal* 21, 5539–5547. <https://doi.org/10.1093/emboj/cdf547>

- Nkanga, V.D., Henrissat, B., Drancourt, M., 2017. Archaea: Essential inhabitants of the human digestive microbiota. *Human Microbiome Journal* 3, 1–8. <https://doi.org/10.1016/j.humic.2016.11.005>
- Noller, H.F., Chaires, J.B., 1972. Functional Modification of 16S Ribosomal RNA by Kethoxal. *Proceedings of the National Academy of Sciences* 69, 3115–3118. <https://doi.org/10.1073/pnas.69.11.3115>
- Nunoura, T., Takaki, Y., Kakuta, J., Nishi, S., Sugahara, J., Kazama, H., Chee, G.-J., Hattori, M., Kanai, A., Atomi, H., Takai, K., Takami, H., 2011. Insights into the evolution of Archaea and eukaryotic protein modifier systems revealed by the genome of a novel archaeal group. *Nucleic Acids Res.* 39, 3204–3223. <https://doi.org/10.1093/nar/gkq1228>
- O'Connor, M., Thomas, C.L., Zimmermann, R.A., Dahlberg, A.E., 1997. Decoding fidelity at the ribosomal A and P sites: influence of mutations in three different regions of the decoding domain in 16S rRNA. *Nucleic Acids Res.* 25, 1185–1193. <https://doi.org/10.1093/nar/25.6.1185>
- O'Farrell, H.C., Musayev, F.N., Scarsdale, J.N., Rife, J.P., 2012. Control of substrate specificity by a single active site residue of the KsgA methyltransferase. *Biochemistry* 51, 466–474. <https://doi.org/10.1021/bi201539j>
- O'Farrell, H.C., Pulicherla, N., Desai, P.M., Rife, J.P., 2006. Recognition of a complex substrate by the KsgA/Dim1 family of enzymes has been conserved throughout evolution. *RNA* 12, 725–733. <https://doi.org/10.1261/rna.2310406>
- O'Farrell, H.C., Rife, J.P., 2012. *Staphylococcus aureus* and *Escherichia coli* have disparate dependences on KsgA for growth and ribosome biogenesis. *BMC Microbiology* 12, 244. <https://doi.org/10.1186/1471-2180-12-244>
- O'Farrell, H.C., Scarsdale, J.N., Rife, J.P., 2004. Crystal Structure of KsgA, a Universally Conserved rRNA Adenine Dimethyltransferase in *Escherichia coli*. *Journal of Molecular Biology* 339, 337–353. <https://doi.org/10.1016/j.jmb.2004.02.068>
- O'Farrell, H.C., Xu, Z., Culver, G.M., Rife, J.P., 2008. Sequence and structural evolution of the KsgA/Dim1 methyltransferase family. *BMC Res Notes* 1, 108. <https://doi.org/10.1186/1756-0500-1-108>
- Ohmayer, U., Gamalinda, M., Sauert, M., Ossowski, J., Pöll, G., Linnemann, J., Hierlmeier, T., Perez-Fernandez, J., Kumcuoglu, B., Leger-Silvestre, I., Faubladiet, M., Griesenbeck, J., Woolford, J., Tschochner, H., Milkereit, P., 2013. Studies on the assembly characteristics of large subunit ribosomal proteins in *S. cerevisiae*. *PLoS ONE* 8, e68412. <https://doi.org/10.1371/journal.pone.0068412>
- Okamoto, S., Tamaru, A., Nakajima, C., Nishimura, K., Tanaka, Y., Tokuyama, S., Suzuki, Y., Ochi, K., 2007. Loss of a conserved 7-methylguanosine modification in 16S rRNA confers low-level streptomycin resistance in bacteria. *Mol. Microbiol.* 63, 1096–1106. <https://doi.org/10.1111/j.1365-2958.2006.05585.x>
- Olsen, G.J., Woese, C.R., Overbeek, R., 1994. The winds of (evolutionary) change: breathing new life into microbiology. *Journal of Bacteriology* 176, 1–6. <https://doi.org/10.1128/JB.176.1.1-6.1994>
- Oren, A., 2008. Microbial life at high salt concentrations: phylogenetic and metabolic diversity. *Saline Systems* 4, 2. <https://doi.org/10.1186/1746-1448-4-2>
- Oren, A., Arahall, D.R., Ventosa, A., 2009. Emended descriptions of genera of the family Halobacteriaceae. *Int J Syst Evol Microbiol* 59, 637–642. <https://doi.org/10.1099/ijs.0.008904-0>
- O'Toole, G.A., 2011. Microtiter Dish Biofilm Formation Assay. *JoVE (Journal of Visualized Experiments)* e2437. <https://doi.org/10.3791/2437>
- Palade, G.E., 1955. A SMALL PARTICULATE COMPONENT OF THE CYTOPLASM. *The Journal of Biophysical and Biochemical Cytology* 1, 59–68. <https://doi.org/10.1083/jcb.1.1.59>
- Park, A.K., Kim, H., Jin, H.J., 2010. Phylogenetic analysis of rRNA methyltransferases, Erm and KsgA, as related to antibiotic resistance: Phylogenetic analysis of Erm and KsgA/Dim1. *FEMS Microbiology Letters* no-no. <https://doi.org/10.1111/j.1574-6968.2010.02031.x>
- Peña, C., Hurt, E., Panse, V.G., 2017. Eukaryotic ribosome assembly, transport and quality control. *Nat. Struct. Mol. Biol.* 24, 689–699. <https://doi.org/10.1038/nsmb.3454>

- Penev, P.I., Fakhretaha-Aval, S., Patel, V.J., Cannone, J.J., Gutell, R.R., Petrov, A.S., Williams, L.D., Glass, J.B., 2019. Supersized ribosomal RNA expansion segments in Asgard archaea (preprint). *Evolutionary Biology*. <https://doi.org/10.1101/2019.12.25.888164>
- Peng, N., Han, W., Li, Y., Liang, Y., She, Q., 2017. Genetic technologies for extremely thermophilic microorganisms of *Sulfolobus*, the only genetically tractable genus of crenarchaea. *Sci. China Life Sci.* 60, 370–385. <https://doi.org/10.1007/s11427-016-0355-8>
- Pérez-Fernández, J., Román, Á., De Las Rivas, J., Bustelo, X.R., Dosil, M., 2007. The 90S Preribosome Is a Multimodular Structure That Is Assembled through a Hierarchical Mechanism. *MCB* 27, 5414–5429. <https://doi.org/10.1128/MCB.00380-07>
- Phipps, K.R., Charette, J.M., Baserga, S.J., 2011. The small subunit processome in ribosome biogenesis—progress and prospects. *Wiley Interdiscip Rev RNA* 2, 1–21. <https://doi.org/10.1002/wrna.57>
- Pletnev, P., Guseva, E., Zanina, A., Evfratov, S., Dzama, M., Treshin, V., Pogorel'skaya, A., Osterman, I., Golovina, A., Rubtsova, M., Serebryakova, M., Pobeguts, O.V., Govorun, V.M., Bogdanov, A.A., Dontsova, O.A., Sergiev, P.V., 2020. Comprehensive Functional Analysis of *Escherichia coli* Ribosomal RNA Methyltransferases. *Front. Genet.* 11, 97. <https://doi.org/10.3389/fgene.2020.00097>
- Poldermans, B., Roza, L., Van Knippenberg, P.H., 1979. Studies on the function of two adjacent N6,N6-dimethyladenosines near the 3' end of 16 S ribosomal RNA of *Escherichia coli*. III. Purification and properties of the methylating enzyme and methylase-30 S interactions. *J. Biol. Chem.* 254, 9094–9100.
- Pöll, G., Braun, T., Jakovljevic, J., Neueder, A., Jakob, S., Woolford, J.L., Tschochner, H., Milkereit, P., 2009. rRNA maturation in yeast cells depleted of large ribosomal subunit proteins. *PLoS ONE* 4, e8249. <https://doi.org/10.1371/journal.pone.0008249>
- Popova, A.M., Williamson, J.R., 2014. Quantitative analysis of rRNA modifications using stable isotope labeling and mass spectrometry. *J. Am. Chem. Soc.* 136, 2058–2069. <https://doi.org/10.1021/ja412084b>
- Pühler, G., Leffers, H., Gropp, F., Palm, P., Klenk, H.P., Lottspeich, F., Garrett, R.A., Zillig, W., 1989. Archaeobacterial DNA-dependent RNA polymerases testify to the evolution of the eukaryotic nuclear genome. *Proceedings of the National Academy of Sciences of the United States of America* 86, 4569.
- Pulicherla, N., Pogorzala, L.A., Xu, Z., O'Farrell, H.C., Musayev, F.N., Scarsdale, J.N., Sia, E.A., Culver, G.M., Rife, J.P., 2009. Structural and Functional Divergence within the Dim1/KsgA Family of rRNA Methyltransferases. *Journal of Molecular Biology* 391, 884–893. <https://doi.org/10.1016/j.jmb.2009.06.015>
- Qi, L., Li, J., Jia, J., Yue, L., Dong, X., 2020. Comprehensive analysis of the pre-ribosomal RNA maturation pathway in a methanoarchaeon exposes the conserved circularization and linearization mode in archaea. *RNA Biology* 15476286.2020.1771946. <https://doi.org/10.1080/15476286.2020.1771946>
- Qu, H.L., Michot, B., Bachellerie, J.P., 1983. Improved methods for structure probing in large RNAs: a rapid “heterologous” sequencing approach is coupled to the direct mapping of nuclease accessible sites. Application to the 5' terminal domain of eukaryotic 28S rRNA. *Nucleic Acids Res.* 11, 5903–5920. <https://doi.org/10.1093/nar/11.17.5903>
- Rabl, J., Leibundgut, M., Ataide, S.F., Haag, A., Ban, N., 2011. Crystal structure of the eukaryotic 40S ribosomal subunit in complex with initiation factor 1. *Science* 331, 730–736. <https://doi.org/10.1126/science.1198308>
- Rake, A.V., Graham, A.F., 1964. KINETICS OF INCORPORATION OF URIDINE-C14 INTO L CELL RNA. *Biophys. J.* 4, 267–284. [https://doi.org/10.1016/s0006-3495\(64\)86782-5](https://doi.org/10.1016/s0006-3495(64)86782-5)
- Rampelotto, P.H., 2013. Extremophiles and extreme environments. *Life (Basel)* 3, 482–485. <https://doi.org/10.3390/life3030482>
- Raveh, A., Margalioth, M., Sontag, E.D., Tuller, T., 2016. A model for competition for ribosomes in the cell. *J. R. Soc. Interface* 13, 20151062. <https://doi.org/10.1098/rsif.2015.1062>
- Razi, A., Davis, J.H., Hao, Y., Jahagirdar, D., Thurlow, B., Basu, K., Jain, N., Gomez-Blanco, J., Britton, R.A., Vargas, J., Guarné, A., Woodson, S.A., Williamson, J.R., Ortega, J., 2019. Role of Era in assembly and homeostasis of the ribosomal small subunit. *Nucleic Acids Res* 47, 8301–8317. <https://doi.org/10.1093/nar/gkz571>

- Razi, A., Guarné, A., Ortega, J., 2017. The cryo-EM structure of YjeQ bound to the 30S subunit suggests a fidelity checkpoint function for this protein in ribosome assembly. *Proc. Natl. Acad. Sci. U.S.A.* 114, E3396–E3403. <https://doi.org/10.1073/pnas.1618016114>
- Ree, H.K., Zimmermann, R.A., 1990. Organization and expression of the 16S, 23S and 5S ribosomal RNA genes from the archaebacterium *Thermoplasma acidophilum*. *Nucleic Acids Res.* 18, 4471–4478. <https://doi.org/10.1093/nar/18.15.4471>
- Rife, J.P., Cheng, C.S., Moore, P.B., Strobel, S.A., 1998. N 2-methylguanosine is iso-energetic with guanosine in RNA duplexes and GNRA tetraloops. *Nucleic Acids Res.* 26, 3640–3644. <https://doi.org/10.1093/nar/26.16.3640>
- Rife, J.P., Moore, P.B., 1998. The structure of a methylated tetraloop in 16S ribosomal RNA. *Structure* 6, 747–756. [https://doi.org/10.1016/S0969-2126\(98\)00076-8](https://doi.org/10.1016/S0969-2126(98)00076-8)
- Rodgers, M.L., Woodson, S.A., 2019. Transcription Increases the Cooperativity of Ribonucleoprotein Assembly. *Cell* 179, 1370–1381.e12. <https://doi.org/10.1016/j.cell.2019.11.007>
- Rogers, K.C., Crescenzo, A.T., Söll, D., 1995. Aminoacylation of transfer RNAs with 2-thiouridine derivatives in the wobble position of the anticodon. *Biochimie* 77, 66–74. [https://doi.org/10.1016/0300-9084\(96\)88106-5](https://doi.org/10.1016/0300-9084(96)88106-5)
- Röhl, R., Nierhaus, K.H., 1982. Assembly map of the large subunit (50S) of *Escherichia coli* ribosomes. *Proc. Natl. Acad. Sci. U.S.A.* 79, 729–733. <https://doi.org/10.1073/pnas.79.3.729>
- Rosado, I.V., Dez, C., Lebaron, S., Caizergues-Ferrer, M., Henry, Y., de la Cruz, J., 2007a. Characterization of *Saccharomyces cerevisiae* Npa2p (Urb2p) reveals a low-molecular-mass complex containing Dbp6p, Npa1p (Urb1p), Nop8p, and Rsa3p involved in early steps of 60S ribosomal subunit biogenesis. *Mol. Cell. Biol.* 27, 1207–1221. <https://doi.org/10.1128/MCB.01523-06>
- Rosado, I.V., Kressler, D., de la Cruz, J., 2007b. Functional analysis of *Saccharomyces cerevisiae* ribosomal protein Rpl3p in ribosome synthesis. *Nucleic Acids Res.* 35, 4203–4213. <https://doi.org/10.1093/nar/gkm388>
- Rouskin, S., Zubradt, M., Washietl, S., Kellis, M., Weissman, J.S., 2014. Genome-wide probing of RNA structure reveals active unfolding of mRNA structures in vivo. *Nature* 505, 701–705. <https://doi.org/10.1038/nature12894>
- Rovera, G., Berman, S., Baserga, R., 1970. Pulse labeling of RNA of mammalian cells. *Proc. Natl. Acad. Sci. U.S.A.* 65, 876–883. <https://doi.org/10.1073/pnas.65.4.876>
- Roy, M.K., Singh, B., Ray, B.K., Apirion, D., 1983. Maturation of 5-S rRNA: ribonuclease E cleavages and their dependence on precursor sequences. *Eur. J. Biochem.* 131, 119–127.
- Roy-Chaudhuri, B., Kirthi, N., Culver, G.M., 2010. Appropriate maturation and folding of 16S rRNA during 30S subunit biogenesis are critical for translational fidelity. *Proceedings of the National Academy of Sciences* 107, 4567–4572. <https://doi.org/10.1073/pnas.0912305107>
- Rozhdestvensky, T.S., Tang, T.H., Tchirkova, I.V., Brosius, J., Bachellerie, J.-P., Hüttnerhofer, A., 2003. Binding of L7Ae protein to the K-turn of archaeal snoRNAs: a shared RNA binding motif for C/D and H/ACA box snoRNAs in Archaea. *Nucleic Acids Res.* 31, 869–877. <https://doi.org/10.1093/nar/gkg175>
- Sá-Moura, B., Kornprobst, M., Kharde, S., Ahmed, Y.L., Stier, G., Kunze, R., Sinning, I., Hurt, E., 2017. Mpp10 represents a platform for the interaction of multiple factors within the 90S pre-ribosome. *PLoS ONE* 12, e0183272. <https://doi.org/10.1371/journal.pone.0183272>
- Sanghai, Z.A., Miller, L., Molloy, K.R., Barandun, J., Hunziker, M., Chaker-Margot, M., Wang, J., Chait, B.T., Klinge, S., 2018. Modular assembly of the nucleolar pre-60S ribosomal subunit. *Nature* 556, 126–129. <https://doi.org/10.1038/nature26156>
- Santama, N., Ogg, S.C., Malekkou, A., Zographos, S.E., Weis, K., Lamond, A.I., 2005. Characterization of hCINAP, a novel coilin-interacting protein encoded by a transcript from the transcription factor TAFII32 locus. *J. Biol. Chem.* 280, 36429–36441. <https://doi.org/10.1074/jbc.M501982200>
- Sas-Chen, A., Thomas, J.M., Matzov, D., Taoka, M., Nance, K.D., Nir, R., Bryson, K.M., Shachar, R., Liman, G.L.S., Burkhart, B.W., Gamage, S.T., Nobe, Y., Briney, C.A., Levy, M.J., Fuchs, R.T., Robb, G.B., Hartmann, J., Sharma, S., Lin, Q., Florens, L., Washburn, M.P., Isobe, T., Santangelo, T.J., Shalev-Benami, M., Meier, J.L., Schwartz, S., 2020. Dynamic

- RNA acetylation revealed by quantitative cross-evolutionary mapping. *Nature* 583, 638–643. <https://doi.org/10.1038/s41586-020-2418-2>
- Sato, K., Kato, Y., Hamada, M., Akutsu, T., Asai, K., 2011. IPknot: fast and accurate prediction of RNA secondary structures with pseudoknots using integer programming. *Bioinformatics* 27, i85–93. <https://doi.org/10.1093/bioinformatics/btr215>
- Scaiola, A., Peña, C., Weisser, M., Böhringer, D., Leibundgut, M., Klingauf-Nerurkar, P., Gerhardy, S., Panse, V.G., Ban, N., 2018. Structure of a eukaryotic cytoplasmic pre-40S ribosomal subunit. *EMBO J* 37. <https://doi.org/10.15252/embj.201798499>
- Schäfer, T., Strauß, D., Petfalski, E., Tollervey, D., Hurt, E., 2003. The path from nucleolar 90S to cytoplasmic 40S pre-ribosomes. *The EMBO Journal* 22, 1370–1380. <https://doi.org/10.1093/emboj/cdg121>
- Scherrer, K., Darnell, J.E., 1962. Sedimentation characteristics of rapidly labelled RNA from HeLa cells. *Biochem. Biophys. Res. Commun.* 7, 486–490. [https://doi.org/10.1016/0006-291x\(62\)90341-8](https://doi.org/10.1016/0006-291x(62)90341-8)
- Schiller, H., Schulze, S., Mutan, Z., de Vault, C., Runcie, C., Schwartz, J., Rados, T., Bisson Filho, A.W., Pohlschroder, M., 2020. *Haloferax volcanii* immersed liquid biofilms develop independently of known biofilm machineries and exhibit rapid honeycomb pattern formation (preprint). *Microbiology*. <https://doi.org/10.1101/2020.07.18.206797>
- Schlegel, H.G., Zaborosch, C., 1992. *Allgemeine Mikrobiologie: 41 Tabellen*, 7., überarb. Aufl. ed, Flexibles Taschenbuch Bio. Thieme, Stuttgart.
- Schluckebier, G., Zhong, P., Stewart, K.D., Kavanaugh, T.J., Abad-Zapatero, C., 1999. The 2.2 Å structure of the rRNA methyltransferase ErmC' and its complexes with cofactor and cofactor analogs: implications for the reaction mechanism. *Journal of Molecular Biology* 289, 277–291. <https://doi.org/10.1006/jmbi.1999.2788>
- Schnare, M.N., Gray, M.W., 2011. Complete Modification Maps for the Cytosolic Small and Large Subunit rRNAs of *Euglena gracilis*: Functional and Evolutionary Implications of Contrasting Patterns between the Two rRNA Components. *Journal of Molecular Biology* 413, 66–83. <https://doi.org/10.1016/j.jmb.2011.08.037>
- Schulze, S., Adams, Z., Cerletti, M., De Castro, R., Ferreira-Cerca, S., Fufezan, C., Giménez, M.I., Hippler, M., Jevtic, Z., Knüppel, R., Legerme, G., Lenz, C., Marchfelder, A., Maupin-Furlow, J., Paggi, R.A., Pfeiffer, F., Poetsch, A., Urlaub, H., Pohlschroder, M., 2020. The Archaeal Proteome Project advances knowledge about archaeal cell biology through comprehensive proteomics. *Nat Commun* 11, 3145. <https://doi.org/10.1038/s41467-020-16784-7>
- Schuwirth, B.S., Day, J.M., Hau, C.W., Janssen, G.R., Dahlberg, A.E., Cate, J.H.D., Vila-Sanjurjo, A., 2006. Structural analysis of kasugamycin inhibition of translation. *Nat. Struct. Mol. Biol.* 13, 879–886. <https://doi.org/10.1038/nsmb1150>
- Schwanhäusser, B., Busse, D., Li, N., Dittmar, G., Schuchhardt, J., Wolf, J., Chen, W., Selbach, M., 2011. Global quantification of mammalian gene expression control. *Nature* 473, 337–342. <https://doi.org/10.1038/nature10098>
- Seistrup, K.H., Rose, S., Birkedal, U., Nielsen, H., Huber, H., Douthwaite, S., 2016. Bypassing rRNA methylation by RsmA/Dim1 during ribosome maturation in the hyperthermophilic archaeon *Nanoarchaeum equitans*. *Nucl. Acids Res.* gkw839. <https://doi.org/10.1093/nar/gkw839>
- Sengupta, J., Bussiere, C., Pallesen, J., West, M., Johnson, A.W., Frank, J., 2010. Characterization of the nuclear export adaptor protein Nmd3 in association with the 60S ribosomal subunit. *J Cell Biol* 189, 1079–1086. <https://doi.org/10.1083/jcb.201001124>
- Sergiev, P.V., Golovina, A.Y., Sergeeva, O.V., Osterman, I.A., Nesterchuk, M.V., Bogdanov, A.A., Dontsova, O.A., 2012. How much can we learn about the function of bacterial rRNA modification by mining large-scale experimental datasets? *Nucleic Acids Research* 40, 5694–5705. <https://doi.org/10.1093/nar/gks219>
- Sharma, I.M., Woodson, S.A., 2020. RbfA and IF3 couple ribosome biogenesis and translation initiation to increase stress tolerance. *Nucleic Acids Res.* 48, 359–372. <https://doi.org/10.1093/nar/gkz1065>
- Sharma, M.R., Barat, C., Wilson, D.N., Booth, T.M., Kawazoe, M., Hori-Takemoto, C., Shirouzu, M., Yokoyama, S., Fucini, P., Agrawal, R.K., 2005. Interaction of Era with the 30S

- ribosomal subunit implications for 30S subunit assembly. *Mol. Cell* 18, 319–329. <https://doi.org/10.1016/j.molcel.2005.03.028>
- Sharma, S., Hartmann, J.D., Watzinger, P., Klepper, A., Peifer, C., Kötter, P., Lafontaine, D.L.J., Entian, K.-D., 2018. A single N1-methyladenosine on the large ribosomal subunit rRNA impacts locally its structure and the translation of key metabolic enzymes. *Sci Rep* 8, 11904. <https://doi.org/10.1038/s41598-018-30383-z>
- Shen, H., Stoute, J., Liu, K.F., 2020. Structural and catalytic roles of the human 18S rRNA methyltransferases DIMT1 in ribosome assembly and translation. *J. Biol. Chem.* <https://doi.org/10.1074/jbc.RA120.014236>
- Siibak, T., Remme, J., 2010. Subribosomal particle analysis reveals the stages of bacterial ribosome assembly at which rRNA nucleotides are modified. *RNA* 16, 2023–2032. <https://doi.org/10.1261/rna.2160010>
- Sloan, K.E., Knox, A.A., Wells, G.R., Schneider, C., Watkins, N.J., 2019. Interactions and activities of factors involved in the late stages of human 18S rRNA maturation. *RNA Biology* 16, 196–210. <https://doi.org/10.1080/15476286.2018.1564467>
- Sloan, K.E., Warda, A.S., Sharma, S., Entian, K.-D., Lafontaine, D.L.J., Bohnsack, M.T., 2016. Tuning the ribosome: The influence of rRNA modification on eukaryotic ribosome biogenesis and function. *RNA Biol* 14, 1138–1152. <https://doi.org/10.1080/15476286.2016.1259781>
- Smith, B.A., Gupta, N., Denny, K., Culver, G.M., 2018. Characterization of 16S rRNA Processing with Pre-30S Subunit Assembly Intermediates from *E. coli*. *J. Mol. Biol.* 430, 1745–1759. <https://doi.org/10.1016/j.jmb.2018.04.009>
- Smola, M.J., Weeks, K.M., 2018. In-cell RNA structure probing with SHAPE-MaP. *Nat Protoc* 13, 1181–1195. <https://doi.org/10.1038/nprot.2018.010>
- Song, W.-S., Lee, M., Lee, K., 2011. RNase G participates in processing of the 5'-end of 23S ribosomal RNA. *J. Microbiol.* 49, 508–511. <https://doi.org/10.1007/s12275-011-1198-7>
- Sowers, K.R., Schreier, H.J., 1999. Gene transfer systems for the Archaea. *Trends in Microbiology* 7, 212–219. [https://doi.org/10.1016/S0966-842X\(99\)01492-4](https://doi.org/10.1016/S0966-842X(99)01492-4)
- Spang, A., Saw, J.H., Jørgensen, S.L., Zaremba-Niedzwiedzka, K., Martijn, J., Lind, A.E., van Eijk, R., Schleper, C., Guy, L., Ettema, T.J.G., 2015. Complex archaea that bridge the gap between prokaryotes and eukaryotes. *Nature* 521, 173–179. <https://doi.org/10.1038/nature14447>
- Spitale, R.C., Crisalli, P., Flynn, R.A., Torre, E.A., Kool, E.T., Chang, H.Y., 2013. RNA SHAPE analysis in living cells. *Nat Chem Biol* 9, 18–20. <https://doi.org/10.1038/nchembio.1131>
- Stachler, A.-E., Marchfelder, A., 2016. Gene Repression in Haloarchaea Using the CRISPR (Clustered Regularly Interspaced Short Palindromic Repeats)-Cas I-B System. *J. Biol. Chem.* 291, 15226–15242. <https://doi.org/10.1074/jbc.M116.724062>
- Stage-Zimmermann, T., Schmidt, U., Silver, P.A., 2000. Factors affecting nuclear export of the 60S ribosomal subunit in vivo. *Molecular Biology of the Cell* 11, 3777–3789.
- Steffen, K.K., McCormick, M.A., Pham, K.M., MacKay, V.L., Delaney, J.R., Murakami, C.J., Kaerberlein, M., Kennedy, B.K., 2012. Ribosome deficiency protects against ER stress in *Saccharomyces cerevisiae*. *Genetics* 191, 107–118. <https://doi.org/10.1534/genetics.111.136549>
- Stroud, A., Liddell, S., Allers, T., 2012. Genetic and Biochemical Identification of a Novel Single-Stranded DNA-Binding Complex in *Haloferax volcanii*. *Front. Microbio.* 3. <https://doi.org/10.3389/fmicb.2012.00224>
- Strunk, B.S., Loucks, C.R., Su, M., Vashisth, H., Cheng, S., Schilling, J., Brooks, C.L., Karbstein, K., Skiniotis, G., 2011. Ribosome Assembly Factors Prevent Premature Translation Initiation by 40S Assembly Intermediates. *Science* 333, 1449–1453. <https://doi.org/10.1126/science.1208245>
- Strunk, B.S., Novak, M.N., Young, C.L., Karbstein, K., 2012a. A translation-like cycle is a quality control checkpoint for maturing 40S ribosome subunits. *Cell* 150, 111–121. <https://doi.org/10.1016/j.cell.2012.04.044>
- Strunk, B.S., Novak, M.N., Young, C.L., Karbstein, K., 2012b. Joining of 60S subunits and a translation-like cycle in 40S ribosome maturation. *Cell* 150, 111–121. <https://doi.org/10.1016/j.cell.2012.04.044>

- Stupar, D.Z., Bajic, J.S., Joza, A.V., Dakic, B.M., Slankamenac, M.P., Zivanov, M.B., Cibula, E., 2012. Remote monitoring of water salinity by using side-polished fiber-optic U-shaped sensor, in: 2012 15th International Power Electronics and Motion Control Conference (EPE/PEMC). Presented at the 2012 EPE-ECCE Europe Congress, IEEE, Novi Sad, Serbia, p. LS4c.4-1-LS4c.4-5. <https://doi.org/10.1109/EPEPEMC.2012.6397458>
- Sulthana, S., Deutscher, M.P., 2013. Multiple Exoribonucleases Catalyze Maturation of the 3' Terminus of 16S Ribosomal RNA (rRNA). *J Biol Chem* 288, 12574–12579. <https://doi.org/10.1074/jbc.C113.459172>
- Summer, S., Smirnova, A., Gabriele, A., Toth, U., Fasemore, A.M., Förstner, K.U., Kuhn, L., Chicher, J., Hammann, P., Mitulović, G., Entelis, N., Tarassov, I., Rossmann, W., Smirnov, A., 2020. YBEY is an essential biogenesis factor for mitochondrial ribosomes. *Nucleic Acids Res.* <https://doi.org/10.1093/nar/gkaa148>
- Sun, Q., Zhu, X., Qi, J., An, W., Lan, P., Tan, D., Chen, R., Wang, B., Zheng, S., Zhang, C., Chen, X., Zhang, W., Chen, J., Dong, M.-Q., Ye, K., 2017. Molecular architecture of the 90S small subunit pre-ribosome. *Elife* 6. <https://doi.org/10.7554/eLife.22086>
- Sun, Y., Liu, Y., Pan, J., Wang, F., Li, M., 2020. Perspectives on Cultivation Strategies of Archaea. *Microb Ecol* 79, 770–784. <https://doi.org/10.1007/s00248-019-01422-7>
- Swiatkowska, A., Wlotzka, W., Tuck, A., Barrass, J.D., Beggs, J.D., Tollervey, D., 2012. Kinetic analysis of pre-ribosome structure in vivo. *RNA* 18, 2187–2200. <https://doi.org/10.1261/rna.034751.112>
- Synowiecki, J., Grzybowska, B., Zdziebło, A., 2006. Sources, Properties and Suitability of New Thermostable Enzymes in Food Processing. *Critical Reviews in Food Science and Nutrition* 46, 197–205. <https://doi.org/10.1080/10408690590957296>
- Takahashi, M.K., Watters, K.E., Gasper, P.M., Abbott, T.R., Carlson, P.D., Chen, A.A., Lucks, J.B., 2016. Using in-cell SHAPE-Seq and simulations to probe structure–function design principles of RNA transcriptional regulators. *RNA* 22, 920–933. <https://doi.org/10.1261/rna.054916.115>
- Talkington, M.W.T., Siuzdak, G., Williamson, J.R., 2005. An assembly landscape for the 30S ribosomal subunit. *Nature* 438, 628–632. <https://doi.org/10.1038/nature04261>
- Talkish, J., May, G., Lin, Y., Woolford, J.L., McManus, C.J., 2014. Mod-seq: high-throughput sequencing for chemical probing of RNA structure. *RNA* 20, 713–720. <https://doi.org/10.1261/rna.042218.113>
- Tamm, T., Kisly, I., Remme, J., 2019. Functional Interactions of Ribosomal Intersubunit Bridges in *Saccharomyces cerevisiae*. *Genetics* 213, 1329–1339. <https://doi.org/10.1534/genetics.119.302777>
- Tan, Z.-J., Chen, S.-J., 2011. Salt contribution to RNA tertiary structure folding stability. *Biophys. J.* 101, 176–187. <https://doi.org/10.1016/j.bpj.2011.05.050>
- Tang, T.H., Rozhdestvensky, T.S., d'Orval, B.C., Bortolin, M.-L., Huber, H., Charpentier, B., Branlant, C., Bachellerie, J.-P., Brosius, J., Hüttenhofer, A., 2002. RNomics in Archaea reveals a further link between splicing of archaeal introns and rRNA processing. *Nucleic Acids Res.* 30, 921–930.
- Thammana, P., Held, W.A., 1974. Methylation of 16S RNA during ribosome assembly in vitro. *Nature* 251, 682–686. <https://doi.org/10.1038/251682a0>
- The Ban Lab ETH Zurich [WWW Document], 2020. . Eukaryotic Cytosolic Ribosomes. URL https://bangroup.ethz.ch/research/eukaryotic_ribosome.html (accessed 3.31.20).
- Theobald, D.L., 2010. A formal test of the theory of universal common ancestry. *Nature* 465, 219–222. <https://doi.org/10.1038/nature09014>
- Thompson, N.L., Burghardt, T.P., Axelrod, D., 1981. Measuring surface dynamics of biomolecules by total internal reflection fluorescence with photobleaching recovery or correlation spectroscopy. *Biophys. J.* 33, 435–454. [https://doi.org/10.1016/S0006-3495\(81\)84905-3](https://doi.org/10.1016/S0006-3495(81)84905-3)
- Thomson, E., Ferreira-Cerca, S., Hurt, E., 2013. Eukaryotic ribosome biogenesis at a glance. *J. Cell. Sci.* 126, 4815–4821. <https://doi.org/10.1242/jcs.111948>
- Thomson, E., Tollervey, D., 2010. The Final Step in 5.8S rRNA Processing Is Cytoplasmic in *Saccharomyces cerevisiae*. *MCB* 30, 976–984. <https://doi.org/10.1128/MCB.01359-09>

- Thore, S., Mayer, C., Sauter, C., Weeks, S., Suck, D., 2003. Crystal structures of the *Pyrococcus abyssi* Sm core and its complex with RNA. Common features of RNA binding in archaea and eukarya. *J. Biol. Chem.* 278, 1239–1247. <https://doi.org/10.1074/jbc.M207685200>
- Thurlow, B., Davis, J.H., Leong, V., Moraes, T.F., Williamson, J.R., Ortega, J., 2016. Binding properties of YjeQ (RsgA), RbfA, RimM and Era to assembly intermediates of the 30S subunit. *Nucleic Acids Res.* 44, 9918–9932. <https://doi.org/10.1093/nar/gkw613>
- Toh, S.-M., Xiong, L., Bae, T., Mankin, A.S., 2008. The methyltransferase YfgB/RlmN is responsible for modification of adenosine 2503 in 23S rRNA. *RNA* 14, 98–106. <https://doi.org/10.1261/rna.814408>
- Tokuhiya, J.G., Vijayan, P., Feldmann, K.A., Browse, J.A., 1998. Chloroplast development at low temperatures requires a homolog of DIM1, a yeast gene encoding the 18S rRNA dimethylase. *Plant Cell* 10, 699–711. <https://doi.org/10.1105/tpc.10.5.699>
- Tomecki, R., Labno, A., Drakowska, K., Cysewski, D., Dziembowski, A., 2015. hUTP24 is essential for processing of the human rRNA precursor at site A₁, but not at site A₀. *RNA Biology* 12, 1010–1029. <https://doi.org/10.1080/15476286.2015.1073437>
- Trapman, J., Planta, R.J., 1975. Detailed analysis of the ribosomal RNA synthesis in yeast. *Biochim. Biophys. Acta* 414, 115–125. [https://doi.org/10.1016/0005-2787\(75\)90214-2](https://doi.org/10.1016/0005-2787(75)90214-2)
- Trapman, J., Retèl, J., Planta, R.J., 1975. Ribosomal precursor particles from yeast. *Exp. Cell Res.* 90, 95–104.
- Traub, P., Nomura, M., 1968. Structure and function of *E. coli* ribosomes. V. Reconstitution of functionally active 30S ribosomal particles from RNA and proteins. *Proc. Natl. Acad. Sci. U.S.A.* 59, 777–784.
- Tschochner, H., Hurt, E., 2003. Pre-ribosomes on the road from the nucleolus to the cytoplasm. *Trends Cell Biol.* 13, 255–263.
- Tu, C., Zhou, X., Tarasov, S.G., Tropea, J.E., Austin, B.P., Waugh, D.S., Court, D.L., Ji, X., 2011. The Era GTPase recognizes the GAUCACCUCC sequence and binds helix 45 near the 3' end of 16S rRNA. *Proceedings of the National Academy of Sciences* 108, 10156–10161. <https://doi.org/10.1073/pnas.1017679108>
- Turowski, T.W., Lebaron, S., Zhang, E., Peil, L., Dudnakova, T., Petfalski, E., Granneman, S., Rappsilber, J., Tollervey, D., 2014. Rio1 mediates ATP-dependent final maturation of 40S ribosomal subunits. *Nucleic Acids Res.* 42, 12189–12199. <https://doi.org/10.1093/nar/gku878>
- Turowski, T.W., Tollervey, D., 2015. Cotranscriptional events in eukaryotic ribosome synthesis. *Wiley Interdiscip Rev RNA* 6, 129–139. <https://doi.org/10.1002/wrna.1263>
- Uicker, W.C., Schaefer, L., Britton, R.A., 2006. The essential GTPase RbgA (YlqF) is required for 50S ribosome assembly in *Bacillus subtilis*. *Mol. Microbiol.* 59, 528–540. <https://doi.org/10.1111/j.1365-2958.2005.04948.x>
- Van Buul, C.P., Hamersma, M., Visser, W., Van Knippenberg, P.H., 1984. Partial methylation of two adjacent adenosines in ribosomes from *Euglena gracilis* chloroplasts suggests evolutionary loss of an intermediate stage in the methyl-transfer reaction. *Nucleic Acids Res* 12, 9205–9208.
- van Buul, C.P.J.J., Visser, W., van Knippenberg, P.H., 1984. Increased translational fidelity caused by the antibiotic kasugamycin and ribosomal ambiguity in mutants harbouring the *ksgA* gene. *FEBS Letters* 177, 119–124. [https://doi.org/10.1016/0014-5793\(84\)80994-1](https://doi.org/10.1016/0014-5793(84)80994-1)
- Van Charldorp, R., Heus, H.A., Van Knippenberg, P.H., Joordens, J., De Bruin, S.H., Hilbers, C.W., 1981. Destabilization of secondary structure in 16S ribosomal RNA by dimethylation of two adjacent adenosines. *Nucleic Acids Res.* 9, 4413–4422. <https://doi.org/10.1093/nar/9.17.4413>
- Van Knippenberg, P.H., Van Kimmenade, J.M.A., Heus, H.A., 1984. Phylogeny of the conserved 3' terminal structure of the RNA of small ribosomal subunits. *Nucl Acids Res* 12, 2595–2604. <https://doi.org/10.1093/nar/12.6.2595>
- Vanrobays, E., 2004. Dim2p, a KH-domain protein required for small ribosomal subunit synthesis. *RNA* 10, 645–656. <https://doi.org/10.1261/rna.5162204>
- Vanrobays, E., Gelugne, J.-P., Gleizes, P.-E., Caizergues-Ferrer, M., 2003. Late Cytoplasmic Maturation of the Small Ribosomal Subunit Requires RIO Proteins in *Saccharomyces*

- cerevisiae. *Mol. Cell. Biol.* 23, 2083–2095. <https://doi.org/10.1128/MCB.23.6.2083-2095.2003>
- Veith, T., Martin, R., Wurm, J.P., Weis, B.L., Duchardt-Ferner, E., Safferthal, C., Hennig, R., Mirus, O., Bohnsack, M.T., Wöhnert, J., Schleiff, E., 2012. Structural and functional analysis of the archaeal endonuclease Nob1. *Nucl. Acids Res.* 40, 3259–3274. <https://doi.org/10.1093/nar/gkr1186>
- Veldman, G.M., Klootwijk, J., van Heerikhuizen, H., Planta, R.J., 1981. The nucleotide sequence of the intergenic region between the 5.8S and 26S rRNA genes of the yeast ribosomal RNA operon. Possible implications for the interaction between 5.8S and 26S rRNA and the processing of the primary transcript. *Nucl Acids Res* 9, 4847–4862. <https://doi.org/10.1093/nar/9.19.4847>
- Venema, J., Tollervey, D., 1995. Processing of pre-ribosomal RNA in *Saccharomyces cerevisiae*. *Yeast* 11, 1629–1650. <https://doi.org/10.1002/yea.320111607>
- Vercruyssen, M., Köhrer, C., Shen, Y., Proulx, S., Ghosal, A., Davies, B.W., RajBhandary, U.L., Walker, G.C., 2016. Identification of YbeY-Protein Interactions Involved in 16S rRNA Maturation and Stress Regulation in *Escherichia coli*. *mBio* 7, e01785-16. <https://doi.org/10.1128/mBio.01785-16>
- Vesper, O., Amitai, S., Belitsky, M., Byrgazov, K., Kaberdina, A.C., Engelberg-Kulka, H., Moll, I., 2011. Selective Translation of Leaderless mRNAs by Specialized Ribosomes Generated by MazF in *Escherichia coli*. *Cell* 147, 147–157. <https://doi.org/10.1016/j.cell.2011.07.047>
- Vierbuchen, T., Bang, C., Rosigkeit, H., Schmitz, R.A., Heine, H., 2017. The Human-Associated Archaeon *Methanosphaera stadtmanae* Is Recognized through Its RNA and Induces TLR8-Dependent NLRP3 Inflammasome Activation. *Front. Immunol.* 8, 1535. <https://doi.org/10.3389/fimmu.2017.01535>
- Vila-Sanjurjo, A., Dahlberg, A.E., 2001. Mutational analysis of the conserved bases C1402 and A1500 in the center of the decoding domain of *Escherichia coli* 16 S rRNA reveals an important tertiary interaction. *J. Mol. Biol.* 308, 457–463. <https://doi.org/10.1006/jmbi.2001.4576>
- Vila-Sanjurjo, A., Squires, C.L., Dahlberg, A.E., 1999. Isolation of kasugamycin resistant mutants in the 16 S ribosomal RNA of *Escherichia coli*. *Journal of Molecular Biology* 293, 1–8. <https://doi.org/10.1006/jmbi.1999.3160>
- Vogel, A., Schilling, O., Späth, B., Marchfelder, A., 2005. The tRNase Z family of proteins: physiological functions, substrate specificity and structural properties. *Biological Chemistry* 386. <https://doi.org/10.1515/BC.2005.142>
- Voss, N.R., Gerstein, M., Steitz, T.A., Moore, P.B., 2006. The Geometry of the Ribosomal Polypeptide Exit Tunnel. *Journal of Molecular Biology* 360, 893–906. <https://doi.org/10.1016/j.jmb.2006.05.023>
- Waegel, I., Schmid, G., Thumann, S., Thomm, M., Hausner, W., 2010. Shuttle Vector-Based Transformation System for *Pyrococcus furiosus*. *Appl Environ Microbiol* 76, 3308–3313. <https://doi.org/10.1128/AEM.01951-09>
- Wagner, M., van Wolferen, M., Wagner, A., Lassak, K., Meyer, B.H., Reimann, J., Albers, S.-V., 2012. Versatile Genetic Tool Box for the Crenarchaeote *Sulfolobus acidocaldarius*. *Front Microbiol* 3, 214. <https://doi.org/10.3389/fmicb.2012.00214>
- Wang, S., Wang, J., Zhang, Xiaoe, Fu, B., Song, Y., Ma, P., Gu, K., Zhou, Xin, Zhang, Xiaolian, Tian, T., Zhou, Xiang, 2016. N⁶-Methyladenine hinders RNA- and DNA-directed DNA synthesis: application in human rRNA methylation analysis of clinical specimens. *Chem. Sci.* 7, 1440–1446. <https://doi.org/10.1039/C5SC02902C>
- Wang, X.D., Padgett, R.A., 1989. Hydroxyl radical “footprinting” of RNA: application to pre-mRNA splicing complexes. *Proc. Natl. Acad. Sci. U.S.A.* 86, 7795–7799. <https://doi.org/10.1073/pnas.86.20.7795>
- Warner, J.R., 1999. The economics of ribosome biosynthesis in yeast. *Trends Biochem. Sci.* 24, 437–440. [https://doi.org/10.1016/s0968-0004\(99\)01460-7](https://doi.org/10.1016/s0968-0004(99)01460-7)
- Waters, E., Hohn, M.J., Ahel, I., Graham, D.E., Adams, M.D., Barnstead, M., Beeson, K.Y., Bibbs, L., Bolanos, R., Keller, M., Kretz, K., Lin, X., Mathur, E., Ni, J., Podar, M., Richardson, T., Sutton, G.G., Simon, M., Soll, D., Stetter, K.O., Short, J.M., Noordewier, M., 2003. The genome of *Nanoarchaeum equitans*: insights into early archaeal evolution and derived

- parasitism. *Proc. Natl. Acad. Sci. U.S.A.* 100, 12984–12988. <https://doi.org/10.1073/pnas.1735403100>
- Watters, K.E., Yu, A.M., Strobel, E.J., Settle, A.H., Lucks, J.B., 2016. Characterizing RNA structures in vitro and in vivo with selective 2'-hydroxyl acylation analyzed by primer extension sequencing (SHAPE-Seq). *Methods* 103, 34–48. <https://doi.org/10.1016/j.ymeth.2016.04.002>
- Waudby, C.A., Launay, H., Cabrita, L.D., Christodoulou, J., 2013. Protein folding on the ribosome studied using NMR spectroscopy. *Progress in Nuclear Magnetic Resonance Spectroscopy* 74, 57–75. <https://doi.org/10.1016/j.pnmrs.2013.07.003>
- Weeks, K.M., 2010. Advances in RNA structure analysis by chemical probing. *Curr. Opin. Struct. Biol.* 20, 295–304. <https://doi.org/10.1016/j.sbi.2010.04.001>
- Weeks, K.M., Mauger, D.M., 2011. Exploring RNA Structural Codes with SHAPE Chemistry. *Acc Chem Res* 44, 1280–1291. <https://doi.org/10.1021/ar200051h>
- Weichmann, F., Hett, R., Schepers, A., Ito-Kureha, T., Flatley, A., Slama, K., Hastert, F., Angstmann, N., Cardoso, C.M., König, J., huettelmaier, stefan, Dieterich, C., Canzar, S., Helm, M., Heissmeyer, V., Feederle, R., Meister, G., 2020. Validation strategies for antibodies targeting modified ribonucleotides. *RNA* rna.076026.120. <https://doi.org/10.1261/rna.076026.120>
- Weisblum, B., 1995. Erythromycin resistance by ribosome modification. *Antimicrobial Agents and Chemotherapy* 39, 577–585. <https://doi.org/10.1128/AAC.39.3.577>
- Wells, G.R., Weichmann, F., Colvin, D., Sloan, K.E., Kudla, G., Tollervey, D., Watkins, N.J., Schneider, C., 2016. The PIN domain endonuclease Utp24 cleaves pre-ribosomal RNA at two coupled sites in yeast and humans. *Nucleic Acids Res* 44, 5399–5409. <https://doi.org/10.1093/nar/gkw213>
- Widmann, B., Wandrey, F., Badertscher, L., Wyler, E., Pfannstiel, J., Zemp, I., Kutay, U., 2012. The kinase activity of human Rio1 is required for final steps of cytoplasmic maturation of 40S subunits. *Mol. Biol. Cell* 23, 22–35. <https://doi.org/10.1091/mbc.E11-07-0639>
- Wilkinson, K.A., Gorelick, R.J., Vasa, S.M., Guex, N., Rein, A., Mathews, D.H., Giddings, M.C., Weeks, K.M., 2008. High-throughput SHAPE analysis reveals structures in HIV-1 genomic RNA strongly conserved across distinct biological states. *PLoS Biol.* 6, e96. <https://doi.org/10.1371/journal.pbio.0060096>
- Willkomm, S., Zander, A., Grohmann, D., 2017. Site-Specific Fluorescent Labeling of Argonaute for FRET-Based Bio-Assays. *Methods Mol. Biol.* 1517, 291–304. https://doi.org/10.1007/978-1-4939-6563-2_20
- Wilson, D.N., Nierhaus, K.H., 2007. The Weird and Wonderful World of Bacterial Ribosome Regulation. *Critical Reviews in Biochemistry and Molecular Biology* 42, 187–219. <https://doi.org/10.1080/10409230701360843>
- Wilson, D.N., Nierhaus, K.H., 2005. Ribosomal proteins in the spotlight. *Crit. Rev. Biochem. Mol. Biol.* 40, 243–267. <https://doi.org/10.1080/10409230500256523>
- Woese, C.R., 1994. There must be a prokaryote somewhere: microbiology's search for itself. *Microbiol. Rev.* 58, 1–9.
- Woese, C.R., Fox, G.E., 1977. Phylogenetic structure of the prokaryotic domain: the primary kingdoms. *Proceedings of the National Academy of Sciences of the United States of America* 74, 5088.
- Woese, C.R., Kandler, O., Wheelis, M.L., 1990. Towards a natural system of organisms: proposal for the domains Archaea, Bacteria, and Eucarya. *Proceedings of the National Academy of Sciences of the United States of America* 87, 4576.
- Woolford, J.L., Baserga, S.J., 2013. Ribosome biogenesis in the yeast *Saccharomyces cerevisiae*. *Genetics* 195, 643–81. <https://doi.org/10.1534/genetics.113.153197>
- Woolfs, H.A., Lamanna, A.C., Karbstein, K., 2011. Roles of Dim2 in Ribosome Assembly. *J. Biol. Chem.* 286, 2578–2586. <https://doi.org/10.1074/jbc.M110.191494>
- Wurtzel, O., Sapra, R., Chen, F., Zhu, Y., Simmons, B.A., Sorek, R., 2010. A single-base resolution map of an archaeal transcriptome. *Genome Res.* 20, 133–141. <https://doi.org/10.1101/gr.100396.109>

- Xu, Y., Zhou, P., Tian, X., 1999. Characterization of two novel haloalkaliphilic archaea *Natronorubrum bangense* gen. nov., sp. nov. and *Natronorubrum tibetense* gen. nov., sp. nov. *Int. J. Syst. Bacteriol.* 49 Pt 1, 261–266. <https://doi.org/10.1099/00207713-49-1-261>
- Xu, Z., O'Farrell, H.C., Rife, J.P., Culver, G.M., 2008. A conserved rRNA methyltransferase regulates ribosome biogenesis. *Nat Struct Mol Biol* 15, 534–536. <https://doi.org/10.1038/nsmb.1408>
- Xue, S., 2006. RNA Recognition and Cleavage by a Splicing Endonuclease. *Science* 312, 906–910. <https://doi.org/10.1126/science.1126629>
- Yip, W.S.V., Vincent, N.G., Baserga, S.J., 2013. Ribonucleoproteins in archaeal pre-rRNA processing and modification. *Archaea* 2013, 614735. <https://doi.org/10.1155/2013/614735>
- Yoshida, K., Shoji, H., Niki, Y., Hanaki, H., Yanagisawa, C., Ikeda-Dantsuji, Y., Fukuchi, K., Adachi, M., 2009. Linezolid-resistant methicillin-resistant *Staphylococcus aureus* isolated after long-term, repeated use of linezolid. *Journal of Infection and Chemotherapy* 15, 417–419. <https://doi.org/10.1007/s10156-009-0727-3>
- Young, R.A., Steitz, J.A., 1978. Complementary sequences 1700 nucleotides apart form a ribonuclease III cleavage site in *Escherichia coli* ribosomal precursor RNA. *Proceedings of the National Academy of Sciences of the United States of America* 75, 3593.
- Youvan, D.C., Hearst, J.E., 1979. Reverse transcriptase pauses at N2-methylguanine during in vitro transcription of *Escherichia coli* 16S ribosomal RNA. *Proceedings of the National Academy of Sciences* 76, 3751–3754. <https://doi.org/10.1073/pnas.76.8.3751>
- Yuan, B.-F., 2017. Liquid Chromatography-Mass Spectrometry for Analysis of RNA Adenosine Methylation, in: Lusser, A. (Ed.), *RNA Methylation, Methods in Molecular Biology*. Springer New York, New York, NY, pp. 33–42. https://doi.org/10.1007/978-1-4939-6807-7_3
- Yusupova, G.Z., Yusupov, M.M., Cate, J.H., Noller, H.F., 2001. The path of messenger RNA through the ribosome. *Cell* 106, 233–241. [https://doi.org/10.1016/s0092-8674\(01\)00435-4](https://doi.org/10.1016/s0092-8674(01)00435-4)
- Yutin, N., Puigbò, P., Koonin, E.V., Wolf, Y.I., 2012. Phylogenomics of prokaryotic ribosomal proteins. *PLoS ONE* 7, e36972. <https://doi.org/10.1371/journal.pone.0036972>
- Zaremba-Niedzwiedzka, K., Caceres, E.F., Saw, J.H., Bäckström, D., Juzokaite, L., Vancaester, E., Seitz, K.W., Anantharaman, K., Starnawski, P., Kjeldsen, K.U., Stott, M.B., Nunoura, T., Banfield, J.F., Schramm, A., Baker, B.J., Spang, A., Ettema, T.J.G., 2017. Asgard archaea illuminate the origin of eukaryotic cellular complexity. *Nature* 541, 353–358. <https://doi.org/10.1038/nature21031>
- Zemp, I., Wild, T., O'Donohue, M.-F., Wandrey, F., Widmann, B., Gleizes, P.-E., Kutay, U., 2009. Distinct cytoplasmic maturation steps of 40S ribosomal subunit precursors require hRio2. *J Cell Biol* 185, 1167–1180. <https://doi.org/10.1083/jcb.200904048>
- Zhang, J., Harnpicharnchai, P., Jakovljevic, J., Tang, L., Guo, Y., Oeffinger, M., Rout, M.P., Hiley, S.L., Hughes, T., Woolford, J.L., 2007. Assembly factors Rpf2 and Rrs1 recruit 5S rRNA and ribosomal proteins rpL5 and rpL11 into nascent ribosomes. *Genes Dev.* 21, 2580–2592. <https://doi.org/10.1101/gad.1569307>
- Zhang, L., Wu, C., Cai, G., Chen, S., Ye, K., 2016. Stepwise and dynamic assembly of the earliest precursors of small ribosomal subunits in yeast. *Genes Dev.* 30, 718–732. <https://doi.org/10.1101/gad.274688.115>
- Zhong, P., Pratt, S.D., Edalji, R.P., Walter, K.A., Holzman, T.F., Shivakumar, A.G., Katz, L., 1995. Substrate requirements for ErmC' methyltransferase activity. *Journal of bacteriology* 177, 4327–4332. <https://doi.org/10.1128/JB.177.15.4327-4332.1995>
- Zhou, D., Zhu, X., Zheng, S., Tan, D., Dong, M.-Q., Ye, K., 2019. Cryo-EM structure of an early precursor of large ribosomal subunit reveals a half-assembled intermediate. *Protein Cell* 10, 120–130. <https://doi.org/10.1007/s13238-018-0526-7>
- Zhou, G.-J., Zhang, Y., Wang, J., Guo, J.-H., Ni, J., Zhong, Z.-M., Wang, L.-Q., Dang, Y.-J., Dai, J.-F., Yu, L., 2004. Cloning and characterization of a novel human RNA binding protein gene PNO1. *DNA Seq.* 15, 219–224. <https://doi.org/10.1080/10425170410001702159>
- Ziehler, W.A., Engelke, D.R., 2000. Probing RNA Structure with Chemical Reagents and Enzymes. *Current Protocols in Nucleic Acid Chemistry* 00, 6.1.1-6.1.21. <https://doi.org/10.1002/0471142700.nc0601s00>

- Zillig, W., 1991. Comparative biochemistry of Archaea and Bacteria. *Current Opinion in Genetics & Development* 1, 544–551. [https://doi.org/10.1016/S0959-437X\(05\)80206-0](https://doi.org/10.1016/S0959-437X(05)80206-0)
- Zorbas, C., Nicolas, E., Wacheul, L., Huvelle, E., Heurgué-Hamard, V., Lafontaine, D.L.J., 2015. The human 18S rRNA base methyltransferases DIMT1L and WBSCR22-TRMT112 but not rRNA modification are required for ribosome biogenesis. *Mol. Biol. Cell* 26, 2080–2095. <https://doi.org/10.1091/mbc.E15-02-0073>

12 PUBLICATIONS

- 2020 Knüppel, R.,** Fenk, M., Jüttner, M., Ferreira-Cerca, S., 2020.
In Vivo RNA Chemical Footprinting Analysis in Archaea, in: Heise, T. (Ed.), *RNA Chaperones, Methods in Molecular Biology*. Springer US, New York, NY, pp. 193–208
- Schulze, S., Adams, Z., Cerletti, M., De Castro, R., Ferreira-Cerca, S., Fufezan, C., Giménez, M.I., Hippler, M., Jevtic, Z., **Knüppel, R.**, Legerme, G., Lenz, C., Marchfelder, A., Maupin-Furlow, J., Paggi, R.A., Pfeiffer, F., Poetsch, A., Urlaub, H., Pohlschroder, M., 2020.
The Archaeal Proteome Project advances knowledge about archaeal cell biology through comprehensive proteomics. *Nat Commun* 11, 3145.
- 2019 Grünberger, F., Knüppel, R.,** Jüttner, M., Fenk, M., Borst, A., Reichelt, R., Hausner, W., Soppa, J., Ferreira-Cerca, S., Grohmann, D.
Nanopore-based native RNA sequencing provides insights into prokaryotic transcription, operon structures, rRNA maturation and modifications (preprint). *Microbiology*
- 2019 Ignatov, A., Lebius, C., Ignatov, T., Ivros, S., Knueppel, R.,** Papatthemelis, T., Ortmann, O., Eggemann, H., 2019.
Lymph node micrometastases and outcome of endometrial cancer. *Gynecologic Oncology* 154, 475–479
- 2019 Jüttner, M., Weiß, M., Ostheimer, N., Reglin, C., Kern, M., Knüppel, R.,** Ferreira-Cerca, S.
A versatile cis-acting element reporter system to study the function, maturation and stability of ribosomal RNA mutants in archaea. *Nucleic Acids Res*
- 2018 Knüppel, R.,** Christensen, R.H., Gray, F.C., Esser, D., Strauß, D., Medenbach, J., Siebers, B., MacNeill, S.A., LaRonde, N., Ferreira-Cerca, S.
Insights into the evolutionary conserved regulation of Rio ATPase activity. *Nucleic Acids Res.* 46, 1441–1456.
- 2017 Knüppel, R.,** Kuttenger, C., Ferreira-Cerca, S.
Toward Time-Resolved Analysis of RNA Metabolism in Archaea Using 4-Thiouracil. *Front. Microbiol.* 8.

13 DANKSAGUNG

Als erstes möchte ich mich bei allen bedanken die mir bei der Vervollständigung dieser Arbeit geholfen haben.

Mein erster und größter Dank gilt meinem Betreuer Sébastien der es seit dem ersten Praktikum vor 7 Jahren so lange mit mir ausgehalten hat! Ich habe in diesen vielen Jahren viel von dir gelernt, wissenschaftlich, wie menschlich und bin sehr froh über diese manchmal doch Anstrengende (dieser scheiß Binde Assay...) aber immer wieder Spaßige Zeit. Insbesondere die freundschaftlichen Momente die zwar häufig wieder in begeisterteren Wissenschafts(-politik) Diskussionen geendet sind haben mir viel bedeutet. Es muss ja nicht immer nur „Science“ sein! Cognac im Flugzeug, die verrückte Airbnb Geschichte in Montreal :-D, lange Abende auf Konferenzen, Hochzeit und noch so viel mehr. Das entgegengebrachte Vertrauen: „mach einfach mal, das kriegst du schon hin“, hat zwar manchmal etwas mehr Zeit verschlungen, aber wenn ich nicht weiter kam konnte ich immer fragen und Lösungen Diskutieren. Plus es hat sehr viel zum eigenständigen wissenschaftlichen Denken und Selbstvertrauen beigetragen, „so schwer kann das schon nicht sein“. Nach den Anfangsjahren gemeinsam im Labor, das viele rumprobieren und kennenlernen der neuen Organismen und der gemeinsame Musikgeschmack haben natürlich gut zusammengeschweißt und irgendwie wars dann doch komisch, als du zum „Award-Winning PD“ wurdest und nur noch vorm PC saßt. Dafür hat das viele vor dem PC sitzen nach vielem Hin und Her endlich zum heißersehten DFG Grant geführt!!! Vielen dank dafür, dass du dich immer für mich eingesetzt hast und mir diese Doktorarbeit ermöglicht hast! Vielen Dank, dass du mir immer bei meinen Anträgen und den Korrekturen der Arbeiten ausgiebig zur Seite gestanden hast! Ich wünsche Dir, Dani, Emma, Lilly und Mathilda für die Zukunft nur das Beste! Dass du in diesem, doch schwierigen Business, deine Ideen und Begeisterung nachhaltig und dauerhaft unterbringen kannst und weiter deine Arbeitsgruppen so leiten wirst, wie du das bisher mit den Archaea Gringos getan hast und tust!

Als nächstes gilt mein Dank natürlich, Herrn Prof. Dr. Herbert Tschochner, der mich an seinem Lehrstuhl promovieren lies und immer wieder Gelder für mich aufgetrieben hat damit ich diese Doktorarbeit bestreiten konnte. Neben dem wissenschaftlichen Mentorat möchte ich mich auch noch ausdrücklich für das Klettermentorat bedanken, dass mir die Furcht vor dem Seilklettern und der damit verbundenen Höhe genommen hat und dadurch ins Sport und Freizeit Repertoire aufgenommen wurde (wird aber leider für die Zeit in Hamburg etwas pausiert werden ... bis wir zurück in Bayern sind also nur Bouldern).

Bei Prof. Dr. Gunter Meister möchte ich mich dafür bedanken, dass er sich bereit erklärt hat, meine Arbeit als Zweitgutachter zu bewerten und dementsprechend auch Teil meines Prüfungskomitees zu sein.

Bei Prof. Dr. Dina Grohmann möchte ich mich als erstes für die Zusammenarbeit bedanken und die immer netten Gespräche in und außerhalb der Universität sowie an der Konferenz und dem Dinner in Wien. Aber natürlich auch dafür, dass sie im Rahmen dieser Arbeit als Drittprüferin im Prüfungskomitee bereitsteht!

Auch bei Prof. Dr. Klaus Grasser bedanke ich mich, dass er sofort zugesagt hat, als Ersatzprüfer in meinem Prüfungskomitee zu fungieren.

Bei Prof. Dr. Denis Lafontaine, dass er sich zu meinem Mentorat zur Doktorarbeit bereit erklärt hat und trotz Blitzeis Umstände sich für die Präsentation meiner Arbeit Zeit genommen hat, sowie auch in Kanada am Poster zu später Stunde sich die neuesten Erkenntnisse angehört und Diskutiert hat.

Als ein Teil der RiboNoc Gruppe möchte ich mich auch noch bei Achim, Jorge und Philipp bedanken die mit ihrem unendlichen (Literatur) Wissen zu gefühlt jeder Frage etwas hilfreiches Beitragen konnten.

Bei meinen „Partners in Crime“, mit denen ich das doch unübliche Vergnügen hatte fast gleichzeitig mit der Promotion anzufangen und auch fast gleichzeitig fertig zu werden möchte ich mich natürlich auch herzlichst bedanken! Christina (AKA Schmiddy, Schmiddsalicious, Schmiddsodian Rhapsody), Christopher und Fabian unzählbare eXpressos diverse Freitagabendfeierabendbiere Dult, Gäubodenfest (mieh...), Konferenzen (leider ohne Christopher in Kanada), haben die Laborzeit doch deutlich besser gemacht, das gemeinsame Leiden unter fehlgeschlagenen Experimenten sowieso. Ich kann mir keine besseren Mitdoktoranden vorstellen! Die vielen Jahren im (gefühl) selben Büro haben zusammengeschweißt und insbesondere die Gemeinsamkeiten als Kinder vom Land bleiben mir in wohliger Erinnerung. Die gemeinsamen Boulderabende, wo sich jeder gegenseitig zu Höchstleistung motiviert hat (wie im Labor natürlich auch). Ich hoffe unsere „Nachfolger“ Kathi, Katha, Nicolas, Sebastian, Maresa und Simon werden die Zeit genauso nutzen wie wir und dadurch gut durch den Dschungel der Doktorarbeit und des Labors finden. Ich wünsche euch alles gute und bin froh, dass wir z.T. doch viel Überlapp hatten und schon die ein oder andere Weihnachts und Grillfeier zusammen hatten!

Meinem Laborkollegen und Archaea Gringo Michael (MJ oder Coach) möchte ich auch nochmal separat danken da wir ja doch sehr, sehr viel Zeit zusammen an der Bench und darüber hinaus verbracht haben. Irgendwie kennengelernt in Berlin dann als Praktikant wieder kennengelernt was dann zum Glück zu einer prämierten Masterarbeit und folgenden Doktorarbeit führte. Ich hoffe ich konnte dir ein paar archaeele weißheiten mitgeben, die dir in der verbleibenden Doktorarbeit weiterhelfen. Wenn ich mir eine Sache wünschen darf: halt die Musikalische Woche am Leben (sobald der PC wieder da ist...). Vielen Dank für die vermittelte Boulder- und Kletterbegeisterung, wird auf jeden Fall im Norden fortgeführt und bei Besuchen in Regensburg oder auch in Corona freien Kletterurlaube? Vielen Dank für deine Motivationskünste und Durchhalteparolen am Fels, Kletterwand, an der Bench (ich wiederhole mich ... schieß Binde Assay) und am Schreibtisch! Danke für das durchlesen und die peniblen Korrekturvorschläge! Auch wenn wir manchmal nicht einer Meinung waren, lobe ich weiterhin unsere ausgeprägte, aber faire Diskussions- und Streitkultur! Podcast incoming!

Meinem externen Archaea Gringo Felix Grünberger in der Mikrobiologie möchte auch danken für die viele Bioinformatische Hilfe, Freundschaft, diverse Biere in der Abendsonne verteilt über die Stufen Regensburgs, hervorragende Ideen im Kloster zur Lösung Regensburger Verkehrsprobleme, Kaffee Genuss in der Mikrobiologie oder Biochemie. Science Diskussionen und grillen am Balkon und diverse Radtouren (mit und ohne Michi).

Vielen Lieben dank auch an unsere drei TAs Kristin Tobi und Giesela. Die einem immer geholfen haben und das Labor am Leben gehalten haben und auch Fehler verzeihen konnten, wenn man sich mal wieder dumm angestellt hat! Giesela dir speziell wünsche ich eine schöne „Pension“ (Rente ist ja was für Senioren) an eurem baldigen Seehäuschen und bedanke mich für die Labornachbarschaft und die viele Hilfe! Auf, dass du nie wieder dich mit Enzymbestellungen rum ärgern musst! Tobi und Kristin ihr werdet das Schiff weiter erfolgreich schaukeln!

Auch über die Laborgrenzen hinaus vielen Dank an alle Mitarbeiter des gesamten Lehrstuhls für die Tolle Zeit!

Bei Kevin Kramm und Leonhard Jakob für die Hilfe am TIRF und FCS.

Bei Tessa Quaxx für die schöne Zeit in Freiburg und die Hilfe bei den Experimenten!

An all meinen Freunde mit denen ich von Studienbeginn bis heute weiterhin sehr gut befreundet bin, die Zahlreichen (Ski-)Urlaube, Festivals, Hochzeiten, Geburtstage und Parties, vielen Dank!

Vielen Dank auch an Kinga Ay und Carolin Apfel die, die PR-Gruppe sehr gut geleitet haben und darüber hinaus auch die manchmal doch etwas verwirrende RIGEL Geschichte gut erklärt haben!

Auch wenn es schon lange her ist... aber bei PD Dr. Jan Oettler und Dr. Lukas Schrader möchte ich mich nochmal sehr herzlich für die vermittelte Wissenschaftsbegeisterung am Anfang meiner Universitäts-/Forschungskarriere (Bachelorarbeit) und Freundschaft bedanken!

Meinen Eltern möchte ich für die langjährige Unterstützung danken, die sich jetzt seit über 32 Jahren hinzieht. Für die Unterstützung während der Studienzeit und danach in der Doktorarbeit. Ohne euch wäre ich sicherlich nicht an diesen Punkt gekommen.

Zu guter Letzt gilt mein Dank meiner lieben Frau und besten Freundin Chrissi! Die all die Jahre an meiner Seite stand und das hin und her mit der Doktorarbeit mitgemacht hat! Mit wenig Murren, als es dann doch noch länger gedauert hat und du für eine Weile schon allein in Hamburg warst. Vielen Dank, dass du die ganze Verrücktheit in dieser Wissenschaftswelt so lange ertragen hast (jaja ich bin gleich fertig im Labor, ich komm gleich nach Hause..., ich fahr schnell ins Labor Zellen animpfen). Vielen Dank für das Verständnis mir gegenüber in der Schreibphase in der ich z.T. kaum Ansprechbar war und irgendwo im Limbo zwischen Wahnsinn und Wirklichkeit getaumelt bin. Dank Corona warst du dann doch schon etwas früher wieder in Regensburg und wir haben die Zeit vor der Geburt noch in unserer schönen Heimat genossen. Die Geburt unseres Sohnes war für den Schreibprozess nicht sehr förderlich aber wir haben es geschafft inmitten einer Pandemie ein Kind zu kriegen. Jetzt heißt es den kleinen Racker am Leben zu halten!

An meinen Sohn Felix: Falls du das liest bist du vermutlich schon etwas älter und denkst, „Mann was hat der denn da für komische Sachen erforscht und warum eigentlich in Archäeen?“ Lass dir sagen, wenn man sich für etwas begeistert und wirklich interessiert dann bleibt man dabei, egal wie viele Fehlschläge es mit sich zieht. Genauso wie du grade immer probierst, mit deiner rechten Hand das Plüschschiff in deinem Mobile zu bewegen, wenn es funktioniert freust du dich, wenn nicht dann halt nicht und versuchst es dann zur Sicherheit doch noch mal...

Als Abschluss noch ein Dank an den Treuen (Labor) Hund Pebbles! Dafür, dass Proben zu Geneart bringen, auch gleichzeitig Gassigehen war und das Büro mit guter Laune gefüllt war. Auf dass du noch viele Löcher buddeln wirst!

